Evolutionarily Conserved Function of Huntingtin in Cellular Dynamics Related to Cell Adhesion and the Cytoskeleton

Professor Marcy E. MacDonald Morgan Nicole Thompson

Evolutionarily Conserved Function of Huntingtin in Cellular Dynamics Related to Cell Adhesion and the Cytoskeleton

Abstract

Huntington's disease (HD) is a rare, dominantly inherited neurodegenerative disorder characterized by progressive chorea, emotional and behavioral disturbances, and cognitive decline. The single, causative mutation is an expanded trinucleotide repeat of cytosine, adenosine, and guanine (CAG) of more than 37 residues in the HD gene (currently referred to as *HTT*). Genetic evidence suggests that the CAG repeat expansion results in a gain of huntingtin function. While huntingtin and its numerous interactors have been implicated in a variety of essential cellular processes, the role of the full-length, endogenous protein remains unclear. Multiple studies have implicated huntingtin in processes related to cytoskeletal structure and dynamics in HD patients and model organisms. However, alterations in cellular dynamics related to the cytoskeleton – including cell adhesion – have not been characterized in a comprehensive, rigorous manner. Using *Mus musculus* genetic models of the HD mutation and/or deficiency and a *Dictyostelium discoideum* genetic deficiency model, I have undertaken an investigation of evolutionarily conserved huntingtin function in the cytoskeleton and cell adhesion. The results of these studies support a role for huntingtin in cell-cell and cell-substrate adhesion, as well as maintaining actin cytoskeletal structure. Furthermore, my thesis research sets the stage for future work to elucidate the molecular mechanism by which huntingtin is acting and determine the effect of the CAG repeat expansion on huntingtin function. Evolutionary conservation affords an invaluable tool to identify crucial function(s) of the huntingtin molecule and the effect of the pathogenic HD mutation on function, enabling therapeutic development while providing novel insights into cytoskeletal biology and cell adhesion.

Table of Contents

Acknowledgements

I would like to thank my advisor, Dr. Marcy MacDonald, for her tireless enthusiasm, support, and mentorship. Dr. MacDonald afforded me the opportunity to pursue my own lines of interest and inquiry in the lab, while also promoting my involvement in formal and informal science education and outreach. I am indebted to and humbled by her faith in my abilities as a scientist and individual. The MacDonald lab provided an environment of collaborative people and resources that were invaluable. My work using the model organism *Dictyostelium* would not have been possible without the close rapport and continual interaction between research groups within the Center for Human Genetic Research, particularly the enthusiastic support of Dr. Jim Gusella, former chair of my thesis committee and initiator of the *Dictyostelium* model. I am indebted to all of my fellow lab members who are helpful, kind, and generous people in and outside of the lab. Particular gratitude goes out to my closest research collaborators – Marta Biagoli, Amanda Lumsden, Michael Myre, Surya Reis, Ihn Sik Seong, and Randy Singh – and additional friends and colleagues – Sunita Biswas, Elisa Fossale, Tammy Gillis, Jessie Jacobsen, Vidya Murthy, and Ravi Vijayvargia – who supported me throughout my thesis work. I must also thank the guidance of my thesis committee: Dr. Kami Ahmad, Dr. Chad Cowan (current chair), Dr. Jim Gusella (former chair), and Dr. Andrea McClatchey. A special appreciation to the Huntington's disease community and the HOPES (Huntington's Disease Outreach Project for Education at Stanford) students and supporters, for letting me play a part.

Huge support has come from wonderful family, friends, and colleagues, too numerous to name. Special thanks to those who changed my life – Dr. Jon Beckwith, Dr. Lee Gehrke, Dr. Vishal Gohil, Dr. Prachi Trivedi Gohil, Dr. Miriam Greenberg, Nancy Houfek, Mr. Jack Lawrence, and Dr. Sheila Thomas, and for their professional and personal guidance and friendship; my parents, Ken and Mary, who instilled the curiosity and creativity that seeded this journey; my sister, Alexandra, and grandparents, Jeanette and Bob, for their unending love and confidence; Doruk, Cristina, Amber, Jess, Megan, Sara, Izzy, Emily, Shirin; and my other half, Alex.

List of figures[1]

[1] Figures are numbered with the chapter number followed by the numerical order in which they appear in that chapter.

Chapter 1:

Introduction

The genetic basis of Huntington's disease

Huntington's disease (HD) is a fatal, late-onset neurodegenerative disorder affecting approximately 1 in 10,000 individuals [1]. Although age of onset of symptoms varies, patients are most likely to experience diagnosed symptoms in mid-life – including uncontrolled, choreic movement and progressive decline of cognitive, behavioral, and motor function [2]. Unlike many other complex genetic neurodegenerative diseases, HD pathogenesis is due to a single causative mutation in the HD gene (recently renamed *HTT*)[2], which is dominantly inherited [3]. The pathogenic mutation results in an expanded version of a normally polymorphic polyglutamine (polyQ) tract in the huntingtin protein [4]. The HD mutation was identified by genomic mapping without prior understanding of underlying biology [5]. However, knowledge of huntingtin normal function is essential to developing targeted therapeutics for intervention at the earliest stages of HD because of the need to both fully understand the HD initiating process and to inform strategies aimed at decreasing huntingtin levels, such as RNA interference (RNAi)

[2] An effort was made to keep HD gene and protein nomenclature consistent throughout this manuscript. However, it is important to note that the name of the *HD* gene was recently changed to *HTT*. The cellular and whole organism models generated in our lab were named under the previous guidelines and therefore reflect the original *HD* (Huntington's disease) or *Hdh* (HD homolog) gene names. These original lab strain names have been retained in this manuscript. Except in rare instances, the protein name huntingtin has been spelled out in its entirety throughout the manuscript to indicate reference to the full-length protein. All of the model organisms described in this manuscript express a form of full-length huntingtin.

Organism	Official nomenclature		Alternate nomenclature
	Gene	Protein	
Homo sapiens	*HTT*	HTT	HD, IT15
Mus musculus	*Htt*	Htt	Hdh
Dictyostelium discoideum	*htt*	htt	hd

technology which is the strategy currently on track to be the first disease modifying HD therapeutic to be assessed in clinical trials. [6, 7].

Genotype-phenotype studies of HD patients have produced a set of genetic criteria that characterize the disease. First, mutant huntingtin displays dominance over the wild-type protein [8, 9]. Second, though age at onset of clinical HD symptoms varies widely, there is an inverse relationship between the CAG repeat length and age at onset, such that over half of the variance can be explained by length of the CAG expansion (Figure 1.1) [9]. However, there remains significant variation in age at onset even in individuals with the same CAG repeat length (Figure 1.1, gray shading). This variation appears to be highly heritable, suggesting that other genetic factors act to modulate HD pathogenesis [10, 11]. Third, the disease-causing mutation leads to progressive neuronal death in a variety of brain regions, but particularly acute and selective loss of medium spiny neurons in the striatum [6].

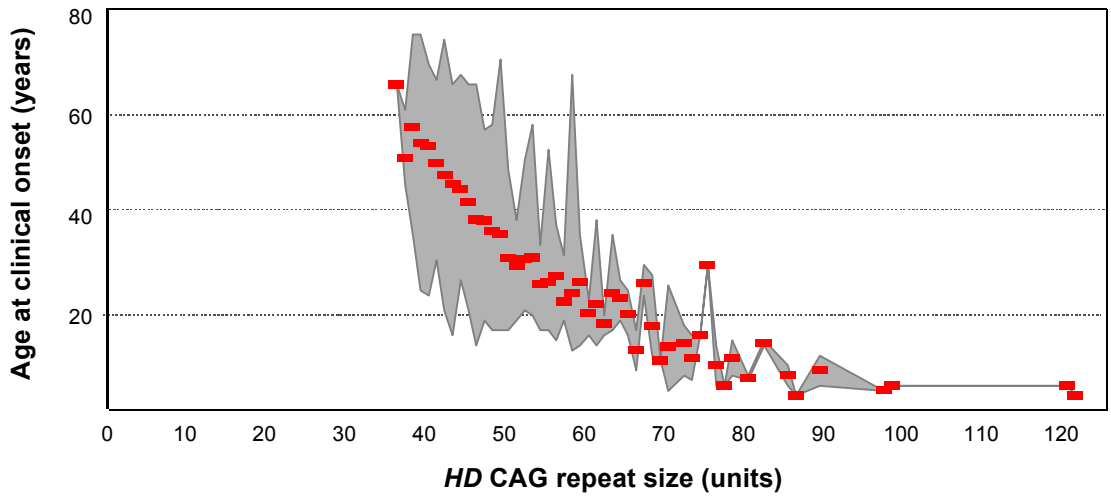

Figure 1.1 CAG repeat length-dependence of age at clinical onset of HD. Each red data point represents the average age at clinical onset for patients with a given HD CAG repeat length. Gray shading indicates the variation in age at onset of clinical symptoms in patients with a given HD CAG repeat length. (Figure courtesy of Dr. Marcy MacDonald)

The pathogenic mechanism of HD is not primarily due to loss of huntingtin activity because heterozygous *HTT* inactivation, via rare translocations, has been reported in humans

and these individuals do not display phenotypic abnormalities [12, 13]. Similarly, mice hemizygous for *Htt* are phenotypically normal and do not develop HD-like phenotypes [12-14]. A complete dominant-negative inhibition of huntingtin function is also unlikely because although human patients homozygous for the HD mutation are indistinguishable from heterozygous siblings [15, 16], homozygous inactivation of the mouse *Htt* gene results in early embryonic lethality at approximately E7.5 [14]. At this time the most parsimonious genetic explanation for the HD trigger is that the polymorphic CAG repeat region confers enhanced huntingtin molecular function.

Huntingtin normal function and its relation to structure and CAG repeat length

Despite two decades of research, the normal function of huntingtin has remained elusive due to a variety of challenges related to the protein's unique structural and physical properties. Huntingtin is a large, 3,144 amino acid (~350 kDa) protein that is expressed ubiquitously throughout all tissues [17]. Based upon sequence prediction and biochemical analysis of purified full-length recombinant huntingtin, the protein is a hinged α-helical solenoid spanned by HEAT (Huntingtin, elongation factor 2, protein phosphatase 2A PR65/A subunit, and target of rapamycin) repeats [18, 19]. Figure 1.2 is a representation of our current understanding of the conserved structural domains of huntingtin created by sequence-based prediction software [20]. Proteins predominantly comprised of HEAT domains – such as importin-β and protein phosphatase 2A PR65/A [21, 22] – are flexible molecules that facilitate macromolecular complexes and contribute to an array of cell signaling pathways [19, 23]. Over 100 distinct conformations of recombinant full-length huntingtin were identified by negative stain electron microscopy [20] and epitopes of endogenous huntingtin display differential accessibility [6]. These data imply structural flexibility of huntingtin that may allow the protein to organize members of dynamic complexes, similar to other canonical HEAT proteins. Consistent with this hypothesis, huntingtin participates in more than 70 putative protein interactions [19, 24, 25] and can directly bind DNA and RNA [26], implicating it in a wide variety of cellular processes –

including transcriptional regulation and DNA maintenance, cytoskeletal and transport processes, cell signaling and fate, protein synthesis and turnover, and cellular metabolism [24, 27-37].

Genetic models to study evolutionarily conserved huntingtin structure/function

Murine genetic models

To narrow down the vast number of putative huntingtin interactors and identify the essential activities of huntingtin, genetic strategies are indispensable because they hold the potential to reveal the unexpected and dissect causal relationships. Our lab generated precise genetic models that replicate the human HD mutation or produce huntingtin deficiency. In the allelic series of knock-in (KI) mouse models, a portion of exon 1 of the murine *Htt* was replaced with a human *HTT* exon 1 of varying CAG (Q) repeat length (*Hdh*^{Q7}, *Hdh*^{Q20}, *Hdh*^{Q91}, *Hdh*^{Q111}), such that the chimeric mouse:human exon 1 (or humanized exon 1) is expressed from the endogenous murine *Htt* promoter along with the rest of the 66 exons encoding the full-length huntingtin protein [38]. Furthermore, mice homozygous or heterozygous (*Hdh*$^{Q7/7}$, *Hdh*$^{Q20/7}$, *Hdh*$^{Q91/Q7}$, *Hdh*$^{Q111/Q7}$) for the HD mutation were generated to enable investigation of possible dominant negative effects; striatal cell lines were isolated and immortalized [8] and embryonic stem (ES) cell lines were derived [39]. A homozygous deficiency mutant model was also created where exons 4 and 5 of the mouse *Htt* gene were replaced with a neomycin (*Neo*) resistance cassette (*Hdh*$^{ex4/5/ex4/5}$) [14]. This genetic strain has a detectable mRNA product, but no huntingtin protein expression. Mice homozygous for *Htt* inactivation were embryonic lethal at approximately E7.5, showing that huntingtin is needed for proper development. Huntingtin is not required for cell growth in culture since ES cells were isolated and viable [39].

Figure 1.2 Conserved segmental domains of huntingtin. Schematic of huntingtin (open line) with amino acid coordinates above, black box representing the polyglutamine tract, and blue boxes representing NORSp predicted disordered regions. Trypsin digestion cleaves the protein at residue 1250, indicating an accessible hinge region. PROF predictions where pH_sec, pE_sec and pL_sec represent the probability (1=high, 0=low) for helical (red), strand (blue), or neither helical nor strand (green) structure. Below this is a compressed multisequence alignment of huntingtin from 8 chordates with increasing intensity of blue shading if the residue is identical in four or more organisms. Followed by Jalview physico-chemical properties conserved for each amino acid position, from least (dark brown) to most (bright yellow) conserved, with height corresponding to increasing conservation. (Figure reproduced with permission from [20])

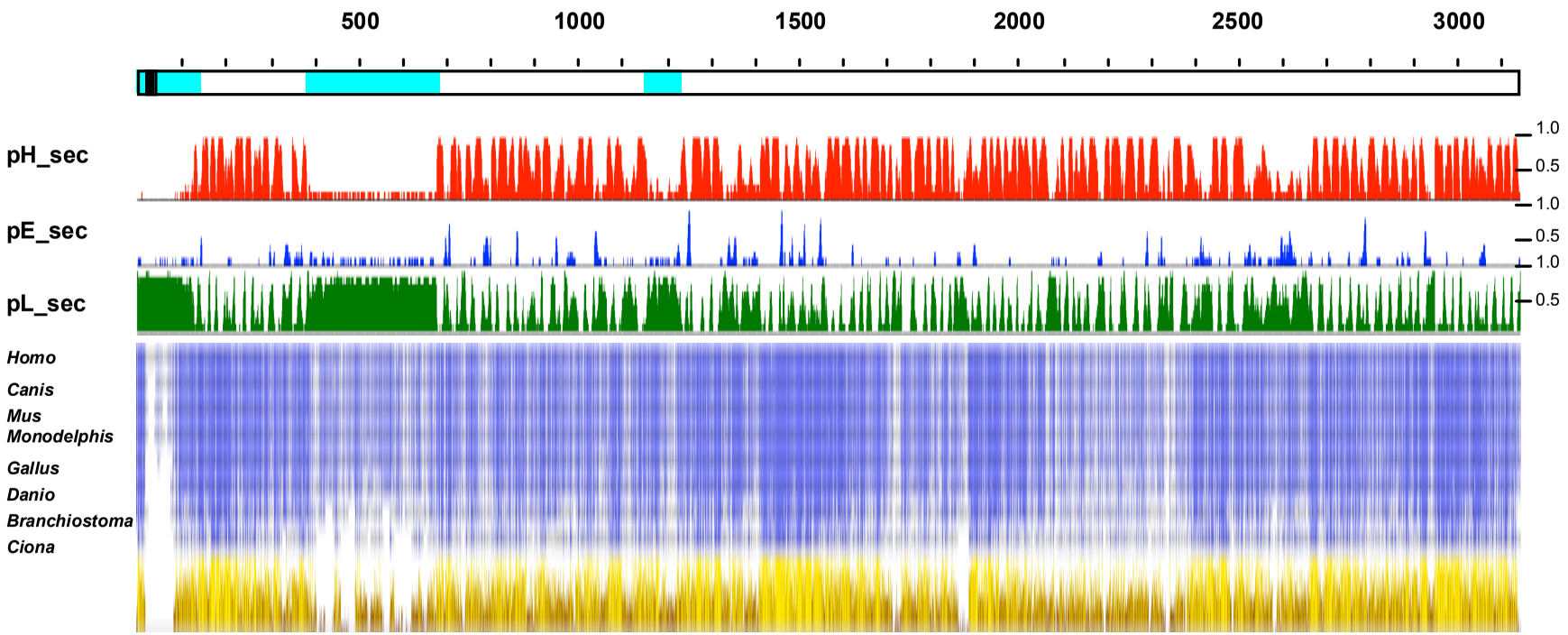

Dictyostelium discoideum huntingtin deficiency model

Given the difficulties in identifying crucial normal functions of full-length huntingtin and the fact that structural properties of huntingtin are highly conserved through multicellular evolution, interest in non-mammalian models to study conserved function of huntingtin has increased and resulted in a number of experimental organisms in nematode worms (*Caenorhabditis elegans)* [40, 41]*,* fruit flies (*Drosophila melanogaster*) [42, 43]*,* zebrafish (*Danio rerio*) [44], and slime mold (*Dictyostelium discoideum*) [45-47]. All of these possess the benefits of reducing the cost and time course of experimentation [17]. *D. discoideum* is particularly intriguing based on a few distinct properties: 1) *D. discoideum* is the most evolutionarily ancient organism known to possess a huntingtin ortholog; 2) While *D. discoideum* can be induced to undergo a diploid phase, they primarily exist in a haploid state throughout their development and in laboratory culture, providing for ease of genetic manipulation; 3) Given the known importance of huntingtin in developmental processes, *D. discoideum* possess a primitive form of multicellular development and cellular differentiation that is well characterized, relatively simpler than mammalian systems, and can be interrogated for potentially conserved huntingtin function.

Translation to human disease

Translation back to mammalian and ideally human systems is necessary to evaluate the relevance of phenotypes and conserved function(s), identified in non-mammalian experimental systems, to HD pathogenesis. Our lab possesses a large repository of human fibroblast and lymphoblast cell lines from patients with various CAG repeat length *HTT* mutations. Furthermore, recent advances in stem cell technology allow new, patient-specific cellular resources to be generated by reprogramming adult, differentiated cells to induced pluripotent stem (iPS) cells [48]. Colleagues in the lab are developing differentiation protocols to take cells from iPS pluripotency to neuronal progenitors and an array of differentiated neuronal subtypes, including cells that phenotypically resemble primary striatal cultures. Thus,

studies in murine and *D. discoideum* cellular models presented here are ripe for parallel investigations in human models to verify their relevance to disease and determine the effect of CAG repeat length on the huntingtin function(s) identified.

Huntingtin in cell adhesion and the cytoskeleton

Mounting evidence supports the hypothesis that huntingtin plays a subtle, but vital functional role in cytoskeletal structure and function, including cell adhesion. The molecular machinery of cytoskeletal and cell adhesion biology is highly conserved and, where direct conservation of specific molecular players is lacking, there remain some unifying mechanistic principles across model organisms [49].

HD patient phenotypes

In human patients, levels of the actin binding protein profilin – a key regulator of actin polymerization and crucial player in neuronal differentiation and synaptic plasticity [50] – are reduced progressively with stage of disease in the cortical brain region of presymptomatic, early stage, and late stage HD patients compared to age-matched controls [51]. Furthermore, coimmunoprecipitation of huntingtin and β-tubulin has been achieved from human patient lymphocytes and rat brain [52]. These studies suggest an interaction between huntingtin and β-tubulin. The association of huntingtin with the microtubule cytoskeleton through interaction of huntingtin with tubulin allows for efficient trafficking of the protein to the cell nucleus. Thus, huntingtin has been strongly implicated as a player in both the actin and microtubule cytoskeletal systems, although its exact role remains unclear.

Phenotypes in murine genetic models

A number of preliminary studies using murine *Htt* deficiency models and *Htt* polyQ expansion models that replicate the precise genetic mutation in HD, suggested that aspects of cytoskeletal and adhesion dynamics are subtly altered both by lack of huntingtin and by the presence of mutant huntingtin. Huntingtin deficient ES cells – as well as zebrafish – have revealed a role for the protein in homotypic adhesion of neuroepithelial cells by modulating

activity of the metalloprotease ADAM10 and cleavage of N-cadherin [47]. Additionally, huntingtin is a well-established enhancer of vesicular transport facilitated by its microtubule-based associations with HAP1, dynactin, and $p150^{glued}$ [27, 53-55]. Actin cytoskeletal effects are also apparent in immortalized striatal murine cells, including colocalization of huntingtin with cofilin-actin stress rods in the cell nucleus and defective actin remodeling [56].

Phenotypes in Dictyostelium discoideum deficiency model

Due to the high degree of evolutionary conservation of many of the key molecules involved in cytoskeletal biology, *D. discoideum* is increasingly being recognized as an excellent tool for dissecting actin-related human diseases, including Alzheimer's disease and spastic paraplegia [57]. Similarly, cell adhesion machinery is highly conserved [58] and two of the main developmentally-regulated cell adhesion molecules, cad1 and csA, are putative orthologs of human cadherin and neuronal cell adhesion molecule, respectively [59]. Figure 1.3 provides a representation of the *D. discoideum* life cycle, which occurs in a 24-hour period upon starvation and is known to be regulated by three adhesion molecules – cad1, csA, and lagC – whose expression peaks successively. Recently, two novel models of huntingtin deficiency have been independently made in *D. discoideum* [45, 46]. Initial phenotypes in the *D. discoideum* huntingtin deficiency model, detailed in Chapter 4, were reminiscent of mammalian models and mirrored known phenotypes of cytoskeletal and cell adhesion mutants, prompting further investigation and in-depth characterization.

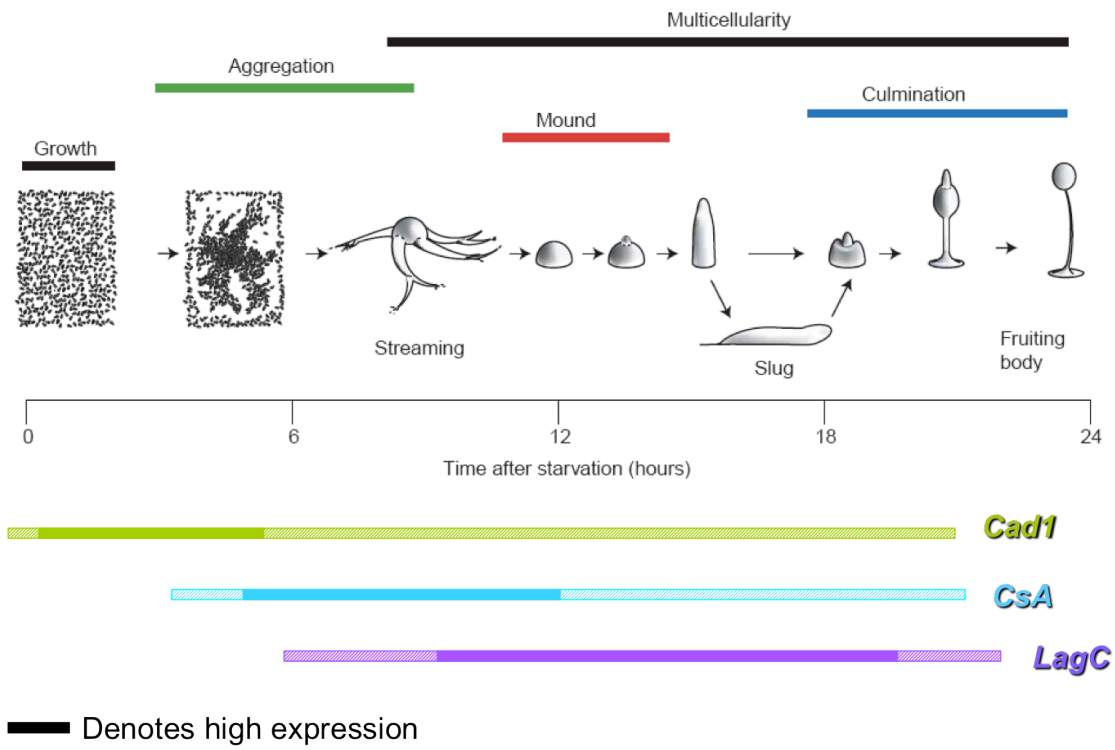

Figure 1.3. Schematic of *D. discoideum* development. The developmental life cycle progresses upon starvation to completion within a 24-hour cycle. Cell adhesion is critical to the complex intracellular and intercellular coordination and movement necessary to accomplish this feat. Cad1, csA, and lagC are the three canonical adhesion molecules known to govern adhesion during development and their expression peaks successively (indicated by solid bars). (Figure modified from [59])

My thesis aimed to further characterize and define evolutionarily conserved functions of huntingtin in cellular dynamics related to the cytoskeleton and cell adhesion. Chapter 2 details the published characterization of cell adhesion and the actin cytoskeleton in the murine striatal genetic knock-in models of HD [60]. Chapter 3 describes optimization of growth conditions and characterization of the murine ES knock-out and knock-in genetic models [39]. Chapter 4 discusses an evolutionarily conserved role for huntingtin in cell adhesion in huntingtin deficient *D. discoideum* [45]. This adhesion phenotype was first described in the original publication characterizing the newly created *D. discoideum* model [45] and Chapter 4 represents a manuscript in preparation that further elucidates the adhesion defect.

Chapter 2:

Striatal neurons expressing full-length mutant huntingtin exhibit decreased N-Cadherin and altered neuritogenesis[3]

Surya A. Reis[1~], Morgan N. Thompson[1], Jong-Min Lee[1], Elisa Fossale[1], Hyung-Hwan Kim[2], James K. Liao[2], Michael A. Moskowitz[3], Stanley Y. Shaw[4], Linda Dong[1], Stephen J. Hagarty[5], Marcy E. MacDonald[1] and Ihn Sik Seong[1*]

[1] Molecular Neurogenetics Unit, Center for Human Genetic Research, Massachusetts General Hospital, 185 Cambridge Street, Boston MA 02114, USA

[2] Vascular Medicine Research Unit, Brigham and Women's Hospital and Harvard Medical School, Cambridge, MA 02139, USA

[3] Stroke and Neurovascular Regulation, Massachusetts General Hospital, Charlestown, MA, 02129, USA

[4] Center for Systems Biology, Massachusetts General Hospital, 185 Cambridge Street, Boston MA 02114, USA

[5] Chemical Biology Program, Center for Human Genetic Research, Massachusetts General Hospital, 185 Cambridge Street, Boston MA 02114, USA

[~] Current address: Chemical Biology Programs, Center for Human Genetic Research, Massachusetts General Hospital, 185 Cambridge Street, Boston MA 02114, USA

[*] To whom correspondence should be addressed:

Email: iseong@chgr.mgh.harvard.edu; Tel: 617-643-9851 ; Fax: 617-643-3202

[3] This chapter is reprinted with permission and minor modifications for formatting and nomenclature consistency from: Reis, S.A., et al., *Striatal neurons expressing full-length mutant huntingtin exhibit decreased N-cadherin and altered neuritogenesis.* Hum Mol Genet, 2011. **20**(12): p. 2344-55.

Attribution

The work in this chapter is a collaborative project conducted in the MacDonald lab, primarily with colleagues Dr. Surya Reis and Dr. Ihn Sik Seong. I conducted the research on actin cytoskeletal phenotypes in the immortalized striatal cell models detailed in Figure 2.5. I identified a novel cofilin phenotype in the striatal cells that was included in the manuscript (Appendix A). Dr. Reis conducted the whole organism and primary striatal cell culture studies, as well as initially identifying the aberrant phalloidin immunofluorescence staining in the immortalized striatal cell system, which I went on to further characterize and quantify. Dr. Seong performed the majority of the biochemical experiments detailed in the manuscript.

Abstract

The expanded HD CAG repeat that causes striatal cell vulnerability in Huntington's disease (HD) encodes a polyglutamine tract in full-length huntingtin that is correlated with cellular [ATP] and [ATP/ADP]. Since striatal neurons are vulnerable to energy deficit, we have investigated – in *Hdh* CAG knock-in mice and striatal cells – the hypothesis that decreased energetics may affect N-cadherin, a candidate energy-sensitive adhesion protein that may contribute to HD striatal cell sensitivity. *In vivo* N-cadherin was sensitive to ischemia and to the effects of full-length mutant huntingtin, progressively decreasing in Hdh^{Q111} striatum with age. In cultured striatal cells, N-cadherin was decreased by ATP-depletion and $STHdh^{Q111}$ striatal cells exhibited dramatically decreased N-cadherin, due to decreased *Cad2* mRNA and enhanced N-cadherin turnover, which was partially normalized by adenine supplementation, to increase [ATP] and [ATP/ADP]. Consistent with decreased N-cadherin function, $STHdh^{Q111}$ striatal cells displayed profound deficits in calcium-dependent N-cadherin-mediated cell clustering and cell-substratum adhesion, and primary Hdh^{Q111} striatal neuronal cells exhibited decreased N-cadherin and an abundance of immature neurites, featuring diffuse, rather than clustered, staining for N-cadherin and synaptic vesicle markers, that was partially rescued by adenine treatment. Thus, mutant full-length huntingtin, via energetic deficit, contributes to

decreased N-cadherin levels in striatal neurons, with detrimental effects on neurite maturation, strongly suggesting that N-cadherin mediated signaling merits investigation early in the HD pathogenic disease process.

Introduction

The CAG expansion mutation that causes Huntington's disease (HD) elongates a polymorphic polyglutamine segment in the huntingtin protein. Full-length huntingtin with a polyglutamine region of more than about 37 residues initiates a disease process that culminates in the loss of neurons, especially in the striatum, and the onset of the motor, psychiatric and cognitive symptoms [61, 62]. Understanding the rate-limiting events that contribute to the early vulnerability of striatal neurons would guide efforts to track the natural history of the disease and may provide new avenues for therapeutic development.

Studies investigating the earliest consequences of full-length mutant huntingtin, in HD patient cells and tissues – and in accurate genetic *Hdh* CAG knock-in mouse cells and tissues – have revealed perturbations in membrane vesicle trafficking, gene transcription, intracellular signaling pathways [55, 63, 64], as well as altered energetics, characterized by decreased [ATP] and [ATP/ADP], that is correlated with size of the polyglutamine-repeat [65-67]. We have been studying the effects of altered energetics, as the correlation of energetic measures with polyglutamine-repeat in full-length huntingtin implies a dominant effect that conforms to the genetic features of the HD trigger mechanism, and energetic defects, thought to be important to striatal cells, may be evident through the lifetime of the cell, perhaps from birth [65-67]. Certainly, early weight loss in HD patients and a systemic metabolic defect in branched chain amino acids (BCAA), are consistent with a systemic attempt to compensate for an early energy deficit [68].

Neuronal (N)-cadherin, which is intimately involved in neuronal cell adhesion signaling, differentiation and synapse function [69, 70], is a prime candidate for being affected by energy deficit. Members of the cadherin family exhibit selective degradation in response to renal

ischemia/ATP depletion [71-73], and in normal rat kidney cells via cleavage by membrane-type 1-matrix metalloprotease (MT-MMP) [74]. However, N-cadherin has not been studied either in acute neuronal ischemia/ATP depletion or in the response to the HD mutation, which elicits a chronic energy deficit in a process that culminates in neurodegeneration.

N-cadherin is a transmembrane cell adhesion glycoprotein comprised of an extracellular domain, a single pass transmembrane region, and a cytoplasmic tail [75]. N-cadherin molecules make calcium-dependent homophilic bonds between their extracellular domains [76]. The cytoplasmic domain contains two main binding regions, the C-terminal domain (CTD) and the juxtamembrane domain (JMD). The CTD domain binds β- and γ- catenin, which in turn associates with the actin cytoskeleton to modulate cell adhesion and mobility via α-catenin [77, 78]. The JMD interacts with p120-catenin and with presenilin 1 (PS1), which has emerged as a potential regulator of cell adhesion and neuronal physiology [79, 80].

Here, we have assessed the candidacy of N-cadherin as an energy-sensitive contributor to the striatal cell vulnerability that ensues from the HD mutation. Specifically, we have investigated N-cadherin in *Hdh*^{Q111} CAG knock-in mouse striatum and cultured *STHdh*^{Q111} striatal neuronal cells, which express endogenous full-length 111-glutamine mutant huntingtin. We first tested whether N-cadherin was sensitive to acute ATP depletion/ischemia and to the chronic effects of full-length mutant huntingtin protein and then we evaluated immortalized *STHdh*^{Q111} and primary *Hdh*^{Q111} striatal neurons to explore N-cadherin ATP-sensitivity and the phenotypic consequences of decreased N-cadherin function. Our findings reveal that N-cadherin is an ATP-sensitive protein that is associated with altered HD CAG striatal cell adhesion and neuritogenesis.

Results

Striatal N-cadherin was sensitive to acute ischemia and to the HD CAG mutation

To assess whether N-cadherin might be affected in a mild ischemic brain injury paradigm, where the striatum displays early vulnerability, we performed transient middle

cerebral artery occlusion (MCA-O) with 12-month-old wild-type and mutant *Hdh*$^{Q111/Q111}$ knock-in mice. For both genotypes, immunoblot of protein extracts at 24 hours after reperfusion (Figure 2.1 A and 2.1 B) revealed robustly decreased N-cadherin in the ischemic, compared to the contralateral, striatal hemispheres. By contrast, full-length wild-type 7-glutamine huntingtin and 111-glutamine mutant huntingtin, cleaved by calpains in response to severe ischemia [81], and α-catenin and β-catenin, were not decreased, though p120 was slightly reduced by ischemia, attesting to the mildness of the lesion and demonstrating the exquisite sensitivity of N-cadherin in striatum to ischemia/ATP-depletion.

The immunoblot results also revealed reduced N-cadherin in contralateral *Hdh*$^{Q111/Q111}$ striata, compared to the wild-type striata, suggesting an effect of the CAG mutation. This was confirmed by immunoblot analysis of wild-type and *Hdh*$^{Q111/Q111}$ striatal tissues at different ages, which revealed a progressive decrease in N-cadherin (normalized to α -tubulin) from 3 months to 5 months of age that reached statistical significance by 12 months of age (Figure 2.2).

Notably, *Cad2* mRNA levels were not reduced, in total striatal tissue, following ischemic reperfusion or in response to the CAG mutation (data not shown), implying that cell-specific and/or multiple mechanisms may contribute to energy-dependent N-cadherin decrease in vivo.

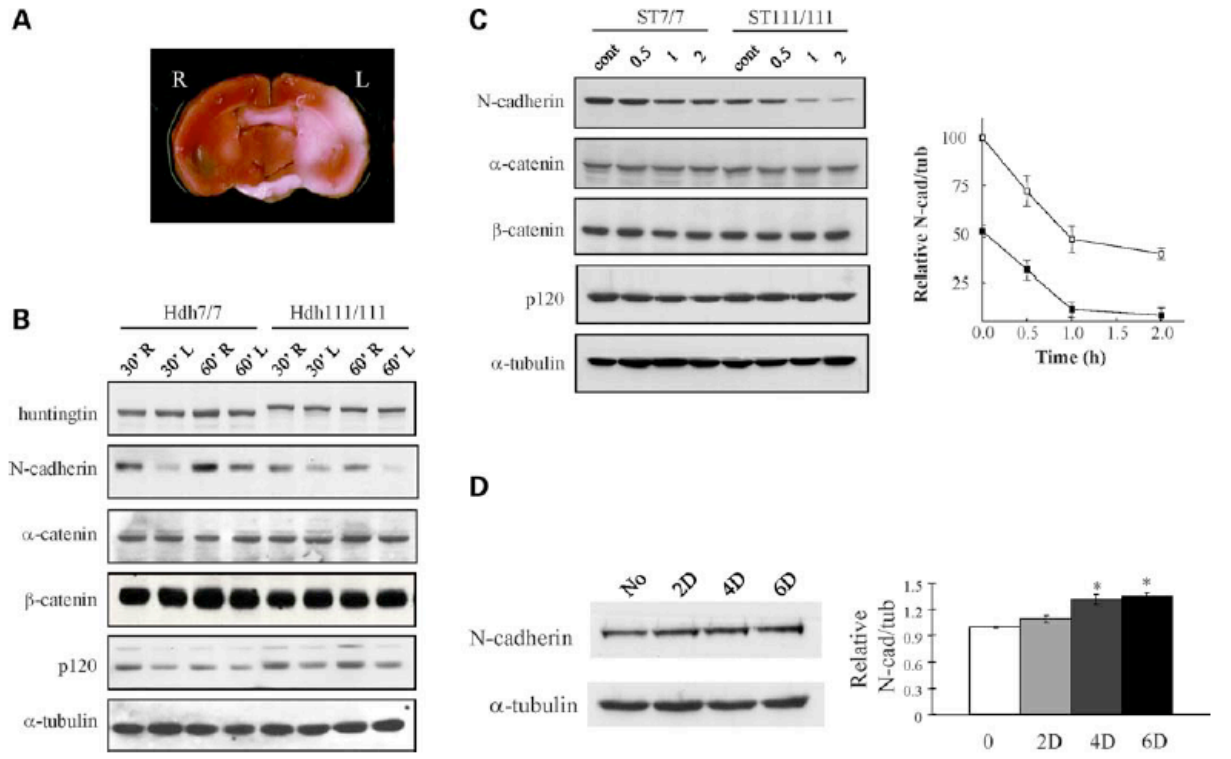

Figure 2.1. ATP-sensitive N-cadherin stability. A) A representative coronal section of wild-type *Hdh*$^{Q7/Q7}$ mouse brain, following MCA occlusion/reperfusion, stained with 2,3,5-triphenyltetrazolium chloride (TTC), to demonstrate the infarct region (white area) in the left hemisphere (L), as well as the contralateral right hemisphere (R). The infarct sizes (mm^3 and mean ± standard errors) were measured from mice brains of both genotypes at 30 and 60 min MCA occlusion as 33.9 ± 3.64 and 35.2 ± 3.55 for wild-type brain at 30 and 60 min and 41.5 ± 5.97 and 43.1 ± 6.81 for mutant brain and showed no significant differences by genotypes and times (n=3), consistent with the previous report (23). B) Immunoblot showing bands of N-cadherin, β-catenin, α-catenin and p120 detected in protein extracts of striata from the MCA-occluded hemisphere (L) and contralateral hemisphere (R) for wild-type *Hdh*$^{Q7/Q7}$ (Hdh7/7) and mutant *Hdh*$^{Q111/Q111}$ (Hdh111/111) mice, with 30 min MCA occlusion (30**"**) or 60 min MCA occlusion (60"), demonstrating decreased N-cadherin on the lesion side, relative to the α-tubulin loading control band. However, the reduction in N-cadherin was not statistically different between two genotypes or two occlusion times (n=3). C) Immunoblot showing bands of N-cadherin, β-catenin, α-catenin and p120 detected in protein extracts of wild-type *STHdh*$^{Q7/Q7}$ (ST7/7) and mutant *STHdh*$^{Q111/Q111}$ (ST111/111) cells, at time 0 (cont), and 0.5, 1 and 2 h in ATP-depletion medium. The adjacent graph plots the relative band intensity of N-cadherin normalized to α-tubulin in the same lane (Y-axis), with the time in ATP-depleting medium (X-axis), illustrating decreased N-cadherin in mutant cells at baseline and ATP-sensitive degradation of N-cadherin in cells of both genotypes. Bars denote the standard deviation from three independent experiments. D) Immunoblot showing N-cadherin in extracts of *STHdh*$^{Q111/Q111}$ cells, after incubation in medium supplemented with 10 μM adenine for 0, 2, 4 and 6 days (D), relative to the α-tubulin band. The adjacent bar graph plots the relative N-cadherin intensities normalized to the α-tubulin band intensities (Y-axis) for the time points analyzed (X-axis). Relative to the untreated control, N-cadherin levels were significantly elevated by day 4 (*P<0.05, n=3).

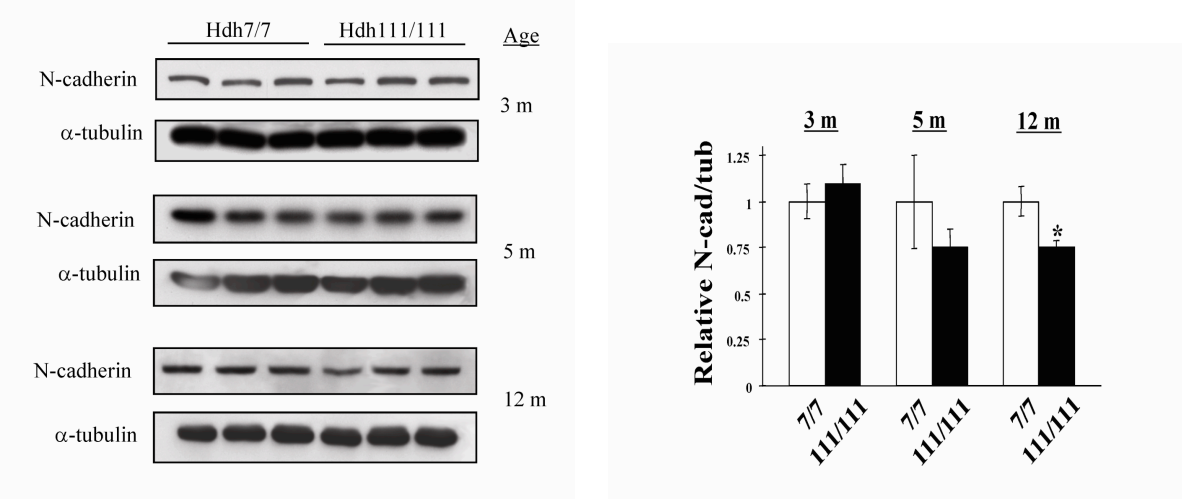

Figure 2.2. N-cadherin was decreased with age in striata of *Hdh*$^{Q111/Q111}$ mice. Immunoblot showing bands of N-cadherin for striata from three *Hdh*$^{Q7/Q7}$ (Hdh7/7) and three *Hdh*$^{Q111/Q111}$ (Hdh111/111) littermates, demonstrating progressively decreased N-cadherin at 3, 5, and 12 months of age. The bar graph below shows relative N-cadherin band-intensity normalized to the α-tubulin band-intensity and expressed relative to the wild-type ratio (Relative N-cad/tub), which was significantly decreased at 12 months in *Hdh*$^{Q111/Q111}$striatum (*P<0.05, n=3). Error bars represent standard deviation (±SD).

Striatal cell N-cadherin was sensitive to ATP-depletion and the HD CAG mutation

We then assessed whether N-cadherin might be sensitive to ATP-depletion and to the CAG mutation in cultured *STHdh*$^{Q7/7}$ and *STHdh*$^{Q111/Q111}$ striatal neuronal cells, expressing wild-type (7-glutamine) and mutant (111-glutamine) full-length huntingtin, respectively. Cells were treated with 2-deoxyglucose and antimycin A, to inhibit both glycolysis and mitochondrial respiration, and nucleotides in cellular extracts were measured by HPLC analysis. As reported previously [65, 67], the baseline [ATP/ADP] was significantly lower in mutant compared to wild-type, striatal cells, and for both genotypes, [ATP/ADP] was dramatically decreased within two hours of energy-depletion (Figure 2.3 A) although cell viability was not significantly changed (Figure 2.3 B).

Immunoblot analysis revealed that N-cadherin was decreased at baseline in mutant striatal cell extracts compared to wild-type, with a progressive reduction over the time-course of ATP-depletion for both genotypes (Figure 2.1 C). By contrast, α-catenin, β-catenin, and p120 levels were similar for cells of either genotype and were not changed by ATP-depletion (Figure 2.1 C). Thus, N-cadherin level was reduced concomitant with decreased [ATP/ADP], both due

to purposeful energy depletion and in response to ATP-deficit due to full-length mutant huntingtin.

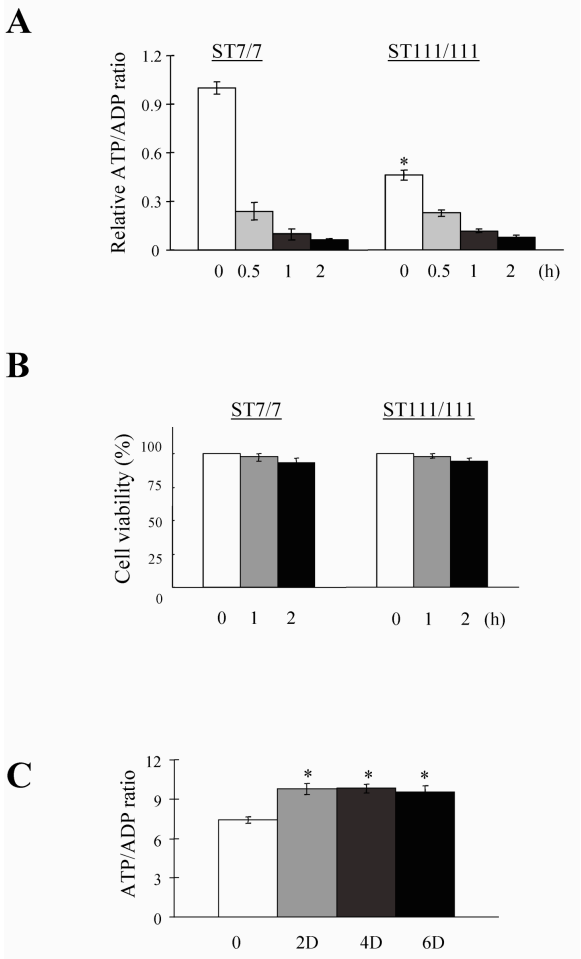

Figure 2.3. ATP/ADP and MTS measurement for ATP-depletion and adenine supplementation. A) The bar graph summarizes HPLC measurements, showing progressively decreased [ATP/ADP], relative to no treatment of wild-type cells (Y-axis), for wild-type ST*Hdh*$^{Q7/Q7}$ (ST7/7) and mutant *Hdh*$^{Q111/Q111}$ (ST111/111) striatal cell extracts, with time in ATP-depletion media (X-axis). The baseline [ATP/ADP] of mutant striatal cells was significantly decreased compared to wild-type striatal cells (*P<0.005, n=3), as previously reported, and was not as affected by ATP-depletion conditions as the wild-type. B) The bar graph plots the results of MTS cell viability (Y-axis), with time in ATP-depletion media (X-axis), revealing no change of wild-type (ST7/7) or mutant striatal cell (ST111/111) viability. C) The bar graph summarizes HPLC measurements, showing progressively increased (*P<0.05, n=3) [ATP/ADP] ratios (Y-axis) for *Hdh*$^{Q111/Q111}$ (ST111/111) striatal cell extracts, with time in adenine supplemented media (X-axis). Error bars represent standard deviation (±SD).

Further analyses demonstrated that decreased N-cadherin in mutant, compared to wild-type, striatal cells, reflected decreased *Cdh2* mRNA, as demonstrated by the results of RT-PCR analysis (Figure 2.4 A), as well as increased turnover rate of the protein, which had a half-life of about two hours in *STHdh*$^{Q111/Q111}$ cells compared to a half-life of more than four hours in wild-type cells (Figure 2.4 B).

To explore the energy-sensitivity of these measures, mutant striatal cell culture medium was supplemented with adenine, a precursor of high-energy nucleotides. By two days, [ATP/ADP] was mildly but significantly elevated (Figure 2.3 C) and by four days of treatment N-

cadherin was modestly but consistently increased (Figure 2.1 D), though *Cad2* mRNA levels were not altered over the entire six day time course (data not shown). These results suggested that enhanced N-cadherin protein turnover in the mutant striatal cells may involve an energy-sensitive process, while altered *Cad2* mRNA may reflect a different underlying process. However, assays to explore the involvement of metalloproteases, activated in ischemia, failed to disclose elevated MT-MMP and MT-MMP inhibition with GM-6001 did not alter the half-life of N-cadherin in mutant striatal cells (data not shown).

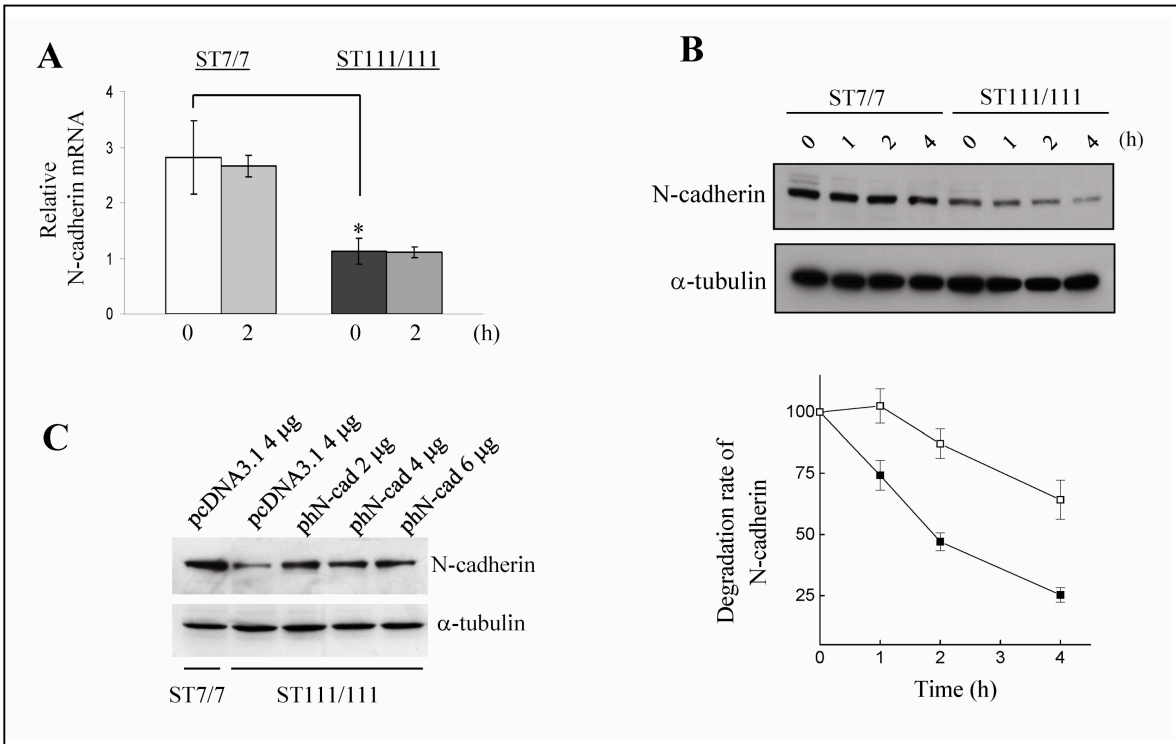

Figure 2.4. N-cadherin expression, turnover, ATP-depletion and N-cadherin overexpression. A) The bar graph presents the results of quantitative RT-PCR analysis of *Cdh2* mRNA normalized to β-actin (Y-axis) for mRNA extracted from wild-type *Hdh*$^{Q7/Q7}$ (ST7/7) and *Hdh*$^{Q111/Q111}$ mutant (ST111/111) striatal cells incubated in ATP-depletion media for 0 or 2 hours (X-axis). *Cdh2* mRNA was significantly decreased in mutant cells (*P < 0.005, n = 3), but was not affected by ATP-depletion. B) Immunoblot showing bands of N-cadherin and a-tubulin for ST*Hdh*$^{Q7/Q7}$ (ST7/7) and ST*Hdh*$^{Q111/Q111}$ (ST111/111) striatal cell extracts, after cells were incubated in cyclohexamide for 0-4 hours to follow the rate of N-cadherin degradation (turnover). The graph below plots the half-life of N-cadherin (Y-axis degradation rate) by time in cyclohexamide (X-axis), calculated by taking the N-cadherin/a-tubulin band intensity ratio relative to the ratio at time=0, for wild-type (open square) and mutant (closed square) striatal cells, showing the short half-life of N-cadherin in mutant striatal cells (about 2 h) compared to wild-type striatal cells (longer than 4 h). Results represent three independent experiments and error bars represent standard deviation (±SD). C) Immunoblot showing bands of N-cadherin and a-tubulin in extracts of wild-type (ST7/7) and mutant (ST111/111) striatal cells transfected with 4 μg of control vector (pcDNA3.1) or 2-6 μg of N-cadherin expression vector (phN-cad), demonstrating increased N-cadherin in mutant striatal cells transfected with phN-cad.

STHdh$^{Q111/Q111}$ cells exhibited deficits in N-cadherin mediated cell-cell adhesion

The potential functional consequences of decreased N-cadherin in mutant striatal cells were then evaluated, beginning with confocal microscopy to investigate N-cadherin sub-cellular localization. The wild-type *STHdh$^{Q7/Q7}$* cells exhibited prominent N-cadherin immunostain at cell-cell contacts, whereas mutant striatal cells displayed decreased N-cadherin signal that was not prominent at cell-cell contacts (Figure 2.5 A), strongly implying a defect in calcium dependent N-cadherin mediated cell-cell adhesion [82, 83]. To assess this possibility, wild-type *STHdh$^{Q7/Q7}$* and mutant *STHdh$^{Q111/Q111}$* cells were evaluated in a cell-clustering assay, which measured the time taken for detached single cells to form clusters (Figure 2.5 B). Within 30 minutes of dispersal to single cells, 70% of the wild-type cells, but only 30% of the mutant striatal cells, formed clusters in Ca^{2+}-containing media, though cells of both genotypes exhibited similar Ca^{2+}-independent (in EGTA) cell-clustering. This phenotype was N-cadherin dependent, as exogenous expression of N-cadherin, after transfection, raised N-cadherin levels to about 50% of wild-type levels (Figure 2.4 C) and partially rescued the mutant cell deficit in Ca^{2+}-dependent cluster formation. At 30 minutes after being dispersed, about 20% more N-cadherin transfected mutant striatal cells formed clusters in Ca^{2+} media, compared to mutant cells transfected with the control vector (Figure 2.5 C). In the absence of Ca^{2+} (in EGTA), the transfection of N-cadherin had no effect on cell-cell adhesion.

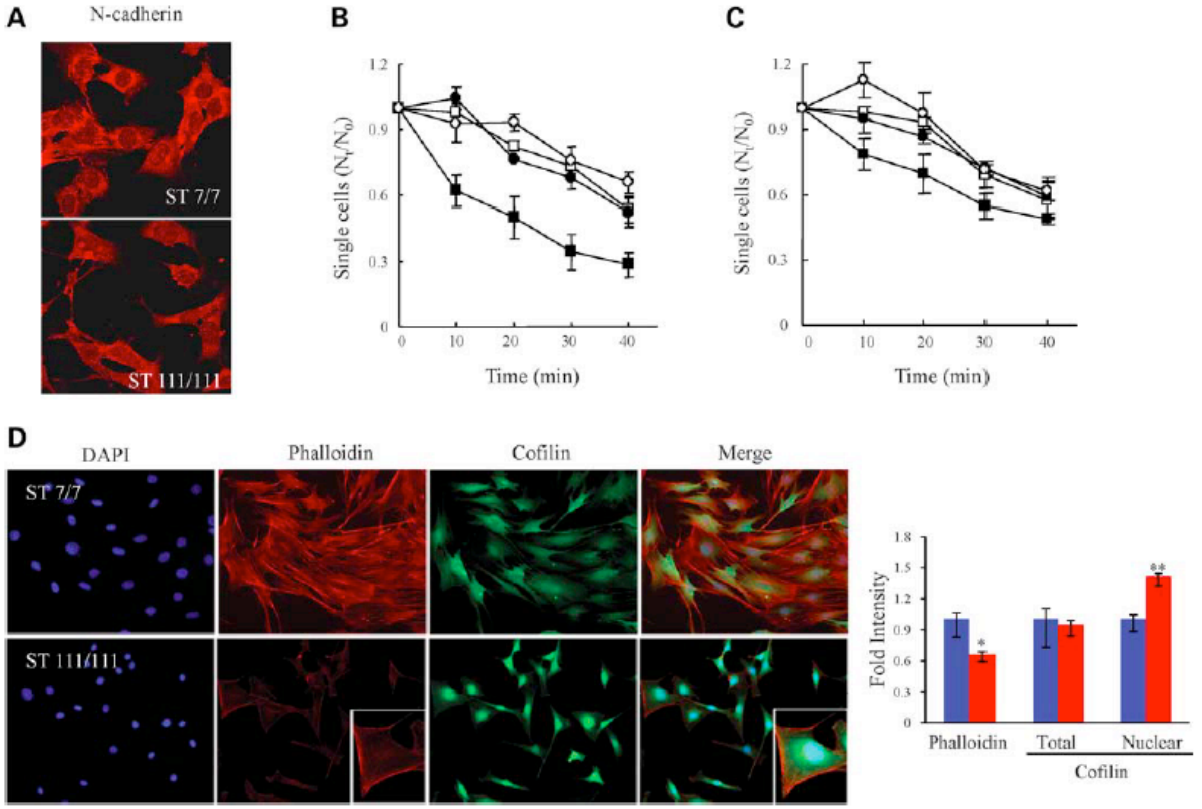

Figure 2.5. *STHdh*$^{Q111/Q111}$ striatal cells exhibited decreased N-cadherin function. A) Confocal images of the N-cadherin immunostain signal (red) in wild-type *STHdh*$^{Q7/Q7}$ (ST7/7) and *STHdh*$^{Q111/Q111}$ (ST111/111) striatal cells, indicating decreased N-cadherin signal at *STHdh*$^{Q111/Q111}$ cell–cell contacts. B) Plot summarizing the results of three independent cell-clustering assays, showing the proportion of single cells compared with time zero (N_t/N_0) (Y-axis) relative to time of clustering (X-axis) for *STHdh*$^{Q7/Q7}$ (square) and *STHdh*$^{Q111/Q111}$ (circle) striatal cells, in the absence (open symbols) and presence (closed symbols) of Ca^{2+}, illustrating that mutant striatal cells exhibit impaired calcium-dependent clustering. Error bars denote the standard deviation. C) Plot summarizing the results of three independent *STHdh*$^{Q111/Q111}$ cell-clustering assays for cells transfected with the phN-cad human N-cadherin expression vector (squares) or with the control vector (circles), performed in the absence (open symbols) and presence (closed symbols) of Ca^{2+}. Error bars denote the standard deviation. D) Fluorescence images of *STHdh*$^{Q7/Q7}$ (ST7/7) and *STHdh*$^{Q111/Q111}$ (ST111/111) striatal cells, showing the pattern of DAPI (blue) nuclei, TRITC–phalloidin (red) F-actin signal and anti-cofilin (green) immunostain, illustrating decreased nuclear size, paucity of actin stress fibers and bright perinuclear cofilin stain of the mutant cells, consistent with an elongated rounded-up (less flat) morphology. The adjacent bar graph shows the average phalloidin signal and the total or nuclear area cofilin intensities. The average intensity of the phalloidin signal was significantly reduced in mutant striatal cells (*P<0.001) and the inset was taken at different exposure conditions to examine the pattern of the phalloidin signal in mutant cells. The average intensity of the total cofilin signal was not altered but its localization was shifted to the nuclear and perinuclear region (**P<0.001). Error bars represent standard errors.

STHdh$^{Q111/Q111}$ cells exhibited deficits in cell-substratum adhesion

N-cadherin is known to regulate cell-substratum adhesion [84] and actin cytoskeleton dynamics [85, 86]. Consequently, co-stained striatal cells were monitored by confocal microscopy, to detect DAPI-stained nuclei and F-actin cytoskeleton binding proteins (Figure 2.5 D). Compared to wild-type *STHdh$^{Q7/Q7}$* cells, the mutant *STHdh$^{Q111/Q111}$* striatal cells appeared smaller with elongated shapes, and decreased stress fiber-like rhodamine-phalloidin signal, though in flattened cells the pattern of phalloidin-signal resembled that of wild-type cells (Figure 2.5 D). Consistent with the elongated (less flat) morphology, mutant striatal cells exhibited smaller DAPI-stained nuclei and the significant intense cofilin-stain of the mutant cells was localized to the nuclear and perinuclear region, although quantification demonstrated that the total cofilin signal in mutant and wild-type cells was similar (Figure 2.5 D). The mutant striatal cells also exhibited a similar nuclear/perinuclear immunostaining pattern for profilin, another F-actin-binding protein, which, like cofilin, is involved in actin filament structure and dynamics [87] (data not shown). Notably, immunoblot revealed similar levels of F-actin and the actin monomer (G-actin) in extracts of mutant and wild-type striatal cells (data not shown). Thus, rather than lacking an actin cytoskeleton, the altered subcellular patterns of actin-associated proteins, along with decreased N-cadherin, were consistent with the elongated less-flat morphology of the striatal cells expressing full-length mutant huntingtin and strongly implied deficits in cell-substrate adhesion, as well as cell-cell adhesion.

Hdh$^{Q111/Q111}$ primary striatal neuronal cells exhibited decreased N-cadherin and immature neurites

N-cadherin mediated cell-substrate adhesion promotes neurite outgrowth [84] and N-cadherin is required for proper vesicle clustering essential for neurite formation and maturation [88-91]. To evaluate the potential impact of full-length mutant huntingtin on N-cadherin function in developing striatal neurons, we examined primary neuronal cell cultures from the striatum of E14 control and *Hdh$^{Q111/Q111}$* knock-in mouse embryos. At day 10 of differentiation (div10), F-

actin rhodamine-phalloidin binding was assessed by confocal microscopy, as a surrogate for proper actin cytoskeleton/cell substratum adhesion, and cultures were immunostained to detect MAP2, a neuronal cell microtubule associated protein, to evaluate the developing neuronal cell projections. Compared to wild-type primary striatal neuronal cells, the primary *Hdh*$^{Q111/Q111}$ cells exhibited decreased rhodamine-phalloidin stain and an abnormally robust network of fine MAP2-stained projections, which confirmed neuronal cell differentiation, while implying altered adhesion and development (Figure 2.6).

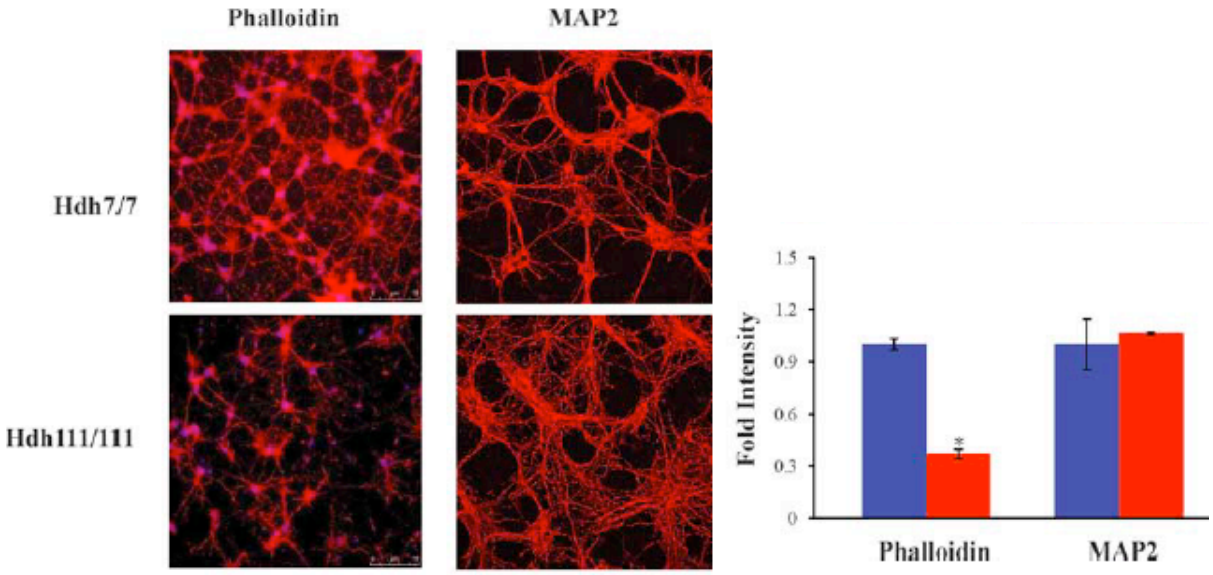

Figure 2.6. Primary *Hdh*$^{Q111/Q111}$ striatal neurons exhibit altered cytoskeletal elements. Confocal images of primary *Hdh*$^{Q7/Q7}$ (Hdh7/7) and *Hdh*$^{Q111/Q111}$ (Hdh111/111) striatal cell cultures at 10 days (div10), showing the pattern of rhodamine–phalloidin F-actin signal (left) and anti-MAP2 microtubule immunostain (right), illustrating decreased phalloidin signal and an abundance of fine MAP2-positive projections of the mutant neuronal cells, consistent with impaired adhesion and altered neuronal cell development. The bar graph below plots the fold intensity of the signal in mutant cells relative to wild-type cells (*P<0.001). Error bars represent standard errors.

Consistent with decreased N-cadherin function, co-staining revealed dramatically decreased N-cadherin signal, detected in β-III-tubulin-positive *Hdh*$^{Q111/Q111}$ striatal neuronal cells, compared to the signal intense signal of wild-type striatal cells (Figure 2.7 A), with only weak diffuse-stain along cellular the projections instead of the bright punctate pattern of wild-type cells (Figure 2.7 A inset, quantified in Figure 2.8 A and B). This observation implied that

the synaptic vesicles that transport N-cadherin were not clustered, as expected of matured neurites, but instead were distributed along the processes in the diffuse pattern characteristic of immature neurons [92].

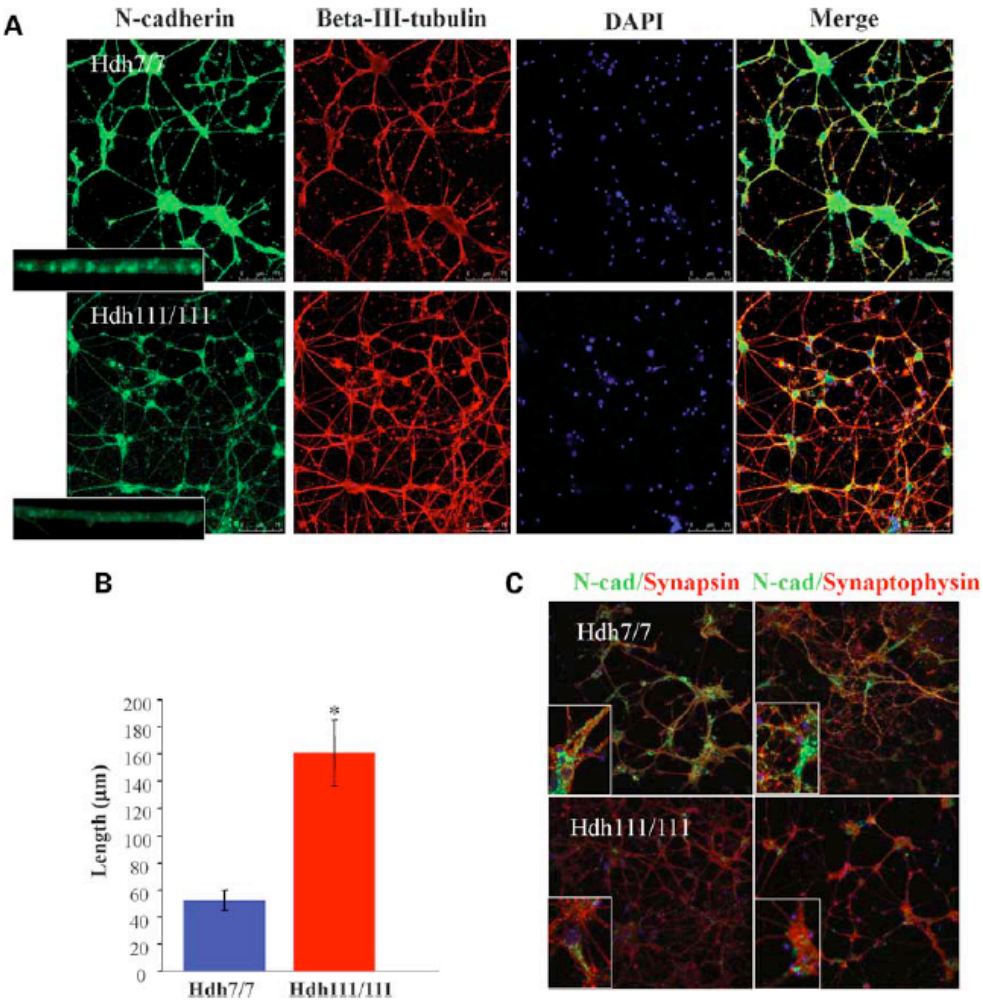

Figure 2.7. Primary *Hdh*$^{Q111/Q111}$ striatal neurons displayed decreased N-cadherin signal and abnormally extensive neurite networks. A) Confocal images of primary *Hdh*$^{Q7/Q7}$ (Hdh7/7) and *Hdh*$^{Q111/Q111}$ (Hdh111/111) striatal cell cultures, at 10 days (div10), showing the pattern of N-cadherin immunostain (green), β-III-tubulin microtubule immunostain (red) and DAPI-signal marking nuclei (blue), with an overlay of all layers (merge), showing in mutant cells decreased N-cadherin signal intensity and paucity of bright puncta (inset), concomitant with an extensive network of β-III-tubulin-positive extensions (neurites). B) Bar graph plotting the total β-III-tubulin-positive neurite length per cell, which was significantly increased in the div10 primary *Hdh*$^{Q111/Q111}$ (Hdh111/111) striatal neuronal cells compared with the wild-type *Hdh*$^{Q7/Q7}$ (Hdh7/7) cells (*P<0.005). Error bars represent standard errors. C) As a consequence of HD mutation, several markers of synaptic development showed decreased signal intensity, such as N-cadherin (green) and presynaptic markers, synapsin 1 (red in the left column) and synaptophysin (red in the right column). Along with a decrease in the markers for synaptic development in the *Hdh*$^{Q111/Q111}$ neurons, there was also a diffuse staining pattern in contrast to a punctuated pattern in the wild-type processes.

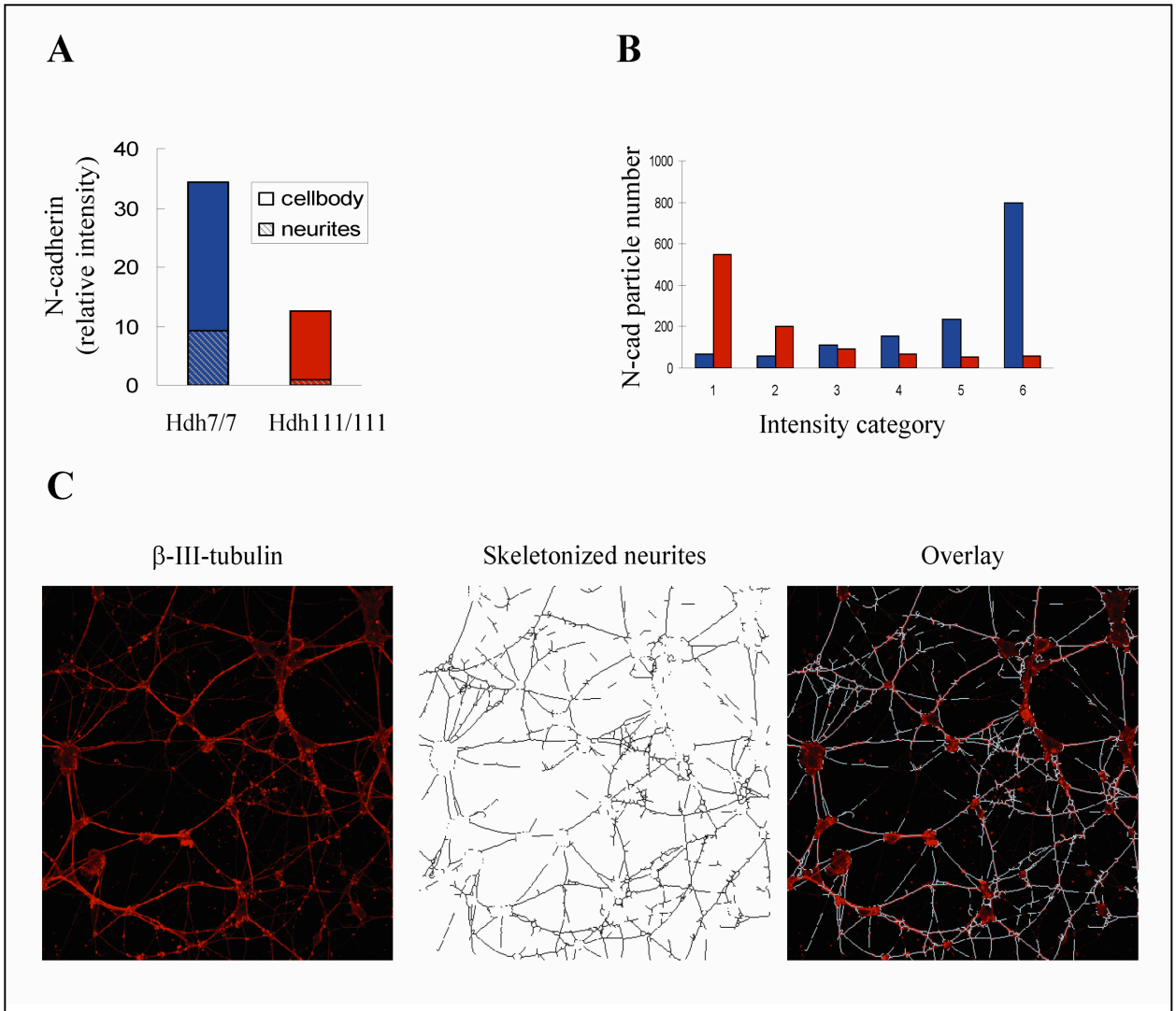

Figure 2.8. Quantification of N-cadherin localization and β-III tubulin-positive neurites. A) The bar graph shows the relative amounts of N-cadherin immunosignal compared to mutant neurites (Y-axis) for primary wild-type *Hdh*$^{Q7/Q7}$ (Hdh7/7) and *Hdh*$^{Q111/Q111}$ (Hdh111/111) neuronal cultures (X-axis), in cell bodies (solid color) or in projections, here called neurites (hatched), demonstrating significantly decreased N-cadherin signal in primary mutant striatal neuronal cells, in the cell bodies ($P<0.01$) as well as the neurites ($P<0.01$). B) The bar graph plots the number of N-cadherin-signal puncta or 'particles' (Y-axis) along neurites, as counted in 6 different signal-intensity bins (categories) (X-axis) for wild-type *Hdh*$^{Q7/Q7}$ (blue) and *Hdh*$^{Q111/Q111}$ (red) striatal neuronal primary cell cultures, illustrating that most wild-type neurite particles are of high signal-intensity, while most of the particles in mutant striatal neuronal cells are of low-signal intensity, consistent with impaired N-cadherin vesicle clustering. C) The montage of images demonstrates the procedure used to determine primary striatal cell β-tubulin-positive neurite length in a given field; the β-III-tubulin image was used to define the neurite-signal above background-signal (left). The image of the skeletonized neurites was converted into a graph where each β-III-tubulin positive neurite was assigned a width of 1 pixel, to equate thick and thin neurites (middle), and the sum of all neurites within a field was then calculated by adding total assigned neurite pixels. The overlay between the original β-III-tubulin signal and the skeletonized neurites is provided (right), to demonstrate that this approach accurately captures the neuronal cell neurites.

To explore the potential developmental deficits, the β-III tubulin positive neuronal cell processes (here called neurites) of day 10 primary neuronal cells were quantified. Automated image analysis revealed that mutant cells exhibited a three-fold increase in total length of β-III tubulin positive neurites, compared to wild-type striatal neuronal cells (Figure 2.7 B, quantification in Figure 2.8), implying delayed maturation of the neurite network. Moreover, co-staining to detect N-cadherin and markers of synaptic vesicles, synapsin and synaptophysin, confirmed this interpretation. The decreased N-cadherin signal, as well as the synapsin and synaptophysin vesicle-signals were distributed diffusely within the processes of the mutant *Hdh*$^{Q111/Q111}$ striatal neuronal cells, rather than assuming the bright punctuate matured appearance of these markers in wild-type *Hdh*$^{Q7/Q7}$ striatal cells (Figure 2.7 C). This immature pattern, which prominently featured decreased N-cadherin [92], was consistent with decreased N-cadherin function and delayed maturation of the network of developing neurites and synapses elaborated by the mutant primary neuronal cells.

Hdh$^{Q111/Q111}$ *primary striatal developmental deficit was partially rescued with adenine*

As adenine treatment of mutant *STHdh*^{Q111} immortalized striatal cells partially elevated [ATP/ADP] (Figure 2.3 C) and partially normalized N-cadherin level (Figure 2.1 D), we determined whether adenine treatment might modulate the propensity of primary div 10 E14 *Hdh*$^{Q111/Q111}$ striatal neurons to form abnormally extensive neurite networks. As shown in Figure 2.9, after treatment with adenine for 10 days the div 10 *Hdh*$^{Q111/Q111}$ striatal cultures exhibited MAP2 positive neuronal cells with fewer neurites per cell body, compared to DMSO vehicle treated cultures, though the number of cell bodies was not appreciably altered, as shown by DAPI nuclear staining. Consistent with the ameliorative effect of adenine on energy measures and N-cadherin levels, demonstrated in *STHdh*^{Q111} cells, these findings suggest that the delayed development of mutant primary neuronal cells may, at least in part, reflect decreased function of the ATP-sensitive N-cadherin adhesion molecule.

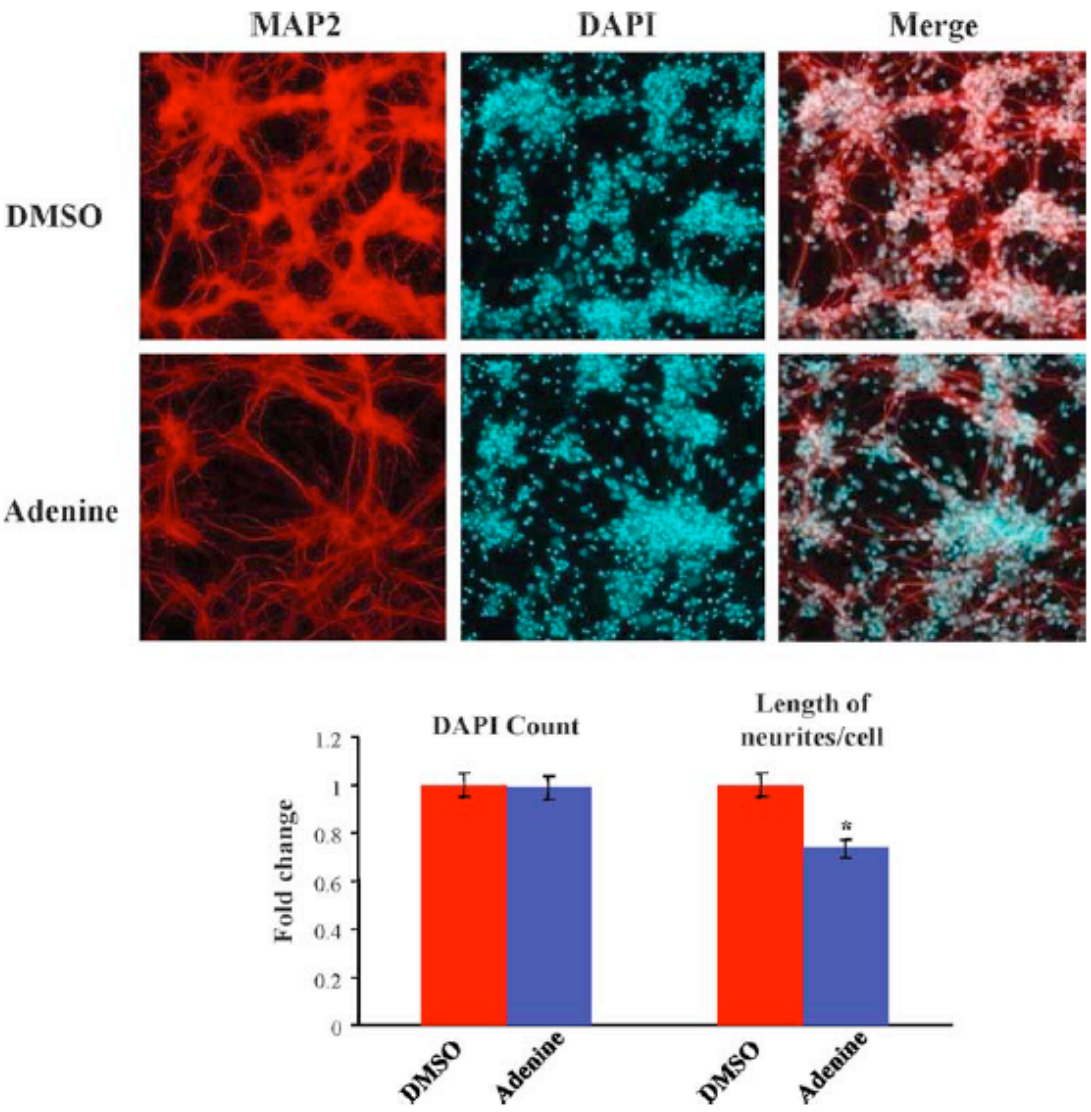

Figure 2.9. Adenine ameliorated altered *Hdh*$^{Q111/Q111}$ primary striatal neuron neuritogenesis. Confocal images of primary *Hdh*$^{Q111/Q111}$ striatal cell cultures at 10 days (div10), after culture in media supplemented with vehicle (DMSO) or with adenine (Adenine), showing MAP2-immunostained microtubules (red) and DAPI-stained nuclei (blue) and overlapped images (merge), illustrating that adenine-treated neuronal cells displayed a less branched neurite network than vehicle-treated cells. The bar graph below shows that adenine supplementation significantly decreased the total length of neurites/cell by 25% (*P<0.001), while a similar number of DAPI-stained nuclei confirmed that adenine did not result in toxicity or loss of cells. Error bars represent standard errors.

Discussion

Huntington's disease is a progressive neurodegenerative disorder, with marked loss of the major population of neurons in the striatum (medium size spiny neurons), which are

vulnerable to acute energetic challenge. The neuronal specificity of HD stems from the effects of the HD CAG repeat, encoding a polyglutamine repeat in the full-length huntingtin protein of more than about 37 residues. Multiple groups including our own have discovered that the polyglutamine repeat modulates the, as yet unknown, role of full-length huntingtin in negatively regulating measures of energy metabolism in human cells and in genetically accurate CAG knock-in mice and striatal cells [65, 66, 93]. In the current study, in order to guide *in vivo* investigations of striatal cell vulnerability, we have explored the hypothesis that chronically decreased energetics, due to endogenous full-length mutant huntingtin, may affect critical aspects of the biology of cultured striatal neuronal cells.

In a candidate approach, we have evaluated N-cadherin, an integrator of adhesion and cytoskeleton signaling required for proper neuronal cell development and synaptic function. N-cadherin was sensitive to acute ATP-depletion, in striatal tissue and cultured striatal neuronal cells, and was strikingly sensitive to the effects of full-length mutant huntingtin. N-cadherin was progressively reduced with age in Hdh^{Q111} knock-in mouse striatum and, consistent with a defect from birth, was dramatically decreased in cultured $STHdh^{Q111}$ immortalized neuronal cells, generated from embryonic Hdh^{Q111} striatal primordia [94], and in primary cultures of embryonic Hdh^{Q111} striatal neurons.

The molecular basis of decreased N-cadherin in response to full-length mutant huntingtin is not yet clear, but in Hdh^{Q111} striatal cells appears to involve regulation of *Cad2* mRNA, as well as N-cadherin protein stability. Chronic energy deficit appears to contribute to the latter, but not the former, as adenine nucleotide was able to elevate both [ATP/ADP] and N-cadherin levels and the rate of N-cadherin turnover was increased, with decreasing ATP and [ATP/ADP], while these manipulations did not affect *Cad2* mRNA levels, which instead may reflect a role for full-length huntingtin in mediating some aspect of *Cad2* gene expression or mRNA stability. Enhanced N-cadherin turnover in $STHdh^{Q111}$ striatal cells did not appear to involve metalloproteinase-1 (MMP-1, which mediates ischemia-induced turnover of cadherin

[73, 74]. MMP-1 levels were not increased in mutant STHdhQ111 striatal cells and N-cadherin turnover was unaffected by GM-6001, a specific MMP inhibitor (data not shown). Rather, elevated N-cadherin instability may entail altered GTPase regulated N-cadherin phosphorylation [8, 95], consistent with decreased *STHdh*^{Q111} striatal cell GTP and [GTP/GDP], as well as ATP and [ATP/ADP] [65]. However, there are other possibilities: altered calcium-dependent ligand or catenin binding and internalization, consistent with full-length huntingtin/syntaxin 1A regulation of N-type calcium channels [96], or abnormal N-cadherin trafficking and/or glycosylation, as implied by the findings that *STHdh*^{Q111} and primary *Hdh*^{Q111} neuronal cells demonstrated a paucity of clustered N-cadherin and synaptic marker-positive vesicles. Certainly, *Hdh*^{Q111} striatal cells display diverse membrane trafficking defects, involving endocytic vesicles [97, 98], autophagic vacuole cargo engulfment [99], and the ER/Golgi network [94], attesting to the impact of the polyglutamine repeat on full-length huntingtin function in regulating membrane trafficking [94, 98, 100].

N-cadherin mediated calcium-dependent adhesion-cytoskeletal organization and signaling is especially needed for normal neuronal cell development and functionality, for example to achieve proper neurite outgrowth, synaptic vesicle clustering in maturing neurons, and synapse formation, maturation and dynamics [84, 86, 101-103]. *Hdh*^{Q111} striatal cells exhibited impaired cell-cell, as well as cell-substrate adhesion, deficits in N-cadherin, synaptophysin and synapsin vesicle clustering, and immature neurite networks, strongly suggesting delayed developmental maturation. In part, chronic energetic deficit contributed to impaired N-cadherin function, perhaps via decreased N-cadherin half-life. Adenine, which partially normalized *STHdh*^{Q111} striatal cell ATP and N-cadherin levels, significantly rescued primary *Hdh*^{Q111} striatal cell neurite development, consistent with the hypothesis that energetic state may be a prominent factor in determining N-cadherin levels and function, in cells expressing full-length mutant huntingtin.

HD is typically assumed to be due to a disease process that begins later in life. However, our observation of decreased N-cadherin and delayed development of embryonic *Hdh*^{Q111} striatal neurons in vitro offers a possible explanation for impaired development of the striatum in E13.5-15.5 *Hdh*^{Q111} embryos [104], and for decreased measures of brain neurodevelopment in humans with expanded CAG repeats [105], which demonstrate effects of the HD CAG repeat that become manifest even before birth. Later in life, N-cadherin was progressively decreased, with age, in *Hdh*^{Q111} striatum, implying chronic synaptic dysfunction, as N-cadherin orchestrates activity-modulated CNS synapses [92]. Indeed decreased N-cadherin may contribute to impaired actin polymerization and long-term potentiation detected in HdhQ92 mice [106, 107].

Accumulated evidence now supports CAG-dependent energetic deficits in human cells and tissues, before onset of overt clinical symptoms, as well as in the brains of symptomatic individuals [67, 68, 108-110]. Therefore, it will be of interest to determine whether decreased levels of N-cadherin may contribute to the HD pathogenic process, either by contributing to subtly altered development that may sensitize striatal cells to the disease process or by representing a rate-limiting step in the disease process that is initiated by the impact of the polyglutamine-repeat on full-length huntingtin.

Materials and Methods

Mice and striatal neuronal cell cultures

Hdh$^{Q111/Q111}$ knock-in mice have been described previously [111]. Striata were dissected from genotyped homozygous mutant *Hdh*$^{Q111/Q111}$ and wild-type *Hdh*$^{Q7/Q7}$ littermates from heterozygous *Hdh*$^{Q111/Q7}$ matings, at various ages. Conditionally immortalized wild-type

STHdh$^{Q7/Q7}$ striatal cells and homozygous mutant *STHdh*$^{Q111/Q111}$ striatal cells, generated from *Hdh*$^{Q111/Q111}$ and *Hdh*$^{Q7/Q7}$ littermate embryos were described previously [94]. The striatal cells were grown at 33°C in Dulbecco's modified Eagle's medium supplemented with 10% fetal bovine serum, 1% nonessential amino acids, 2 mM L-glutamine, and 400 mg/mL

G418 (geneticin; Invitrogen). Primary neuronal cell cultures were set up from striata dissected from E14 wild-type *Hdh*$^{Q7/Q7}$ and mutant *Hdh*$^{Q111/Q111}$ embryos, from heterozygous *Hdh*$^{Q111/Q7}$ matings.

The striata were dissociated with trypsin (0.5%), trypsin inhibitor (0.1%) and DNAse [228 U/mL] treatments for 1 minute each in a 37°C warm water bath. Dissociated cells were plated onto poly-L-lysin [0.1 mg/mL] and laminin [50 µg/mL] (Sigma) double-coated coverslips in neurobasal medium (GIBCO) supplemented with 2% B27 and 1% penicillin/streptomycin/gentamycin. Cells were cultured for 10 days (DIV 10) at 37°C and 5% CO_2.

Focal ischemia

All focal ischemia experiments were conducted in accordance with National Institutes of Health, and Massachusetts General Hospital institutional guidelines on animal experimentation.

Three wild-type *Hdh*$^{Q7/Q7}$ and three *Hdh*$^{Q111/Q111}$ mice (12 months of age) mice were anesthetized with 2% halothane in 70% N2O and 30% O2, and then maintained on 1% halothane in a similar gaseous mixture. Transient focal cerebral ischemia was performed using an 8-0 nylon monofilament coated with silicone, which was introduced into the internal carotid artery via the external carotid artery and then advanced 10 mm distal to the carotid bifurcation to occlude the middle cerebral artery (MCA) as described [112]. Laser Doppler flowmetry (PF2B; Perimed Stockholm) of relative cerebral blood fluid (CBF) was used to verify successful occlusion (<20% baseline value). The MCA was occluded for 0.5 and 1 hour followed by withdrawal of filament and reperfusion for 24 hours. Relative CBF returned to >95% of baseline values, indicating almost complete reperfusion without residual occlusion. After reperfusion, right (control hemisphere) and left (infarct hemisphere) striata from each mouse brain were dissected for tissue extraction and immunoblot analysis.

MTT assay

The metabolic activity of mitochondria as indicator of cell viability was estimated by MTT assay, based on the conversion of yellow MTT tetrazolium salt to blue insoluble MTT formazan product by mitochondrial succinic dehydrogenase. After incubation under ATP depletion conditions, the cells were washed twice with PBS and MTT (0.5 mg/mL in PBS) was added to each well and incubated for two hours at 33°C. The medium was carefully removed and 200 µl of acidified isopropyl alcohol was added to solubilize the colored formazan product. Absorbance was read at 550 nm on a multi-well spectrophotometer (Molecular Devices).

Immunoblot analysis

Whole cell protein extracts were prepared from harvested striata and striatal cells by lysis on ice for 30 minutes in a buffer containing 20 mM HEPES (pH 7.6), 1 mM EDTA, 0.5% Triton X-100, protease inhibitor mixture (Roche, Indianapolis, IN), and 1 mM PMSF (phenylmethyl sulfonyl fluoride), mixing by tapping every 10 minutes. The total lysates were cleared by centrifugation at 14,000g for 30 minutes and the supernatants were collected. The protein concentration was determined by using Bio-Rad (detergent compatible) protein assay. 25 µg of protein extract was mixed with 4X SDS sample buffer, boiled for 2 minutes, and subjected to 6 or 10% SDS-PAGE. After electrophoresis, the proteins were transferred to nitrocellulose membranes (Schleicher & Schuell) and incubated for 30 minutes in blocking solution containing 5% nonfat powered milk in TBS-T (50 mM Tris-HCl, 150 mM NaCl, pH 7.4, 0.1% Tween 20). The blots were probed overnight at 4°C with primary antibodies: MAB2166 for huntingtin (Chemicon), N-cadherin (BD-bioscience), α-catenin (Chemicon), β-catenin (Sigma), p120 (Sigma), and α-tubulin (Sigma). After four washes of 10 minutes each, in TBS-T, the blots were incubated for one hour at room temperature with horseradish peroxidase-conjugated anti-mouse or anti-rabbit antisera. After a 30-minute wash, the membranes were processed using an ECL chemiluminiscence substrate kit (New England Biolabs, Beverly, MA) and exposed to autoradiographic film (Hyperfilm ECL; Amersham Bioscience). Quantification of

the immunoreactive bands was performed by scanning and analysis using the GS-800 Calibrated Densitometer and the Quantity One software (BioRad, Hercules, CA).

Immunocytochemistry

Wild-type *STHdh*$^{Q7/Q7}$ and homozygous mutant *STHdh*$^{Q111/Q111}$ cells were grown on four-chamber glass slides at a density of $2*10^5$ cells/well. The cells were fixed in 4% paraformaldehyde for 20 minutes, permeabilized for five minutes in 0.1% Triton X-100 in PBS, treated for 30 minutes in blocking buffer (2% bovine serum albumin in PBS) and incubated for two hours in blocking solution containing anti-N-cadherin. After several washes in PBS (3 X 5 min), cells were then incubated for one hour in blocking solution containing anti-mouse fluorescent secondary antibody.

Cells were imaged with a laser confocal microscope (Bio Rad, Hercules, CA) using a 60X oil objective. Primary cells were fixed with 4% formaldehyde for 10 min followed by 20 min of 100% MeOH for permeabilization. Single or double incubation of neurons with various primary antibodies was performed overnight at 4°C. The primary antibodies in this study were N-cadherin antibody (Abcam; 1:200), β-III-tubulin (Chemicon; 1:500), Cofilin (Sigma: 1:1000), Synapsin-1 (Synaptic Systems: 1:1000), Synaptophysin-1 (Synaptic Systems 1:200), and MAP2 (EnCor Biotechnology Inc: 1:10,000). For visualization, one-hour treatment with Alexa-488 and Alexa-568 secondary antibodies (both Molecular Probes, 1:500) was performed. Phalloidin-TRITC (Sigma: 1:1000) signal was visualized without secondary antibody. Coverslips were fixed onto object glasses using ProLong Gold antifade reagent containing DAPI (Invitrogen) for subsequent laser confocal microscopy (Leica).

Cell-clustering assay

Sub-confluent striatal cell cultures were incubated for 10 minutes in cold PBS and the cells were then collected with a scraper. After washing twice with PBS containing 10 mM HEPES-NaOH (pH 7.4), cells were resuspended in PBS containing 10 mM HEPES-NaOH (pH 7.4), 1 mg/mL BSA, 1 mM EGTA and maintained at 4°C. Before the start of clustering assays,

cells were carefully resuspended to ensure single cell suspensions and viability of cells (>90%) was confirmed by trypan blue exclusion. Clustering assays, which were performed at 33°C with rotation in non-tissue culture 24 well Falcon dishes to prevent cell-dish attachment, were started by addition of 50 µl cell suspension (5 Í 106 cells/mL) to 500 µl pre-warmed (33°C) PBS containing 1 mg/mL BSA, 10 mM HEPES-NaOH (pH 7.4) and either 2 mM $CaCl_2$ or 2 mM EGTA. Incubations were terminated by addition of 500 µl of 5% glutaraldehyde in PBS and particle numbers were determined on a Coulter Counter Model Z2 (Beckman Coulter, Fullerton, CA). Clustering is expressed as the fractional loss of particle number, N_t/N_0, where N_0 is the particle number at time 0 and N_t the particle number after any given time point.

RNA extraction and quantitative RT-PCR

Harvested striatal cells or dissected striata were extracted with TRIzol reagent (Invitrogen) and total RNA was extracted according to the manufacturer's instructions. Synthesis of cDNA was performed using Oligo(dT)15 primer and Reverse Transcription System (Promega) according to the manufacturer's instructions. Amplification by PCR was performed with 10 µl aliquots of cDNA in a total volume of 50 µl using iQTM SYBR Green Supermix (Bio Rad) with a Bio-Rad iCycler (Hercules, CA). Expression of *Cdh2* was specifically detected using two primers; Cdh2 forward, 5'-AGAGGCCTATCCATGCTGAG-3' and Cdh2 reverse, 5'-AGCAGCTTTAAGGCCCTCAT-3'. The thermocycling program used was 30 cycles of 95°C

for 15 seconds, 56°C for 20 seconds, 72°C for 15 seconds, preceded by incubation at 95°C for 1 minute. A primer set of β-actin, forward, 5'-GACGGCCAGGTCATCACTAT-3'; reverse, 5'-ATGCCACAGGATTCCATACC-3', was used as a positive control to ensure the integrity and quantity of RNA. PCR amplification was performed for β-actin under the following conditions: 95°C for 1 minute; 30 cycles of 95°C for 15 seconds, 54°C for 20 seconds, 72°C for 20 seconds.

ΔΔCT method was used to calculate gene expression levels from quantitative RT-RCR [113].

N-cadherin half-life

STHdh$^{Q7/Q7}$ and *STHdh*$^{Q111/Q111}$ cells plated on 6-well dishes were incubated in growth medium containing cyclohexamide at a final concentration of 30 µg/mL for 0, 1, 2, and 4 hours. At each time point the cells were washed once with ice-cold phosphate-buffered saline and lysed by incubation for 30 minutes in a buffer containing 20 mM HEPES (pH 7.6), 1 mM EDTA, 0.5% Triton X-100, protease inhibitor mixture (Roche, Indianapolis, IN), and 1 mM PMSF, followed by tapping every 10 minutes. The total lysates were then cleared by centrifugation at 14,000g for 30 minutes and the supernatants were collected. The protein concentration was determined using the Bio-Rad (detergent compatible) protein assay and equal amounts of protein from each lysate were resolved by 10% SDS PAGE. The proteins were transferred to nitrocellulose membranes, blocked in 5% nonfat milk TBS-T, and incubated overnight at 4°C with a monoclonal anti N-cadherin antibody. The immunoblot was then probed with horseradish peroxidase-conjugated secondary antibody and visualized by ECL reagents.

ATP depletion

STHdh$^{Q7/Q7}$ and *STHdh*$^{Q111/Q111}$ cells plated on 6-well dishes were washed twice with phosphate-buffered saline (PBS) and then were incubated at 33°C in either normal growth medium (control cells) or glucose-free DMEM containing 10 mM 2-deoxyglucose and 10 µM antimycin A to yield ATP-depleted cells. After incubation for 0.5, 1, 2 hours, cells were collected with a scraper and extracts were generated for immunoblot analysis.

After ATP-depletion, cells were washed three times with PBS and viability was assessed by the MTS assay kit (Promega, Madison, WI). MTS (3-(4,5-dimethylthiazol-2-yl)-5-(3-carboxymethoxyphenyl)-2-(4-sulfophenyl)-2H-tetrazolium, inner salt) solution was added to each well, followed by incubation at 33°C for 2 hours. Absorbance was measured at 490 nm on a multi-well spectrophotometer (Molecular Devices). For measuring altered ATP nucleotide in cells after ATP depletion, HPLC analysis was performed as described previously [67].

Image analysis of primary cultures

Quantification of immunostain was performed using ImageJ, image analysis software available through the NIH website (http://rsb.info.nih.gov/ij/). To determine the area for cells (cell bodies and neurites separately) the number of β-III-positive pixels were counted within a field of view. For cell bodies, β-III-tubulin staining defined the edges of the cell body, so that the total area of the cell body could be determined. Four different fields per genotype were analyzed. For quantification of N-cadherin, intensity histograms of N-cadherin in β-III-tubulin defined neurites and cell bodies were measured. To obtain the amounts of N-cadherin-signal for a specific genotype and the respective cell part, the products of each intensity over a threshold value multiplied by the percentage of the area covered by that intensity were added up:

$$\sum_{i = \text{minimum intensity}}^{i = \text{maximum intensity}} \text{intensity}_i * \text{pixel}_i/\text{total pixel number}$$

To compare the four different amounts to one another (wild-type cell body, wild-type neurites, mutant cell body, mutant cell neurites), the signal-amount in mutant neurites was defined as one, and the other three signal amounts were expressed in ratio to this. The number of N-cadherin signal particles was determined by using the Analyze particle plug-in of ImageJ. 30 images of neurites per genotype were analyzed. Images were thresholded 6 times for different signal intensity intervals (intensity 30-90, 40-90, 50-90 etc. till 80-90) For each thresholded image, the number of particles was calculated (i.e. $I_{30\text{-}90}$, $I_{40\text{-}90}$, $I_{50\text{-}90}$, … $I_{80\text{-}90}$). To obtain the number of particles with a specific highest intensity (40, 50, … 90), the number of particles within one intensity interval was subtracted from the one of the next lower interval (i.e. $N_{30\text{-}40} = I_{30\text{-}90} - I_{40\text{-}90}$). The number of particles was also normalized to the length of neurites. In order to determine the total neurite length, in four fields of view per genotype of β-III-tubulin images, the cell bodies were removed. The resulting images were skeletonized and the length

of the skeleton was measured and subsequently divided by the number of DAPI-positive nuclei in the appropriate field.

Statistical analysis

All cell images were quantified in 10 randomly chosen groups comprising at least 100 cells and other experiments, such as immunoblot and ATP/ADP measurement, in three independent experiments. The mean, standard deviation (SD) and standard error (SE) were calculated and statistical significance analyzed using an unpaired two-sample t-test.

Chapter 3:

Characterization of murine embryonic stem cell model of Huntington's disease[4]

Attribution

Colleagues in the MacDonald lab created the ES cell genetic models of huntingtin deficiency and the HD genetic mutation [39]. When I undertook my graduate work, these cell systems had fallen out of use. I revived and re-optimized the growth conditions for these cells to return them to optimal morphology and pluripotency. I began a preliminary characterization of the cytoskeletal structure in the ES models and found initial evidence of a defect in cellular adhesion. We quickly decided that neuronal differentiation would be essential to in-depth analyses of the cytoskeleton and cell adhesion. Colleagues in the lab began pursuing optimization of neuronal differentiation protocols and have, to date, succeeded in deriving neuronal progenitor and mature neuronal populations.

I contributed cellular resources and data to a publication (Appendix B) on gene expression profiling of the knock-out and knock-in ES cell models (Figure 3.1) [39]. I also supported the training of new lab members in murine ES culturing. In collaboration with my colleague, Dr. Marta Biagoli, I contributed cell resources to a characterization of the ES model – including pluripotency markers and epigenetic state – under different growth conditions. Dr. Biagoli is chiefly responsible for optimizing the neuronal differentiation protocols which can now be employed to conduct a more thorough characterization of cytoskeletal phenotypes and validate huntingtin conserved function(s) identified in the *D. discoideum* model. Dr. Randy Singh has collaborated with me to investigate cell adhesion phenotypes in the ES cells based upon results from the murine striatal cell and *D. discoideum* models. His work has yielded a

[4] This chapter contains data that contributed to the following publication and is reprinted here with permission: Jacobsen, J.C., et al., *HD CAG-correlated gene expression changes support a simple dominant gain of function.* Hum Mol Genet, 2011. **20**(14): p. 2846-60.

cell-substrate adhesion assay in the ES cell system that has been optimized for screening with small molecules and RNAi.

Abstract

We sought a model cellular system in which effects of huntingtin deficiency, as well as the CAG repeat expansion, could be studied to elucidate huntingtin function in the cytoskeleton and cell adhesion and its relation to HD. Growth conditions have been optimized for maintenance of pluripotent potential and stem cell state on gelatin and mouse embryonic fibroblast feeder cells. Preliminary results, suggested that there might be a cell adhesion defect related to CAG repeat expansion in ES cells.

Results and discussion

An allelic series of heterozygous knock-in (KI) ES cells with varying polyQ lengths, as well as a knock-out (dKO) ES cell line have been generated in our lab [14, 38, 39, 114, 115]. I undertook an optimization of growth conditions for the murine ES cells WT ($Hdh^{Q7/7}$), dKO ($Hdh^{ex4/5/ex4/4}$), KI ($Hdh^{Q20/7}$, $Hdh^{Q50/7}$, $Hdh^{Q91/7}$, $Hdh^{Q111/7}$) (Figure 3.1).

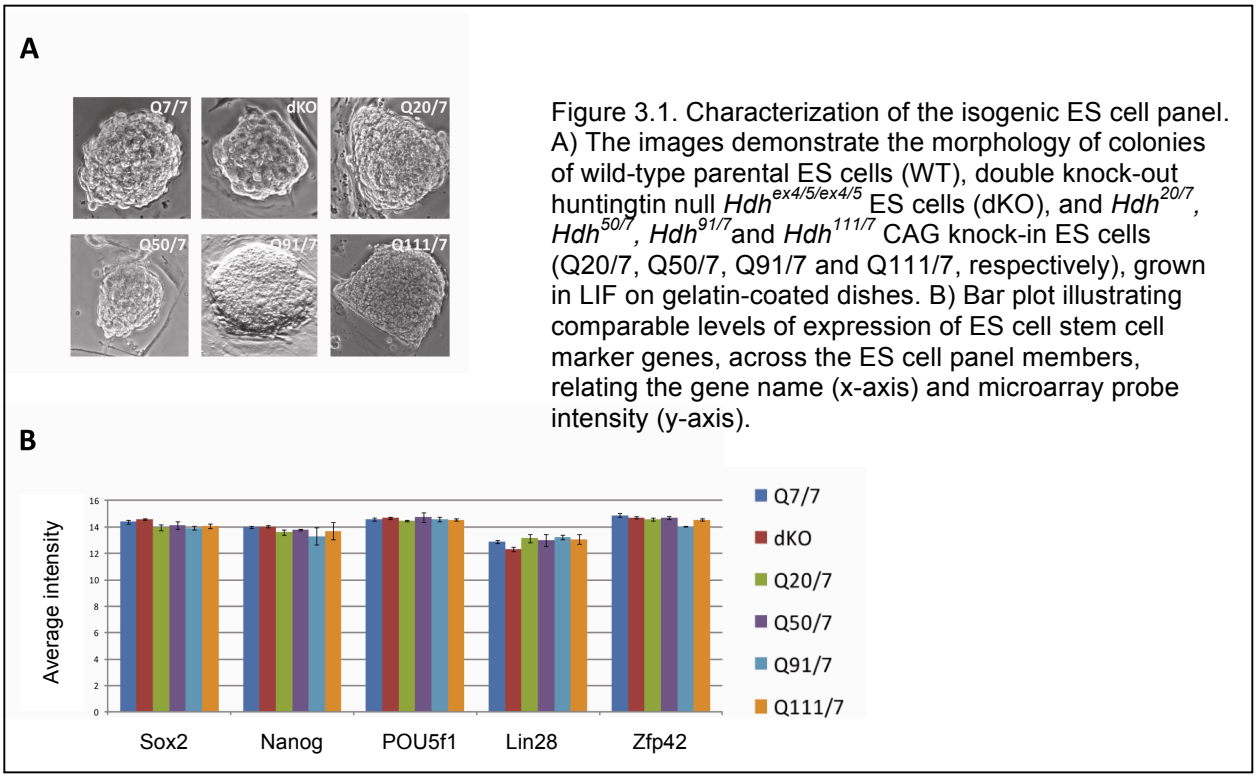

Figure 3.1. Characterization of the isogenic ES cell panel. A) The images demonstrate the morphology of colonies of wild-type parental ES cells (WT), double knock-out huntingtin null $Hdh^{ex4/5/ex4/5}$ ES cells (dKO), and $Hdh^{20/7}$, $Hdh^{50/7}$, $Hdh^{91/7}$and $Hdh^{111/7}$ CAG knock-in ES cells (Q20/7, Q50/7, Q91/7 and Q111/7, respectively), grown in LIF on gelatin-coated dishes. B) Bar plot illustrating comparable levels of expression of ES cell stem cell marker genes, across the ES cell panel members, relating the gene name (x-axis) and microarray probe intensity (y-axis).

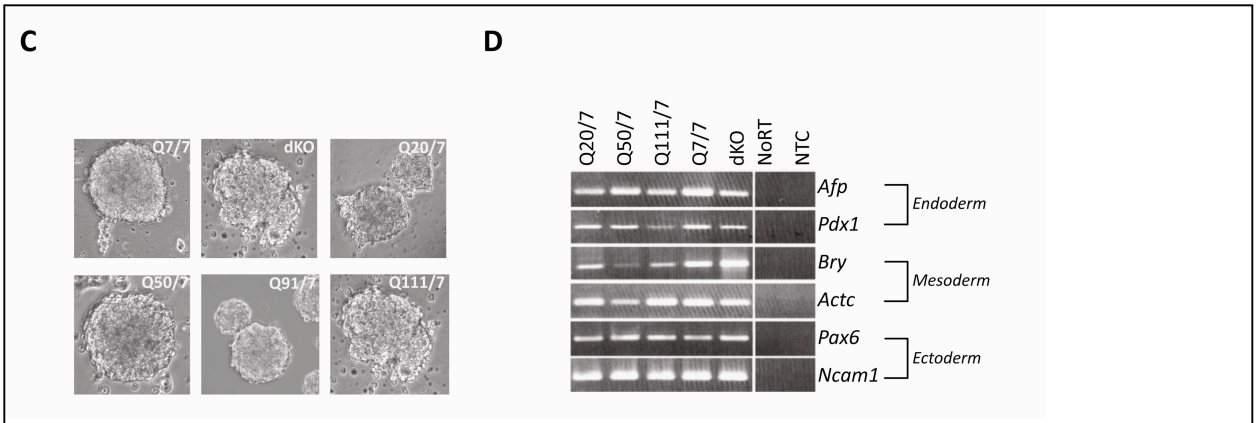

Figure 3.1 (continued). Characterization of the isogenic ES cell panel. C) The images demonstrate the morphology of day 4 embryoid bodies, following withdrawal of LIF, for wild-type parental ES cells (Q7/7), double knock-out huntingtin null $Hdh^{ex4/5/ex4/5}$ ES cells (dKO), and $Hdh^{20/7}$, $Hdh^{50/7}$, $Hdh^{91/7}$ and $Hdh^{111/7}$ CAG knock-in ES cells (Q20/7, Q50/7, Q91/7 and Q111/7, respectively). D) Composite images of bands of RT-PCR amplification products, summarizing the results of analysis of day 4 embryoid bodies, from members of the ES cell panel, for the expression of endoderm, mesoderm and ectoderm marker genes, demonstrating differentiation into the three primary germ layers. Endoderm markers: *Afp* = alpha-fetoprotein, *Pdx1* = pancreatic and duodenal homeobox 1; Mesoderm markers: *Actc* = alpha cardiac actinin, *Bry* = Brachyury and Ectoderm markers: *Ncam1* = neural cell adhesion molecule, *Pax6* = paired box gene 6. The results for $Hdh^{91/7}$ EBs are not shown but confirm formation of primary germ layers. Figure reprinted with permission from [39].

Microarray profiling followed by pathway analysis, revealed that the comparison of genome-wide expression changes across the polyQ series and the comparison of deficiency versus WT produces two different gene sets with minimal overlap [39]. However, upon pathway analysis, there were 13 shared pathways, indicating that the effects of huntingtin deficiency are distinct from, but related to, the effects of polyQ expansion. The cytoskeleton and adhesion as well as pathways related to cytoskeletal function – including lipid metabolism, energy metabolism, reproduction/development/growth, signal transduction, nucleotide metabolism, and amino acid/peptide/protein metabolism – were amongst the top pathways to emerge from the analysis.

I conducted a preliminary investigation of cytoskeletal structure in the undifferentiated ES cells. Possible changes in the cell/colony morphology exist between the genotypes WT, $Hdh^{ex4/5/ex4/5}$, and $Hdh^{Q111/7}$ ES cells on gelatin substrate (Figure 3.2). Most notably, immunofluorescence data as well as observations while culturing the cells and differentiating

them to embryoid bodies suggest that CAG repeat expansion has an effect on cell adhesion, with *Hdh*$^{Q111/7}$ cells failing to form tight colonies on gelatin.

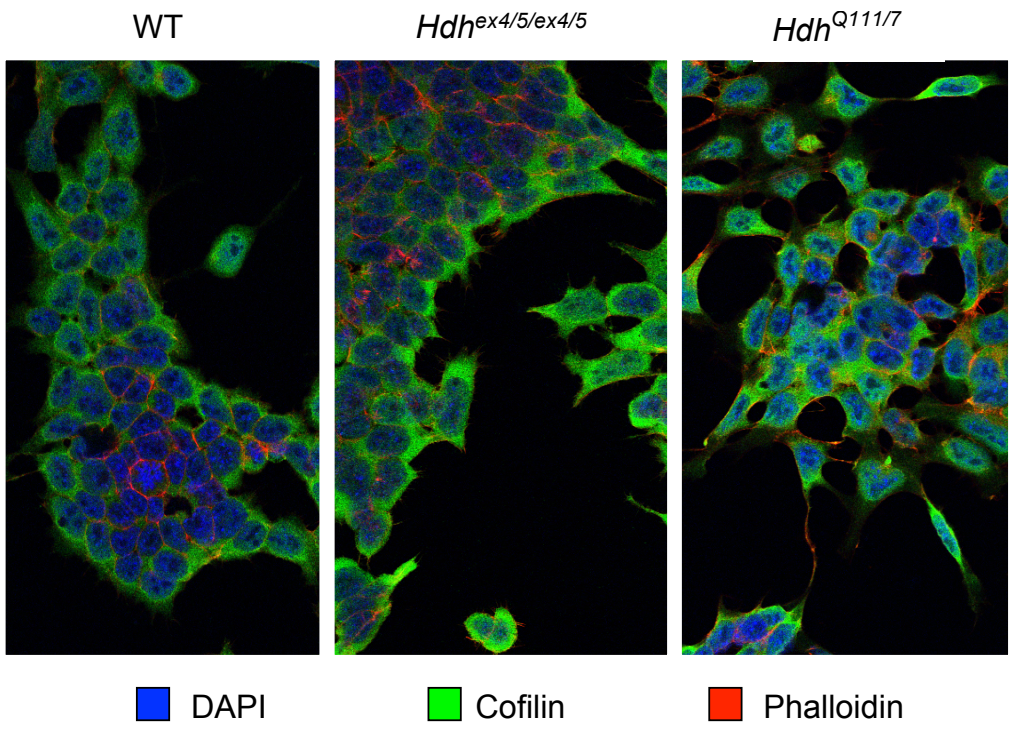

Figure 3.2. Comparison of staining for F-actin (phalloidin, red), cofilin (green), and nucleus (DAPI, blue) in WT, *Hdh*$^{Q7/7}$.and *Hdh*$^{Q111/111}$ mouse ES cells. Cells were cultured on gelatin for at least three passages and then replated on laminin-coated glass coverslips and allowed to settle overnight. The next day cells were fixed with 4% formaldehyde and permeabilized with 1% Triton-100, followed by co-immunostaining with cofilin and phalloidin antibodies. Coverslips were mounted with Prolong Gold reagent containing DAPI. Images are representative of three experiments. 20X magnification.

The localization of cytoskeletal markers is hard to assess given the relative lack of cytoskeletal architecture in undifferentiated ES cells. Therefore, I repeated the experiment with retinoic acid (RA) differentiated ES cells and assessed the following markers: phalloidin, cofilin, N-cadherin, Ezh2, cortactin (data not shown). RA differentiation had a high degree of cell toxicity resulting in variable cell density and morphology, which may be related to different adhesion properties of the cells with different huntingtin genotypes. Therefore, the localizations of cytoskeletal markers were variable and it was difficult to determine trends. A neuronal differentiation protocol has now been optimized in the lab that will allow investigation of cytoskeletal structure and cell adhesion to be carried out in neuronal progenitors and terminally

differentiated neurons derived from the knock-out and knock-in ES cells. Moreover, encouraged by observations of apparently different adhesion properties of the knock-in neurons differentiated from the ES cells, as well as the *STHdh*^{Q111} striatal cells (Chapter 2), my colleague Dr. Randy Singh has now generated cell adhesion assays that distinguish human neuronal progenitor cell lines (from iPS cell lines) with different CAG repeat alleles [48]. Meanwhile, I became interested in gaining greater insight into evolutionarily conserved cytoskeletal and adhesion functions of huntingtin in the hopes that ancient roles of the protein will be crucial to its normal function, help to guide studies of the functional consequences of the CAG repeat expansion of the protein in HD, and more quickly yield mechanistic insights which can be validated in the optimized mammalian cell systems.

Methods:

Modified from: Embryonic Stem Cells: Methods and Procotols. Ed. Turksen, K. Methods in Mol. Bio. v.185. Humana Press, 2002.

Preparation of media

1. Store media at 4°C until used and discard after 14 days.
2. Combine reagents and filter through 0.2 μm filter units.
3. ES cells are sensitive to pH change. When a bottle is half full, filter remaining medium into a smaller bottle to minimize air space in the bottle that causes the pH to rise as air gases and medium reach equilibrium.
4. Mouse ES cell medium
    a. Ingredients
        i. KO-DMEM (Invitrogen Cat no. 10829-018, 500 mL)
        ii. 15% ES-qualified FBS (Hyclone)

iii. 0.2 mM GlutaMax (Invitrogen)

iv. 0.1 mM MEM nonessential amino acids (NEAA, 100X; Sigma)

v. 0.1 mM 2-mercaptoethanol (BME; Sigma)

vi. 1000 units/mL leukemia inhibitory factor (LIF; Millipore)

vii. 50 U/mL penicillin/50 µg/mL streptomycin (100X; Cellgro)

5. Mouse embryonic fibroblast (MEF) medium (same as above without LIF)

Preparation of gelatin-coated plates

1. Store and use gelatin solution (ES-qualified, Millipore) at room temperature.

2. Transfer enough 0.1% gelatin solution to cover the bottom of the dish or well.

Dish size	Volume gelatin (mL)
4-well	0.5
24-well	0.5
12-well	1.0
6-well	2.0
6 cm (60 mm)	3.0
10 cm (100 mm)	6.0

3. Incubate at room temperature for 30 minutes under the tissue culture hood.

4. Remove excess gelatin solution and use dishes immediately. Do not allow the gelatin to air dry.

Preparation of feeder layers

1. To prepare a fresh 10 cm MEF feeder plate:
    a. Quickly thaw MEF cells. Transfer to 9 mL MEF media in a 15 mL tube and spin to wash. Discard supernatant. Resuspend in fresh MEF media and plate. Allow cells to settle overnight before use.
    b. Discard feeder cells after 7-10 days.
    c. Prior to plating ES cells on MEFs, aspirate media and wash once with fresh ESC media.

Maintenance of ES cells

1. Thawing
    a. Remove a vial of cells from the liquid nitrogen freezer and thaw in a 37°C water bath. Agitate the vial until the frozen suspension becomes slurry.
    b. Sterilize the vial with 70% ethanol and transfer to the tissue culture hood.
    c. Transfer contents of the vial to a prepared feeder plate containing fresh ES cell medium. Vials should have enough cells to evenly plate a 10 cm dish with colonies (~ 4-6*10^6 cells).
    d. Gently swirl the plate to distribute cells over the entire surface.
    e. Label the plate with date, cell line, and passage number before returning to incubator.
2. Daily feeding
    a. Examine the condition of cells and colony formation daily and record observations.
    b. Remove media by aspirating slowly and replace with fresh ES cell media gently by adding media to side of plate at least every other day or daily.

c. Media volume given dish type

Dish size	Media volume (mL)	Cell count
4-well	0.5	Embryos
24-well	1.0	$2.0 *10^4$
12-well	2.0	$3.0 *10^5$
6-well	5.0	$4.0 *10^5$
3.5 cm (35 mm)	3.0	$4.0 *10^5$
6 cm (60 mm)	5.0	$6.0 *10^5$
10 cm (100 mm)	15.0	$2.0 *10^6$
4-chamber slide	1.0	$1.4 *10^5$
8-chamber slide	0.5	$6.0 *10^4$

3. Subculturing

a. Examine colony morphology, density, and size to estimate the ratio at which you wish to split cells and prepare the number of feeder plates needed.

i. Decide the ratio to split cultures based on size and distribution of ES cell colonies. Growth rate of different cell lines often differs and should be determined for each strain.

ii. Even distribution of colonies averaging in size from 200-400 μm diameter and spaced 400 μm apart in a 10 cm plate will have ~ $1\text{-}1.5*10^7$ total cells

iii. Typically split cultures at ratios from 1:6 – 1:8 resulting in ~ $1.5\text{-}2.0*10^6$ cells to be plated to each new 10 cm plate. Avoid overcrowding and undercrowding.

b. Remove media and wash with 10 mL PBS.

c. Remove PBS and add trypsin

   i. Amount trypsin given dish size

Dish size	Volume gelatin (mL)
24-well	4 drops/well
12-well	0.5
6-well	0.5
6 cm (60 mm)	1.5
10 cm (100 mm)	2.0

d. Incubate 1-2 minutes, monitoring the detachment of cells every 30 seconds by gently tapping it against your palm.

e. Once cells are no longer attached, add 8 mL (for 10 cm plate) ES cell media to the trypsin cell suspension. Transfer to 15 mL tube and pipette up and down vigorously to dissociate cells.

f. Plate approximately $2*10^6$ cells in each prepared 10 cm plate. You can cryopreserve remaining cells as described below.

4. Freezing (10 cm plate = 4-5 vials with ~ $3\text{-}6*10^6$ cells/vial)

   a. Freezing medium

      i. 90% ES cell media

      ii. 10% DMSO

   b. Transfer the cell suspension to a 15 mL tube and pellet cells by low speed centrifugation at 100 g for 5 minutes.

c. Remove supernatant without disturbing the cell pellet.

d. Add 1 mL freezing medium for each frozen vial depending on cell number. Pipette up and down to dissociated ES cells and transfer 1 mL of cell suspension into each cryotube.

e. Put cryotubes in a Nalgene controlled-rate freezer box and then put the box in the -80°C freezer overnight.

f. Transfer the vials of frozen ES cells into liquid nitrogen for long-term storage.

Subcloning and expanding ES cell colonies

1. Prepare 24-well plates with a MEF feeder layer as described above at least one day in advance.
2. To pick colonies:
    a. Remove media from each well of 24-well plate and replace with fresh ES cell media.
    b. Select and mark colonies under microscope. Pick colonies that are ~300 μm in diameter using a sterile pipette tip.
    c. Transfer colony to a well of a 24-well dish and pipette repeatedly to disrupt cells. Draw media from the well up and down in the pipette to transfer all ES cells into the well.
    d. Distribute a single colony per well.
3. To expand picked colonies:
    a. In the days after you pick colonies, examine each well for the presence of ES cells. Record average size and morphology of surviving colonies.
    b. When colonies are ~300 μm in diameter dissociate them. If colonies are smaller, gently change the media and leave the cells alone until the next day.

i. Remove old media from wells and wash with 0.5 mL PBS.

ii. Add 4 drops trypsin/well and incubate 1-2 minutes.

iii. After incubation, vigorously tap dish against palm of hand to dislodge cells

iv. Once cells are completely dissociated, add 2 mL ES cell media to each well.

v. The next day, examine each well and record observations of colony morphology and number. Change media in wells with 1.5 mL fresh ES cell media.

vi. To maintain ES cells undifferentiated they must be dissociated usually every other day and the media changed daily or every other day.

vii. Dissociation and/or media changes may need to be done several times in a 24-well dish before there are enough ES cells to split 1:2 (half for freezing, half for replating and other uses).

viii. Not all clones grow at the same rate. Each should be handled as a different cell line.

ix. When there are enough colonies (200-400 μm in diameter) to cover dishes/wells while still being spaced approximately 200-400 μm apart, they are ready to split.

c. To split:

i. Prepare 12-well dishes with MEF feeder layers as described above.

ii. Examine each well and mark colonies that will be dissociated and left in the 24-well dish and colonies that are ready to split 1:2. Record clone numbers.

iii. Remove media from each well and wash with PBS

iv. Add 4 drops trypsin per well and incubate 1-2 min at 37°C

v. Vigorously tap dish to dissociate all cells

vi. For wells that are just being dissociated: add 2 mL media to each well

vii. For each well to be split 1:2: aspirate 3 mL of media into a 5 mL pipette. Transfer 1 mL of this media into 1 well of a trypsinized 24-well dish and transfer to a 12-well dish. Pipette up and down several times to ensure all cells are completely dissociated. Transfer 1.5 mL cell suspension into appropriate pre-labeled cryotube. Leaving remaining cell suspension in the 12-well dish to continue growing.

viii. Pellet cells in cryotubes at 100 g for 5 min. Pour off supernatant and add 0.5 mL freezing medium to each vial. Vigorously shake all the vials and place in a controlled-rate freezer at -80°C.

ix. When all clones are transferred into the 12-well dish, fill each well with ES cell media to a total of 3 mL.

x. The next day, transfer vials to a liquid nitrogen freezer for long-term storage.

Important notes:

1. Use aseptic technique at all times. Never re-enter a bottle with the same pipette
2. Use ES-qualified products
3. ES lines from different strains react differently to serum in the media. When working with cell lines from different strains use ALL strains in tests of different serum lots. This is even necessary for ES-qualified serum.
4. ES cells grow more slowly following freeze-thaw and need time to recover. It is not unusual to dissociate cells within the same dish or split 1:2.

Chapter 4:

Calcium partially restores EDTA-resistant homotypic cell adhesion in huntingtin deficient *Dictyostelium discoideum*[5]

Morgan N. Thompson, James F. Gusella, Marcy E. MacDonald, Michael A. Myre

Attribution

I performed the entire body of research on the *D. discoideum* EDTA-resistant cell adhesion defect in huntingtin deficient cells that is presented in this chapter and a manuscript regarding this work is in preparation for publication. The adhesion defect that I identified was first reported in the original publication characterizing the *D. discoideum* model of huntingtin deficiency, which is also addressed in the introduction to this chapter and included as Appendix C [45].

Abstract

Huntington's disease (HD) results from a single causative mutation in the *HTT* gene consisting of an expanded version of a polymorphic polyglutamine tract in the huntingtin protein. As the earliest known organism to possess a huntingtin ortholog, *D. discoideum* is a powerful system to study conserved, normal function of huntingtin. We have previously demonstrated that huntingtin null (*hd*-) *D. discoideum* cells wholly fail to acquire EDTA-resistant cell adhesion in shaking starvation culture. Contact site A (csA) is the molecular player considered to be primarily responsible for EDTA-resistant adhesion in *D. discoideum*. Protein, but not mRNA, levels of csA are dramatically reduced in *hd*- cells, yet introduction of csA via an overexpression construct fails to rescue the adhesion defect. Interestingly, exogenous calcium supplementation is capable of partially restoring EDTA-resistant adhesion in *hd*- cells in the

[5] This chapter includes data from a manuscript in preparation as well as already published data which is included here and in Appendix C with permission from: Myre, M.A., et al., *Deficiency of huntingtin has pleiotropic effects in the social amoeba Dictyostelium discoideum.* PLoS Genet. **7**(4): p. e1002052.

appropriate developmental timeframe and results in normal levels of csA. No defects were found in localization or glycosylation of the protein, suggesting that csA protein synthesis or turnover is defective in *hd-* cells. Yet, upon addition of calcium, we demonstrate that *hd-* cells possess all of the necessary machinery to produce csA at normal levels and developmental timing. These results spurred an examination of the effects of calcium on EDTA-resistant adhesion in *csA-* cells. Exogenous calcium is able to partially rescue EDTA-resistant adhesion in the absence of csA. Together our data suggest that calcium alone is capable of partially ameliorating the requirement for csA. Therefore, a novel compensatory pathway that supports EDTA-resistant adhesion in the early adhesion phase of *D. discoideum* development must exist independent of csA and huntingtin.

Introduction

Huntingtin is a large, multifunctional protein first identified because of the severe neurodegenerative human genetic disorder Huntington's disease, which results from an CAG triplet repeat expansion in the *HTT* gene [5]. Despite two decades of research, the normal function(s) of the huntingtin protein remain(s) unknown. Huntingtin is expressed ubiquitously, associates with a variety of cellular organelles, interacts with more than 50 proteins, and has been implicated in a many essential cellular processes, including transcription, vesicular transport, cell adhesion, apoptosis, metabolism, autophagy, and microRNA regulation [6]. In mammalian models, polyglutamine expansion of huntingtin alters cellular function long before disease symptoms present, suggesting that the mutation may act to initiate the disease process via some opportunity afforded by the normal function of the full-length huntingtin protein [116]. The difficulty in identifying the normal function of huntingtin in mammalian models encourages the use of lower organism models, including recently developed *D. discoideum* huntingtin deficient cells [45, 46].

Huntingtin appears to have arisen coincidently with multicellularity in evolution. As the most ancient organism known to possess a huntingtin ortholog, *D. discoideum* offers an

exceptional model for investigations of evolutionarily conserved huntingtin function. While the expansion of the polyglutamine tract first appears in deuterostomes [17, 47], the overall structure of huntingtin remains predominately alpha-helical across species [45], lending plausibility to the hypothesis that functional conservation will exist. Although the exact molecular players may differ, investigation of evolutionarily conserved huntingtin function may provide critical insights into essential roles for this protein that can be studied in parallel with mammalian experimental systems.

We previously characterized that loss of huntingtin in *D. discoideum* results in pleiotropic defects in multiple cellular processes throughout different phases of the organisms' lifecycle [45]. Interestingly, *D. discoideum hd-* cells revealed cytoskeletal and cell adhesion defects reminiscent of phenotypes uncovered in mammalian cells that possess the precise genetic mutation observed in HD patients [45, 47, 60]. Cellular morphology appears normal in nutrient medium, but exposure to starvation conditions immediately causes cell rounding in huntingtin deficient cells (Figure 4.1 B, [45]). Phalloidin staining was examined as a direct result of parallel lines of experimentation in immortalized striatal cells – detailed in Chapter 2 – and revealed aberrant localization of F-actin in cells lacking huntingtin under starvation conditions (Figure 4.1 D). Also suggestive of an actin cytoskeletal phenotype is the altered spore shape in the absence of huntingtin (Figure 4.2 A), which is reminiscent of *D. discoideum* actin cytoskeletal mutants [117].

In addition to the cytoskeletal abnormalities, *hd-* cells display defective cell adhesion as revealed by a number of developmental assays. Upon starvation, *D. discoideum* cells enter a complex developmental program, involving polarized motility, multicellularity, and differentiation that culminates in the formation of a fruiting body [59]. The developmental cycle is governed by cyclic AMP (cAMP) pulsing that in turn activates a host of other factors, including cell adhesion proteins [118]. On starvation agar, WT cells migrate in streams to form mounds by six hours (Figure 4.3 A). However, *hd-* cells fail to stream and instead form mounds by accretion (Figure

4.3 B). Furthermore, *hd-* cells submerged under starvation buffer entirely fail to stream. High cell density allowed the *hd-* cells to form mounds with irregular shape, but did not rescue the streaming defect (Figure 4.3 E and F). However, exogenous supplementation with 1mM $CaCl_2$ is capable of restoring normal development in *hd-* cells (Figure 4.3 G and H).

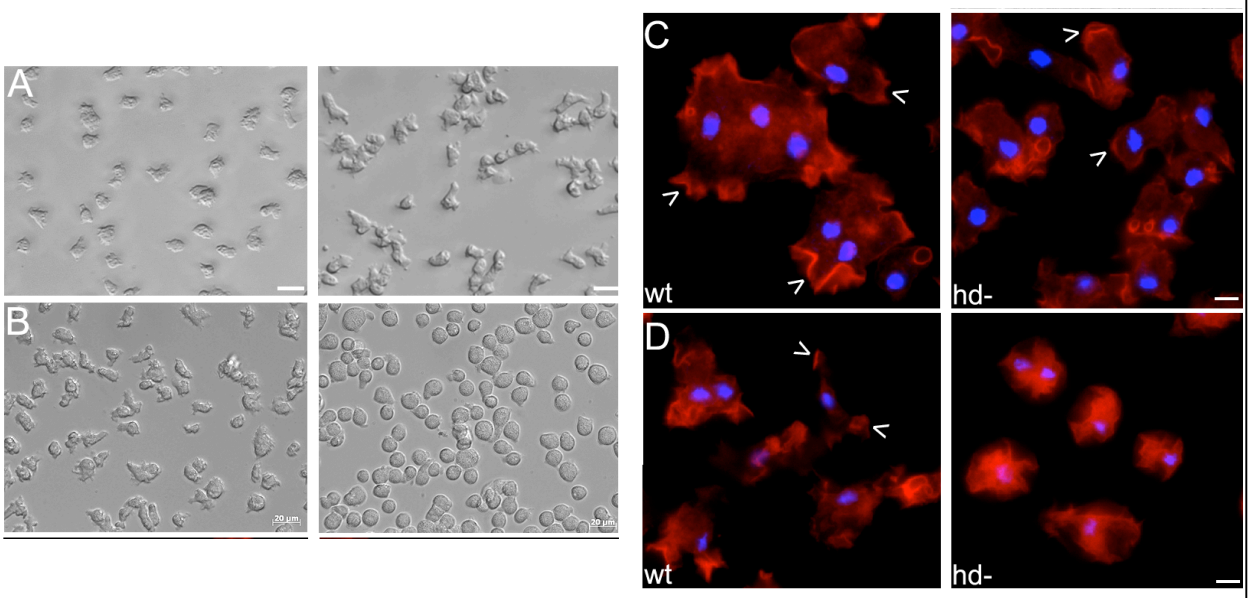

Figure 4.1. Removal of nutrients caused rounding of *hd*$^-$ cells and affects F-actin localization. A) The morphology of *hd*$^-$ cells (*right panel*) grown and photographed as an adherent culture in HL-5 was similar to wild-type cells (*left panel*). Scale bars (20 µm) are shown on the *bottom right*. B) Removal of nutrients (HL-5) and replacement with starvation buffer (KK_2) caused rounding of *hd*$^-$ cells. Cells were photographed 20 minutes after the addition of starvation buffer. Wild-type cells (*left panel*) displayed morphology similar to that observed for cells in HL-5 whereas all *hd*$^-$ cells immediately adopted a rounded morphology (*right panel*). Scale bars (20 µm) are shown on the *bottom right*. C) Aberrant localization of F-actin in starved *hd*$^-$ cells. Vegetative wild-type cells (*left panel*) and *hd*$^-$ cells (*right panel*) collected from axenic medium (HL-5) were deposited into Lab-tek chambered cover glass (8 well) at 1×10^5 cells/cm^2 and allowed to grow overnight in HL-5 at 21°C. For F-actin staining, the cells were fixed with 4% formaldehyde in PDF buffer and then stained with Texas red-phalloidin. Arrows indicate membrane extensions enriched with F-actin. D) Localization of F-actin in cells submerged in starvation buffer (KK_2). One hour after starvation in KK_2, wild-type cells retained their normal amoeboid morphology (*left panel*); *hd*$^-$ cells remained rounded and exhibited a redistribution of F-actin away from the cell cortex as it concentrated in the cytosol (*right panel*). Nuclei were stained with Hoechst 33342. Scale bars (5 µm) are shown on the *bottom right*. Scale bar 10 µm. Figure reproduced here with permission from [45].

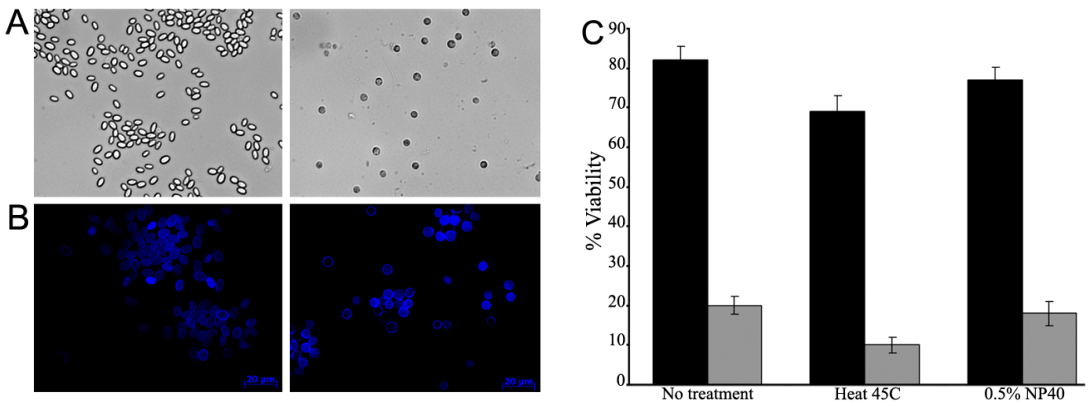

Figure 4.2. *hd*⁻ cells produced round, calcofluor positive spores with reduced viability. A) Wild-type (*left panel*) and *hd*⁻ (*right panel*) spores were collected from 48-72 hour fruiting bodies and viewed using brightfield microscopy. Wild-type spores were refractile with an elliptical morphology; *hd*⁻ fruiting bodies produced spores with a dark, round morphology. B) Wild-type (*left panel*) and *hd*⁻ spores (*right panel*) were stained with 0.01% calcofluor in spore buffer and viewed by fluorescent microscopy. Scale bar 20 mM. C) The viability of wild-type (*black bars*) and *hd*⁻ (*grey bars*) spores was assessed. Untreated spores were heated to 45°C for 10 minutes or incubated with 0.5% NP40 detergent for 5 minutes and aliquots of 100 spores were plated in triplicate onto SM-5 agar plates in a suspension of bacteria and grown for 7 days at 21°C. The relative viability of *hd*⁻ spores was assessed by counting the number of clear plaques on the bacterial lawns. Results are representative of three independent experiments. Figure reproduced here with permission from [45].

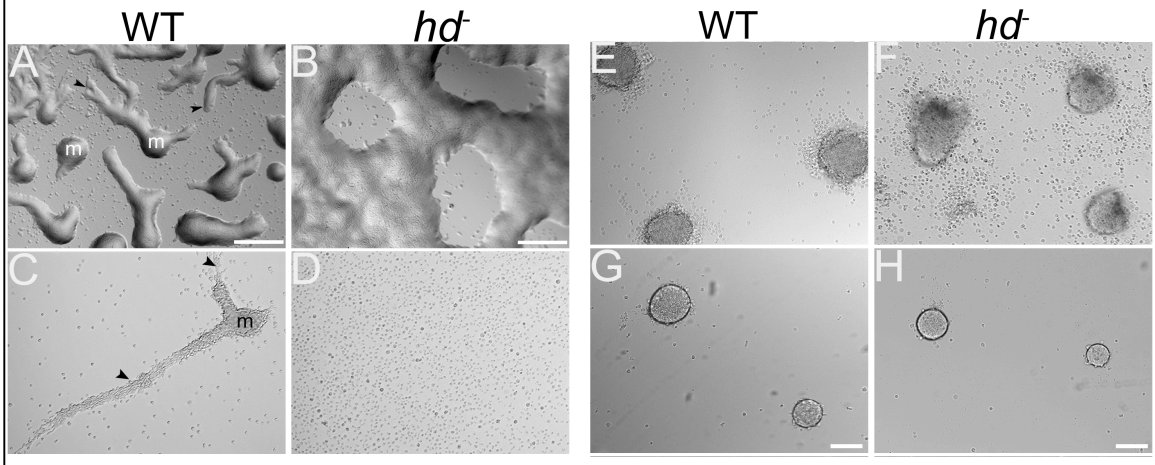

Figure 4.3. *hd*⁻ cells displayed aggregation defects and failed to stream under submerged culture. Wild-type and *hd*⁻ cells (1×10^6 cells/mL) were deposited on non-nutrient KK_2 agar plates and visualized by brightfield microscopy. Images are top view. A) Wild-type cells migrated in streams (*arrows*) to form aggregation territories (*m*) by ~6 hours. B) *hd*⁻ cells did not form well-defined streams, but rather clusters of cells that formed aggregation centers largely by accretion. Scale bar 100 µm. C) Wild-type and D) *hd*⁻ cells (1×10^5 cells/cm^2) were submerged under KK_2 and allowed to develop for 6 hours. Streams (*arrows*) of wild-type cells moving into an aggregation center (*m*) were readily apparent (*left panel*) whereas *hd*⁻ cells failed to stream (*right panel*). E) Wild-type and F) *hd*⁻ cells were submerged under buffer at high density (5×10^6 cells/cm^2) and imaged after 20 hours. Under these conditions, wild-type cells readily formed distinct organized mounds; high density partially restored the ability of *hd*⁻ cells to form aggregation territories but with an irregular polarized shape. (G) Wild-type and (H) *hd*⁻ cells (1×10^5 cells/cm^2) were submerged under KK_2 in the presence of 1 mM $CaCl_2$ and imaged after 20 hours; under these conditions exogenous calcium rescues early development of *hd*⁻ cells. Scale bar 100 µm. Figure reproduced here with permission from [45].

Cell adhesion in the early aggregation phase of *Dictyostelium* development is known to be facilitated by two glycoproteins whose expression peaks successively, cad1 and csA [59] (Figure 1.3 and 4.5), and can be monitored using an assay that takes advantage of the unique ability of *Dictyostelium* cells to acquire EDTA-resistant adhesion within four hours of initiation of development by starvation, in shaking suspension culture [119]. Using this assay I explored the homotypic cell adhesion properties of *hd-* cells in comparison to WT. I discovered that the *hd-* cells wholly failed to acquire EDTA-resistant homotypic adhesion (Figure 4.4) [45]. This phenotype mimics the well-characterized adhesion defect of *csA-* cells.

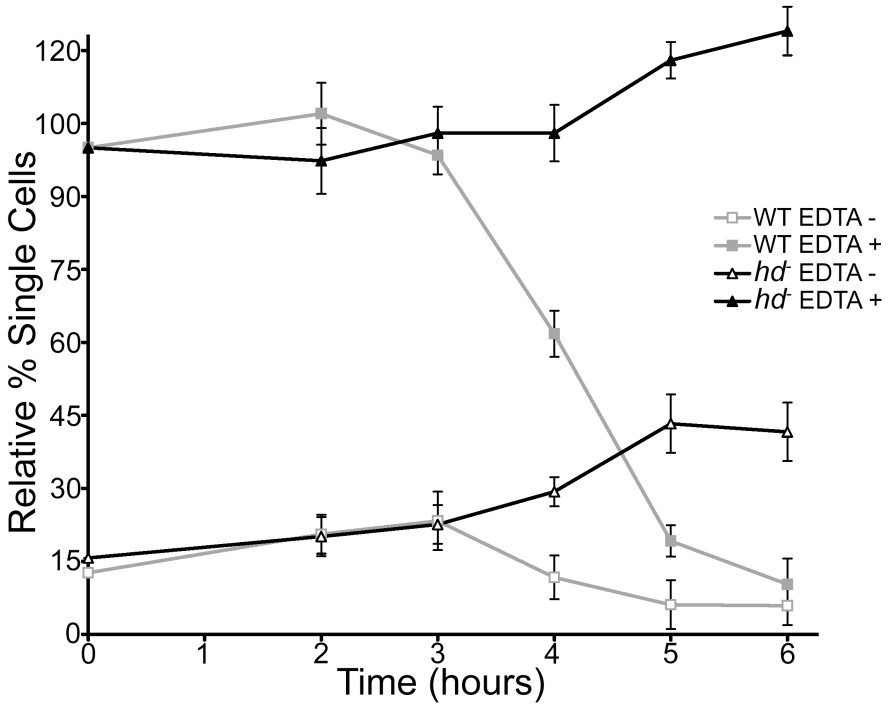

Figure 4.4. Loss of EDTA-resistant adhesion in *hd-* cells. Wild-type and *hd-* cells (5×106 cells/mL) were developed in Soerensen's buffer at 150 rpm and 21°C. Samples were collected at the start of the assay and at one hour time points over a period of 6 hours. For each collection point, cells were dissociated by vortexing and then incubated in the presence or absence of 10 mM EDTA for 30 minutes, fixed with 2% glutaraldehyde (10 min.) and single cells were counted in duplicate using a hemocytometer. All experiments were performed in duplicate at least three times and the mean value for single cells in duplicate samples, expressed as percentage of total cells, was plotted over time.

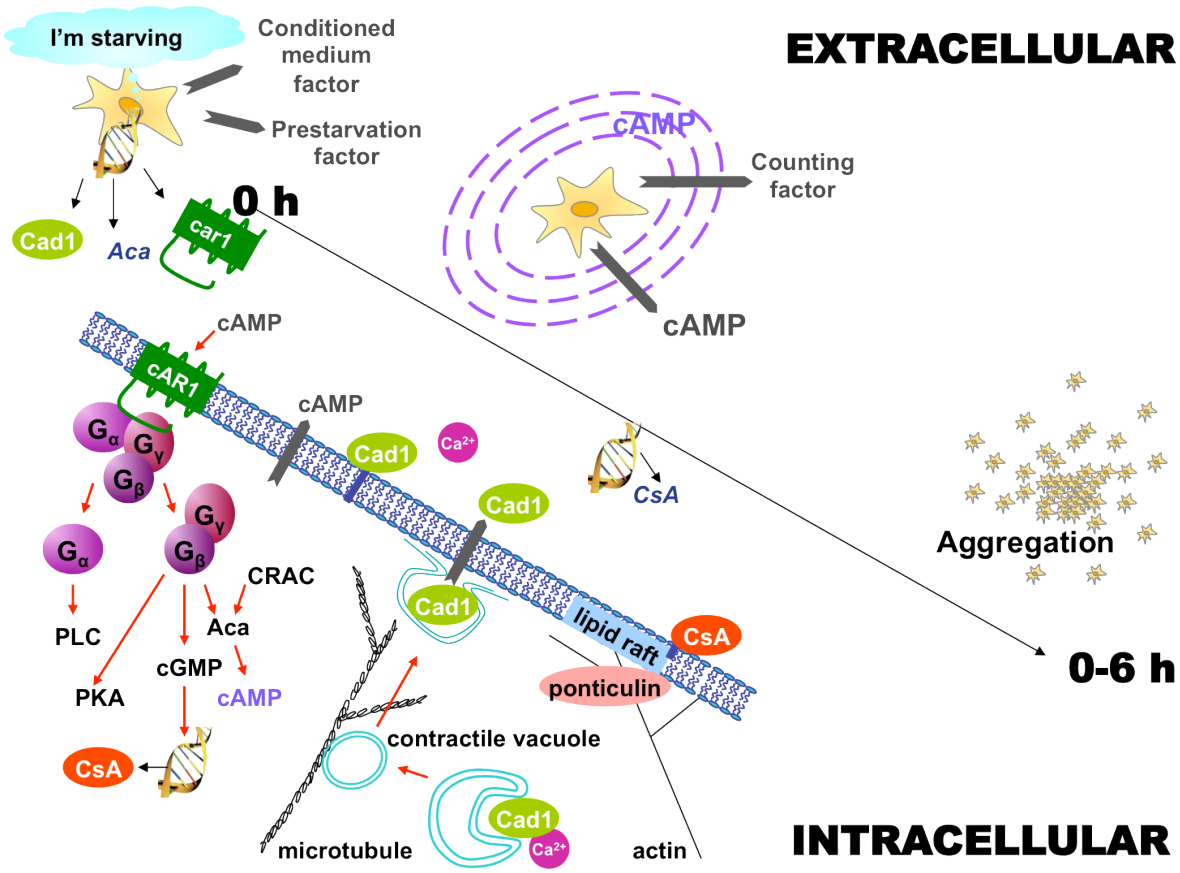

Figure 4.5. Signaling events in the early aggregation stages of *Dictyostelium* development. Starving amoebae secrete glycoprotein factors, including prestarvation factor and conditioned medium factor, that trigger the onset of multicellular development by inducing full expression of early genes and a low rate of expression of aggregation genes, including car1 and acA, which in turn initiate pulsatile cAMP signaling. cAMP in the cellular and extracellular environment is rapidly hydrolyzed by phosphodiesterases to allow for transient pulsing. Cad1 is expressed at basal levels in amoebae and is the first adhesion molecule whose expression is upregulated during development to form weak, homophilic, EDTA-sensitive interactions. Cad1 is unique in that it is soluble, secreted via the non-canonical contractile vacuole system, and comprises part of the extracellular matrix. As development continues, csA accumulates and is responsible for the acquisition of EDTA-resistant homotypic cell adhesion. CsA associates with the plasma membrane via a ceramide-like linkage and indirectly associates with the actin binding protein ponticulin. Abbreviations: **C**yclic **AMP** (cAMP), **C**yclic **GMP** (cGMP), **C**alcium-dependent **AD**hesion Molecule-1(cad1)**, C**ontact **S**ite **A** protein (csA)**, L**oose **AG**regate **C** (lagC)**, cA**MP **R**eceptor- 1 (car1)**, C**ytosolic **R**egulator of **A**denylate **C**yclase (CRAC)**, A**denylate **C**yclase of **A**ggregation Stage (acA)**, P**hosho**l**ipase **C** (PLC)**,** cAMP-dependent **P**rotein **K**inase **A** (PKA)

Our current study provides evidence that *hd-* cells fail to produce the csA protein, although normal levels of csA mRNA are present. However, lack of csA alone is not responsible for the inability of *hd-* cells to acquire EDTA-resistant adhesion since we

demonstrate that constitutive overexpression of csA is unable to rescue the defect, despite the fact that the overexpressed protein is properly localized. Supplementation with calcium or magnesium is capable of partially restoring EDTA-resistant adhesion and restores normal csA protein levels. Interestingly, the EDTA-resistant adhesion defect of *csA*- cells is also partially rescued by calcium supplementation. These data suggest that calcium is interacting with another novel factor independent of csA or huntingtin to facilitate EDTA-resistant adhesion.

Results

Huntingtin null cells fail to accumulate csA protein upon starvation

Previous studies indicate that the csA protein chiefly governs the maintenance of EDTA-resistant homotypic cell adhesion [120, 121]. Therefore, we examined levels of csA in *hd*- cells to determine whether the defect in cell adhesion we observe is due to the csA protein (Figure 4.6). As expected, csA protein is present at barely detectable basal levels prior to starvation, but accumulates dramatically by six hours of starvation in WT cells. By contrast, *hd*- cells fail to accumulate csA protein in the normal developmental timeframe (Figure 4.6 B). To determine if the failure to accumulate csA protein was due to improper gene expression, *csA* levels were assessed by RT-PCR (Figure 4.6 C). CsA mRNA levels in *hd*- cells mirrored WT, indicating that the homotypic cell adhesion defect resulting from huntingtin deficiency was instead at the level of either protein translation or stability. Despite the artificiality of the EDTA-resistant adhesion assay, this experimental method is an effective way of interrogating aspects of real biology since disruption of cell-cell contact in early adhesion – in this case, due to absence of huntingtin – has developmental consequences when cells are plated on an agar-based starvation substrate and allowed to develop normally (Figure 4.6 D).

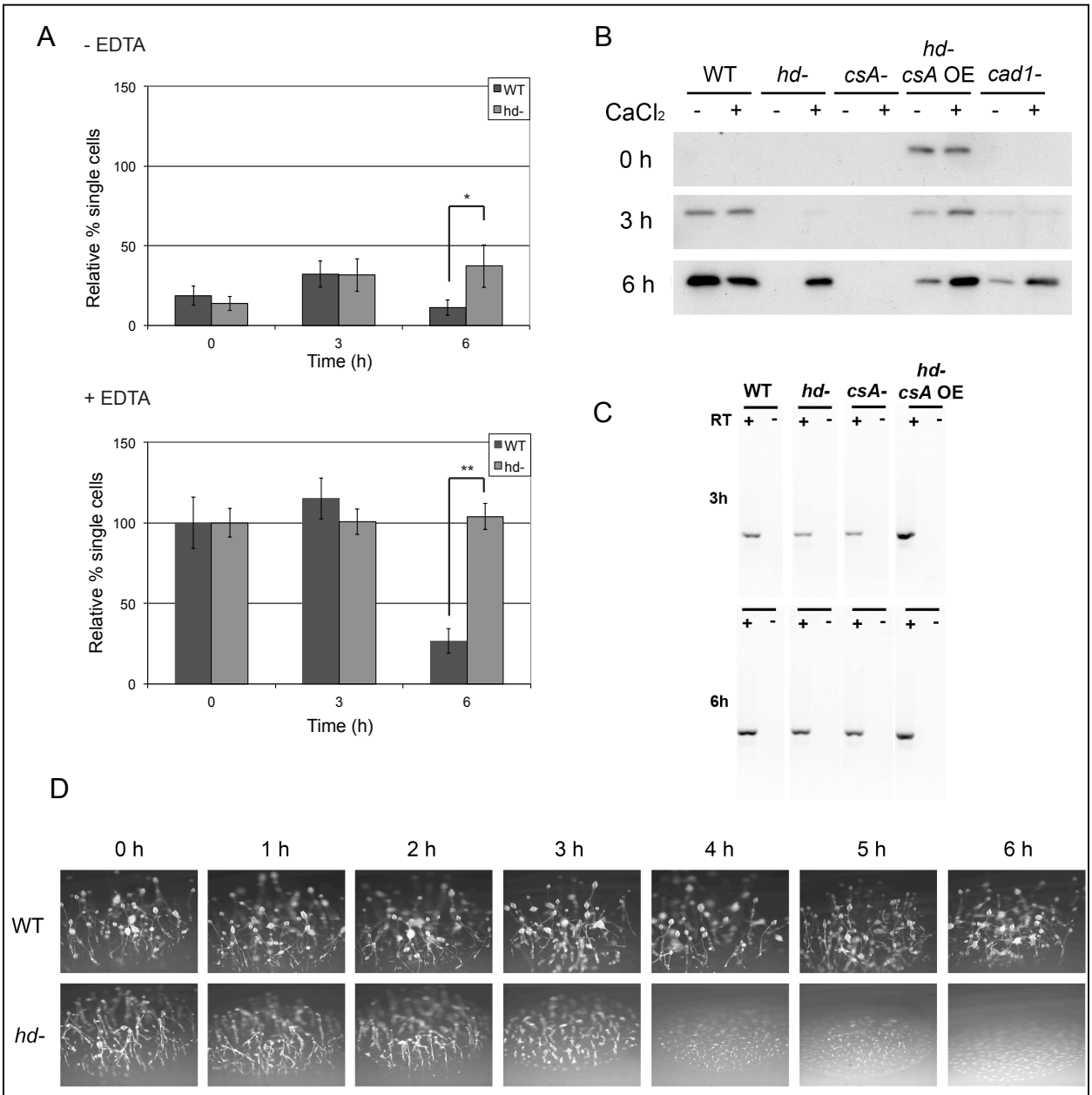

Figure 4.6. Huntingtin deficient cells fail to acquire EDTA-resistant homotypic cell adhesion in shaking starvation culture. A) *hd-* cells fail to acquire EDTA resistant cell adhesion in the presence of EDTA as measured by relative % single cells. * p-value = 0.0001 ** p-value – $2.6*10^{-13}$ Error bars = standard deviation of cell counts; N=7. B) Protein levels of csA (80 kD) at 0, 3, and 6 hours of development in shaking starvation culture in WT, *hd-*, *csA-*, *hd- csA* OE (overexpression), and *cad1-* cells probed with 1:100 csA antibody. C) RT-PCR of *csA* at 3 and 6 hours of development in shaking starvation culture. RT +/- indicates presence or absence of reverse transcriptase. D) Defective cell-cell adhesion results in disruption of developmental potential of *hd-* cells plated on starvation agar after 0-6 hours of starvation in liquid shaking culture.

Cad1 protein levels and localization are normal in huntingtin deficient cells

The defect in cell adhesion could be due to the upstream molecule Cad1 which has been proposed to influence csA levels by an unknown mechanism [59]. I established that cad1 levels were not significantly altered in the *hd-* cells (Figure 4.7 A). Therefore, I sought to address by immunofluorescence microscopy whether cad1 localization was affected (Figure 4.7 B). In WT cells at six hours of starvation, cad1 signal concentrated near the plasma membrane or in distinct puncta, appearing to decorate contractile vacuoles known to traffic cad1 [122, 123]. No significant differences were observed in *hd-* cells except for a decrease in signal at contractile vacuoles (Figure 2 B), which is expected given prior evidence that the contractile vacuole system is severely affected by loss of huntingtin [45].

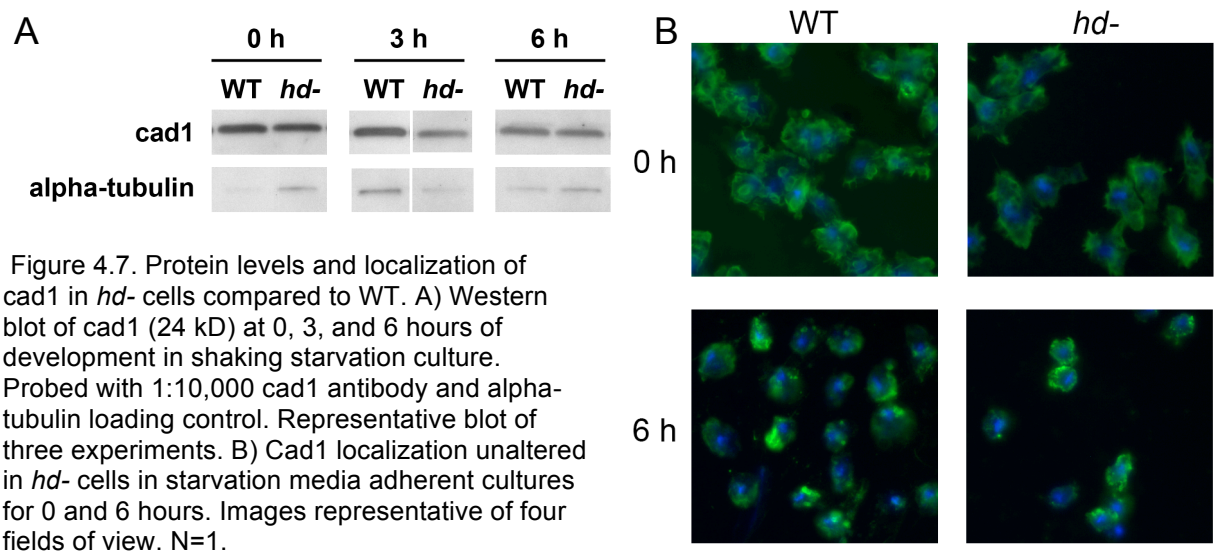

Figure 4.7. Protein levels and localization of cad1 in *hd-* cells compared to WT. A) Western blot of cad1 (24 kD) at 0, 3, and 6 hours of development in shaking starvation culture. Probed with 1:10,000 cad1 antibody and alpha-tubulin loading control. Representative blot of three experiments. B) Cad1 localization unaltered in *hd-* cells in starvation media adherent cultures for 0 and 6 hours. Images representative of four fields of view. N=1.

Overexpression of csA fails to rescue the homotypic adhesion defect in huntingtin deficient cells

Constitutive overexpression of csA has been previously demonstrated to rescue the absence of EDTA-resistant adhesion in *csA-* cells [124]. We obtained and introduced this expression construct into *hd-* cells and evaluated EDTA resistant adhesion. Overexpression of *csA* was achieved (Figure 4.6 B and C), but failed to rescue EDTA-resistant adhesion (Fig. 4.8 A) despite proper localization of the overexpressed protein (Figure 4.8 B).

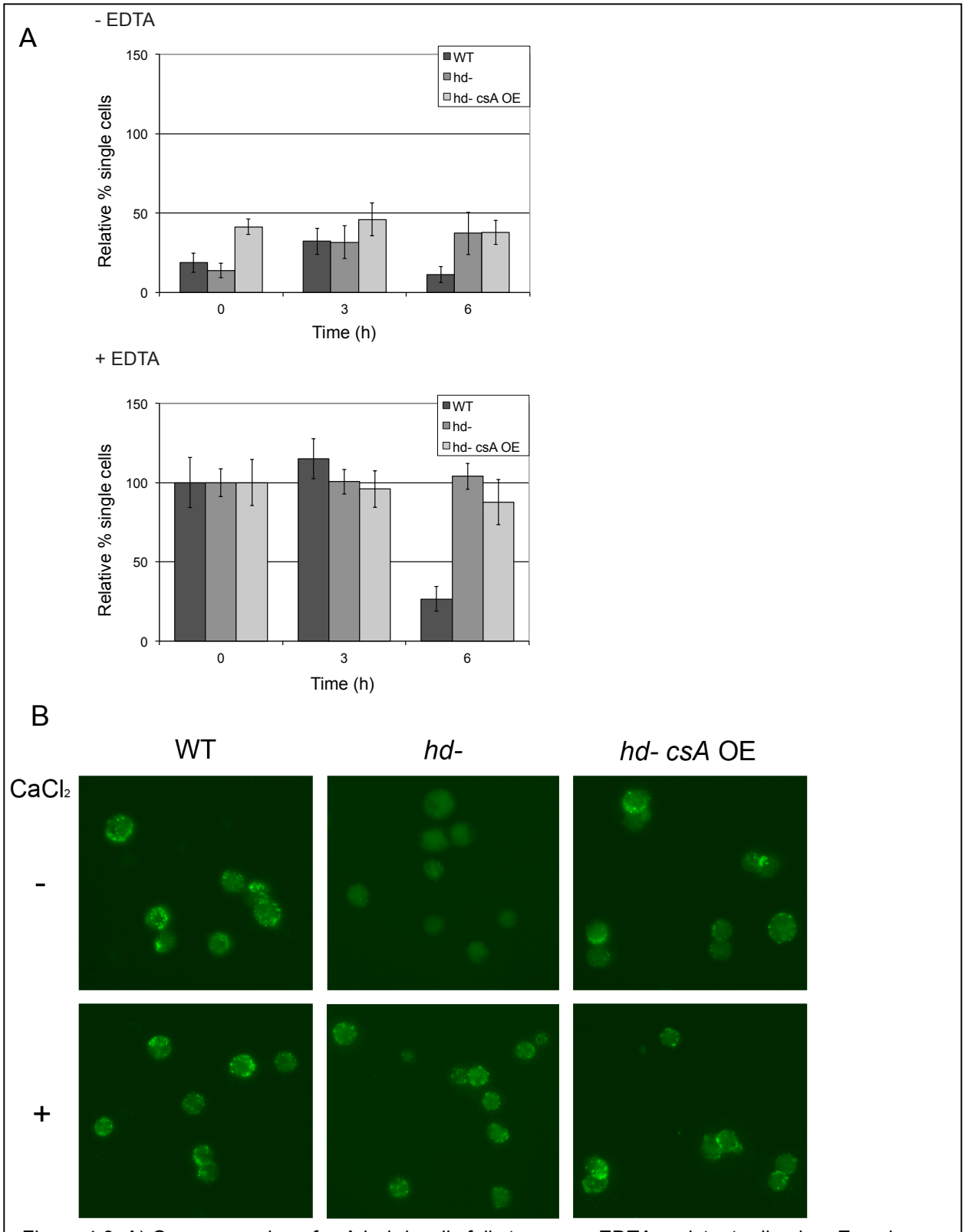

Figure 4.8. A) Overexpression of csA in *hd-* cells fails to rescue EDTA-resistant adhesion. Error bars = standard deviation of cell counts; N=3. B) Localization of csA in WT, *hd-*, and *hd-* cells overexpressing *csA* (csA OE) after one hour in starvation medium with (+) and without (-) exogenous 1mM $CaCl_2$. Representative images from four fields of view.

Homotypic cell adhesion in huntingtin deficient cells is not rescued by cAMP pulsing

Proper timing and progression of development is governed by cAMP pulsing which is suggested to affect csA levels by an unknown mechanism [59]. Huntingtin deficient cells grown on a substrate have a characterized defect in synchronicity of cAMP pulsing, which can be overcome by exogenous cAMP pulsing [45]. Therefore, I examined whether the defective homotypic adhesion of the *hd-* cells was due to improper extracellular cAMP pulsing by providing pulses of 75 nM cAMP every seven minutes for the duration of the adhesion assay (Figure 4.9). In WT cells, supplementation with 75 nM cAMP speeds up development such that when six hour-starved cells are plated on glass slides, they immediately enter the developmental program and begin to stream and develop faster than non-pulsed WT cells (Figure 4.9 A). By contrast, *hd-* cells fail to acquire EDTA resistant adhesion even with cAMP pulsing in the adhesion assay (Figure 4.9 B) and remain unable to stream on glass slides (Figure 4.9 A). Failure of extracellular cAMP to rescue the *hd-* adhesion defect suggests that the defect is not at the level of synchronicity of pulsing. To determine whether cells lacking huntingtin respond appropriately to the extracellular cAMP signal, we measured levels of adenylyl cyclase A (acA) expression. As a downstream effector critical for upregulation of intracellular cAMP production, acA expression is an indirect readout of the ability of cAMP to bind and activate the cAMP receptor (car1) and the intervening cAMP signal relay and transport machinery. However, acA mRNA expression was unchanged in *hd-* cells at six hours suggesting that there are no gross abnormalities in cAMP response (Figure 4.9 C).

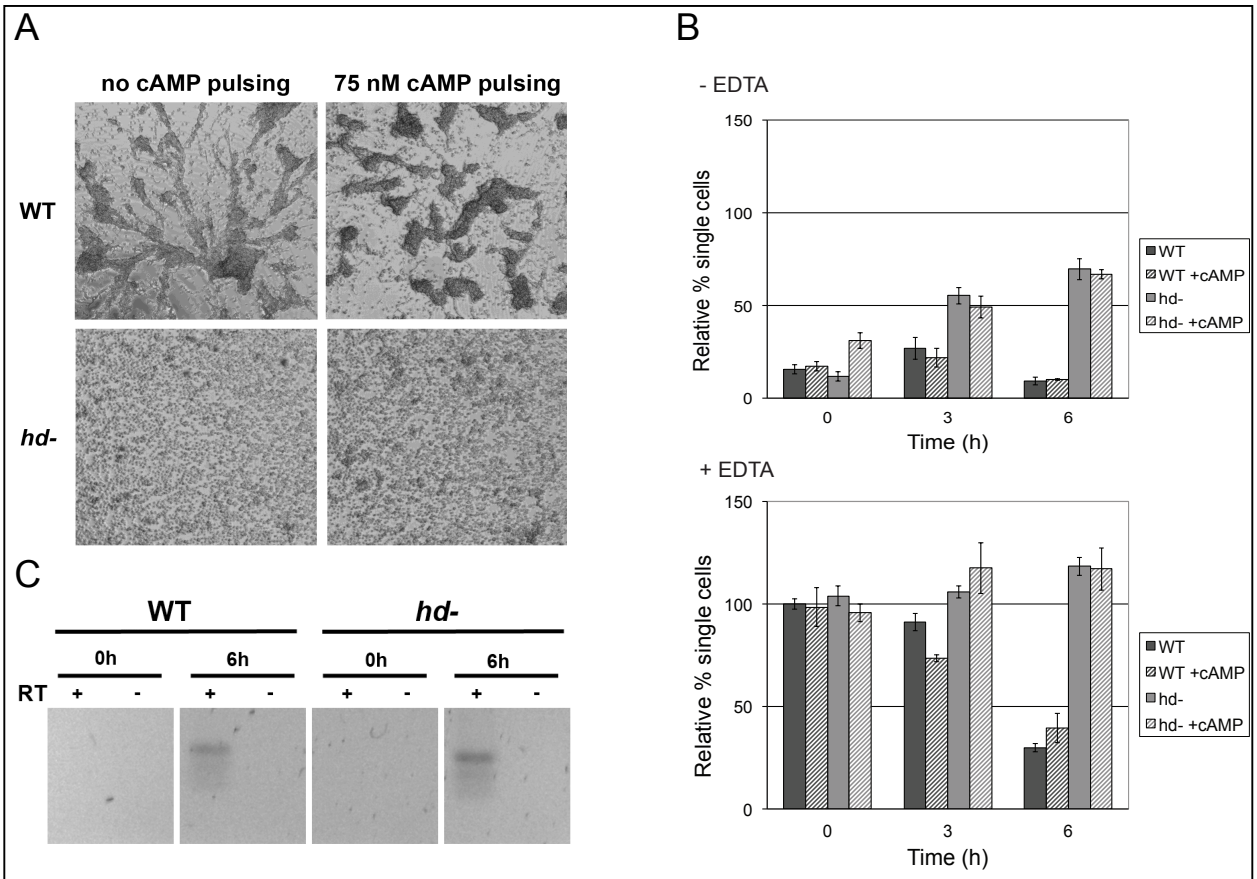

Figure 4.9 Pulsing of cAMP fails to rescue the *hd*- homotypic cell adhesion defect in starvation media. A) Streaming behavior is initiated immediately upon plating of 6h starved cells on glass slides and is accelerated in cells pulsed with 75 nM cAMP. By contrast, *hd*-cells never enter normal streaming behavior and are unaffected by cAMP pulsing. 4X magnification, brightfield image. B) 75 nM pulses of cAMP were added every 7 min. Error bars = standard deviation of cell counts; N=1. C) RT-PCR of *acA* at 0, 3, and 6 hours of starvation in WT and *hd*-cells.

Calcium supplementation restores csA levels in huntingtin deficient cells

Calcium signaling has well-established roles in cell adhesion and cAMP-dependent development [125-127]. Furthermore, the divalent cations magnesium and calcium were previously shown to rescue a developmental streaming defect in *hd*- cells [45]. Therefore, I examined whether supplementation with 1 mM $CaCl_2$ affects the adhesion of *hd*- cells. As seen in Figure 4.10 A, supplementation with calcium restored EDTA-resistant cell adhesion as measured by percentage of single cells in the normal six-hour developmental window (six hour pvalue with EDTA = 0.27 and without EDTA = 0.77). Furthermore, csA protein levels returned to normal in *hd*- cells with calcium supplementation (Fig 4.10 B) and the protein was localized

properly (Figure 4.8 B). Calcium was capable of rescuing the % single cell measure of EDTA-resistant adhesion at concentrations as low as 0.1 mM (data not shown).

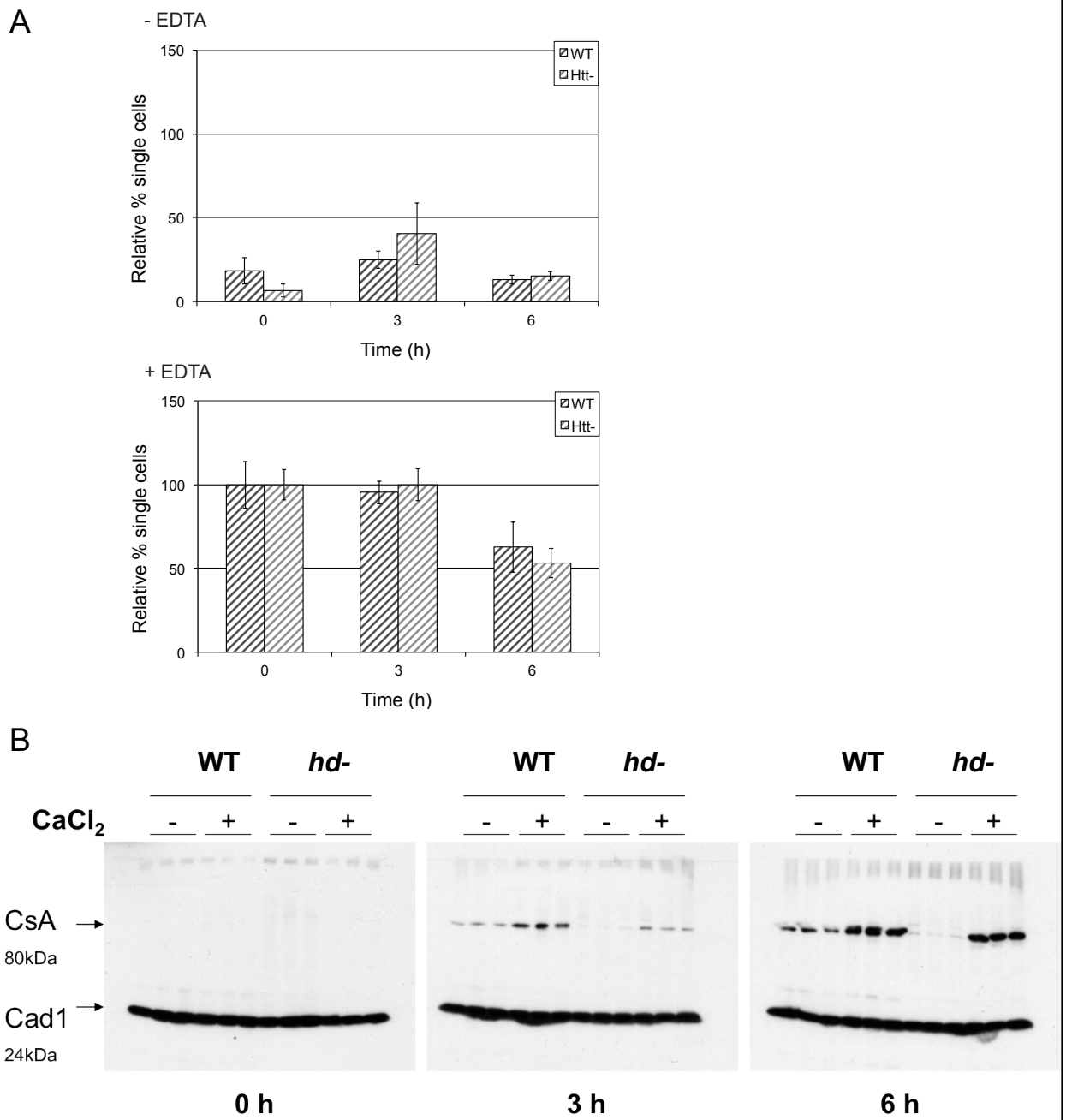

Figure 4.10. Supplementation with calcium partially rescues EDTA-resistant adhesion in *hd-* cells and enables csA protein synthesis. A) Rescue of *hd-* homotypic cell adhesion defect with 1mM $CaCl_2$ supplementation in starvation media. Error bars = standard deviation of cell counts; N=2. B) Western blot of csA levels with $CaCl_2$ supplementation, probed with csA antibody and reprobed with cad1 antibody as a loading control. Loaded in triplicate. Representative blot of three experiments.

We sought to more finely characterize the EDTA-resistant adhesion phenotype by examining more subtle measures of the aggregation phenotype, including aggregate size and morphology. Brightfield microscopy of cells taken from the adhesion assay at the six-hour time point reveals that while calcium supplementation restores *hd*- cell adhesion, as measured by percent single cells in the presence of EDTA, the size of aggregates is dramatically reduced with no large aggregates, similar to the *csA*- cells in the presence of EDTA (Figure 4.11). However, in presence of calcium without EDTA treatment *hd*- cells are capable of normal aggregate formation. By contrast *csA*- cells, in the absence of EDTA form aggregates, but the aggregate morphology is irregular and much less compact that *hd*- or WT cells. These data, combined with the fact that restoring csA levels in *hd*- cells by overexpression fails to restore EDTA-resistant adhesion, suggest that huntingtin is playing an additional novel role in homotypic cell adhesion independent of its effect on csA protein levels.

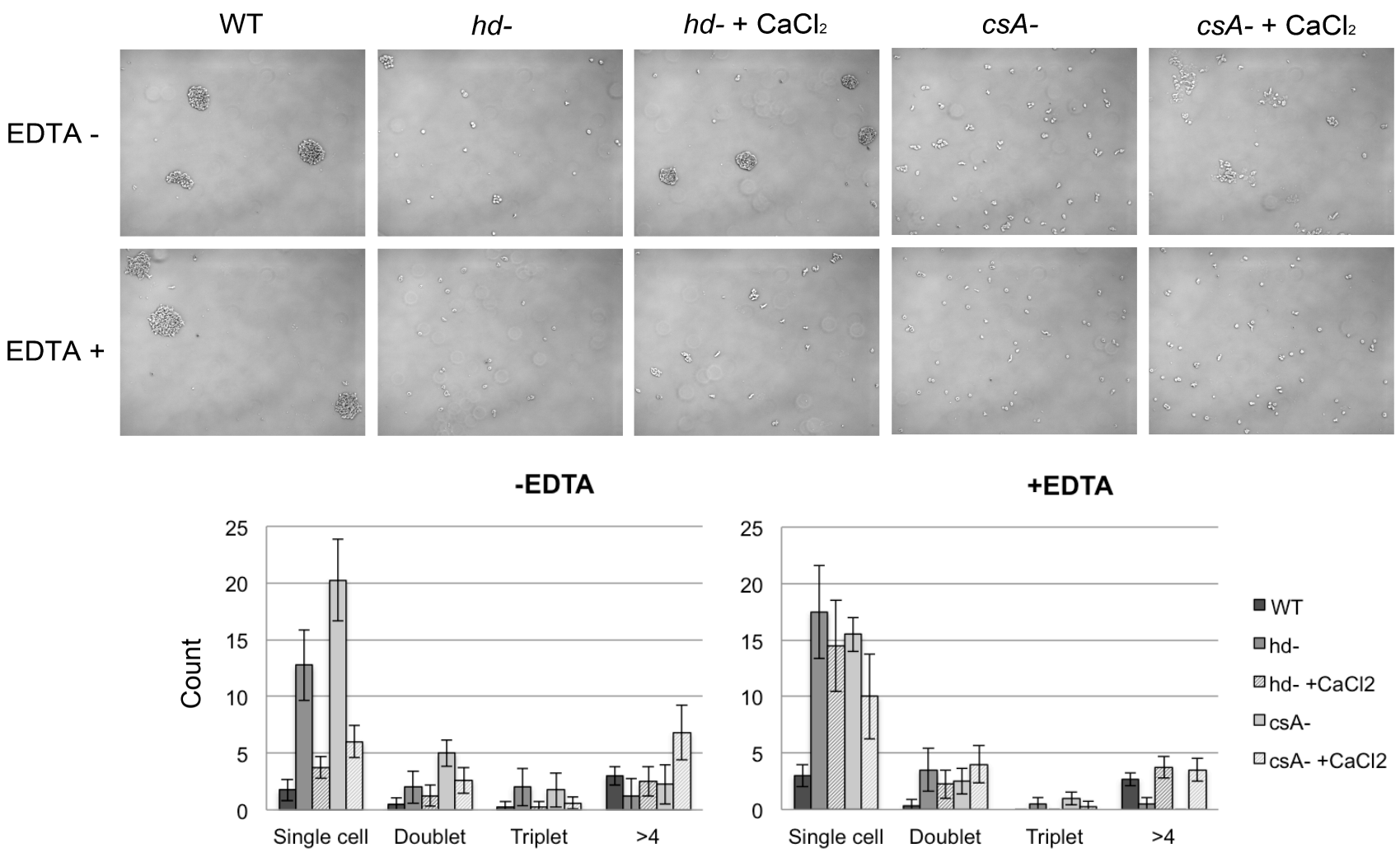

Figure 4.11. Brightfield microscope images (above) of aggregates at 6 hours of starvation in shaking liquid culture in *hd*- and csA- cells in the presence or absence of 1mM $CaCl_2$ compared to WT. 20X magnification. Lower panel shows quantification of average (per field) count of single cells, doublets, triplets, and aggregates composed of >4 cells in the presence and absence of EDTA at six hours starvation. N=3 fields of view per sample. The number of fields counted (3) was determined by the number of fields that must be counted in order to count 100 cells at the zero hour time point in the presence of EDTA when essentially all cells are dissociated.

Inability to produce csA points to a translation defect in the absence of huntingtin

Failure to produce csA in the absence of huntingtin could result from increased turnover or decreased synthesis. Glycosylation of csA is known to affect localization and stability of the protein [128]. Tunicamycin treatment inhibits N-glycosylation and reveals the 50 kDa and 68 kDa precursors of csA, as well as the 80 kDa mature, fully-glycosylated, membrane-bound isoform [128]. Cells were treated with 0.4 µg/mL tunicamycin at 3 hours of starvation and protein extraction was performed at 6 hours of starvation (three hours of tunicamycin treatment). Figure 4.12 shows all three glycosylated forms of csA could be detected in WT cells. Combined with the normal localization of csA in *hd-* cells supplemented with calcium (Figure 4.8 B), these data suggest that improper glycosylation is unlikely to account for the decreased levels of csA in *hd-* cells.

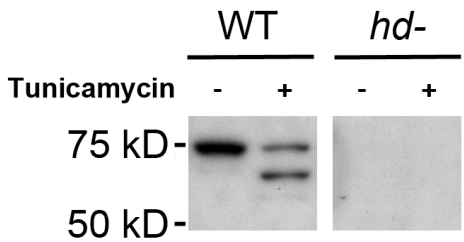

Figure 4.12. Western blot of WT and *hd-* cells at 6 hours of starvation following 0.4 µg/mL tunicamycin treatment from 3-6 hours, probed with 1:1000 csa antibody (33-294-17). Representative blot of n=3 replicates.

To investigate whether reduced csA protein levels resulted from enhanced protein degradation, cells were treated with the proteasome inhibitor lactacystin. After three hours of starvation in liquid shaking culture, cells were treated with 10 µM lactacystin for an additional three hours. Western blot analysis revealed an accumulation of csA protein by six hours of starvation (three hours of lactacystin treatment) in WT cells (Figure 4.13). However, *hd-* cells failed to accumulate csA, providing preliminary evidence that the primary defect resulting in low csA levels in the absence of huntingtin is likely not due to increased protein turnover, but rather aberrant translation.

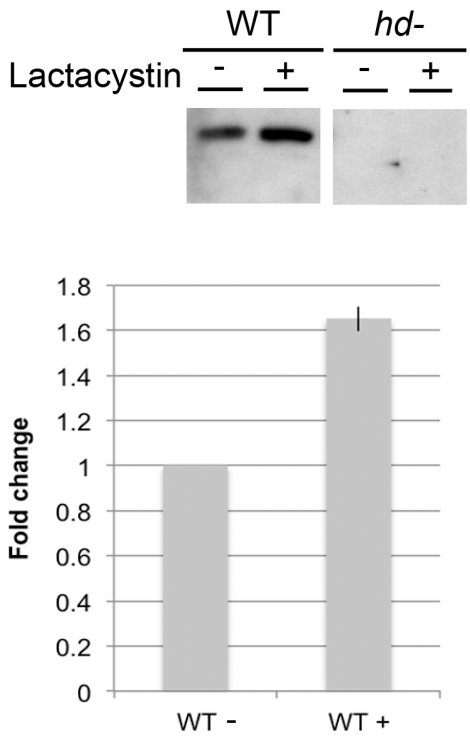

Figure 4.13. Western blot of WT and *hd*- cells at 6 hours of starvation following treatment with 10 μM lactacystin from 3-6 hours of starvation, probed with 1:1000 csa antibody (33-294-17). Quantified by densiometry using ImageJ. Error bar = standard deviation of three replicates; n=3.

Discussion

Taken together, our results suggest that the lack of csA protein in *hd*- cells is not a result of rapid degradation or failure of transcription, but rather reflects a protein synthesis or translation defect in the absence of huntingtin that can be overcome by calcium or magnesium supplementation. The fact that calcium or magnesium alone can partially rescue the cell adhesion phenotype suggests that huntingtin deficient cells possess all of the machinery necessary for csA synthesis and cell adhesion.

Importantly, csA is not capable of completely restoring EDTA-resistant adhesion in the absence of huntingtin, indicating an additional novel role for huntingtin in homotypic cell adhesion that is yet to be identified. In the absence of huntingtin or csA, calcium allows for transient initial cell-cell contact (within 3-5 minutes of starvation) that may activate compensatory intracellular signaling pathways that are capable of supporting homotypic adhesion. Recent sequencing and annotation of the *D. discoideum* genome has identified a

number of putative cell adhesion molecules of unknown function so novel molecular players are likely to be uncovered. Additionally, the known Ca^{2+}-dependent/EDTA sensitive adhesion molecules cad1 and lagC may strengthen cell adhesion in the presence of calcium in a manner sufficient to produce partial rescue of adhesion since compensatory roles for these molecules have been previously identified and *D. discoideum* mutants of the three canonical early adhesion molecules are fully capable of development despite their respective adhesion defects (Figure 1.3) [59].

Exactly how calcium alleviates the csA protein translation defect remains to be determined. However, calcium has been previously shown to be integral to various aspects of protein synthesis [129-131]. Furthermore, colleagues in the lab have characterized a defect in osmoregulation and the contractile vacuole (CV) system in *hd-* cells (manuscript in preparation). The CV network in *D. discoideum*, is a double-membrane structure that helps to regulate water and ion homeostasis and is an important store of intracellular calcium in *D. discoideum* [132, 133]. It will be interesting to investigate whether the defect in the CV system could be affecting calcium signaling or levels in a way that disrupts homotypic cell adhesion in the *hd-* cells.

Our study adds to accumulating evidence that the huntingtin protein is involved in cytoskeletal biology and this conserved role is manifest functionally in cell adhesion in both *D. discoideum* and mammalian models [47, 60]. Future experiments will focus on gaining mechanistic insight into the conserved functional role of huntingtin in the regulation of cell adhesion. These investigations will set the stage for follow-up studies to determine the relationship between the identified huntingtin function(s) and HD pathogenesis.

Methods

Cell culture and development

Dictyostelium discoideum AX3 (WT) cells were grown at 21°C either on SM/2 agar plates (DictyBase) in the presence of *Klebsiella aerogenes*, axenically in tissue culture dishes,

or in HL5 medium (ForMedium; Norfolk, UK) in 50 mL flasks shaking on a platform shaker at 150 rpm. All cells were cultured in the presence of streptomycin (300 µg/ml). The *hd*- cells were grown in blasticidin (25 µg/ml). WT and *hd*- cells were obtained from Dr. Michael Myre, *cad*- cells were from DictyBase, and *csA*- cells were obtained from Dr. Salvo Bozarro.

Homotypic cell adhesion assay

Homotypic cell adhesion was assessed as described previously with the following modifications [134]. Briefly, cells from HL5 shaking cultures were inoculated in fresh HL5 media for overnight culture at a density of 2-3*10^6 cells/mL. Cells were counted by hemocytometer and an aliquot containing 5*10^6 cells/mL was transferred to a 50 mL Falcon tube and centrifuged at 2500 rpm for 5 min. Cells were washed twice in a half volume of chilled Soerensen's buffer (SB) (DictyBase), resuspended in 15 mL SB, transferred to a 50 mL beaker, and placed on a shaking platform at 150 rpm. Cells were collected at various time points in 300 µL aliquots and placed in 300 µL SB either containing or lacking 10 mM EDTA for 30 minutes in 10 mL beakers. Cells were then fixed with glutaraldehyde (company) at a final concentration of 2% for 10 minutes. Single cells were counted using a hemocytometer. All experiments were performed in duplicate and the average of the single cell counts for the replicates was used to calculate the total percentage of single cells normalized to WT and the results were plotted over time. The effect of supplementation with $CaCl_2$, $MgCl_2$, $MgSO_4$, and other divalent cations was tested by making stock solutions in SB media and resuspending cells in SB containing the ions at 0.1-1 mM concentrations from the outset of the adhesion assay after washing.

Immunoblot analysis

Whole cell protein extracts were prepared by lysis on ice for one hour in a buffer containing 1X RIPA buffer and a Complete mini EDTA-free protease inhibitor tablet (Roche) with mixing by tapping every 20 minutes. The total lysates were cleared by centrifugation at 14,000g for 10 minutes and the supernatants were collected. The protein concentration was determined by using the Pierce BCA protein assay (Thermo Scientific) protein assay. 40 µg of protein

extract was mixed with 4X SDS sample buffer, boiled for 5 minutes, and subjected to SDS-PAGE with 4-12%Tris-Glycine gels (Invitrogen). After electrophoresis, the proteins were transferred to Immobilon-P transfer membranes (Millipore) and then incubated for one hour in blocking solution containing 5% nonfat powered milk in TBS-T (50 mM Tris-HCl, 150 mM NaCl, pH 7.4, 0.1% Tween 20). The blots were probed overnight at 4°C with primary antibodies. After four washes of 10 minutes each in TBS-T, the blots were incubated for one hour at room temperature with horseradish peroxidase-conjugated anti-mouse or anti-rabbit antisera. After three 10-minute washes TBS-T, the membranes were processed using a chemiluminiscence detection kit (GE Healthcare) and exposed to autoradiographic film (Hyperfilm ECL; Amersham Bioscience). Quantification of the immunoreactive bands was performed by scanning and analysis using the GS-800 Calibrated Densitometer and the ImageJ software.

For tunicamycin treatment, 0.4 µg/mL tunicamycin was added to the starvation culture at three hours of starvation and cells were assessed by immunoblotting at six hours. For lactacystin treatment, 10 µM lactacystin was added to the starvation culture at three hours of starvation and cells were assessed by immunoblotting at six hours.

CsA antibody (33-294-17 [128, 135]; Developmental Studies Hybridoma Bank, IA) was used at a concentration of 1:1000 for Western blotting. DdCad-1 antiserum was provided by Dr. Chi-hung Siu [136] and used at a concentration of 1:10,000 for Western blotting.

Overexpression of csA

The pDCEV csA expression vector was kindly obtained from DictyBase. This vector results in constitutive overexpression of csA driven by the actin15 promoter as described previously [124]. Transfected cells were kept under constant selection by adding 25 µg/mL G418 to the medium.

Immunofluorescence microscopy

CsA localization was examined by gently mixing a 100 µL aliquot of cells, removed from shaking suspension culture after five hours of starvation, with 100 µL csA antibody (mAb 448;

generously provided by Dr. Salvo Bozarro). The cell-antibody mixture was placed on ice for 20 minutes with vortexing during the incubation to disaggregate cells. Cells were washed twice with PBS, using brief centrifugation to collect cells. Following washes, cells were resuspended in secondary antibody (Alexa 488; Invitrogen) at 1:500 dilution and once again incubated on ice for 20 minutes followed by two PBS washes as described previously and resuspension in PBS. A 20 µL aliquot of cells was placed on a slide and covered with no. 1.5 coverglass. Cells were imaged on a Zeiss microscope at 40 X magnification.

The cad1 localization protocol was modified from [122, 136]. Briefly, $1*10^6$ cells/mL were plated on a coverslip in a 24-well dish with 1 mL per well HL5 medium and allowed to settle overnight. The next day, media was gently aspirated and coverslips were washed two times with Sorenson's starvation buffer. Cells were either fixed immediately (for the zero hour time point) or allowed to starve for six hours in 1 mL fresh Sorenson's starvation buffer (for the six hour time point). Cells were washed once with PBS and the fixed with 3.7% formaldehyde in PBS for 15 min at room temperature. Samples were permeabilized with cold (-20°C) methanol containing 1% formaldehyde for five minutes. Cells were washed once with PBS and blocked with 1% w/v BSA in PBS for 10 minutes, followed by incubation with DdCAD-1 antibody (generously provided by Dr. Chi-hung Siu) at 1:200 dilution in PBS with 0.1% BSA for one hour at room temperature. Samples were washed three times with PBS containing 0.05% Tween 20 and then incubated with Alexa-488 (1:300 dilution) secondary antibody for one hour at room temperature. Samples were washed once in PBS and once in water and then mounted in Prolong Gold Antifade with DAPI reagent. Cells were imaged on a Zeiss microscope at 40 X magnification.

RT-PCR analysis

RNA extraction was performed with the RNeasy mini kit (Qiagen). Levels of csA and acA mRNA expression were measured by RT-PCR using the following primers: for csA forward primer 5'- TAA CCA TGG GAA CCT CAA GC -3' and reverse primer 5'- ACA ATC GAA ACA

TGG GCA TT -3'; for acA forward primer 5'- CAA ACA TTT TCC AAA AAT ATA CTC TCA -3' and reverse primer 5'- AAA TCG CTT CTT TTG TAA ATC CA -3'.

Chapter 5:

Discussion and future directions

Huntingtin has a function in cellular adhesion

Using genetic models of huntingtin polyQ expansion in striatal neuronal progenitor cells, I provided the first evidence that cell-cell and cell-substrate adhesion is altered. This finding has been replicated by a variety of approaches including unbiased gene expression studies [39, 137] and targeted approaches [47]. My preliminary cell biological investigations of adhesion in the mouse embryonic stem cell models of huntingtin deficiency or polyQ expansion suggested that ES cells also display altered cell-cell and cell-substrate and that the alteration was different in huntingtin deficient compared to polyQ huntingtin expansion cells. I contributed ES cell samples to a larger transcriptional profiling study in an effort to gain unbiased global insight into what cell adhesion and cytoskeletal changes may be occurring and to address the question of whether loss of huntingtin mirrors huntingtin polyQ expansion [39]. In fact, it appears that while similar cellular pathways are influenced by either huntingtin deficiency or polyQ expansion, the specific genes altered and the direction of gene expression change differs. These studies also led directly to the development of a quantitative, embryoid body adhesion assay in 96-well format that can be used for future genetic and small molecule screening (Singh-Atwal, et al., manuscript in preparation).

New insights into conserved huntingtin function

The findings in *D. discoideum* greatly reinforce the notion from mammalian cell systems that huntingtin plays a role in cellular dynamics related to the cytoskeleton and cell adhesion, and further indicate that this function may be evolutionarily conserved. Mechanistic understanding of huntingtin function is still lacking, but my results from D. discoideum suggest that huntingtin is affecting both translational regulation and playing a role in a novel cell adhesion mechanism in early development that remains to be characterized. This research now enables dissection of molecular mechanisms through a combination of hypothesis-driven and

screening-based approaches by providing optimized genetic models in multiple organisms with well-characterized and complementary phenotypes ready for further investigation.

D. discoideum deficiency rescue with native and human huntingtin

Rescue of the *hd*- cell phenotypes with Dictyostelium and human huntingtin are essential for ongoing efforts to characterize the normal function of huntingtin and impact of CAG repeat length in this model system and validate the usefulness of the model to support parallel mammalian and human research. Another group claims to have created a full-length *D. discoideum hd* expression construct with an N-terminal GFP fusion product [46]. However, upon obtaining this construct from the DictyBase repository we found that it did not contain the *D. discoideum hd* sequence.

Numerous attempts to create cloning vectors expressing full-length human or *D. discoideum* huntingtin by colleagues in the lab and by the company GeneArt have failed; the main obstacle being the size of the HD gene. Two primary strategies have been tried thus far. The first approach involved cloning either the *D. discoideum hd* cDNA or genomic DNA using standard RT-PCR followed by PCR. However, amplification of the full-length gene product failed likely due to the size and degree of AT richness of the sequence, which produced many homodimers. Altering primers, optimizing polymerases and assay reagents, and attempting to clone in three fragments that could be sequentially stitched together are all strategies that were tried unsuccessfully by my colleagues and GeneArt independently. The second approach was a knock-in homologous recombination strategy to regenerate the genomic *hd* locus by removal of the gene disruption cassette that confers blasticidin resistance and introduction of a GFP product for selection. Clones positive for recombination event – as assessed microscopically by GFP expression – were obtained but all clones remained resistant to blasticidin and displayed characteristics phenotypes of huntingtin deficiency, indicating a failure of the double crossover event.

Interestingly, rescue of knockout *D. discoideum* mutants by electroporating endogenous *D. discoideum* or human protein into cells has been previously demonstrated [138]. My colleague, Dr. Michael Myre has successfully used this approach to demonstrate that introduction of the human huntingtin protein is capable of restoring at least one of the osmolarity-related huntingtin deficiency phenotypes (manuscript in preparation). Although this approach suffers from low and variable transformation efficiency, it provides important preliminary evidence of at least partial conservation of huntingtin function from *D. discoideum* to human. Chimeric mixing experiments with either 1:1 or 2:1 ratios of WT:*hd*- cells that I performed failed to rescue the EDTA-resistant adhesion phenotype (data not shown), suggesting that the low transformation efficiency of electroporated protein is unlikely to achieve effective rescue. However, my colleagues' success in rescue of a single cell *hd*- phenotype with purified full-length human huntingtin indicate that at least some functions of huntingtin are likely to be conserved and has motivated us to focus cloning efforts on human huntingtin expression using newly obtained *D. discoideum* vectors. Initial attempts to create a construct where human huntingtin is expressed from the endogenous *D. discoideum* promoter produced clones expressing the mRNA but that failed to produce the protein, likely as a result of codon bias. My colleagues are currently preparing a vector corrected for *D. discoideum* codon bias and anticipate obtaining and using this construct to validate the effect of the human protein on known *D. discoideum* huntingtin deficiency phenotypes in the next six months. Once this construct is obtained, modified versions of the construct will be developed with varying CAG repeat lengths. These tools are essential for addressing disease relevance of identified conserved functions.

Translation back to mammalian systems and HD

My research has contributed to mounting proof-of-principle evidence that the *D. discoideum* huntingtin deficiency model will prove useful for identifying evolutionarily conserved functions of the huntingtin protein and, by enabling huntingtin-structure function studies, will

prove useful for uncovering the effect of the CAG repeat that may ultimately be relevant to HD. Indeed, my colleague, Dr. Michael Myre is currently developing expression constructs that will lead to establishment of *D. discoideum* models of CAG repeat length modulation of huntingtin function and investigation of the relevance of specific portions of the protein to function. The true potential of *D. discoideum* is not just as a discovery tool of huntingtin conserved function, modifiers and interactors, but also as a more rapid guide to triaging the most important lines of investigation for parallel study in mammalian systems.

Development of the *D. discoideum* model combined with recent advances in the *Mus musculus* genetic models and HD patient-derived cellular systems are currently converging to allow simultaneous, mutually informative experimentation. If genetic pathways affected by CAG repeat-related huntingtin biology in *D. discoideum* overlap to some extent with the pathways discovered in human patient cells, this would validate the huntingtin conserved function approach and facilitate a new round of investigation in *D. discoideum*, where biological discovery may be faster. I have started from the hypothesis that understanding conserved, potentially essential, huntingtin function(s) may be crucial to developing effective disease-modifying therapeutic intervention. If this hypothesis is proven accurate, a synergistic approach – harnessing the strengths of each of the genetic model systems to their greatest utility – could hasten our understanding of the structural/functional features of the molecular mechanism that initiates the disease process that culminates in HD symptoms. This understanding would increase the likelihood of being able to treat patients by intervening at the initiation of the pathogenic process.

Bibliography

1. Pringsheim, T., et al., *The incidence and prevalence of Huntington's disease: A systematic review and meta-analysis.* Mov Disord, 2012. **27**(9): p. 1083-91.

2. Shannon, K.M., *Huntington's disease - clinical signs, symptoms, presymptomatic diagnosis, and diagnosis.* Handb Clin Neurol, 2011. **100**: p. 3-13.

3. Gusella, J.F. and M. Macdonald, *Genetic criteria for Huntington's disease pathogenesis.* Brain Res Bull, 2007. **72**(2-3): p. 78-82.

4. Gusella, J.F., et al., *Molecular genetics of Huntington's disease.* Arch Neurol, 1993. **50**(11): p. 1157-63.

5. Gusella, J.F., et al., *A polymorphic DNA marker genetically linked to Huntington's disease.* Nature, 1983. **306**(5940): p. 234-8.

6. Cattaneo, E., C. Zuccato, and M. Tartari, *Normal huntingtin function: an alternative approach to Huntington's disease.* Nat Rev Neurosci, 2005. **6**(12): p. 919-30.

7. Omi, K., et al., *siRNA-mediated inhibition of endogenous Huntington disease gene expression induces an aberrant configuration of the ER network in vitro.* Biochem Biophys Res Commun, 2005. **338**(2): p. 1229-35.

8. Trettel, F., et al., *Dominant phenotypes produced by the HD mutation in STHdh(Q111) striatal cells.* Hum Mol Genet, 2000. **9**(19): p. 2799-809.

9. Gusella, J.F., F. Persichetti, and M.E. MacDonald, *The genetic defect causing Huntington's disease: repeated in other contexts?* Mol Med, 1997. **3**(4): p. 238-46.

10. Djousse, L., et al., *Interaction of normal and expanded CAG repeat sizes influences age at onset of Huntington disease.* Am J Med Genet A, 2003. **119A**(3): p. 279-82.

11. Wexler, N.S., et al., *Venezuelan kindreds reveal that genetic and environmental factors modulate Huntington's disease age of onset.* Proc Natl Acad Sci U S A, 2004. **101**(10): p. 3498-503.

12. Ambrose, C.M., et al., *Structure and expression of the Huntington's disease gene: evidence against simple inactivation due to an expanded CAG repeat.* Somat Cell Mol Genet, 1994. **20**(1): p. 27-38.

13. Persichetti, F., et al., *Differential expression of normal and mutant Huntington's disease gene alleles.* Neurobiol Dis, 1996. **3**(3): p. 183-90.

14. Duyao, M.P., et al., *Inactivation of the mouse Huntington's disease gene homolog Hdh.* Science, 1995. **269**(5222): p. 407-10.

15. Wexler, N.S., et al., *Homozygotes for Huntington's disease.* Nature, 1987. **326**(6109): p. 194-7.

16. Myers, R.H., et al., *Homozygote for Huntington disease.* Am J Hum Genet, 1989. **45**(4): p. 615-8.

17. Zuccato, C., M. Valenza, and E. Cattaneo, *Molecular mechanisms and potential therapeutical targets in Huntington's disease.* Physiol Rev, 2010. **90**(3): p. 905-81.

18. MacDonald, M.E., *Huntingtin: alive and well and working in middle management.* Sci STKE, 2003. **2003**(207): p. pe48.

19. Harjes, P. and E.E. Wanker, *The hunt for huntingtin function: interaction partners tell many different stories.* Trends Biochem Sci, 2003. **28**(8): p. 425-33.

20. Seong, I.S., et al., *Huntingtin facilitates polycomb repressive complex 2.* Hum Mol Genet, 2010. **19**(4): p. 573-83.

21. Xu, Y., et al., *Structure of the protein phosphatase 2A holoenzyme.* Cell, 2006. **127**(6): p. 1239-51.

22. Lee, S.J., et al., *The adoption of a twisted structure of importin-beta is essential for the protein-protein interaction required for nuclear transport.* J Mol Biol, 2000. **302**(1): p. 251-64.

23. Bossy-Wetzel, E., R. Schwarzenbacher, and S.A. Lipton, *Molecular pathways to neurodegeneration.* Nat Med, 2004. **10 Suppl**: p. S2-9.

24. Goehler, H., et al., *A protein interaction network links GIT1, an enhancer of huntingtin aggregation, to Huntington's disease.* Mol Cell, 2004. **15**(6): p. 853-65.

25. Gusella, J.F. and M.E. MacDonald, *Huntingtin: a single bait hooks many species.* Curr Opin Neurobiol, 1998. **8**(3): p. 425-30.

26. Benn, C.L., et al., *Huntingtin modulates transcription, occupies gene promoters in vivo, and binds directly to DNA in a polyglutamine-dependent manner.* J Neurosci, 2008. **28**(42): p. 10720-33.

27. Marcora, E., K. Gowan, and J.E. Lee, *Stimulation of NeuroD activity by huntingtin and huntingtin-associated proteins HAP1 and MLK2.* Proc Natl Acad Sci U S A, 2003. **100**(16): p. 9578-83.

28. Li, J.L., et al., *A genome scan for modifiers of age at onset in Huntington disease: The HD MAPS study.* Am J Hum Genet, 2003. **73**(3): p. 682-7.

29. Kalchman, M.A., et al., *HIP1, a human homologue of S. cerevisiae Sla2p, interacts with membrane-associated huntingtin in the brain.* Nat Genet, 1997. **16**(1): p. 44-53.

30. Lee, S.J., et al., *E3 ligase activity of RING finger proteins that interact with Hip-2, a human ubiquitin-conjugating enzyme.* FEBS Lett, 2001. **503**(1): p. 61-4.

31. Faber, P.W., et al., *Huntingtin interacts with a family of WW domain proteins.* Hum Mol Genet, 1998. **7**(9): p. 1463-74.

32. Wanker, E.E., et al., *HIP-I: a huntingtin interacting protein isolated by the yeast two-hybrid system.* Hum Mol Genet, 1997. **6**(3): p. 487-95.

33. Hattula, K. and J. Peranen, *FIP-2, a coiled-coil protein, links Huntingtin to Rab8 and modulates cellular morphogenesis.* Curr Biol, 2000. **10**(24): p. 1603-6.

34. Horn, S.C., et al., *Huntingtin interacts with the receptor sorting family protein GASP2.* J Neural Transm, 2006. **113**(8): p. 1081-90.

35. Boutell, J.M., et al., *Huntingtin interacts with cystathionine beta-synthase.* Hum Mol Genet, 1998. **7**(3): p. 371-8.

36. Burke, J.R., et al., *Huntingtin and DRPLA proteins selectively interact with the enzyme GAPDH.* Nat Med, 1996. **2**(3): p. 347-50.

37. Bao, J., et al., *Expansion of polyglutamine repeat in huntingtin leads to abnormal protein interactions involving calmodulin.* Proc Natl Acad Sci U S A, 1996. **93**(10): p. 5037-42.

38. Wheeler, V.C., et al., *Length-dependent gametic CAG repeat instability in the Huntington's disease knock-in mouse.* Hum Mol Genet, 1999. **8**(1): p. 115-22.

39. Jacobsen, J.C., et al., *HD CAG-correlated gene expression changes support a simple dominant gain of function.* Hum Mol Genet, 2011. **20**(14): p. 2846-60.

40. Faber, P.W., et al., *Polyglutamine-mediated dysfunction and apoptotic death of a Caenorhabditis elegans sensory neuron.* Proc Natl Acad Sci U S A, 1999. **96**(1): p. 179-84.

41. Parker, J.A., et al., *Expanded polyglutamines in Caenorhabditis elegans cause axonal abnormalities and severe dysfunction of PLM mechanosensory neurons without cell death.* Proc Natl Acad Sci U S A, 2001. **98**(23): p. 13318-23.

42. Marsh, J.L. and L.M. Thompson, *Drosophila in the study of neurodegenerative disease.* Neuron, 2006. **52**(1): p. 169-78.

43. Zhang, S., et al., *Inactivation of Drosophila Huntingtin affects long-term adult functioning and the pathogenesis of a Huntington's disease model.* Dis Model Mech, 2009. **2**(5-6): p. 247-66.

44. Lumsden, A.L., et al., *Huntingtin-deficient zebrafish exhibit defects in iron utilization and development.* Hum Mol Genet, 2007. **16**(16): p. 1905-20.

45. Myre, M.A., et al., *Deficiency of huntingtin has pleiotropic effects in the social amoeba Dictyostelium discoideum.* PLoS Genet, 2011. **7**(4): p. e1002052.

46. Wang, Y., et al., *Dictyostelium huntingtin controls chemotaxis and cytokinesis through the regulation of myosin II phosphorylation.* Mol Biol Cell, 2011. **22**(13): p. 2270-81.

47. Lo Sardo, V., et al., *An evolutionary recent neuroepithelial cell adhesion function of huntingtin implicates ADAM10-Ncadherin.* Nat Neurosci, 2012. **15**(5): p. 713-21.

48. The Hd Ipsc, C., *Induced Pluripotent Stem Cells from Patients with Huntington's Disease Show CAG-Repeat-Expansion-Associated Phenotypes.* Cell Stem Cell, 2012. **11**(2): p. 264-78.

49. Bowers-Morrow, V.M., S.O. Ali, and K.L. Williams, *Comparison of molecular mechanisms mediating cell contact phenomena in model developmental systems: an exploration of universality.* Biol Rev Camb Philos Soc, 2004. **79**(3): p. 611-42.

50. Birbach, A., *Profilin, a multi-modal regulator of neuronal plasticity.* Bioessays, 2008. **30**(10): p. 994-1002.

51. Burnett, B.G., et al., *Expression of expanded polyglutamine targets profilin for degradation and alters actin dynamics.* Neurobiol Dis, 2008. **30**(3): p. 365-74.

52. Hoffner, G., P. Kahlem, and P. Djian, *Perinuclear localization of huntingtin as a consequence of its binding to microtubules through an interaction with beta-tubulin: relevance to Huntington's disease.* J Cell Sci, 2002. **115**(Pt 5): p. 941-8.

53. Truant, R., R.S. Atwal, and A. Burtnik, *Nucleocytoplasmic trafficking and transcription effects of huntingtin in Huntington's disease.* Prog Neurobiol, 2007. **83**(4): p. 211-27.

54. Colin, E., et al., *Huntingtin phosphorylation acts as a molecular switch for anterograde/retrograde transport in neurons.* Embo J, 2008. **27**(15): p. 2124-34.

55. Gauthier, L.R., et al., *Huntingtin controls neurotrophic support and survival of neurons by enhancing BDNF vesicular transport along microtubules.* Cell, 2004. **118**(1): p. 127-38.

56. Munsie, L., et al., *Mutant huntingtin causes defective actin remodeling during stress: defining a new role for transglutaminase 2 in neurodegenerative disease.* Hum Mol Genet, 2011. **20**(10): p. 1937-51.

57. Carnell, M.J. and R.H. Insall, *Actin on disease--studying the pathobiology of cell motility using Dictyostelium discoideum.* Semin Cell Dev Biol, 2011. **22**(1): p. 82-8.

58. Abedin, M. and N. King, *Diverse evolutionary paths to cell adhesion.* Trends Cell Biol, 2010. **20**(12): p. 734-42.

59. Coates, J.C. and A.J. Harwood, *Cell-cell adhesion and signal transduction during Dictyostelium development.* J Cell Sci, 2001. **114**(Pt 24): p. 4349-58.

60. Reis, S.A., et al., *Striatal neurons expressing full-length mutant huntingtin exhibit decreased N-cadherin and altered neuritogenesis.* Hum Mol Genet, 2011. **20**(12): p. 2344-55.

61. Vonsattel, J.P. and M. DiFiglia, *Huntington disease.* J Neuropathol Exp Neurol, 1998. **57**(5): p. 369-84.

62. *A novel gene containing a trinucleotide repeat that is expanded and unstable on Huntington's disease chromosomes. The Huntington's Disease Collaborative Research Group.* Cell, 1993. **72**(6): p. 971-83.

63. Reddy, P.H., P. Mao, and M. Manczak, *Mitochondrial structural and functional dynamics in Huntington's disease.* Brain Res Rev, 2009. **61**(1): p. 33-48.

64. Truant, R., R. Atwal, and A. Burtnik, *Hypothesis: Huntingtin may function in membrane association and vesicular trafficking.* Biochem Cell Biol, 2006. **84**(6): p. 912-7.

65. Gines, S., et al., *Specific progressive cAMP reduction implicates energy deficit in presymptomatic Huntington's disease knock-in mice.* Hum Mol Genet, 2003. **12**(5): p. 497-508.

66. Lee, J.M., et al., *Unbiased gene expression analysis implicates the huntingtin polyglutamine tract in extra-mitochondrial energy metabolism.* PLoS Genet, 2007. **3**(8): p. e135.

67. Seong, I.S., et al., *HD CAG repeat implicates a dominant property of huntingtin in mitochondrial energy metabolism.* Hum Mol Genet, 2005. **14**(19): p. 2871-80.

68. Mochel, F., et al., *Early energy deficit in Huntington disease: identification of a plasma biomarker traceable during disease progression.* PLoS One, 2007. **2**(7): p. e647.

69. Benson, D.L., D.R. Colman, and G.W. Huntley, *Molecules, maps and synapse specificity.* Nat Rev Neurosci, 2001. **2**(12): p. 899-909.

70. Takeichi, M., *The cadherin superfamily in neuronal connections and interactions.* Nat Rev Neurosci, 2007. **8**(1): p. 11-20.

71. Mandel, L.J., R.B. Doctor, and R. Bacallao, *ATP depletion: a novel method to study junctional properties in epithelial tissues. II. Internalization of Na+,K(+)-ATPase and E-cadherin.* J Cell Sci, 1994. **107 (Pt 12)**: p. 3315-24.

72. Bush, K.T., T. Tsukamoto, and S.K. Nigam, *Selective degradation of E-cadherin and dissolution of E-cadherin-catenin complexes in epithelial ischemia.* Am J Physiol Renal Physiol, 2000. **278**(5): p. F847-52.

73. Covington, M.D., et al., *Ischemia-induced cleavage of cadherins in NRK cells: evidence for a role of metalloproteinases.* Am J Physiol Renal Physiol, 2005. **289**(2): p. F280-8.

74. Covington, M.D., R.C. Burghardt, and A.R. Parrish, *Ischemia-induced cleavage of cadherins in NRK cells requires MT1-MMP (MMP-14).* Am J Physiol Renal Physiol, 2006. **290**(1): p. F43-51.

75. Hatta, K., et al., *Cloning and expression of cDNA encoding a neural calcium-dependent cell adhesion molecule: its identity in the cadherin gene family.* J Cell Biol, 1988. **106**(3): p. 873-81.

76. Takeichi, M., *Cadherins: a molecular family important in selective cell-cell adhesion.* Annu Rev Biochem, 1990. **59**: p. 237-52.

77. Aberle, H., et al., *Assembly of the cadherin-catenin complex in vitro with recombinant proteins.* J Cell Sci, 1994. **107 (Pt 12)**: p. 3655-63.

78. Knudsen, K.A., et al., *Interaction of alpha-actinin with the cadherin/catenin cell-cell adhesion complex via alpha-catenin.* J Cell Biol, 1995. **130**(1): p. 67-77.

79. Baki, L., et al., *Presenilin-1 binds cytoplasmic epithelial cadherin, inhibits cadherin/p120 association, and regulates stability and function of the cadherin/catenin adhesion complex.* Proc Natl Acad Sci U S A, 2001. **98**(5): p. 2381-6.

80. Gumbiner, B.M., *Regulation of cadherin adhesive activity.* J Cell Biol, 2000. **148**(3): p. 399-404.

81. Namura, S., et al., *The HD mutation does not alter neuronal death in the striatum of Hdh(Q92) knock-in mice after mild focal ischemia.* Neurobiol Dis, 2002. **11**(1): p. 147-54.

82. Kim, M., et al., *Huntingtin is degraded to small fragments by calpain after ischemic injury.* Exp Neurol, 2003. **183**(1): p. 109-15.

83. Peyrieras, N., et al., *Uvomorulin: a nonintegral membrane protein of early mouse embryo.* Proc Natl Acad Sci U S A, 1983. **80**(20): p. 6274-7.

84. Yoshida, C. and M. Takeichi, *Teratocarcinoma cell adhesion: identification of a cell-surface protein involved in calcium-dependent cell aggregation.* Cell, 1982. **28**(2): p. 217-24.

85. Bixby, J.L. and R. Zhang, *Purified N-cadherin is a potent substrate for the rapid induction of neurite outgrowth.* J Cell Biol, 1990. **110**(4): p. 1253-60.

86. Goodwin, M. and A.S. Yap, *Classical cadherin adhesion molecules: coordinating cell adhesion, signaling and the cytoskeleton.* J Mol Histol, 2004. **35**(8-9): p. 839-44.

87. Bamji, S.X., *Cadherins: actin with the cytoskeleton to form synapses.* Neuron, 2005. **47**(2): p. 175-8.

88. Bamji, S.X., et al., *Role of beta-catenin in synaptic vesicle localization and presynaptic assembly.* Neuron, 2003. **40**(4): p. 719-31.

89. Muhlrad, A., et al., *Antagonistic effects of cofilin, beryllium fluoride complex, and phalloidin on subdomain 2 and nucleotide-binding cleft in F-actin.* Biophys J, 2006. **91**(12): p. 4490-9.

90. Regalado, M.P., et al., *Transsynaptic signaling by postsynaptic synapse-associated protein 97.* J Neurosci, 2006. **26**(8): p. 2343-57.

91. Togashi, H., et al., *Cadherin regulates dendritic spine morphogenesis.* Neuron, 2002. **35**(1): p. 77-89.

92. Bozdagi, O., et al., *Temporally distinct demands for classic cadherins in synapse formation and maturation.* Mol Cell Neurosci, 2004. **27**(4): p. 509-21.

93. Garner, C.C., C.L. Waites, and N.E. Ziv, *Synapse development: still looking for the forest, still lost in the trees.* Cell Tissue Res, 2006. **326**(2): p. 249-62.

94. Clabough, E.B. and S.O. Zeitlin, *Deletion of the triplet repeat encoding polyglutamine within the mouse Huntington's disease gene results in subtle behavioral/motor phenotypes in vivo and elevated levels of ATP with cellular senescence in vitro.* Hum Mol Genet, 2006. **15**(4): p. 607-23.

95. Braga, V.M., *Small GTPases and regulation of cadherin dependent cell-cell adhesion.* Mol Pathol, 1999. **52**(4): p. 197-202.

96. Watanabe, T., K. Sato, and K. Kaibuchi, *Cadherin-mediated intercellular adhesion and signaling cascades involving small GTPases.* Cold Spring Harb Perspect Biol, 2009. **1**(3): p. a003020.

97. Markianos, M., et al., *Low plasma total cholesterol in patients with Huntington's disease and first-degree relatives.* Mol Genet Metab, 2008. **93**(3): p. 341-6.

98. Swayne, L.A., et al., *Crosstalk between huntingtin and syntaxin 1A regulates N-type calcium channels.* Mol Cell Neurosci, 2005. **30**(3): p. 339-51.

99. Valenza, M., et al., *Cholesterol defect is marked across multiple rodent models of Huntington's disease and is manifest in astrocytes.* J Neurosci, 2010. **30**(32): p. 10844-50.

100. Pardo, R., et al., *pARIS-htt: an optimised expression platform to study huntingtin reveals functional domains required for vesicular trafficking.* Mol Brain, 2010. **3**: p. 17.

101. Martinez-Vicente, M., et al., *Cargo recognition failure is responsible for inefficient autophagy in Huntington's disease.* Nat Neurosci, 2010. **13**(5): p. 567-76.

102. Pal, A., et al., *Huntingtin-HAP40 complex is a novel Rab5 effector that regulates early endosome motility and is up-regulated in Huntington's disease.* J Cell Biol, 2006. **172**(4): p. 605-18.

103. Strehlow, A.N., J.Z. Li, and R.M. Myers, *Wild-type huntingtin participates in protein trafficking between the Golgi and the extracellular space.* Hum Mol Genet, 2007. **16**(4): p. 391-409.

104. Bruses, J.L., *N-cadherin signaling in synapse formation and neuronal physiology.* Mol Neurobiol, 2006. **33**(3): p. 237-52.

105. Tan, Z.J., et al., *N-cadherin-dependent neuron-neuron interaction is required for the maintenance of activity-induced dendrite growth.* Proc Natl Acad Sci U S A, 2010. **107**(21): p. 9873-8.

106. Molero, A.E., et al., *Impairment of developmental stem cell-mediated striatal neurogenesis and pluripotency genes in a knock-in model of Huntington's disease.* Proc Natl Acad Sci U S A, 2009. **106**(51): p. 21900-5.

107. Stan, A., et al., *Essential cooperation of N-cadherin and neuroligin-1 in the transsynaptic control of vesicle accumulation.* Proc Natl Acad Sci U S A, 2010. **107**(24): p. 11116-21.

108. Lynch, G., et al., *Brain-derived neurotrophic factor restores synaptic plasticity in a knock-in mouse model of Huntington's disease.* J Neurosci, 2007. **27**(16): p. 4424-34.

109. Nopoulos, P.C., et al., *Smaller intracranial volume in prodromal Huntington's disease: evidence for abnormal neurodevelopment.* Brain, 2011. **134**(Pt 1): p. 137-42.

110. Simmons, D.A., et al., *Up-regulating BDNF with an ampakine rescues synaptic plasticity and memory in Huntington's disease knockin mice.* Proc Natl Acad Sci U S A, 2009. **106**(12): p. 4906-11.

111. Jenkins, B.G., et al., *1H NMR spectroscopy studies of Huntington's disease: correlations with CAG repeat numbers.* Neurology, 1998. **50**(5): p. 1357-65.

112. Saft, C., et al., *Mitochondrial impairment in patients and asymptomatic mutation carriers of Huntington's disease.* Mov Disord, 2005. **20**(6): p. 674-9.

113. Sturrock, A. and B.R. Leavitt, *The clinical and genetic features of Huntington disease.* J Geriatr Psychiatry Neurol, 2010. **23**(4): p. 243-59.

114. Auerbach, W., et al., *The HD mutation causes progressive lethal neurological disease in mice expressing reduced levels of huntingtin.* Hum Mol Genet, 2001. **10**(22): p. 2515-23.

115. White, J.K., et al., *Huntingtin is required for neurogenesis and is not impaired by the Huntington's disease CAG expansion.* Nat Genet, 1997. **17**(4): p. 404-10.

116. Gusella, J.F. and M.E. Macdonald, *Huntington's disease: seeing the pathogenic process through a genetic lens.* Trends Biochem Sci, 2006. **31**(9): p. 533-40.

117. Noegel, A.A. and M. Schleicher, *The actin cytoskeleton of Dictyostelium: a story told by mutants.* J Cell Sci, 2000. **113 (Pt 5)**: p. 759-66.

118. Siu, C.H., et al., *Regulation of cell-cell adhesion during Dictyostelium development.* Semin Cell Dev Biol, 2004. **15**(6): p. 633-41.

119. Gerisch, G., et al., *Control of cell-contact sites by cyclic AMP pulses in differentiating Dictyostelium cells.* Nature, 1975. **255**(5509): p. 547-9.

120. Noegel, A., et al., *Complete sequence and transcript regulation of a cell adhesion protein from aggregating Dictyostelium cells.* EMBO J, 1986. **5**(7): p. 1473-6.

121. Siu, C.H., A. Cho, and A.H. Choi, *The contact site A glycoprotein mediates cell-cell adhesion by homophilic binding in Dictyostelium discoideum.* J Cell Biol, 1987. **105**(6 Pt 1): p. 2523-33.

122. Sesaki, H., E.F. Wong, and C.H. Siu, *The cell adhesion molecule DdCAD-1 in Dictyostelium is targeted to the cell surface by a nonclassical transport pathway involving contractile vacuoles.* J Cell Biol, 1997. **138**(4): p. 939-51.

123. Sriskanthadevan, S., et al., *Cell adhesion molecule DdCAD-1 is imported into contractile vacuoles by membrane invagination in a Ca2+- and conformation-dependent manner.* J Biol Chem, 2009. **284**(52): p. 36377-86.

124. Faix, J., G. Gerisch, and A.A. Noegel, *Constitutive overexpression of the contact site A glycoprotein enables growth-phase cells of Dictyostelium discoideum to aggregate.* Embo J, 1990. **9**(9): p. 2709-16.

125. Gross, J.D., *Acidic Ca2+ stores, excitability, and cell patterning in Dictyostelium discoideum.* Eukaryot Cell, 2009. **8**(5): p. 696-702.

126. Malchow, D., et al., *Cyclic AMP-induced pH changes in Dictyostelium discoideum and their control by calcium.* Biochim Biophys Acta, 1978. **538**(3): p. 473-80.

127. Wick, U., D. Malchow, and G. Gerisch, *Cyclic-AMP stimulated calcium influx into aggregating cells of Dictyostelium discoideum.* Cell Biol Int Rep, 1978. **2**(1): p. 71-9.

128. Hohmann, H.P., et al., *Two-step glycosylation of the contact site A protein of Dictyostelium discoideum and transport of an incompletely glycosylated form to the cell surface.* J Biol Chem, 1987. **262**(34): p. 16618-24.

129. Hagenston, A.M. and H. Bading, *Calcium signaling in synapse-to-nucleus communication.* Cold Spring Harb Perspect Biol, 2011. **3**(11): p. a004564.

130. West, A.E., et al., *Calcium regulation of neuronal gene expression.* Proc Natl Acad Sci U S A, 2001. **98**(20): p. 11024-31.

131. Iketani, M., et al., *Regulation of neurite outgrowth mediated by localized phosphorylation of protein translational factor eEF2 in growth cones.* Dev Neurobiol, 2012.

132. Marchesini, N., et al., *Acidocalcisomes are functionally linked to the contractile vacuole of Dictyostelium discoideum.* J Biol Chem, 2002. **277**(10): p. 8146-53.

133. Malchow, D., et al., *The contractile vacuole in Ca2+-regulation in Dictyostelium: its essential function for cAMP-induced Ca2+-influx.* BMC Dev Biol, 2006. **6**: p. 31.

134. Bozzaro, S., R. Merkl, and G. Gerisch, *Cell adhesion: its quantification, assay of the molecules involved, and selection of defective mutants in Dictyostelium and Polysphondylium.* Methods Cell Biol, 1987. **28**: p. 359-85.

135. Bertholdt, G., et al., *Carbohydrate and other epitopes of the contact site A glycoprotein of Dictyostelium discoideum as characterized by monoclonal antibodies.* Cell Differ, 1985. **16**(3): p. 187-202.

136. Sesaki, H. and C.H. Siu, *Novel redistribution of the Ca(2+)-dependent cell adhesion molecule DdCAD-1 during development of Dictyostelium discoideum.* Dev Biol, 1996. **177**(2): p. 504-16.

137. Tang, B., et al., *Gene expression profiling of R6/2 transgenic mice with different CAG repeat lengths reveals genes associated with disease onset and progression in Huntington's disease.* Neurobiol Dis, 2011. **42**(3): p. 459-67.

138. Yumura, S., R. Matsuzaki, and T. Kitanishi-Yumura, *Introduction of macromolecules into living Dictyostelium cells by electroporation.* Cell Struct Funct, 1995. **20**(3): p. 185-90.

Appendix A

Reprint of:

Reis, S. A., Thompson, M. N., Lee, J. M., Fossale, E., Kim, H., Liao, J. K., Moskowitz, M. A., Shaw, S. Y., Dong, L., Hagarty, S. J., MacDonald, M. E., Seong, I. S. *Striatal neurons expressing full-length mutant huntingtin exhibit decreased N-cadherin and altered neuritogenesis.* Hum Mol Genet, 2011. **20**(12): p. 2344-55.

Attributions

My question:

Pertaining to this manuscript, the question I personally sought to address was: Is cell adhesion altered in cells appropriately expressing huntingtin with an expanded polyQ tract?

My research contributions:

I performed immunofluorescence microscopy of cytoskeleton & cell adhesion markers (Figure 2.5 A and D) and identified a cell “rounding” phenotype (described in Results section text) in mouse striatal neuronal progenitor cells with the HD mutation.

Significance:

My data was the first demonstration that cell-cell and cell-substrate adhesion are altered by the HD mutation and knowledge of the ‘rounding’ phenotype prompted the neuritogenesis assay showing altered neurite development in primary striatal cultures.

Human Molecular Genetics, 2011, Vol. 20, No. 12 **2344–2355**
doi:10.1093/hmg/ddr127
Advance Access published on March 29, 2011

Striatal neurons expressing full-length mutant huntingtin exhibit decreased N-cadherin and altered neuritogenesis

Surya A. Reis[1,†], Morgan N. Thompson[1], Jong-Min Lee[1], Elisa Fossale[1], Hyung-Hwan Kim[4], James K. Liao[4], Michael A. Moskowitz[5], Stanley Y. Shaw[2], Linda Dong[1], Stephen J. Haggarty[3], Marcy E. MacDonald[1] and Ihn Sik Seong[1,*]

[1]Molecular Neurogenetics Unit, Center for Human Genetic Research, [2]Center for Systems Biology and [3]Chemical Biology Program, Center for Human Genetic Research, Massachusetts General Hospital, 185 Cambridge Street, Boston, MA 02114, USA, [4]Vascular Medicine Research Unit, Brigham and Women's Hospital and Harvard Medical School, Cambridge, MA 02139, USA and [5]Stroke and Neurovascular Regulation, Massachusetts General Hospital, Charlestown, MA 02129, USA

Received February 8, 2011; Revised March 16, 2011; Accepted March 23, 2011

The expanded CAG repeat that causes striatal cell vulnerability in Huntington's disease (HD) encodes a polyglutamine tract in full-length huntingtin that is correlated with cellular [ATP] and [ATP/ADP]. Since striatal neurons are vulnerable to energy deficit, we have investigated, in *Hdh* CAG knock-in mice and striatal cells, the hypothesis that decreased energetics may affect neuronal (N)-cadherin, a candidate energy-sensitive adhesion protein that may contribute to HD striatal cell sensitivity. *In vivo*, N-cadherin was sensitive to ischemia and to the effects of full-length mutant huntingtin, progressively decreasing in Hdh^{Q111} striatum with age. In cultured striatal cells, N-cadherin was decreased by ATP depletion and STHdh^{Q111} striatal cells exhibited dramatically decreased N-cadherin, due to decreased *Cdh2* mRNA and enhanced N-cadherin turnover, which was partially normalized by adenine supplementation to increase [ATP] and [ATP/ADP]. Consistent with decreased N-cadherin function, STHdh^{Q111} striatal cells displayed profound deficits in calcium-dependent N-cadherin-mediated cell clustering and cell–substratum adhesion, and primary Hdh^{Q111} striatal neuronal cells exhibited decreased N-cadherin and an abundance of immature neurites, featuring diffuse, rather than clustered, staining for N-cadherin and synaptic vesicle markers, which was partially rescued by adenine treatment. Thus, mutant full-length huntingtin, via energetic deficit, contributes to decreased N-cadherin levels in striatal neurons, with detrimental effects on neurite maturation, strongly suggesting that N-cadherin-mediated signaling merits investigation early in the HD pathogenic disease process.

INTRODUCTION

The CAG expansion mutation that causes Huntington's disease (HD) elongates a polymorphic polyglutamine segment in the huntingtin protein. Full-length huntingtin with a polyglutamine region of more than ~37 residues initiates a disease process that culminates in the loss of neurons, especially in the striatum, and the onset of the motor, psychiatric and cognitive symptoms (1,2). Understanding the rate-limiting events that contribute to the early vulnerability of striatal neurons would guide efforts to track the natural history of the disease and may provide new avenues for therapeutic development.

Studies investigating the earliest consequences of full-length mutant huntingtin, in HD patient cells and tissues and in genetically accurate *Hdh* CAG knock-in mouse cells and tissues, have revealed perturbations in membrane vesicle trafficking, gene transcription, intracellular signaling pathways

*To whom correspondence should be addressed. Tel: +1 6176439851; Fax: +1 6176433202; Email: iseong@chgr.mgh.harvard.edu
†Present address: Chemical Biology Programs, Center for Human Genetic Research, Massachusetts General Hospital, 185 Cambridge Street, Boston, MA 02114, USA.

(3–6), as well as altered energetics, characterized by decreased [ATP] and [ATP/ADP], which is correlated with the size of the polyglutamine repeat (7–9). We have been studying the effects of altered energetics because the correlation of energetic measures with the polyglutamine repeat in full-length huntingtin implies a dominant effect that conforms to the genetic features of the HD trigger mechanism, and energetic defects, thought to be important to striatal cells, may be evident throughout the lifetime of the cell (7–9). Certainly, early weight loss in HD and a systemic metabolic defect in branched chain amino acids are consistent with a systemic attempt to compensate for an early energy deficit (10).

Neuronal (N)-cadherin, which is intimately involved in neuronal cell adhesion, signaling, differentiation and synapse function (11,12), is a prime candidate for being affected by energy deficit. Members of the cadherin family exhibit selective degradation in response to renal ischemia and ATP depletion (13–15), and in normal rat kidney cells via cleavage by membrane-type 1 matrix metalloprotease (MT-MMP) (16). However, N-cadherin has not been studied either in acute neuronal ischemia and ATP depletion or in response to the HD mutation, which elicits a chronic energy deficit in a process that culminates in neurodegeneration.

N-cadherin is a transmembrane cell adhesion glycoprotein composed of an extracellular domain, a single-pass transmembrane region and a cytoplasmic tail (17). N-cadherin molecules make calcium-dependent homophilic bonds between their extracellular domains (18). The cytoplasmic domain contains two main binding regions, the C-terminal domain (CTD) and the juxtamembrane domain (JMD). The CTD binds β- and γ-catenin, which in turn associate with the actin cytoskeleton to modulate cell adhesion and mobility via α-catenin (19,20). The JMD interacts with p120-catenin and with presenilin 1, which has emerged as a potential regulator of cell adhesion and neuronal physiology (21,22).

Here, we have assessed the candidacy of N-cadherin as an energy-sensitive contributor to the striatal cell vulnerability that ensues from the HD mutation. Specifically, we have investigated N-cadherin in Hdh^{Q111} CAG knock-in mouse striatum and cultured Hdh^{Q111} striatal neuronal cells, which express endogenous full-length 111-glutamine mutant huntingtin. We first tested whether N-cadherin was sensitive to acute ATP depletion/ischemia and to the chronic effects of full-length mutant huntingtin protein and then we evaluated immortalized STHdh^{Q111} and primary Hdh^{Q111} striatal neurons to explore N-cadherin ATP sensitivity and the phenotypic consequences of decreased N-cadherin function. Our findings reveal that N-cadherin is an ATP-sensitive protein that is associated with altered HD CAG striatal cell adhesion and neuritogenesis.

RESULTS

Striatal N-cadherin was sensitive to acute ischemia and to the HD CAG mutation

To assess whether N-cadherin might be affected in a mild ischemic brain injury paradigm where the striatum displays early vulnerability, we performed transient middle cerebral artery (MCA) occlusion with 12-month-old wild-type $Hdh^{Q7/Q7}$ and mutant $Hdh^{Q111/Q111}$ knock-in mice. For both genotypes, immunoblot of protein extracts at 24 h after reperfusion (Fig. 1A and B) revealed robustly decreased N-cadherin in the ischemic, compared with the contralateral, striatal hemispheres. Both the reduction in N-cadherin and the infarct size (at 30 and 60 min) were similar in wild-type and mutant brain, consistent with a previous report demonstrating that CAG expansion did not sensitize to acute ischemic injury (23). In contrast, full-length wild-type 7-glutamine huntingtin and 111-glutamine mutant huntingtin cleaved by calpains in response to severe ischemia (24), α-catenin and β-catenin were not decreased, though p120 was slightly reduced by ischemia, attesting to the mildness of the lesion and demonstrating the exquisite sensitivity of N-cadherin in the striatum to ischemia.

The immunoblot results also revealed reduced N-cadherin in contralateral $Hdh^{Q111/Q111}$ striata compared with wild-type striata, suggesting an effect of the CAG mutation. This was confirmed by immunoblot analysis of wild-type and $Hdh^{Q111/Q111}$ striatal tissues at different ages, which revealed a progressive decrease in N-cadherin (normalized to α-tubulin) from 3 to 5 months of age that reached statistical significance by 12 months of age (Supplementary Material, Fig. S1).

Notably, N-cadherin (*Cdh2*) mRNA levels were not reduced in total striatal tissue, following ischemic reperfusion or in response to the CAG mutation (data not shown), implying that cell-specific and/or multiple mechanisms may contribute to the energy-dependent N-cadherin decrease *in vivo*.

Striatal cell N-cadherin was sensitive to ATP depletion and the HD CAG mutation

We then assessed whether N-cadherin might be sensitive to ATP depletion and to the CAG mutation in cultured ST$Hdh^{Q7/Q7}$ and ST$Hdh^{Q111/Q111}$ striatal neuronal cells expressing wild-type (7-glutamine) and mutant (111-glutamine) full-length huntingtin, respectively. Cells were treated with 2-deoxyglucose and antimycin A, to inhibit both glycolysis and mitochondrial respiration, and nucleotides in cellular extracts were measured by HPLC analysis. As reported previously (7,8), the baseline [ATP/ADP] was significantly lower in mutant, compared with wild-type, striatal cells, and, for both genotypes, [ATP/ADP] was dramatically decreased within 2 h of energy depletion (Supplementary Material, Fig. S2A), although cell viability was not significantly changed (Supplementary Material, Fig. S2B). Immunoblot analysis revealed that N-cadherin was decreased at baseline in mutant, compared with wild-type, striatal cell extracts, with a progressive reduction over the time course of ATP depletion for both genotypes (Fig. 1C). In contrast, α-catenin, β-catenin and p120 levels were similar for cells of either genotype and were not changed by ATP depletion (Fig. 1C). Thus, the N-cadherin level was reduced concomitant with decreased [ATP/ADP], both due to purposeful energy depletion and in response to ATP deficit due to full-length mutant huntingtin.

Further analyses demonstrated that decreased N-cadherin in mutant, compared with wild-type, striatal cells reflected decreased *Cdh2* mRNA, as demonstrated by the results of

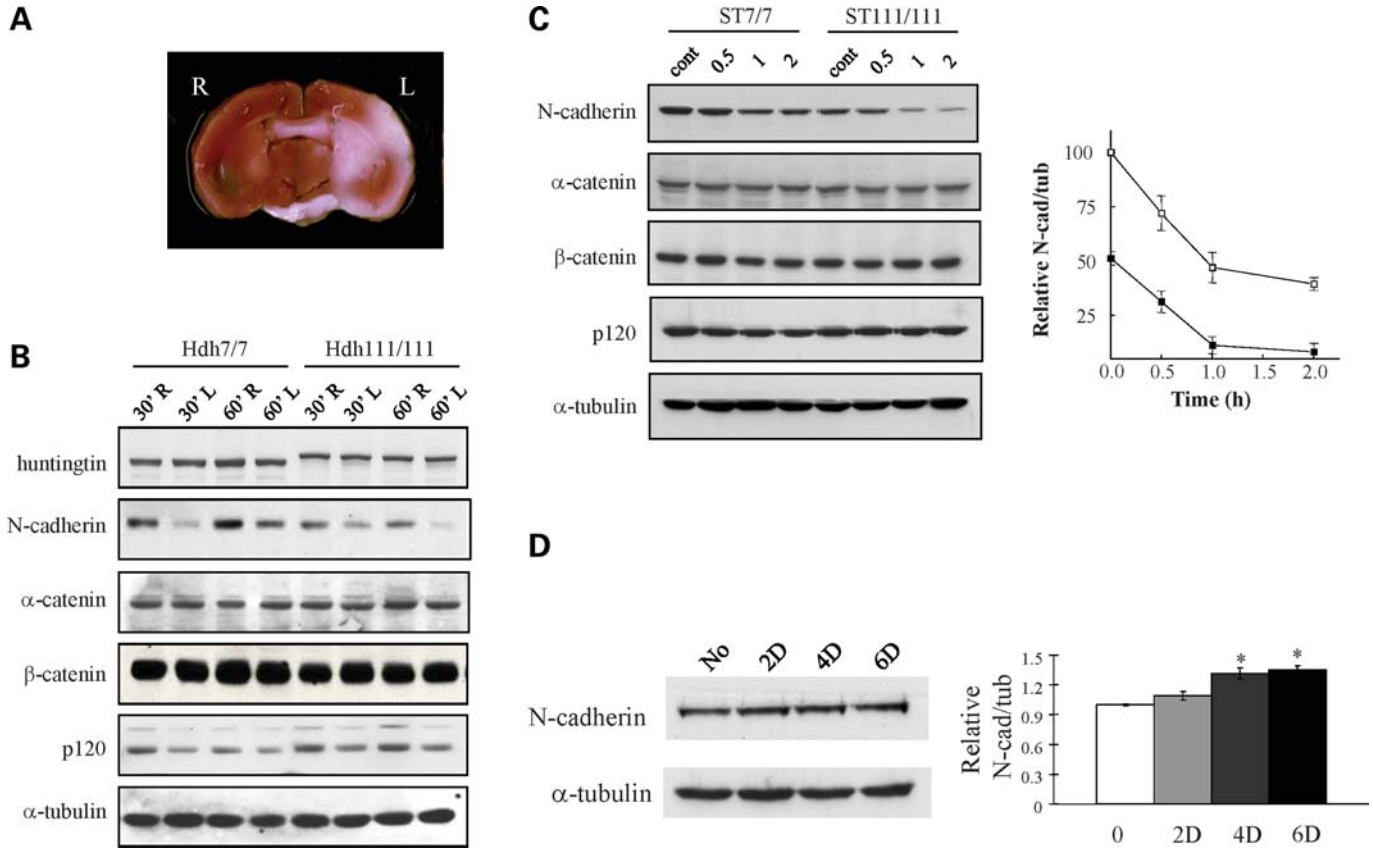

Figure 1. ATP-sensitive N-cadherin stability. (**A**) A representative coronal section of wild-type $Hdh^{Q7/Q7}$ mouse brain, following MCA occlusion/reperfusion, stained with 2,3,5-triphenyltetrazolium chloride (TTC), to demonstrate the infarct region (white area) in the left hemisphere (L), as well as the contralateral right hemisphere (R). The infarct sizes (mm^3 and mean ± standard errors) were measured from mice brains of both genotypes at 30 and 60 min MCA occlusion as 33.9 ± 3.64 and 35.2 ± 3.55 for wild-type brain at 30 and 60 min and 41.5 ± 5.97 and 43.1 ± 6.81 for mutant brain and showed no significant differences by genotypes and times ($n = 3$), consistent with the previous report (23). (**B**) Immunoblot showing bands of N-cadherin, β-catenin, α-catenin and p120 detected in protein extracts of striata from the MCA-occluded hemisphere (L) and contralateral hemisphere (R) for wild-type $Hdh^{Q7/Q7}$ (Hdh7/7) and mutant $Hdh^{Q111/Q111}$ (Hdh111/111) mice, with 30 min MCA occlusion (30′) or 60 min MCA occlusion (60′), demonstrating decreased N-cadherin on the lesion side, relative to the α-tubulin loading control band. However, the reduction in N-cadherin was not statistically different between two genotypes or two occlusion times ($n = 3$). (**C**) Immunoblot showing bands of N-cadherin, β-catenin, α-catenin and p120 detected in protein extracts of wild-type ST$Hdh^{Q7/Q7}$ (ST7/7) and mutant ST$Hdh^{Q111/Q111}$ (ST111/111) cells, at time 0 (cont), and 0.5, 1 and 2 h in ATP-depletion medium. The adjacent graph plots the relative band intensity of N-cadherin normalized to α-tubulin in the same lane (*y*-axis), with the time in ATP-depleting medium (*x*-axis), illustrating decreased N-cadherin in mutant cells at baseline and ATP-sensitive degradation of N-cadherin in cells of both genotypes. Bars denote the standard deviation from three independent experiments. (**D**) Immunoblot showing N-cadherin in extracts of ST$Hdh^{Q111/Q111}$ cells, after incubation in medium supplemented with 10 μM adenine for 0, 2, 4 and 6 days (D), relative to the α-tubulin band. The adjacent bar graph plots the relative N-cadherin intensities normalized to the α-tubulin band intensities (*y*-axis) for the time points analyzed (*x*-axis). Relative to the untreated control, N-cadherin levels were significantly elevated by day 4 ($^*P < 0.05$, $n = 3$).

RT–PCR analysis (Supplementary Material, Fig. S3A), as well as the increased turnover rate of the protein, which had a half-life of ∼2 h in ST$Hdh^{Q111/Q111}$ cells compared with a half-life of >4 h in wild-type cells (Supplementary Material, Fig. S3B). To explore the energy sensitivity of these measures, mutant striatal cell culture medium was supplemented with adenine, a precursor of high-energy nucleotides. By 2 days, [ATP/ADP] was mildly but significantly elevated (Supplementary Material, Fig. S2C), and by 4 days of treatment, N-cadherin was modestly but consistently increased (Fig. 1D), though *Cdh2* mRNA levels were not altered over the entire 6 day time course (data not shown). These results suggested that enhanced N-cadherin protein turnover in the mutant striatal cells may involve an energy-sensitive process, while altered *Cdh2* mRNA may reflect a different underlying process. However, assays to explore the involvement of metalloproteases, activated in ischemia, failed to disclose elevated MT-MMP, and MT-MMP inhibition with GM-6001 did not alter the half-life of N-cadherin in mutant striatal cells (data not shown).

ST$Hdh^{Q111/Q111}$ cells exhibited deficits in N-cadherin-mediated cell–cell adhesion

The potential functional consequences of decreased N-cadherin in mutant striatal cells were then evaluated, beginning with confocal microscopy to investigate N-cadherin subcellular localization. Wild-type ST$Hdh^{Q7/Q7}$ cells exhibited prominent N-cadherin immunostain at cell–cell contacts, whereas mutant striatal cells displayed a decreased N-cadherin signal that was not prominent at cell–cell contacts (Fig. 2A), strongly implying a defect in calcium-dependent

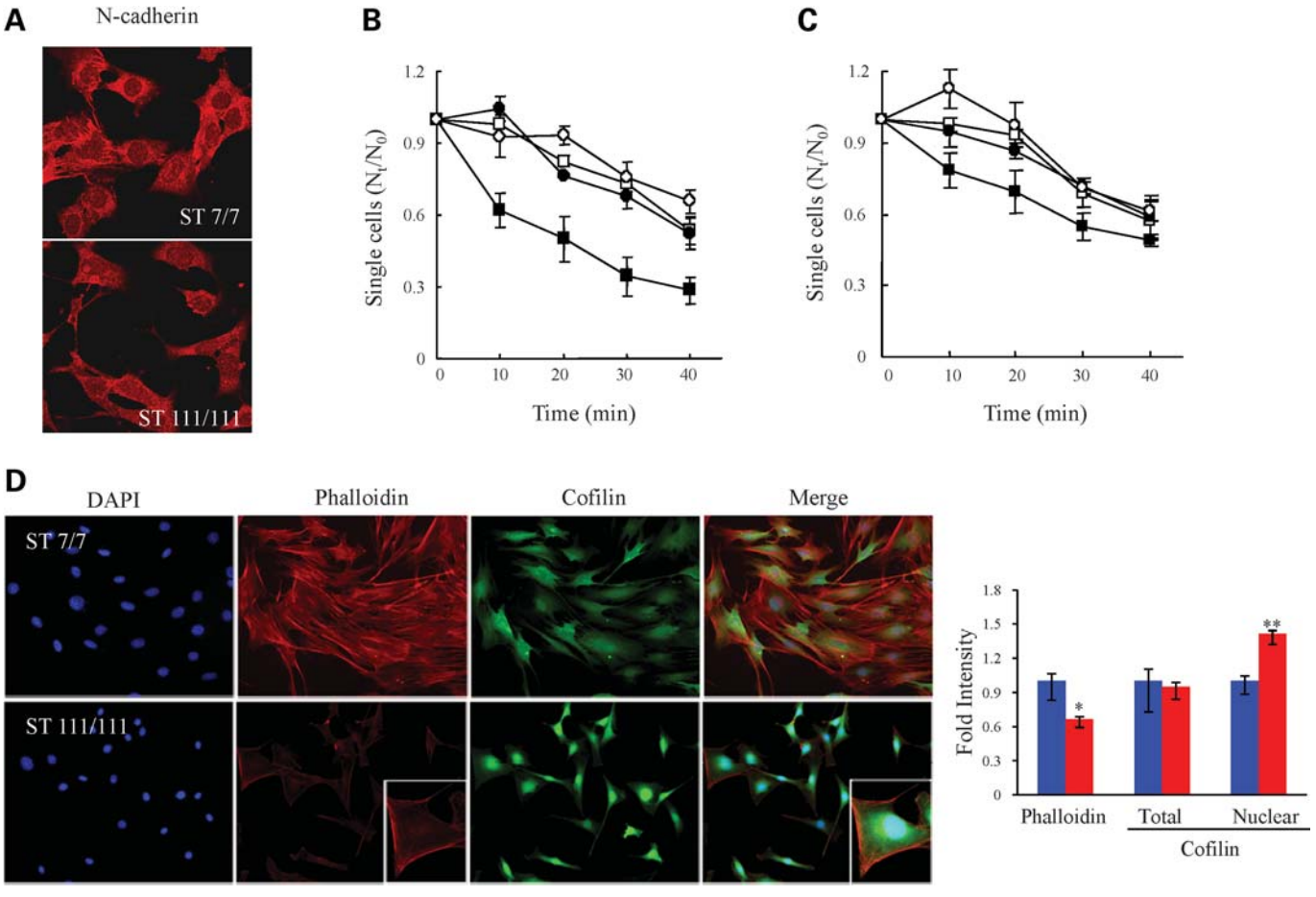

Figure 2. ST*Hdh*$^{Q111/Q111}$ striatal cells exhibited decreased N-cadherin function. (**A**) Confocal images of the N-cadherin immunostain signal (red) in wild-type ST*Hdh*$^{Q7/Q7}$ (ST7/7) and ST*Hdh*$^{Q111/Q111}$ (ST111/111) striatal cells, indicating decreased N-cadherin signal at ST*Hdh*$^{Q111/Q111}$cell–cell contacts. (**B**) Plot summarizing the results of three independent cell-clustering assays, showing the proportion of single cells compared with time zero (N_t/N_0) (*y*-axis) relative to time of clustering (*x*-axis) for ST*Hdh*$^{Q7/Q7}$ (square) and ST*Hdh*$^{Q111/Q111}$ (circle) striatal cells, in the absence (open symbols) and presence (closed symbols) of Ca^{2+}, illustrating that mutant striatal cells exhibit impaired calcium-dependent clustering. Error bars denote the standard deviation. (**C**) Plot summarizing the results of three independent ST*Hdh*$^{Q111/Q111}$ cell-clustering assays for cells transfected with the phN-cad human N-cadherin expression vector (squares) or with the control vector (circles), performed in the absence (open symbols) and presence (closed symbols) of Ca^{2+}. Error bars denote the standard deviation. (**D**) Fluorescence images of ST*Hdh*$^{Q7/Q7}$ (ST7/7) and ST*Hdh*$^{Q111/Q111}$ (ST111/111) striatal cells, showing the pattern of DAPI (blue) nuclei, TRITC–phalloidin (red) F-actin signal and anti-cofilin (green) immunostain, illustrating decreased nuclear size, paucity of actin stress fibers and bright perinuclear cofilin stain of the mutant cells, consistent with an elongated rounded-up (less flat) morphology. The adjacent bar graph shows the average phalloidin signal and the total or nuclear area cofilin intensities. The average intensity of the phalloidin signal was significantly reduced in mutant striatal cells ($^{*}P < 0.001$) and the inset was taken at different exposure conditions to examine the pattern of the phalloidin signal in mutant cells. The average intensity of the total cofilin signal was not altered but its localization was shifted to the nuclear and perinuclear region ($^{**}P < 0.001$). Error bars represent standard errors.

N-cadherin-mediated cell–cell adhesion (25,26). To assess this possibility, wild-type ST*Hdh*$^{Q7/Q7}$ and mutant ST*Hdh*$^{Q111/Q111}$ cells were evaluated in a cell-clustering assay, which measured the time taken for detached single cells to form clusters (Fig. 2B). Within 30 min of dispersal to single cells, 70% of the wild-type cells, but only 30% of the mutant striatal cells, formed clusters in Ca^{2+}-containing media, though cells of both genotypes exhibited similar Ca^{2+}-independent (in EGTA) cell clustering. This phenotype was N-cadherin dependent, as exogenous expression of N-cadherin, after transfection, raised N-cadherin levels to ~50% of wild-type levels (Supplementary Material, Fig. S3C) and partially rescued the mutant cell deficit in Ca^{2+}-dependent cluster formation. At 30 min after being dispersed, ~20% more N-cadherin-transfected mutant striatal cells formed clusters in Ca^{2+} media, compared with mutant cells transfected with the control vector (Fig. 2C). In the absence of Ca^{2+} (in EGTA), the transfection of N-cadherin had no effect on cell–cell adhesion.

ST*Hdh*$^{Q111/Q111}$ cells exhibited deficits in cell–substratum adhesion

N-cadherin is known to regulate cell–substratum adhesion (27) and actin cytoskeleton dynamics (28,29). Consequently, co-stained striatal cells were monitored by epifluorescence microscopy to detect DAPI-stained nuclei and filamentous actin (F-actin) cytoskeletal-binding proteins (Fig. 2D). Compared with wild-type ST*Hdh*$^{Q7Q/7}$ cells, the mutant ST*Hdh*$^{Q111/Q111}$ striatal cells appeared smaller with elongated shapes, and decreased stress fiber-like rhodamine–phalloidin signal, though in the inset the pattern of the phalloidin

signal resembled that of wild-type cells (Fig. 2D). Consistent with the elongated (less flat) morphology, mutant striatal cells exhibited smaller DAPI-stained nuclei and the significant intense cofilin stain of the mutant cells was localized to the nuclear and perinuclear region, although quantification demonstrated that the total cofilin signal in mutant and wild-type cells was similar (Fig. 2D). The mutant striatal cells also exhibited a similar nuclear/perinuclear immunostaining pattern for profilin, another F-actin-binding protein, which, like cofilin, is involved in actin filament structure and dynamics (30) (data not shown). Notably, immunoblot revealed similar levels of F-actin, and actin monomer (G-actin), in extracts of mutant and wild-type striatal cells (data not shown). Thus, rather than lacking an actin cytoskeleton, the altered subcellular patterns of actin-associated proteins, along with decreased N-cadherin, were consistent with the elongated, less flat morphology of the striatal cells expressing full-length mutant huntingtin and strongly implied deficits in cell–substrate adhesion, as well as cell–cell adhesion.

Hdh$^{Q111/Q111}$ primary striatal neuronal cells exhibited decreased N-cadherin and immature neuritis

N-cadherin-mediated cell–substrate adhesion promotes neurite outgrowth (27) and N-cadherin is required for proper vesicle clustering essential for neurite formation and maturation (31–34). To evaluate the potential impact of full-length mutant huntingtin on N-cadherin function in developing striatal neurons, we examined primary neuronal cell cultures from the striatum of E14 control and *Hdh*$^{Q111/Q111}$ knock-in mouse embryos. At day 10 of differentiation (days *in vitro*, *div*10), F-actin rhodamine–phalloidin binding was assessed by confocal microscopy, as a surrogate for proper actin cytoskeleton/cell–substratum adhesion, and cultures were immunostained to detect MAP2, a neuronal cell microtubule-associated protein, to evaluate the developing neuronal cell projections. Compared with wild-type primary striatal neuronal cells, the primary *Hdh*$^{Q111/Q111}$ cells exhibited decreased rhodamine–phalloidin stain and an abnormally robust network of fine MAP2-stained projections, which confirmed neuronal cell differentiation, while implying altered adhesion and development (Fig. 3).

Consistent with decreased N-cadherin function, co-staining revealed dramatically decreased N-cadherin signal, detected in β-III-tubulin-positive *Hdh*$^{Q111/Q111}$ striatal neuronal cells, compared with the intense signal of wild-type striatal cells (Fig. 4A), with only weak diffuse stain along the projections instead of the bright punctate pattern of wild-type cells (Fig. 4A inset, quantified in Supplementary Material, Fig. S4A and B). This observation implied that the synaptic vesicles that transport N-cadherin were not clustered, as expected of mature neurites, but instead were distributed along the processes in the diffuse pattern characteristic of immature neurons (35).

To explore the potential developmental deficits, β-III-tubulin-positive neuronal cell processes (here called neurites) of *div*10 primary neuronal cells were quantified. Automated image analysis revealed that mutant cells exhibited a 3-fold increase in total length of β-III-tubulin-positive neurites, compared with wild-type striatal neuronal cells (Fig. 4B, quantification in Supplementary Material, Fig. S4C), implying

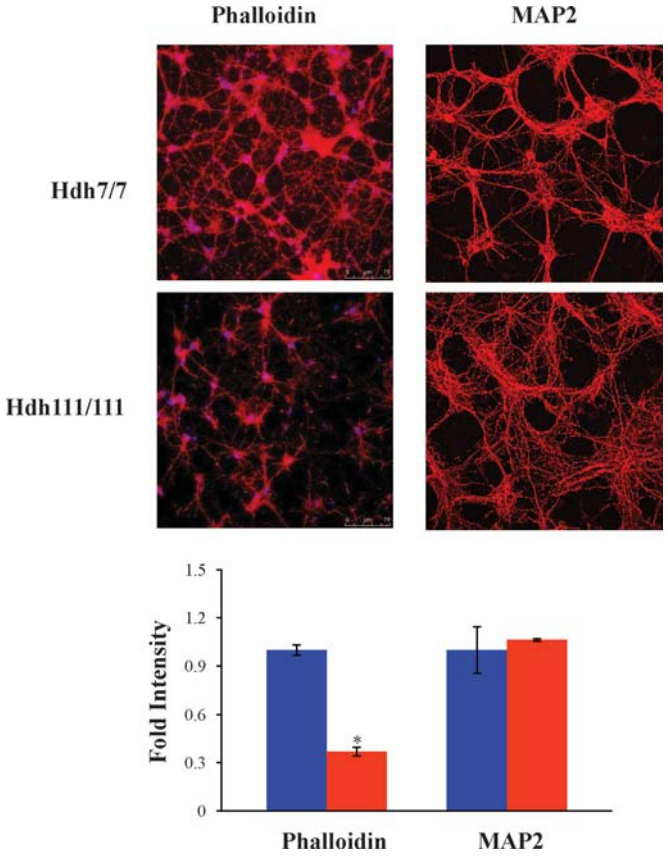

Figure 3. Primary *Hdh*$^{Q111/Q111}$ striatal neurons exhibit altered cytoskeletal elements. Confocal images of primary *Hdh*$^{Q7/Q7}$ (Hdh7/7) and *Hdh*$^{Q111/Q111}$ (Hdh111/111) striatal cell cultures at 10 days (*div*10), showing the pattern of rhodamine–phalloidin F-actin signal (left) and anti-MAP2 microtubule immunostain (right), illustrating decreased phalloidin signal and an abundance of fine MAP2-positive projections of the mutant neuronal cells, consistent with impaired adhesion and altered neuronal cell development. The bar graph below plots the fold intensity of the signal in mutant cells relative to wild-type cells ($^*P < 0.001$). Error bars represent standard errors.

delayed maturation of the neurite network. Moreover, co-staining to detect N-cadherin and markers of synaptic vesicles, synapsin and synaptophysin, confirmed this interpretation. The decreased N-cadherin signal, as well as the synapsin and synaptophysin vesicle signals, was distributed diffusely within the processes of the mutant *Hdh*$^{Q111/Q111}$ striatal neuronal cells, rather than assuming the bright punctuate matured appearance of these markers in wild-type *Hdh*$^{Q7/Q7}$ striatal cells (Fig. 4C). This immature pattern, which prominently featured decreased N-cadherin (35), was consistent with decreased N-cadherin function and delayed maturation of the network of developing neurites and synapses elaborated by the mutant primary neuronal cells.

Hdh$^{Q111/Q111}$ primary striatal developmental deficit was partially rescued with adenine

As adenine treatment of mutant ST*Hdh*$^{Q111/Q111}$-immortalized striatal cells partially elevated [ATP/ADP] (Supplementary Material, Fig. S2C) and partially normalized the N-cadherin level (Fig. 1D), we determined whether adenine treatment

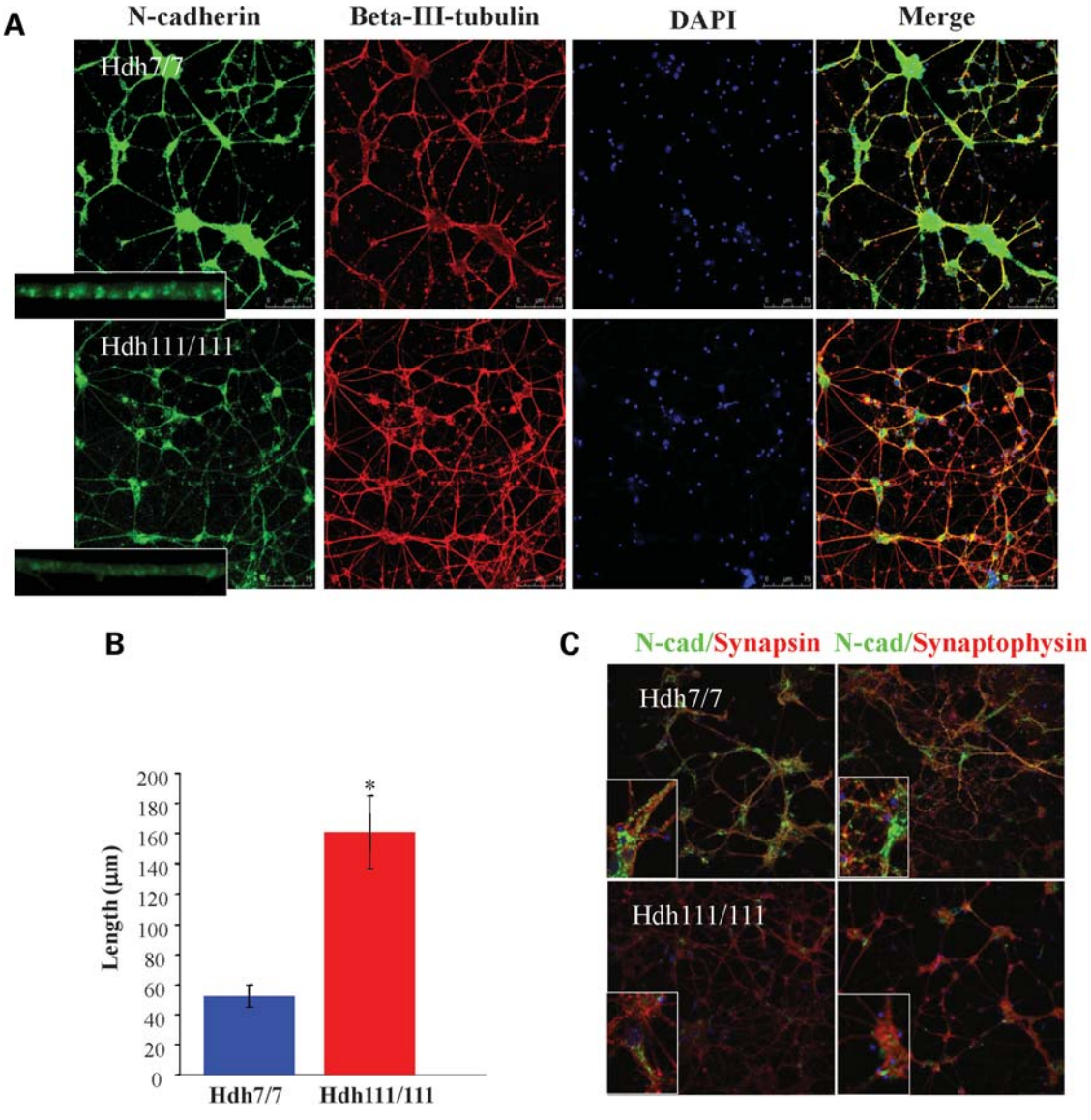

Figure 4. Primary $Hdh^{Q111/Q111}$ striatal neurons displayed decreased N-cadherin signal and abnormally extensive neurite networks. (**A**) Confocal images of primary $Hdh^{Q7/Q7}$ (Hdh7/7) and $Hdh^{Q111/Q111}$ (Hdh111/111) striatal cell cultures, at 10 days (*div*10), showing the pattern of N-cadherin immunostain (green), β-III-tubulin microtuble immunostain (red) and DAPI-signal marking nuclei (blue), with an overlay of all layers (merge), showing in mutant cells decreased N-cadherin signal intensity and paucity of bright puncta (inset), concomitant with an extensive network of β-III-tubulin-positive extensions (neurites). (**B**) Bar graph plotting the total β-III-tubulin-positive neurite length per cell, which was significantly increased in the *div*10 primary $Hdh^{Q111/Q111}$ (Hdh111/111) striatal neuronal cells compared with the wild-type $Hdh^{Q7/Q7}$ (Hdh7/7) cells ($^*P < 0.005$). Error bars represent standard errors. (**C**) As a consequence of HD mutation, several markers of synaptic development showed decreased signal intensity, such as N-cadherin (green) and presynaptic markers, synapsin 1 (red in the left column) and synaptophysin (red in the right column). Along with a decrease in the markers for synaptic development in the $Hdh^{Q111/Q111}$ neurons, there was also a diffuse staining pattern in contrast to a punctuated pattern in the wild-type processes.

might modulate the propensity of primary *div*10 E14 $Hdh^{Q111/Q111}$ striatal neurons to form abnormally extensive neurite networks. As shown in Figure 5, after treatment with adenine for 10 days, the *div*10 $Hdh^{Q111/Q111}$ striatal cultures exhibited MAP2-positive neuronal cells with fewer neurites per cell body compared with DMSO vehicle-treated cultures, though the number of cell bodies was not appreciably altered, as shown by DAPI nuclear staining. Consistent with the ameliorative effect of adenine on energy measures and N-cadherin levels demonstrated in ST$Hdh^{Q111/Q111}$ cells, these findings suggest that the delayed development of mutant primary neuronal cells may, at least in part, reflect decreased function of the ATP-sensitive N-cadherin adhesion molecule.

DISCUSSION

HD is a progressive neurodegenerative disorder, with marked loss of the major population of neurons in the striatum (medium-sized spiny neurons), which are vulnerable to acute energetic challenge. The neuronal specificity of HD stems from the effects of the HD CAG repeat, encoding a

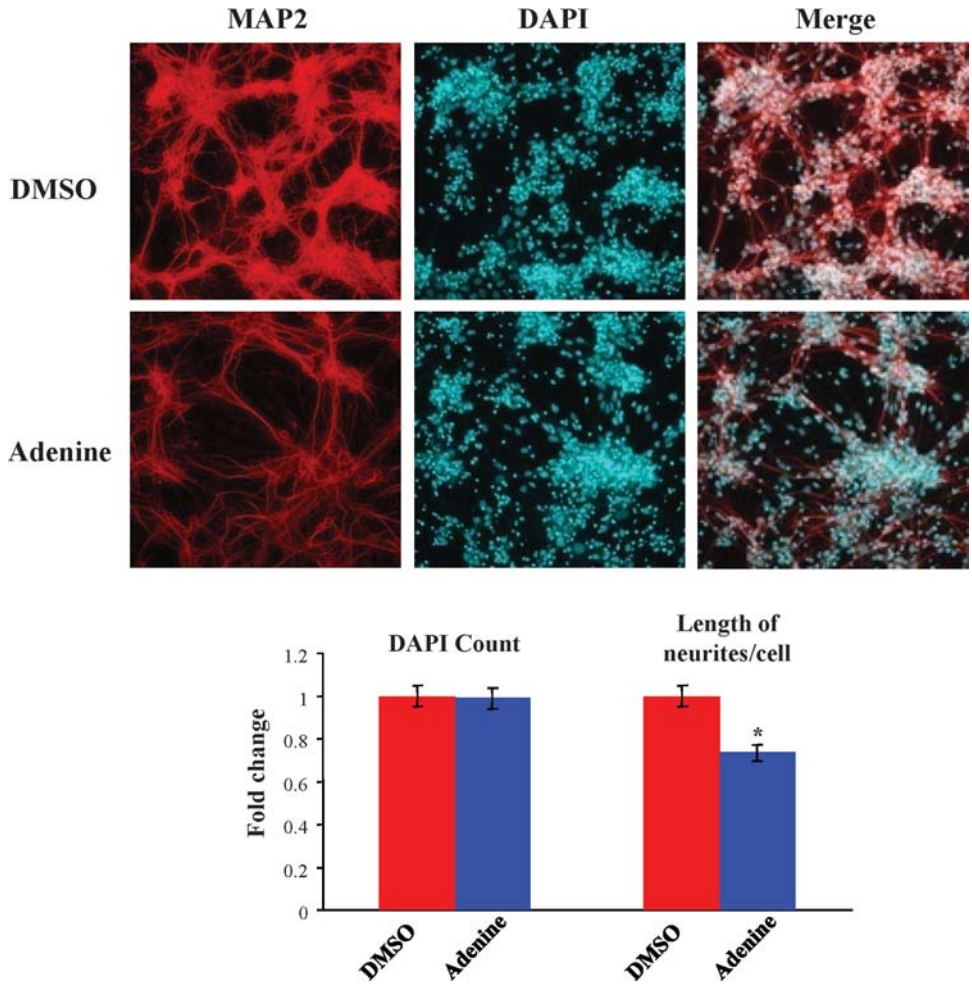

Figure 5. Adenine ameliorated altered $Hdh^{Q111/Q111}$ primary striatal neuron neuritogenesis. Confocal images of primary $Hdh^{Q111/Q111}$ striatal cell cultures at 10 days (*div*10), after culture in media supplemented with vehicle (DMSO) or with adenine (Adenine), showing MAP2-immunostained microtubules (red) and DAPI-stained nuclei (blue) and overlapped images (merge), illustrating that adenine-treated neuronal cells displayed a less branched neurite network than vehicle-treated cells. The bar graph below shows that adenine supplementation significantly decreased the total length of neurites/cell by 25% ($^*P = 0.001$), while a similar number of DAPI-stained nuclei confirmed that adenine did not result in toxicity or loss of cells. Error bars represent standard errors.

polyglutamine repeat in the full-length huntingtin protein of more than ~37 residues. We and others have discovered that the polyglutamine repeat modulates the, as yet unknown, role of full-length huntingtin in negatively regulating measures of energy metabolism in human cells and in genetically accurate CAG knock-in mice and striatal cells (7,8,36). In the current study, in order to guide *in vivo* investigations of striatal cell vulnerability, we have explored the hypothesis that chronically decreased energetics, due to endogenous full-length mutant huntingtin, may affect critical aspects of the biology of cultured striatal neuronal cells.

In a candidate approach, we have evaluated N-cadherin, an integrator of adhesion and cytoskeletal signaling required for proper neuronal cell development and synaptic function. N-cadherin was sensitive to acute ATP depletion, in striatal tissue and cultured striatal neuronal cells, and was strikingly sensitive to the effects of full-length mutant huntingtin. N-cadherin was progressively reduced with age in Hdh^{Q111} knock-in mouse striatum and, consistent with a defect from birth, was dramatically decreased both in cultured STHdh^{Q111} immortalized neuronal cells, generated from embryonic Hdh^{Q111} striatal primordia (37), and in primary cultures of embryonic Hdh^{Q111} striatal neurons.

The molecular basis of decreased N-cadherin in response to full-length mutant huntingtin is not yet clear, but in STHdh^{Q111} striatal cells appears to involve regulation of *Cdh2* mRNA, as well as N-cadherin protein stability. Chronic energy deficit appears to contribute to the latter, but not the former, as adenine nucleotide was able to elevate both [ATP/ADP] and N-cadherin levels, and the rate of N-cadherin turnover was increased under ATP-depletion conditions, while these manipulations did not affect *Cdh2* mRNA levels, which instead may reflect a role for full-length huntingtin in mediating some aspect of *Cdh2* gene expression or mRNA stability. Enhanced N-cadherin turnover in STHdh^{Q111} striatal cells did not appear to involve MMP-1, which mediates ischemia-induced turnover of cadherin (15,16). MMP-1 levels were not increased in mutant STHdh^{Q111} striatal cells and N-cadherin turnover was unaffected by GM-6001, a specific MMP inhibitor (data not shown). Rather, elevated

N-cadherin instability may entail altered GTPase-regulated N-cadherin phosphorylation (38,39), consistent with decreased STHdh^{Q111} striatal cell GTP and [GTP/GDP], as well as ATP and [ATP/ADP] (8). However, other possibilities include: altered calcium-dependent ligand or catenin binding and internalization, consistent with full-length huntingtin/syntaxin 1A regulation of N-type calcium channels (40), impaired N-cadherin membrane association due to altered cholesterol metabolism (41,42) or abnormal N-cadherin precursor processing, trafficking and/or glycosylation, as implied by the findings that STHdh^{Q111} and primary Hdh^{Q111} neuronal cells demonstrated a paucity of clustered N-cadherin and synaptic marker-positive vesicles. Certainly, STHdh^{Q111} striatal cells display diverse membrane trafficking defects, involving endocytic vesicles (43,44), autophagic vacuole cargo engulfment (45) and the ER/Golgi network (37), attesting to the impact of the polyglutamine repeat on full-length huntingtin function in regulating membrane trafficking (37,43,46).

N-cadherin-mediated calcium-dependent adhesion/cytoskeletal organization and signaling are especially needed for normal neuronal cell development and functionality, for example to achieve proper neurite outgrowth, synaptic vesicle clustering in maturing neurons, and synapse formation, maturation and dynamics (27,29,47–49). Mutant striatal cells exhibited impaired cell–cell, as well as cell–substrate adhesion, deficits in N-cadherin, synaptophysin and synapsin vesicle clustering and immature neurite networks, strongly suggesting delayed developmental maturation, though this interpretation remains to be tested. In part, the chronic energetic deficit contributed to impaired N-cadherin function, perhaps via decreased N-cadherin half-life. Adenine, which partially normalized STHdh^{Q111} striatal cell ATP and N-cadherin levels, significantly rescued primary Hdh^{Q111} striatal cell neurite development, consistent with the hypothesis that the energetic state may be a prominent factor in determining N-cadherin levels and function in cells expressing full-length mutant huntingtin.

HD is typically assumed to be due to a disease process that begins later in life. However, our observation of decreased N-cadherin and delayed development of embryonic Hdh^{Q111} striatal neurons *in vitro* offers a possible explanation for impaired development of the striatum in E13.5–15.5 Hdh^{Q111} embryos (50), and for decreased measures of brain neurodevelopment in humans with expanded CAG repeats (51), which demonstrate effects of the HD CAG repeat that become manifest even before birth. Later in life, N-cadherin progressively decreased with age in Hdh^{Q111} striatum, implying chronic synaptic dysfunction, as N-cadherin orchestrates activity-modulated CNS synapses (35). Indeed, decreased N-cadherin may contribute to impaired actin polymerization and long-term potentiation detected in Hdh^{Q92} mice (52,53).

Accumulated evidence now supports CAG-dependent energetic deficits in human cells and tissues, before onset of overt clinical symptoms, as well as in the brains of symptomatic individuals (7,10,54–56). Therefore, it will be important to determine whether decreased levels of N-cadherin may contribute to the HD pathogenic process, in a manner that is specific to striatal neurons, thereby contributing to the early vulnerability of the striatum, compared with other brain regions. Furthermore, it will be of interest to determine whether subtly altered development may sensitize striatal cells, and perhaps other neuronal cells, to the disease process or may represent a rate-limiting step in the disease process that is initiated by the impact of the polyglutamine repeat on full-length huntingtin.

MATERIALS AND METHODS

Mice and striatal neuronal cell cultures

$Hdh^{Q111/Q111}$ knock-in mice have been described previously (57). Striata were dissected from genotyped homozygous mutant $Hdh^{Q111/Q111}$ and wild-type $Hdh^{Q7/Q7}$ littermates from heterozygous $Hdh^{Q111/Q7}$ matings, at various ages. Conditionally immortalized wild-type ST$Hdh^{Q7/Q7}$ striatal cells and homozygous mutant ST$Hdh^{Q111/Q111}$ striatal cells, generated from $Hdh^{Q111/Q111}$ and $Hdh^{Q7/Q7}$ littermate embryos, were described previously (37). The striatal cells were grown at 33°C in Dulbecco's modified Eagle's medium (DMEM) supplemented with 10% fetal bovine serum, 1% non-essential amino acids, 2 mM L-glutamine and 400 μg/ml G418 (Geneticin; Invitrogen). Primary neuronal cell cultures were set up from striata dissected from E14 wild-type $Hdh^{Q7/Q7}$ and mutant $Hdh^{Q111/Q111}$ embryos, from heterozygous $Hdh^{Q111/Q7}$ matings. The striata were dissociated with trypsin (0.5%), trypsin inhibitor (0.1%) and DNase (228 U/ml) treatments for 1 min each in a 37°C warm water bath. Dissociated cells were plated onto poly-L-lysine (0.1 mg/ml) and laminin (50 μg/ml) (Sigma) double-coated coverslips in neurobasal medium (GIBCO) supplemented with 2% B27 and 1% penicillin/streptomycin/gentamycin. Cells were cultured for 10 days (*div*10) at 37°C and 5% CO_2.

Focal ischemia

All focal ischemia experiments were conducted in accordance with the National Institutes of Health and Massachusetts General Hospital institutional guidelines on animal experimentation. Three wild-type $Hdh^{Q7/Q7}$ and three $Hdh^{Q111/Q111}$ mice (12 months of age) were anesthetized with 2% halothane in 70% N_2O and 30% O_2, and then maintained on 1% halothane in a similar gaseous mixture. Transient focal cerebral ischemia was performed using an 8-0 nylon monofilament coated with silicone, which was introduced into the internal carotid artery via the external carotid artery and then advanced 10 mm distal to the carotid bifurcation to occlude the MCA as described (58). Laser Doppler flowmetry (PF2B; Perimed Stockholm) of relative cerebral blood fluid (CBF) was used to verify successful occlusion (<20% baseline value). The MCA was occluded for 0.5 and 1 h followed by withdrawal of filament and reperfusion for 24 h. Relative CBF returned to >95% of baseline values, indicating almost complete reperfusion without residual occlusion. After reperfusion, right (control hemisphere) and left (infarct hemisphere) striata from each mouse brain were dissected for tissue extraction and immunoblot analysis.

Immunoblot analysis

Whole-cell protein extracts were prepared from harvested striata and striatal cells by lysis on ice for 30 min in a buffer

containing 20 mM HEPES (pH 7.6), 1 mM EDTA, 0.5% Triton X-100, protease inhibitor mixture (Roche, Indianapolis, IN, USA) and 1 mM phenylmethyl sulfonyl fluoride (PMSF), mixed by tapping every 10 min. The total lysates were cleared by centrifugation at 14 000*g* for 30 min and the supernatants were collected. Protein concentration was determined by the Bio-Rad (detergent compatible) protein assay. An amount of 25 μg of protein extract was mixed with 4× SDS sample buffer, boiled for 2 min and subjected to 6 or 10% SDS–PAGE. After electrophoresis, the proteins were transferred to nitrocellulose membranes (Schleicher & Schuell) and incubated for 30 min in blocking solution containing 5% non-fat powdered milk in TBS-T (50 mM Tris–HCl, 150 mM NaCl, pH 7.4, 0.1% Tween 20). The blots were probed overnight at 4°C with primary antibodies: MAB2166 for huntingtin (Chemicon), N-cadherin (BD-bioscience), α-catenin (Chemicon), β-catenin (Sigma), p120 (Sigma) and α-tubulin (Sigma). After four washes of 10 min each in TBS-T, the blots were incubated for 1 h at room temperature with horseradish peroxidase-conjugated anti-mouse or anti-rabbit antisera. After a 30 min wash, the membranes were processed using an ECL chemiluminescence substrate kit (New England Biolabs, Beverly, MA, USA) and exposed to autoradiographic film (Hyperfilm ECL; Amersham Bioscience). Quantification of the immunoreactive bands was performed by scanning and analysis using the GS-800 Calibrated Densitometer and the Quantity One software (BioRad, Hercules, CA, USA).

Immunocytochemistry

Wild-type ST*Hdh*$^{Q7/Q7}$ and homozygous mutant ST*Hdh*$^{Q111/Q111}$ cells were grown on 4-chamber glass slides at a density of 2×10^5 cells/well. The cells were fixed in 4% paraformaldehyde for 20 min, permeabilized for 5 min in 0.1% Triton X-100 in phosphate-buffered saline (PBS), treated for 30 min in blocking buffer [2% bovine serum albumin (BSA) in PBS] and incubated for 2 h in blocking solution containing anti-N-cadherin. After several washes in PBS (3 × 5 min), cells were incubated for 1 h in blocking solution containing the anti-mouse fluorescent secondary antibody. Cells were imaged with a laser confocal microscope (Leica) using a 60× oil objective. Primary cells were fixed with 4% formaldehyde for 10 min, followed by 20 min of 100% MeOH for permeabilization. Single or double incubation of neurons with various primary antibodies was performed overnight at 4°C. The primary antibodies in this study were N-cadherin antibody (Abcam; 1:200), β-III-tubulin (Chemicon; 1:500), Cofilin (Sigma: 1:1000), Synapsin-1 (Synaptic Systems: 1:1000), Synaptophysin-1 (Synaptic Systems 1:200) and MAP2 (EnCor Biotechnology Inc: 1:10 000). For visualization, 1 h treatment with Alexa-488 and Alexa-568 secondary antibodies (both Molecular Probes, 1:500) was performed. The Phalloidin–TRITC (Sigma: 1:1000) signal was visualized without the secondary antibody. Coverslips were fixed onto object glasses using ProLong Gold antifade reagent containing DAPI (Invitrogen) for subsequent laser confocal microscopy (Leica) or epifluorescence microscopy (Zeiss).

Cell-clustering assay

Sub confluent striatal cell cultures were incubated for 10 min in cold PBS and the cells were then collected with a scraper. After washing twice with PBS containing 10 mM HEPES–NaOH (pH 7.4), cells were resuspended in PBS containing 10 mM HEPES–NaOH (pH 7.4), 1 mg/ml BSA, 1 mM EGTA and maintained at 4°C. Before the start of clustering assays, cells were carefully resuspended to ensure single-cell suspensions, and viability of cells (>90%) was confirmed by trypan blue exclusion. Clustering assays, which were performed at 33°C with rotation in non-tissue culture 24-well Falcon dishes to prevent cell–dish attachment, were started by addition of 50 μl of cell suspension (5×10^6 cells/ml) to 500 μl of pre-warmed (33°C) PBS containing 1 mg/ml BSA, 10 mM HEPES–NaOH (pH 7.4) and either 2 mM $CaCl_2$ or 2 mM EGTA. Incubations were terminated by addition of 500 μl of 5% glutaraldehyde in PBS and particle numbers were determined on a Coulter Counter Model Z2 (Beckman Coulter, Fullerton, CA, USA). Clustering is expressed as the fractional loss of particle number, N_t/N_0, where N_0 is the particle number at time 0 and N_t is the particle number after any given time point.

RNA extraction and quantitative RT–PCR

Harvested striatal cells or dissected striata were extracted with TRIzol reagent (Invitrogen) to isolate total RNA according to the manufacturer's instructions. cDNA was synthesized using Oligo(dT)15 primer and Reverse Transcription System (Promega) according to the manufacturer's instructions. Amplification by PCR was performed with 10 μl aliquots of cDNA in a total volume of 50 μl using iQTM SYBR Green Supermix (Bio Rad) with a Bio-Rad iCycler (Hercules, CA, USA). Expression of *Cdh2* was specifically detected by using two primers: *Cdh2* forward, 5′-AGAGGCCTATCCATGCT GAG-3′ and *Cdh2* reverse, 5′-AGCAGCTTTAAGGC CCTCAT-3′. The thermocycling program used began with incubation at 95°C for 1 min, followed by 30 cycles of 95°C for 15 s, 56°C for 20 s and 72°C for 15 s. A primer set of β-actin, forward, 5′-GACGGCCAGGTCATCACTAT-3′, reverse, 5′-ATGCCACAGGATTCCATACC-3′, was used as a positive control to ensure the integrity and quantity of RNA. PCR amplification was performed for β-actin under the following conditions: 95°C for 1 min; 30 cycles of 95°C for 15 s, 54°C for 20 s and 72°C for 20 s. The ΔΔCT method was used to calculate gene expression levels from quantitative RT–PCR (59).

N-cadherin half-life

ST*Hdh*$^{Q7/Q7}$ and ST*Hdh*$^{Q111/Q111}$ cells plated on 6-well dishes were incubated in growth medium containing cycloheximide at a final concentration of 30 μg/ml for 0, 1, 2 and 4 h. At each time point, the cells were washed once with ice-cold PBS and lysed by incubation for 30 min in a buffer containing 20 mM HEPES (pH 7.6), 1 mM EDTA, 0.5% Triton X-100, protease inhibitor mixture (Roche, Indianapolis, IN, USA) and 1 mM PMSF, followed by tapping every 10 min. The total lysates were then cleared by centrifugation at 14 000*g* for 30 min and the supernatants were collected. The protein concentration was determined by the Bio-Rad (detergent compatible) protein assay and equal amounts of protein from each lysate were resolved by 10% SDS–PAGE. The proteins were transferred to nitrocellulose membranes, blocked in 5%

non-fat milk TBS-T and incubated overnight at 4°C with a monoclonal anti N-cadherin antibody. The immunoblot was then probed with horseradish peroxidase-conjugated secondary antibody and visualized by ECL reagents.

ATP depletion

ST*Hdh*$^{Q7/Q7}$ and ST*Hdh*$^{Q111/Q111}$ cells plated on 6-well dishes were washed twice with PBS and then were incubated at 33°C in either normal growth medium (control cells) or glucose-free DMEM containing 10 mM 2-deoxyglucose and 10 μM antimycin A to yield ATP-depleted cells. After incubation for 0.5, 1 and 2 h, cells were collected with a scraper and extracts were generated for immunoblot analysis.

After ATP depletion, viability was assessed by the MTS assay kit (Promega, Madison, WI, USA). Prior to the assay, cells were washed three times with PBS. MTS [3-(4,5-dimethylthiazol-2-yl)-5-(3-carboxymethoxyphenyl)-2-(4-sulfophenyl)-2H-tetrazolium, inner salt] solution was added to each well, followed by incubation at 33°C for 2 h. Absorbance was measured at 490 nm on a multi-well spectrophotometer (Molecular Devices). For measuring altered ATP nucleotide in cells after ATP depletion, HPLC analysis was performed as described previously (7).

Image analysis of primary cultures

Quantification of immunostain was performed using ImageJ, image analysis software available through the NIH website (http://rsb.info.nih.gov/ij/). To determine the area for cells (cell bodies and neurites separately), the number of β-III-positive pixels were counted within a field of view. For cell bodies, β-III-tubulin staining defined the edges of the cell body, so that the total area of the cell body could be determined. Four different fields per genotype were analyzed. For quantification of N-cadherin, intensity histograms of N-cadherin in β-III-tubulin-defined neurites and cell bodies were measured. To obtain the amounts of the N-cadherin signal for a specific genotype and the respective cell part, the products of each intensity over a threshold value multiplied by the percentage of the area covered by that intensity were added up $\left(\sum_{\text{i=minimum intensity}}^{\text{i=maximum intensity}} \text{intensity}_i \times \text{pixel}_i/\text{total pixel number}\right)$. To compare the four different amounts with one another (wild-type cell body, wild-type neurites, mutant cell body and mutant cell neurites), the signal amount in mutant neurites was defined as one, and the other three signal amounts were expressed as a ratio. The number of N-cadherin signal particles was determined by using the Analyze Particle plug-in of ImageJ. Thirty images of neurites per genotype were analyzed. Images were thresholded six times for different signal intensity intervals (intensity 30–90; 40–90, 50–90, etc., until 80–90). For each thresholded image, the number of particles was calculated (i.e. I_{30-90}, I_{40-90}, $I_{50-90,\ldots}$, I_{80-90}). To obtain the number of particles with a specific highest intensity (40, 50, …, 90), the number of particles within one intensity interval was subtracted from the one of the next lower interval (i.e. $N_{30-40} = I_{30-90} - I_{40-90}$). The number of particles was also normalized to the length of neurites. In order to determine the total neurite length, in four fields of view per genotype of β-III-tubulin images, the cell bodies were removed. The resulting images were skeletonized and the length of the skeleton was measured. Subsequently, this number was divided by the number of DAPI-positive nuclei in the appropriate field.

Statistical analysis

All cell images were quantified in 10 randomly chosen groups comprising at least 100 cells and other experiments, such as immunoblot and [ATP/ADP] measurement, in three independent experiments. The mean, standard deviation (SD) and standard error (SE) were calculated and statistical significance analyzed using an unpaired two-sample *t*-test.

SUPPLEMENTARY MATERIAL

Supplementary Material is available at *HMG* online.

ACKNOWLEDGEMENTS

The authors thank Dr Anastasios Georgakopoulos from Mount Sinai School of Medicine for a gift of phN-cadherin vector.

Conflict of Interest statement. None declared.

FUNDING

This work was supported by the National Institute of Neurological Disorders and Stroke (NS32765 to M.E.M., NS070001 to J.K.L.); the Massachusetts HD Center Without Walls [NS16367 (Project 3) to M.E.M.]; the Huntington's Disease Society of America Coalition for the Cure Normal Function Team to M.E.M.; the de Gunzburg Family Foundation at Massachusetts General Hospital to S.Y.S.; National Scientist Develoment Grant of the American Heart Association (0930202N to H.-H.K.); and an anonymous donor.

REFERENCES

1. Vonsattel, J.P. and DiFiglia, M. (1998) Huntington disease. *J. Neuropathol. Exp. Neurol.*, **57**, 369–384.
2. The Huntington's Disease Collaborative Research Group. (1993) A novel gene containing a trinucleotide repeat that is expanded and unstable on Huntington's disease chromosomes. *Cell*, **72**, 971–983.
3. Gauthier, L.R., Charrin, B.C., Borrell-Pages, M., Dompierre, J.P., Rangone, H., Cordelieres, F.P., De Mey, J., MacDonald, M.E., Lessmann, V., Humbert, S. *et al.* (2004) Huntingtin controls neurotrophic support and survival of neurons by enhancing BDNF vesicular transport along microtubules. *Cell*, **118**, 127–138.
4. Reddy, P.H., Mao, P. and Manczak, M. (2009) Mitochondrial structural and functional dynamics in Huntington's disease. *Brain Res. Rev.*, **61**, 33–48.
5. Truant, R., Atwal, R. and Burtnik, A. (2006) Hypothesis: huntingtin may function in membrane association and vesicular trafficking. *Biochem. Cell Biol.*, **84**, 912–917.
6. Carnevale, F.A., Macdonald, M.E., Bluebond-Langner, M. and McKeever, P. (2008) Using participant observation in pediatric health care settings: ethical challenges and solutions. *J. Child Health Care*, **12**, 18–32.
7. Seong, I.S., Ivanova, E., Lee, J.M., Choo, Y.S., Fossale, E., Anderson, M., Gusella, J.F., Laramie, J.M., Myers, R.H., Lesort, M. *et al.* (2005) HD CAG repeat implicates a dominant property of huntingtin in mitochondrial energy metabolism. *Hum. Mol. Genet.*, **14**, 2871–2880.

8. Gines, S., Seong, I.S., Fossale, E., Ivanova, E., Trettel, F., Gusella, J.F., Wheeler, V.C., Persichetti, F. and MacDonald, M.E. (2003) Specific progressive cAMP reduction implicates energy deficit in presymptomatic Huntington's disease knock-in mice. *Hum. Mol. Genet.*, **12**, 497–508.
9. Lee, J.M., Ivanova, E.V., Seong, I.S., Cashorali, T., Kohane, I., Gusella, J.F. and MacDonald, M.E. (2007) Unbiased gene expression analysis implicates the huntingtin polyglutamine tract in extra-mitochondrial energy metabolism. *PLoS Genet.*, **3**, e135.
10. Mochel, F., Charles, P., Seguin, F., Barritault, J., Coussieu, C., Perin, L., Le Bouc, Y., Gervais, C., Carcelain, G., Vassault, A. *et al.* (2007) Early energy deficit in Huntington disease: identification of a plasma biomarker traceable during disease progression. *PLoS One*, **2**, e647.
11. Benson, D.L., Colman, D.R. and Huntley, G.W. (2001) Molecules, maps and synapse specificity. *Nat. Rev. Neurosci.*, **2**, 899–909.
12. Takeichi, M. (2007) The cadherin superfamily in neuronal connections and interactions. *Nat. Rev. Neurosci.*, **8**, 11–20.
13. Mandel, L.J., Doctor, R.B. and Bacallao, R. (1994) ATP depletion: a novel method to study junctional properties in epithelial tissues. II. Internalization of Na+,K(+)-ATPase and E-cadherin. *J. Cell Sci.*, **107**, 3315–3324.
14. Bush, K.T., Tsukamoto, T. and Nigam, S.K. (2000) Selective degradation of E-cadherin and dissolution of E-cadherin-catenin complexes in epithelial ischemia. *Am. J. Physiol. Renal Physiol.*, **278**, F847–852.
15. Covington, M.D., Bayless, K.J., Burghardt, R.C., Davis, G.E. and Parrish, A.R. (2005) Ischemia-induced cleavage of cadherins in NRK cells: evidence for a role of metalloproteinases. *Am. J. Physiol. Renal Physiol.*, **289**, F280–F288.
16. Covington, M.D., Burghardt, R.C. and Parrish, A.R. (2006) Ischemia-induced cleavage of cadherins in NRK cells requires MT1-MMP (MMP-14). *Am. J. Physiol. Renal Physiol.*, **290**, F43–F51.
17. Hatta, K., Nose, A., Nagafuchi, A. and Takeichi, M. (1988) Cloning and expression of cDNA encoding a neural calcium-dependent cell adhesion molecule: its identity in the cadherin gene family. *J. Cell Biol.*, **106**, 873–881.
18. Takeichi, M. (1990) Cadherins: a molecular family important in selective cell–cell adhesion. *Annu. Rev. Biochem.*, **59**, 237–252.
19. Aberle, H., Butz, S., Stappert, J., Weissig, H., Kemler, R. and Hoschuetzky, H. (1994) Assembly of the cadherin–catenin complex *in vitro* with recombinant proteins. *J. Cell Sci.*, **107**, 3655–3663.
20. Knudsen, K.A., Soler, A.P., Johnson, K.R. and Wheelock, M.J. (1995) Interaction of alpha-actinin with the cadherin/catenin cell–cell adhesion complex via alpha-catenin. *J. Cell Biol.*, **130**, 67–77.
21. Baki, L., Marambaud, P., Efthimiopoulos, S., Georgakopoulos, A., Wen, P., Cui, W., Shioi, J., Koo, E., Ozawa, M., Friedrich, V.L. Jr *et al.* (2001) Presenilin-1 binds cytoplasmic epithelial cadherin, inhibits cadherin/p120 association, and regulates stability and function of the cadherin/catenin adhesion complex. *Proc. Natl Acad. Sci. USA*, **98**, 2381–2386.
22. Gumbiner, B.M. (2000) Regulation of cadherin adhesive activity. *J. Cell Biol.*, **148**, 399–404.
23. Namura, S., Hirt, L., Wheeler, V.C., McGinnis, K.M., Hilditch-Maguire, P., Moskowitz, M.A., MacDonald, M.E. and Persichetti, F. (2002) The HD mutation does not alter neuronal death in the striatum of Hdh(Q92) knock-in mice after mild focal ischemia. *Neurobiol. Dis.*, **11**, 147–154.
24. Kim, M., Roh, J.K., Yoon, B.W., Kang, L., Kim, Y.J., Aronin, N. and DiFiglia, M. (2003) Huntingtin is degraded to small fragments by calpain after ischemic injury. *Exp. Neurol.*, **183**, 109–115.
25. Peyrieras, N., Hyafil, F., Louvard, D., Ploegh, H.L. and Jacob, F. (1983) Uvomorulin: a nonintegral membrane protein of early mouse embryo. *Proc. Natl Acad. Sci. USA*, **80**, 6274–6277.
26. Yoshida, C. and Takeichi, M. (1982) Teratocarcinoma cell adhesion: identification of a cell-surface protein involved in calcium-dependent cell aggregation. *Cell*, **28**, 217–224.
27. Bixby, J.L. and Zhang, R. (1990) Purified N-cadherin is a potent substrate for the rapid induction of neurite outgrowth. *J. Cell Biol.*, **110**, 1253–1260.
28. Goodwin, M. and Yap, A.S. (2004) Classical cadherin adhesion molecules: coordinating cell adhesion, signaling and the cytoskeleton. *J. Mol. Histol.*, **35**, 839–844.
29. Bamji, S.X. (2005) Cadherins: actin with the cytoskeleton to form synapses. *Neuron*, **47**, 175–178.
30. Muhlrad, A., Ringel, I., Pavlov, D., Peyser, Y.M. and Reisler, E. (2006) Antagonistic effects of cofilin, beryllium fluoride complex, and phalloidin on subdomain 2 and nucleotide-binding cleft in F-actin. *Biophys. J.*, **91**, 4490–4499.
31. Regalado, M.P., Terry-Lorenzo, R.T., Waites, C.L., Garner, C.C. and Malenka, R.C. (2006) Transsynaptic signaling by postsynaptic synapse-associated protein 97. *J. Neurosci.*, **26**, 2343–2357.
32. Togashi, H., Abe, K., Mizoguchi, A., Takaoka, K., Chisaka, O. and Takeichi, M. (2002) Cadherin regulates dendritic spine morphogenesis. *Neuron*, **35**, 77–89.
33. Bamji, S.X., Shimazu, K., Kimes, N., Huelsken, J., Birchmeier, W., Lu, B. and Reichardt, L.F. (2003) Role of beta-catenin in synaptic vesicle localization and presynaptic assembly. *Neuron*, **40**, 719–731.
34. Bozdagi, O., Valcin, M., Poskanzer, K., Tanaka, H. and Benson, D.L. (2004) Temporally distinct demands for classic cadherins in synapse formation and maturation. *Mol. Cell Neurosci.*, **27**, 509–521.
35. Garner, C.C., Waites, C.L. and Ziv, N.E. (2006) Synapse development: still looking for the forest, still lost in the trees. *Cell Tissue Res.*, **326**, 249–262.
36. Clabough, E.B. and Zeitlin, S.O. (2006) Deletion of the triplet repeat encoding polyglutamine within the mouse Huntington's disease gene results in subtle behavioral/motor phenotypes in vivo and elevated levels of ATP with cellular senescence *in vitro*. *Hum. Mol. Genet.*, **15**, 607–623.
37. Trettel, F., Rigamonti, D., Hilditch-Maguire, P., Wheeler, V.C., Sharp, A.H., Persichetti, F., Cattaneo, E. and MacDonald, M.E. (2000) Dominant phenotypes produced by the HD mutation in STHdh(Q111) striatal cells. *Hum. Mol. Genet.*, **9**, 2799–2809.
38. Braga, V.M. (1999) Small GTPases and regulation of cadherin dependent cell–cell adhesion. *Mol. Pathol.*, **52**, 197–202.
39. Watanabe, T., Sato, K. and Kaibuchi, K. (2009) Cadherin-mediated intercellular adhesion and signaling cascades involving small GTPases. *Cold Spring Harb. Perspect. Biol.*, **1**, a003020.
40. Swayne, L.A., Chen, L., Hameed, S., Barr, W., Charlesworth, E., Colicos, M.A., Zamponi, G.W. and Braun, J.E. (2005) Crosstalk between huntingtin and syntaxin 1A regulates N-type calcium channels. *Mol. Cell Neurosci.*, **30**, 339–351.
41. Markianos, M., Panas, M., Kalfakis, N. and Vassilopoulos, D. (2008) Low plasma total cholesterol in patients with Huntington's disease and first-degree relatives. *Mol. Genet. Metab.*, **93**, 341–346.
42. Valenza, M., Leoni, V., Karasinska, J.M., Petricca, L., Fan, J., Carroll, J., Pouladi, M.A., Fossale, E., Nguyen, H.P., Riess, O. *et al.* (2010) Cholesterol defect is marked across multiple rodent models of Huntington's disease and is manifest in astrocytes. *J. Neurosci.*, **30**, 10844–10850.
43. Pardo, R., Molina-Calavita, M., Poizat, G., Keryer, G., Humbert, S. and Saudou, F. (2010) pARIS-htt: an optimised expression platform to study huntingtin reveals functional domains required for vesicular trafficking. *Mol. Brain*, **3**, 17.
44. Pal, A., Severin, F., Lommer, B., Shevchenko, A. and Zerial, M. (2006) Huntingtin-HAP40 complex is a novel Rab5 effector that regulates early endosome motility and is up-regulated in Huntington's disease. *J. Cell Biol.*, **172**, 605–618.
45. Martinez-Vicente, M., Talloczy, Z., Wong, E., Tang, G., Koga, H., Kaushik, S., de Vries, R., Arias, E., Harris, S., Sulzer, D. *et al.* (2010) Cargo recognition failure is responsible for inefficient autophagy in Huntington's disease. *Nat. Neurosci.*, **13**, 567–576.
46. Strehlow, A.N., Li, J.Z. and Myers, R.M. (2007) Wild-type huntingtin participates in protein trafficking between the Golgi and the extracellular space. *Hum. Mol. Genet.*, **16**, 391–409.
47. Bruses, J.L. (2006) N-cadherin signaling in synapse formation and neuronal physiology. *Mol. Neurobiol.*, **33**, 237–252.
48. Tan, Z.J., Peng, Y., Song, H.L., Zheng, J.J. and Yu, X. (2010) N-cadherin-dependent neuron-neuron interaction is required for the maintenance of activity-induced dendrite growth. *Proc. Natl Acad. Sci. USA*, **107**, 9873–9878.
49. Stan, A., Pielarski, K.N., Brigadski, T., Wittenmayer, N., Fedorchenko, O., Gohla, A., Lessmann, V., Dresbach, T. and Gottmann, K. (2010) Essential cooperation of N-cadherin and neuroligin-1 in the transsynaptic control of vesicle accumulation. *Proc. Natl Acad. Sci. USA*, **107**, 11116–11121.
50. Molero, A.E., Gokhan, S., Gonzalez, S., Feig, J.L., Alexandre, L.C. and Mehler, M.F. (2009) Impairment of developmental stem cell-mediated striatal neurogenesis and pluripotency genes in a knock-in model of Huntington's disease. *Proc. Natl Acad. Sci. USA*, **106**, 21900–21905.

51. Nopoulos, P.C., Aylward, E.H., Ross, C.A., Mills, J.A., Langbehn, D.R., Johnson, H.J., Magnotta, V.A., Pierson, R.K., Beglinger, L.J., Nance, M.A. *et al.* (2011) Smaller intracranial volume in prodromal Huntington's disease: evidence for abnormal neurodevelopment. *Brain*, **134**, 137–142.
52. Lynch, G., Kramar, E.A., Rex, C.S., Jia, Y., Chappas, D., Gall, C.M. and Simmons, D.A. (2007) Brain-derived neurotrophic factor restores synaptic plasticity in a knock-in mouse model of Huntington's disease. *J. Neurosci.*, **27**, 4424–4434.
53. Simmons, D.A., Rex, C.S., Palmer, L., Pandyarajan, V., Fedulov, V., Gall, C.M. and Lynch, G. (2009) Up-regulating BDNF with an ampakine rescues synaptic plasticity and memory in Huntington's disease knockin mice. *Proc. Natl Acad. Sci. USA*, **106**, 4906–4911.
54. Jenkins, B.G., Rosas, H.D., Chen, Y.C., Makabe, T., Myers, R., MacDonald, M., Rosen, B.R., Beal, M.F. and Koroshetz, W.J. (1998) 1H NMR spectroscopy studies of Huntington's disease: correlations with CAG repeat numbers. *Neurology*, **50**, 1357–1365.
55. Saft, C., Zange, J., Andrich, J., Muller, K., Lindenberg, K., Landwehrmeyer, B., Vorgerd, M., Kraus, P.H., Przuntek, H. and Schols, L. (2005) Mitochondrial impairment in patients and asymptomatic mutation carriers of Huntington's disease. *Mov. Disord.*, **20**, 674–679.
56. Sturrock, A. and Leavitt, B.R. (2010) The clinical and genetic features of Huntington disease. *J. Geriatr. Psychiatry Neurol.*, **23**, 243–259.
57. Wheeler, V.C., Auerbach, W., White, J.K., Srinidhi, J., Auerbach, A., Ryan, A., Duyao, M.P., Vrbanac, V., Weaver, M., Gusella, J.F. *et al.* (1999) Length-dependent gametic CAG repeat instability in the Huntington's disease knock-in mouse. *Hum. Mol. Genet.*, **8**, 115–122.
58. Endres, M., Laufs, U., Huang, Z., Nakamura, T., Huang, P., Moskowitz, M.A. and Liao, J.K. (1998) Stroke protection by 3-hydroxy-3-methylglutaryl (HMG)-CoA reductase inhibitors mediated by endothelial nitric oxide synthase. *Proc. Natl Acad. Sci. USA*, **95**, 8880–8885.
59. Livak, K.J. and Schmittgen, T.D. (2001) Analysis of relative gene expression data using real-time quantitative PCR and the 2(-Delta Delta C(T)) method. *Methods*, **25**, 402–408.

Appendix B

Reprint of:

Jacobsen, J. C., Gregory, G. C., Woda, J. M., Thompson, M. N., Coser, K. R., Murthy, V., Kohane, I. S., Gusella, J. F., Seong, I. S., MacDonald, M. E., Shioda, T., Lee, J. M. *HD CAG-correlated gene expression changes support a simple dominant gain of function.* Hum Mol Genet, 2011. **20**(14): p. 2846-60.

Attributions

My questions:

Pertaining to this manuscript, the question I personally sought to address was: Do the cell adhesion & cytoskeletal phenotypes represent a normal function of huntingtin revealed by huntingtin deficiency and, if so, might huntingtin with longer polyQ tracts alter adhesion in the same way or in a different way?

My research contributions:

I reestablished and optimized growth conditions for multiple clones of mouse ES cell lines, including wild-type ($Hdh^{Q7/7}$), knock-out ($Hdh^{ex4/5/ex4/5}$)*, and* knock-in ($Hdh^{Q20/7}$, $Hdh^{Q50/7}$, $Hdh^{Q91/7}$, $Hdh^{Q111/7}$) alleles. Subsequently, I demonstrated the stem cell character of the allelic cell series by morphology (Supplemental Figure 1 A), RT-PCR marker panel (Supplemental Figure 1 B and D, Supplemental Figure 2 A and D), and developmental potential by embryoid body formation (Supplemental Figure 1 C). I used these reagents for cell biological investigations that uncovered evidence of distinct adhesion phenotypes for null and knock-in ES cell colonies as judged by colony morphology that has been further characterized by my colleague Dr. Randy Singh Atwal (manuscript in preparation).

Significance:

My research led directly to transcriptional profiling, which demonstrated that cellular adhesion processes are differentially altered in null and CAG knock-in ES cells as detailed in the manuscript included as Appendix B. Furthermore, identification of cell adhesion changes in

the ES allelic series led directly to development of quantitative embryoid body adhesion assays by my colleague Dr. Randy Singh Atwal; a manuscript detailing this work is currently in preparation.

Human Molecular Genetics, 2011, Vol. 20, No. 14 **2846–2860**
doi:10.1093/hmg/ddr195
Advance Access published on May 2, 2011

HD CAG-correlated gene expression changes support a simple dominant gain of function

Jessie C. Jacobsen[1], Gillian C. Gregory[1], Juliana M. Woda[1,†], Morgan N. Thompson[1], Kathryn R. Coser[2], Vidya Murthy[1], Isaac S. Kohane[3,4,5], James F. Gusella[1], Ihn Sik Seong[1], Marcy E. MacDonald[1], Toshi Shioda[2] and Jong-Min Lee[1,*]

[1]Center for Human Genetic Research, Massachusetts General Hospital, 185 Cambridge Street, Boston, MA 02114, USA, [2]Center for Cancer Research, Massachusetts General Hospital Cancer Center, 149, 13th Street, Charlestown, MA 02129, USA, [3]Informatics Program, Children's Hospital, 300 Longwood Avenue, Boston, MA 02115, USA, [4]Center for Biomedical Informatics, Harvard Medical School, 10 Shattuck Street, Boston, MA 02114, USA and [5]i2b2 National Center for Biomedical Computing, Boston, MA 02115, USA

Received March 2, 2011; Revised April 14, 2011; Accepted April 27, 2011

Huntington's disease is initiated by the expression of a CAG repeat-encoded polyglutamine region in full-length huntingtin, with dominant effects that vary continuously with CAG size. The mechanism could involve a simple gain of function or a more complex gain of function coupled to a loss of function (e.g. dominant negative-graded loss of function). To distinguish these alternatives, we compared genome-wide gene expression changes correlated with CAG size across an allelic series of heterozygous CAG knock-in mouse embryonic stem (ES) cell lines (*Hdh*$^{Q20/7}$, *Hdh*$^{Q50/7}$, *Hdh*$^{Q91/7}$, *Hdh*$^{Q111/7}$), to genes differentially expressed between *Hdh*$^{ex4/5/ex4/5}$ huntingtin null and wild-type (*Hdh*$^{Q7/7}$) parental ES cells. The set of 73 genes whose expression varied continuously with CAG length had minimal overlap with the 754-member huntingtin-null gene set but the two were not completely unconnected. Rather, the 172 CAG length-correlated pathways and 238 huntingtin-null significant pathways clustered into 13 shared categories at the network level. A closer examination of the energy metabolism and the lipid/sterol/lipoprotein metabolism categories revealed that CAG length-correlated genes and huntingtin-null-altered genes either were different members of the same pathways or were in unique, but interconnected pathways. Thus, varying the polyglutamine size in full-length huntingtin produced gene expression changes that were distinct from, but related to, the effects of lack of huntingtin. These findings support a simple gain-of-function mechanism acting through a property of the full-length huntingtin protein and point to CAG-correlative approaches to discover its effects. Moreover, for therapeutic strategies based on huntingtin suppression, our data highlight processes that may be more sensitive to the disease trigger than to decreased huntingtin levels.

INTRODUCTION

Huntington's disease (HD) features degeneration, especially of the striatum, along with motor, cognitive and psychiatric symptoms (1). All cases of HD are caused by an expanded CAG trinucleotide repeat in one copy of the 4p16.3 *HD* gene (2). In humans, the CAG alleles span a continuum from fully penetrant HD alleles (≥40 CAGs), which lead to HD pathology and clinical symptoms, through alleles with progressively reduced penetrance that can often (36–39 CAGs) (2–4), or only very rarely (27–35 CAGs), result in overt HD (5), to the shorter, more frequent, 'normal' alleles at the lower end of the distribution (6–26 CAGs), for which no HD case has been reported (6).

The dominant effects of endogenous CAG repeats are graded with the allele size. In the fully penetrant range, CAG length is inversely correlated with the age at onset of

*To whom correspondence should be addressed at: Center for Human Genetic Research, Massachusetts General Hospital, Simches Research Building, Room 5818, 185 Cambridge Street, Boston, MA 02114, USA. Tel: +1 617 643 9714; Fax: +1 617 726 5735. Email: jlee51@partners.org
†Present address: Athersys, Inc., 3201 Carnegie Avenue, Cleveland, OH 44115, USA.

overt HD symptoms in humans (2,7,8) and with the onset of striatal phenotypes in heterozygote Huntington's disease homolog (*Hdh*) CAG repeat knock-in mice (made to replicate the human CAG spectrum) (9–16). Graded effects of the polymorphic CAG stretch are also evident through the reduced penetrance HD range, for example, in sensitizing major depressive disorder (17), as well as in the normal range, as part of a continuous relationship of CAG size with ATP/ADP levels in human lymphoblastoid cells (18). Thus, the CAG repeat is a functional polymorphism, specifying a polyglutamine region in the full-length 3144 amino acid huntingtin protein (2), such that most humans express full-length huntingtins with polyglutamine repeats of different sizes. This large alpha-helical HEAT domain protein (19–22) is thought to act as a mechanical facilitator of multi-subunit complexes (21), as suggested for other predominantly HEAT proteins (23).

The preponderance of evidence argues that the polyglutamine segment modulates the full-length huntingtin in a manner most consistent with a simple gain of a novel function, rather than either a simple or a dominant-negative loss of function. Chiefly, huntingtin deficiency fails to mimic CAG expansion. Individuals with a balanced chromosomal translocation inactivating one HD allele express 50% of normal levels of huntingtin without exhibiting HD symptoms (24). In mice, more severe decreases in full-length huntingtin levels, below 50%, produce developmental defects and embryonic lethality (9,25–28). Yet HD homozygote humans (29,30) and knock-in mice (9,13,15,16,31) do exist, despite expressing no normal-range full-length huntingtin. There is mounting evidence that the polyglutamine repeat, though not required for basal activity (32), enhances, rather than impairs, the full-length huntingtin function in repressing energy metabolism (18,32) and in stimulating the multi-subunit enzyme, polycomb repressive complex 2 (21).

However, some findings from studies on CAG knock-in and full-length HD transgenic mouse systems seem more consistent with a dominant-negative effect or a combination of gain of function and loss of function. These include the failure of the full-length mutant huntingtin to exhibit functional activities attributed to the normal protein, such as in NRSE/REST target gene transcription (33), as well as SREBP (34–36) and LXR (37) regulated transcription of genes involved in cholesterol and lipid metabolism that lead to decreased biosynthetic intermediates. The alternate to the simple gain-of-function hypothesis is that the polyglutamine repeat confers a novel property on the full-length huntingtin that produces, or combines with, a loss of huntingtin function (37–40).

To more fully understand the molecular response to the impact of the polyglutamine region on the full-length huntingtin, and to reconcile seemingly conflicting evidence, we have created an isogenic allelic panel of heterozygous CAG knock-in mouse embryonic stem (ES) cells, augmenting an existing wild-type and huntingtin-null knock-out ES cell panel. With this new resource, we have conducted an unbiased genome-wide search for dominant CAG length-dependent gene expression changes and tested the validity of predictions that distinguish the alternate hypotheses: CAG-length-dependent gene changes would either be novel (simple gain of function) or overlap with the molecular effects of absent huntingtin (dominant-negative loss of function or combined gain and loss of function). The results of our analyses distinguish these alternatives and offer insights into the biology of the full-length huntingtin, as revealed by structure–function and deficiency analyses.

RESULTS

An isogenic panel of heterozygous CAG knock-in ES cell lines

To enable a discovery strategy based on the continuous relationship between CAG size and phenotype, we generated an allelic series of heterozygous *Hdh* CAG knock-in mouse ES cell lines, which would appropriately express full-length huntingtins from endogenous alleles. This series was produced from a matching series of targeted 'PGKneo-in' CAG exon 1 knock-in (CAG 18, CAG 48, CAG 89 and CAG 109) ES cell lines (14,27). As the 'neo-in' alleles express decreased levels of full-length huntingtin, due to the floxed PGKneo cassette in the promotor region (9,27), the selection cassette (conferring G418 resistance) was removed by Cre-recombinase-mediated excision (Fig. 1A) and multiple G418-sensitive ES subclones were identified for each line (Fig. 1B) (Materials and Methods). The results of polymerase chain reaction (PCR) amplification assays with genomic DNAs confirmed proper PGKneo excision (Fig. 1C), and DNA sequence analysis confirmed the size of the CAG repeat (data not shown). Immunoblot analysis revealed the ~350 kDa band of the wild-type full-length huntingtin with seven glutamines and, with progressively decreased mobility, a band of full-length huntingtin with a polyglutamine region from the normal human range (Q20), the adult-onset (Q50) and the juvenile-onset (Q91 and Q111) HD range (Fig. 1D). As expected, the wild-type parental ES cells expressed only the 7-glutamine full-length huntingtin and no huntingtin band was detected in the extract of double knock-out (null) $Hdh^{ex4/5/ex4/5}$ ES cells (25) (Fig. 1D).

The entire allelic panel comprises three to four heterozygous CAG knock-in ES cell subclones for each repeat length, and subclones of wild-type ES cells and double knock-out $Hdh^{ex4/5/ex4/5}$ ES cells, that were chosen based upon morphological, developmental and molecular criteria. The chosen subclones displayed an appropriate stem cell morphology (Supplementary Material, Fig. S1A), the expression of stem cell marker mRNAs (Supplementary Material, Fig. S1B), the ability to develop into embryoid bodies (Supplementary Material, Fig. S1C) and the expression of germ-layer marker mRNAs (Supplementary Material, Fig. S1D).

The members of this heterozygous *Hdh* CAG knock-in ES cell panel, which share an 129Sv genetic background with the wild-type $Hdh^{Q7/7}$ and huntingtin-null $Hdh^{ex4/5/ex4/5}$ ES cell lines, are named $Hdh^{Q20/7}$, $Hdh^{Q50/7}$, $Hdh^{Q91/7}$ and $Hdh^{Q111/7}$ to denote the polyglutamine region, encoded by the pure CAG tract and adjacent CAA, CAG codons, in the endogenous full-length huntingtin proteins expressed from the wild-type and targeted CAG alleles.

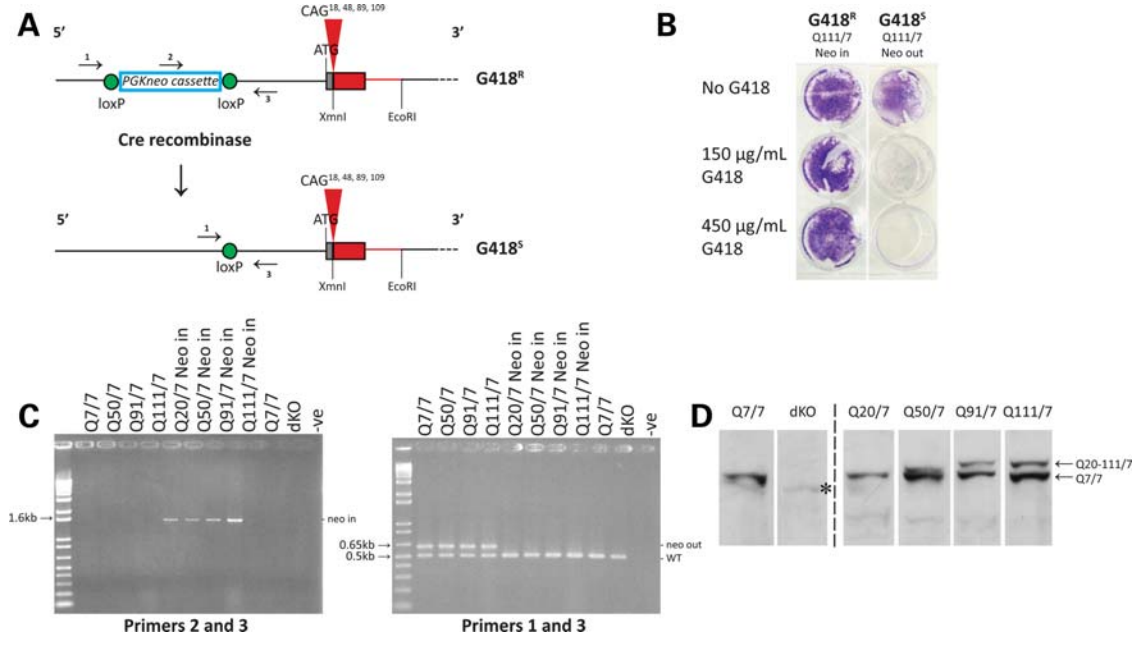

Figure 1. Generation of an allelic panel of heterozygous CAG knock-in ES cell lines. (**A**) The upper schematic depicts the targeted *Hdh* CAG knock-in allele in heterozygous $Hdh^{neo20/7}$, $Hdh^{neo50/7}$, $Hdh^{neo91/7}$ and $Hdh^{neo111/7}$ ES cell lines, with the location of the loxP-flanked PGKneo selection cassette in the promotor region upstream of the chimeric mouse (gray)/human (red) exon 1 with different CAG repeat sizes (CAG 18, CAG 48, CAG 89 and CAG 109), encoding adjacent CAA, CAG codons, the polyglutamine repeat in the full-length endogenous huntingtin. The corresponding PGKneo-out-targeted allele in the cognate $Hdh^{20/7}$, $Hdh^{50/7}$, $Hdh^{91/7}$ and $Hdh^{111/7}$ ES cell subclones created by Cre-recombinase-mediated excision is depicted below. Arrows denote the locations of primer sets for 'neo-in' (2 and 3) and 'neo-out' (1 and 3) PCR amplification assays. The schematic is not drawn to scale. The wild-type allele is not shown. (**B**) Trypan blue staining reveals the growth of G418-resistant ($G418^R$) $Hdh^{neo111/7}$ (Q111 neo-in) ES cells and the lack of growth of a subclone of G418-sensitive ($G418^S$) $Hdh^{111/7}$ (Q111 neo-out) ES cells, derived by Cre-recombinase excision of the pGKneo selection cassette. (**C**) Agarose gel analysis of PCR amplification products generated by specific PGKneo-in (left gel) and PGKneo-out (right gel) assays. The expected bands confirmed the presence of the PGKneo cassette in the parental $Hdh^{neo20/7}$, $Hdh^{neo50/7}$, $Hdh^{neo91/7}$and $Hdh^{neo111/7}$ ES cell genomic DNAs (lanes left gel) and the proper removal of the PGKneo cassette from the targeted allele in the cognate neo-out $Hdh^{20/7}$, $Hdh^{50/7}$, $Hdh^{91/7}$ and $Hdh^{111/7}$ ES cell DNAs (lanes on the left gel). The latter assay also amplifies the expected product from the wild-type allele present in all of the ES cell lines, including the $Hdh^{ex4/5/ex4/5}$ ES cell genomic DNA (dKO), which harbor alleles with a targeted inactivating mutation replacing/deleting exons 4 and 5 (data not shown). PCR products were not detected in genomic DNA minus lanes (−ve) for each assay. (**D**) The immunoblot, detected with mAb2166, confirms proper expression of both full-length wild-type huntingtin (7 glutamines) and, migrating more slowly, huntingtins from the targeted allele with distinct polyglutamine tracts (Q20, Q50, Q91 and Q111) in protein extracts of $Hdh^{20/7}$, $Hdh^{50/7}$, $Hdh^{91/7}$ and $Hdh^{111/7}$ ES cells, respectively. Wild-type ES cells (Q7/7) express full-length 7-glutamine huntingtin from both alleles and $Hdh^{ex4/5}/Hdh^{ex4/5}$-null ES cells (dKO) express no full-length huntingtin. mAb2166 and other anti-huntingtin antibodies differentially detect the huntingtin with the shorter polyglutamine tract, compared with those with the longer tracts, for reasons that are not yet understood. Bands are ∼350 kDa (the position of the 250 kDa marker is not depicted on this immunoblot). An asterisk indicates a cross-reacting band, previously noted (25).

ATP/ADP ratio decreased with increased CAG length

The ATP/ADP ratio, a dominant quantitative phenotype known to vary with CAG size in human lymphoblastoid cells (18), was measured in all members of the ES cell panel, to assess the utility of this new resource for evaluating dominant CAG-correlated effects. Results of the HPLC analysis demonstrated that huntingtin-null $Hdh^{ex4/5/ex4/5}$ cells showed a trend toward higher ATP/ADP ratios than the wild-type $Hdh^{Q7/7}$ ES cells (Fig. 2A), consistent with the proposal that the full-length huntingtin negatively regulates this energy measure (18,32). In contrast, across the $Hdh^{Q20/7}$, $Hdh^{Q50/7}$, $Hdh^{Q91/7}$ and $Hdh^{Q111/7}$ ES cell panel, ATP/ADP ratios decreased concomitantly (Pearson's correlation test, $P = 0.018$) with the increased size of the longer CAG allele (Fig. 2B), confirming that lengthening the polyglutamine region in full-length huntingtin expressed from one allele enhanced the negative regulation of this energy measure, as reported previously (18,32).

In demonstrating the utility of the allelic ES cell panel for assessing a candidate CAG length-dependent phenotype, these results also implied that comprehensive phenotyping across the members of the panel would permit the discovery of new dominant CAG length-dependent responses.

Continuous analysis effectively identified changes correlated with CAG size

As an unbiased discovery approach, we utilized Affymetrix Mouse 430 2.0 gene chips to generate genome-wide gene expression datasets from RNA isolated from three independent subclones for each of the $Hdh^{Q20/7}$, $Hdh^{Q50/7}$, $Hdh^{Q91/7}$ and $Hdh^{Q111/7}$ ES cell genotypes (12 samples), as well as six wild-type $Hdh^{Q7/7}$ and six null $Hdh^{ex4/5/ex4/5}$ ES cell replicates (12 samples). The raw data sets were subject to standard quality control filtering steps (Materials and Methods).

The 12 CAG knock-in ES cell data sets were then analyzed to identify probes/genes with expression altered progressively with the CAG repeat size. As the CAG length is a single source of variation expected to produce subtle incremental changes, we reasoned that a continuous analytic strategy

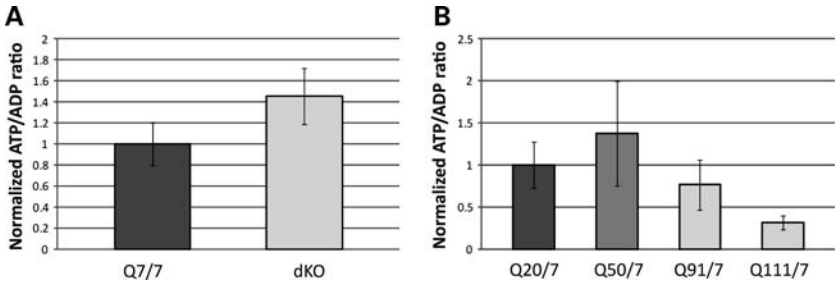

Figure 2. ATP/ADP ratio across the members of the ES cell panel. (**A**) The bar plot summarizes the results of HPLC determination of ATP/ADP ratio for replicates of $Hdh^{ex4/5}/Hdh^{ex4/5}$-null ES cells (dKO), expressed as a percentage of the parental wild-type ES cell ATP/ADP ratio, showing a trend ($P = 0.057$) toward increased ATP/ADP ratio in the absence of full-length huntingtin. All data points are included. (**B**) The bar plot summarizes the results of HPLC determination of ATP/ADP ratio for two biological replicates performed in duplicate for each member of the $Hdh^{20/7}$, $Hdh^{50/7}$, $Hdh^{91/7}$ and $Hdh^{111/7}$ knock-in ES series, expressed as a percentage of the $Hdh^{20/7}$ ATP/ADP ratio, demonstrating a decrease with increasing CAG repeat length (Pearson's correlation coefficient $P = 0.018$). All data points are included.

should effectively identify such alterations from among the gene expression changes due to all other factors (technical, biological and chance), whereas the standard dichotomous comparison (normal range versus HD range) would be expected to highlight any probes with altered expression, regardless of the cause.

Continuous analysis to uncover graded differences in signal intensity, with increased CAG size, was conducted by comparing the probe intensities from the $Hdh^{Q20/7}$, $Hdh^{Q50/7}$, $Hdh^{Q91/7}$ and $Hdh^{Q111/7}$ data sets with the CAG length of the corresponding cell lines using Pearson's correlation analysis. A total of 73 probes (Supplementary Material, Table S1) passed a rigorous statistical cut-off (absolute correlation coefficient > 0.8; $P < 0.001$). Of these, 48 probes were negatively correlated and 25 probes were positively correlated with the length of the CAG allele. Validation of a subset of these genes, by RT Q-PCR assay, verified that the RNA levels of the majority were significantly altered in the predicted direction (Supplementary Material, Fig. S2), strongly implying that the RNA levels of most of the genes in the set identified by this continuous analysis approach were likely to truly vary in a continuous fashion with CAG length.

The dichotomous normal-range versus HD-range allele analysis was conducted by comparing the normalized average signal intensity for each probe from the combined expanded CAG data sets ($Hdh^{Q50/7}$, $Hdh^{Q91/7}$ and $Hdh^{Q111/7}$) with the average signal intensity in the normal human CAG allele datasets ($Hdh^{Q20/7}$). Thirteen probes met stringent statistical criteria (Student's *t*-test, $P < 0.001$; absolute fold-change > 1.5) and 37 probes passed a less stringent cut-off ($P < 0.005$; absolute fold-change > 1.5), providing a set of probes whose expression differed significantly between ES cells with short and long CAGs (Supplementary Material, Table S2). However, as shown in the volcano plots presented in Figure 3, none of the 13 high-stringency probes (Fig. 3A) and only one of the 37 relaxed-stringency probes (Fig. 3B, filled red circle) exhibited a signal intensity that correlated with the CAG size. These results indicated that the traditional dichotomous analytical approach, most often used in the HD field, disclosed variation due to non-CAG repeat factors and did not efficiently uncover gene expression changes continuously correlated with the CAG length.

Genes altered with CAG size are distinct from genes altered with lack of huntingtin

Identification of a set of probes/genes whose expression conformed to the HD trigger mechanism (dominant, continuous with CAG length) allowed an empirical test to distinguish the main alternative hypotheses for the effects of the impact of the polyglutamine region on the full-length huntingtin: a simple gain of a novel function versus a more complex gain-of-function/loss-of-function scenario, including a dominant-negative loss of function. We determined whether the probes altered in a dominant CAG-continuous fashion, as outcomes of the full-length huntingtin gain of function might also be prominent in the ES cell response to the absence of huntingtin. Any model in which the expanded CAG contributes to a loss of huntingtin function would predict an extensive overlap in the molecular responses observed. However, the simple gain of a novel function hypothesis does not require any overlap.

First, the set of probes/genes with expression that differed between the $Hdh^{ex4/5/ex4/5}$ and wild-type ES cell data sets was identified by Student's *t*-test (Material and Methods). This comparison disclosed 754 probes with significantly different signal intensities (absolute fold-change > 1.5; $P < 0.001$): 398 increased and 356 decreased in the huntingtin-null ES data sets (Supplementary Material, Table S3). RT Q-PCR analysis of a subset of these genes generally confirmed the microarray data (Supplementary Material, Fig. S2A), though one gene (*Mest*), altered 20-fold in the RT Q-PCR analysis, was an outlier on the microarray platform (200-fold change).

Comparison of the 'huntingtin-null' probe set with the set of probes whose expression was continuously altered with CAG length revealed virtually no overlap; 99.6% (751 of 754) of the probes altered in cells lacking full-length huntingtin did not vary with CAG size (Fig. 3C) and 96% (70 of 73) of the CAG-correlated probes did not distinguish wild-type and full-length huntingtin-null ES cells (Fig. 3D). Probes for only three genes (*Mapt*, *Erdr1* and *Mll5*) were altered in both genetic paradigms. A second more global analytical approach, gene set enrichment analysis, also failed to disclose a significant overlap. The rank order of the probes significant in one paradigm, when assessed in the entire ~45 000 probe data set from the other paradigm, did not differ from what might be

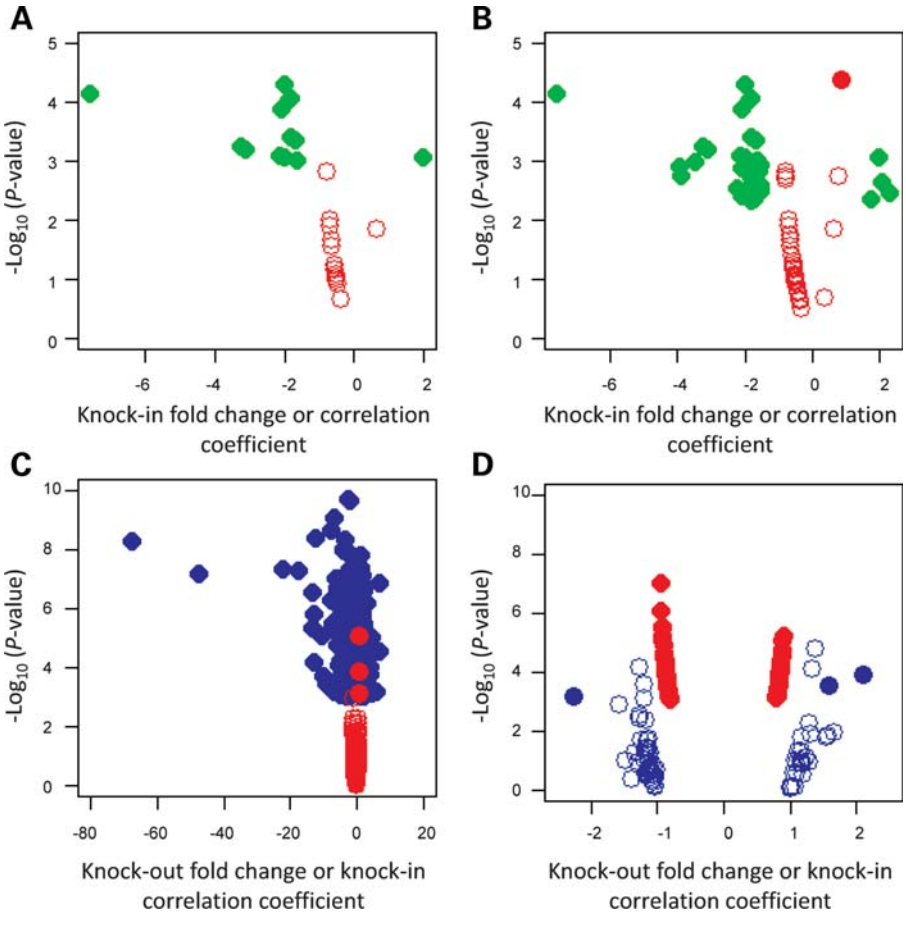

Figure 3. Comparisons of CAG-correlated and huntingtin-null gene sets. (**A**) Volcano plot showing $-\log_{10}(P)$ (*Y*-axis) for the 13 probes discovered by the dichotomous analysis of the CAG knock-in ES cell data sets at high statistical stringency ($P < 0.001$) relative to fold-change (*X*-axis) (green symbols) and the $-\log_{10}(P)$ (*Y*-axis) for each of these probes in the continuous analysis across the CAG knock-in ES cell data sets relative to Pearson's correlation coefficient (*X*-axis) (red symbols), demonstrating that none of the significant probes in the dichotomous analysis of the CAG knock-in ES cells was significantly correlated with the CAG repeat size. (**B**) Volcano plot showing $-\log_{10}(P)$ (*Y*-axis) for the 37 probes discovered by the dichotomous analysis of the CAG knock-in ES cell data sets at more relaxed statistical stringency ($P < 0.005$) relative to fold-change (*X*-axis) (green symbols) and the $-\log_{10}(P)$ (*Y*-axis) for each of these probes in the continuous analysis across the CAG knock-in ES cell data sets relative to Pearson's correlation coefficient (*X*-axis) (red symbols), demonstrating that only one probe from the less-stringent dichotomous analysis of the CAG knock-in ES cells was significantly correlated with the CAG repeat size (filled red circle). (**C**) Volcano plot showing $-\log_{10}(P)$ (*Y*-axis) for the 754 probes significantly ($P < 0.001$) different in huntingtin-null ES cell data sets, compared with wild-type parental ES cell data sets ($P < 0.001$) relative to fold-change (*X*-axis) (blue symbols) and the $-\log_{10}(P)$ (*Y*-axis) for each of these probes in the continuous analysis across the CAG knock-in ES cell data sets relative to Pearson's correlation coefficient (*X*-axis) (red symbols), revealing that few of the significant probes in the huntingtin-null ES cells were significantly correlated with the CAG repeat size. *Mest*, an outlier, was excluded from this analysis. (**D**) Volcano plot showing $-\log_{10}(P)$ (*Y*-axis) for the 73 probes with expression significantly ($P < 0.001$) correlated with CAG repeat length across the CAG knock-in ES cell data sets relative to Pearson's correlation coefficient > 0.8 (*X*-axis) (red symbols) and the $-\log_{10}(P)$ (*Y*-axis) for each of these probes in the huntingtin-null versus wild-type ES cell data set comparison relative to fold-change (*X*-axis) (blue symbols), demonstrating that most of the CAG-correlated probes were not significantly changed in the absence of huntingtin. The *X*-axis corresponds to fold-change for the dichotomous analysis and Pearson's correlation coefficient for continuous analysis. Open and filled circles represent non-significant and significant probes, respectively.

observed by chance, with low enrichment scores and high nominal *P*-values (Fig. 4).

The dominant molecular effects of extending the polyglutamine region in the full-length huntingtin, therefore, did not mimic the responses to lack of huntingtin function, contradicting dominant-negative loss of function or mixed gain-of-function/loss-of-function mechanisms, but consistent with a simple gain of a novel function hypothesis.

Related huntingtin pathways

If extending the polyglutamine region in the full-length huntingtin confers a simple gain of function, how then to explain reports of phenotypes implying loss of function? We reasoned that the response to the polyglutamine region in the full-length huntingtin (a structural alteration with a dominant impact, potentially acting through an intrinsic activity of huntingtin) and the response to lack of huntingtin (classic deficiency) might be expected to engage related pathways, predicting that the probe sets from the two genetic paradigms, though almost completely distinct, might actually be connected via common pathways.

sigPathway analysis identified 238 pathways significantly (gene set permutation $q < 0.01$ and phenotype permutation $q < 0.01$) altered between wild-type and huntingtin-null ES cell data sets (Supplementary Material, Table S4) and 172

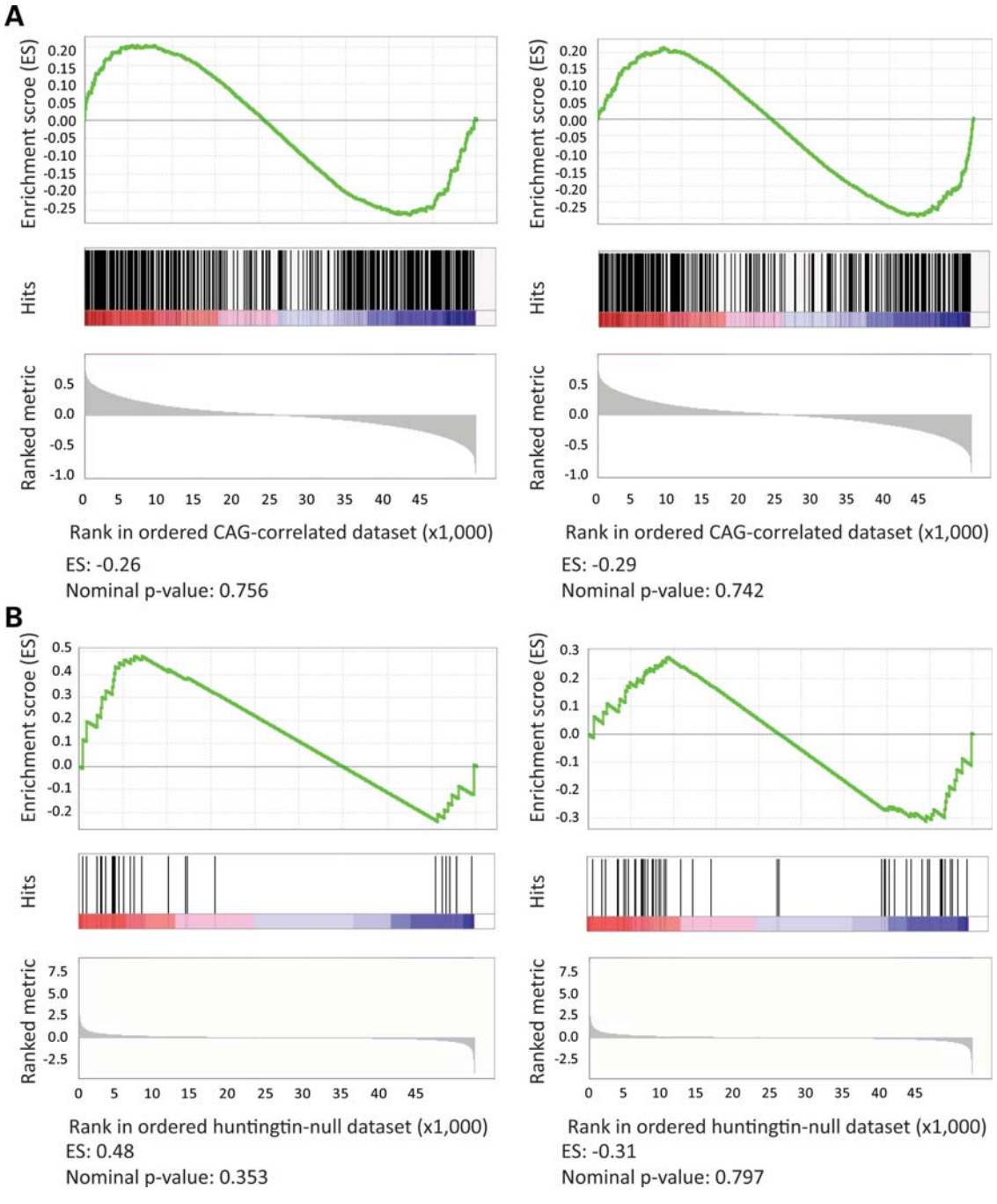

Figure 4. Tests of gene set enrichment by phenotype permutation analysis. The results of GSEA, using phenotype permutation (1000 iterations), are presented. *Top*: enrichment score (ES) representing the degree to which the test gene set is overrepresented at the top or bottom of the ranked genes from the other data set; *middle*: position of the test set probes in the other dataset; *bottom*: ranked metric (Pearson's correlation coefficient for the CAG-correlated data set or *t*-statistic for the huntingtin-null data set). The enrichment score (ES) and nominal *P*-value are shown at the bottom. (**A**) The probes with significantly increased (left panel) or decreased (right panel) expression in the huntingtin-null ES cell comparison were not significantly enriched in the CAG-correlated knock-in ES cell data set. (**B**) The probes with expression significantly positively correlated (left) or negatively correlated (right) with the CAG length in the knock-in ES cell data sets were not significantly enriched in the huntingtin-null ES cell data set.

pathways that correlated with CAG size across the knock-in ES cell panel data sets (Supplementary Material, Table S5). In support of overlap at the pathway, if not the probe level, 74 pathways were significant in both genetic paradigms (Supplementary Material, Table S6), and the gene set enrichment analysis (GSEA) with the top 20 ranked pathways from each paradigm disclosed significant enrichment in the entire 1947 pathways for the other paradigm (Fig. 5A and B). These results were unlikely to have been produced by chance because the true enrichment score (i.e. average rank of top 20 pathways in the other paradigm) significantly deviated from the majority of the enrichment scores obtained from

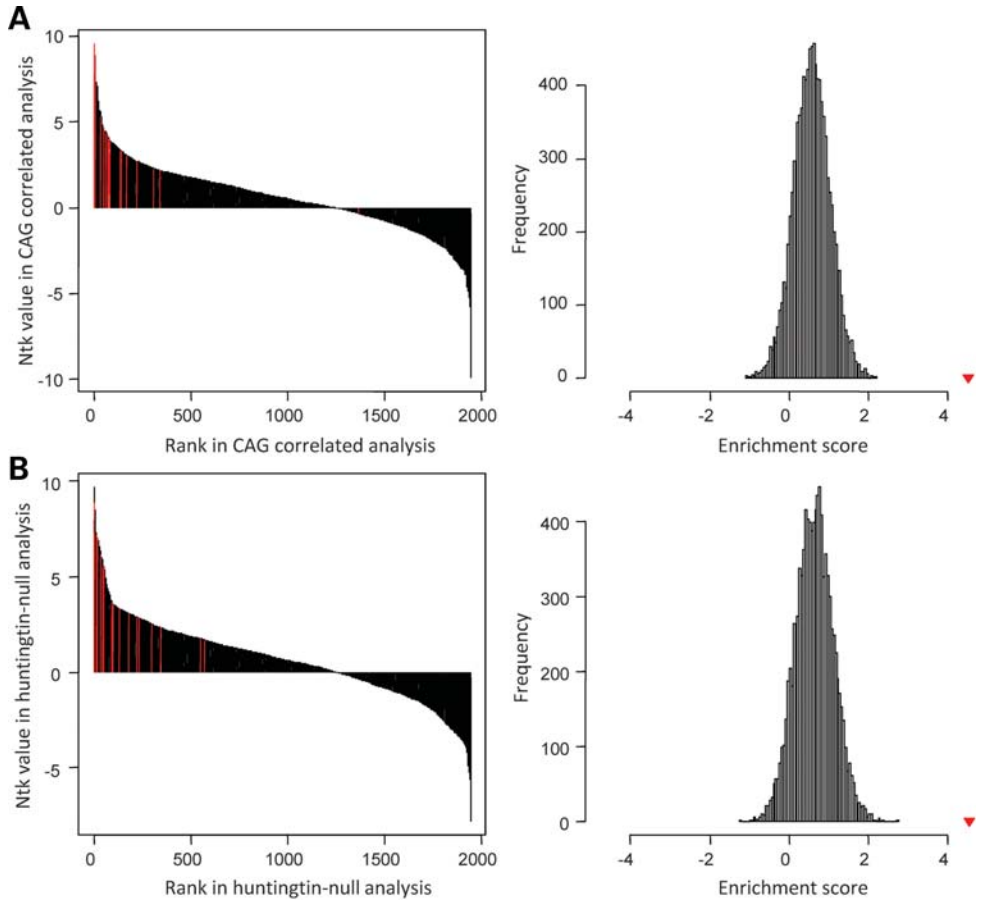

Figure 5. Tests of enrichment of significant pathways by permutation analysis. The results of permutation-based enrichment analysis to test whether a sort of the top 20 significant pathways in one paradigm was also significantly enriched in the other paradigm. *Left*: original sigPathway results (black bars) representing rank (*X*-axis) and NTk value from gene set permutations (*Y*-axis), with the rank of test pathways highlighted (red bars). *Right*: average ranks of test pathways (enrichment score) compared with the distribution obtained from a random sampling of 20 pathways from the compared data set (10 000 permutations). (**A**) Top 20 huntingtin-null significant pathways in CAG-correlated knock-in ES cell pathways indicated significant enrichment, with an enrichment score of 4.51, compared with a distribution of enrichment scores obtained from a random selection of 20 pathways in knock-in pathway results. (**B**) Top 20 CAG-correlated pathways in huntingtin-null pathways indicated significant enrichment, with an enrichment score of 4.55, compared with a distribution of enrichment scores obtained from a random selection of 20 pathways in knock-out pathway results. Red triangles in the right panels represent true enrichment scores.

simulations for each paradigm, with 10 000 iterations of permuted data sets. In addition, the majority of these pathways could be assigned to 13 categories at the network level, though, as shown in Figure 6A, six clusters were more prominently altered in the huntingtin-null ES cells (reproduction/development/growth, amino acid/peptide/protein metabolism, chromatin regulation, immune process, transcription/translation and signal transduction) and seven clusters were more prominently altered by extending the polyglutamine region in the full-length huntingtin (nucleotide metabolism, energy metabolism, regulation of cell cycle/death, RNA metabolism/ribosomal process, cell structure/adhesion, cellular component and lipid/sterol/lipoprotein metabolism).

Despite these general features of commonality and interconnection of the pathways altered in the two genetic paradigms, statistical analysis continued to highlight the lack of one-to-one correspondence between the specific alterations detected in these pathway data sets. The alterations of the 238 significant pathways in huntingtin-null were mildly predictive of a significant effect on the same pathways in the continuous CAG comparison (Spearman's rho 0.291; $P = 5.08\text{E}-6$) (Fig. 6B). However, alterations of the 172 full-length huntingtin polyglutamine region-correlated pathways were not at all predictive of a significant effect in the wild-type/huntingtin-null data set comparison (Spearman's rho 0.142; $P = 0.06282$) (Fig. 6C). Nor did the alterations observed in the 74 common pathways predict statistical significance from one genetic comparison to the other (Spearman's rho 0.147; $P = 0.2117$) (Fig. 6D). Therefore, while the huntingtin-null pathways captured a portion of the dominant response to increase the full-length huntingtin polyglutamine region, the conversing was not true.

Taken together, these findings implied that the probes/genes contributing to the CAG-correlation genetic paradigm and those contributing to the huntingtin-null genetic paradigm represent either different members of the same pathways or members of distinct but interconnected pathways within the same category networks.

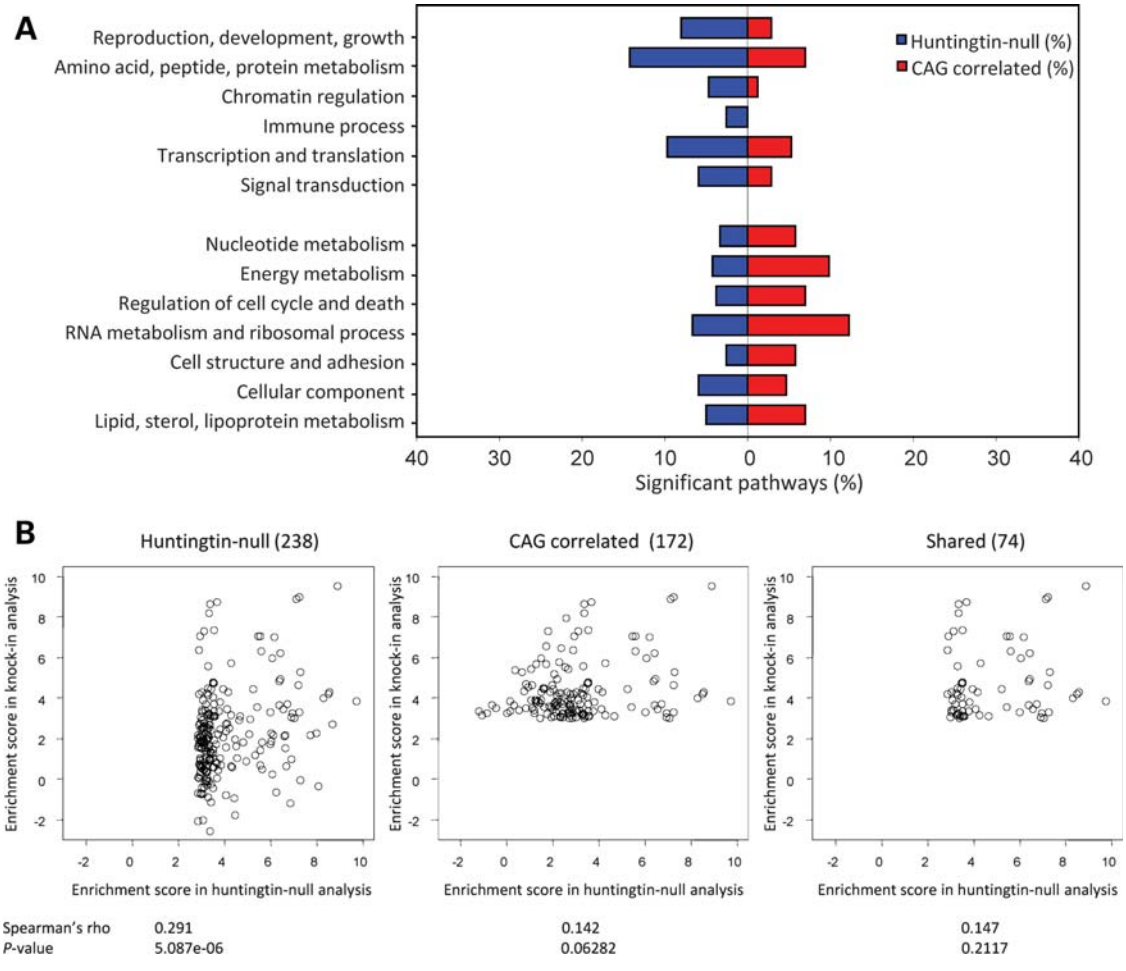

Figure 6. CAG-correlated and huntingtin-null pathway categories. A summary of sigPathway analysis results, with significant pathways for each paradigm grouped by category is presented (**A**), with results of correlation analysis testing the relationship between huntingtin-null significant pathways (KO) and the CAG-correlated pathways (KI) (**B**–**D**). (A) Bar plot of the proportion (*X*-axis) of the 238 pathways significantly enriched in the huntingtin-null ES cell comparison (blue) and the 172 significantly CAG-correlated pathways across the knock-in ES cell data sets (red) within 13 shared categories (*Y*-axis). (B) Left scatter plot displays the relationship of the enrichment scores of 238 huntingtin-null significant pathways (*X*-axis; NTk values) with the enrichment score for these pathways in the continuous CAG ES cell knock-in pathways analysis (*Y*-axis; NTk values). The Spearman's rank correlation statistic (rho) and the significant *P*-value indicate that the huntingtin-null pathways capture to some extent the CAG-correlated pathway set. Middle scatter plot displays the relationship of the enrichment scores of the 172 continuous CAG-correlated pathways (*X*-axis) with the enrichment score for these pathways from the huntingtin-null analysis (*Y*-axis). The Spearman's rank correlation statistic (rho) and the non-significant *P*-value indicate that the pathways significantly altered with the CAG size are not altered by the absence of huntingtin. The right scatter plot shows the relationship between the enrichment scores of 74 pathways significant in both the huntingtin-null ES cell analysis (*X*-axis) and the CAG continuous ES cell data analysis (*Y*-axis). The Spearman's rank correlation statistic (rho) and the non-significant *P*-value indicate that the enrichment score in one analysis does not predict the enrichment score in the other paradigm, indicating that these pathways are not consistently altered in the different paradigms.

Interconnectedness of CAG-correlated and huntingtin-null pathways

To explore this possibility, we examined the hierarchical relationships of the pathways in the energy and lipid/cholesterol/sterol categories. The energy network (24 pathways) (Fig. 7 and Supplementary Material, Fig. S3) comprised pathways altered with the size of the full-length huntingtin polyglutamine region (carbohydrate metabolism, glycolysis) and other pathways prominent in huntingtin deficiency (mitochondrial, TCA cycle, oxidative respiration) with only a few pathways common to both. In contrast, the lipid/sterol/lipoprotein network (17 pathways) (Fig. 8 and Supplementary Material, Fig. S4) comprised nearly equal proportions of processes prominent in the response to extending the full-length huntingtin polyglutamine region (phospholipid metabolism), pathways prominent in the wild-type/huntingtin-null comparison (acetyl-CoA, glycerophospholipid metabolism) and shared pathways common to both genetic paradigms (cholesterol, sterol).

These hierarchies demonstrated that some of the genes that were uniquely changed with increasing CAG repeat length were different members of the same pathways as genes that were altered by the complete absence of huntingtin, while other CAG-repeat-altered genes were members of distinct pathways that were not significantly affected by the lack of huntingtin. However, even the latter CAG-correlated pathways, though distinct, were often closely connected in the network to the pathways changed in the absence of

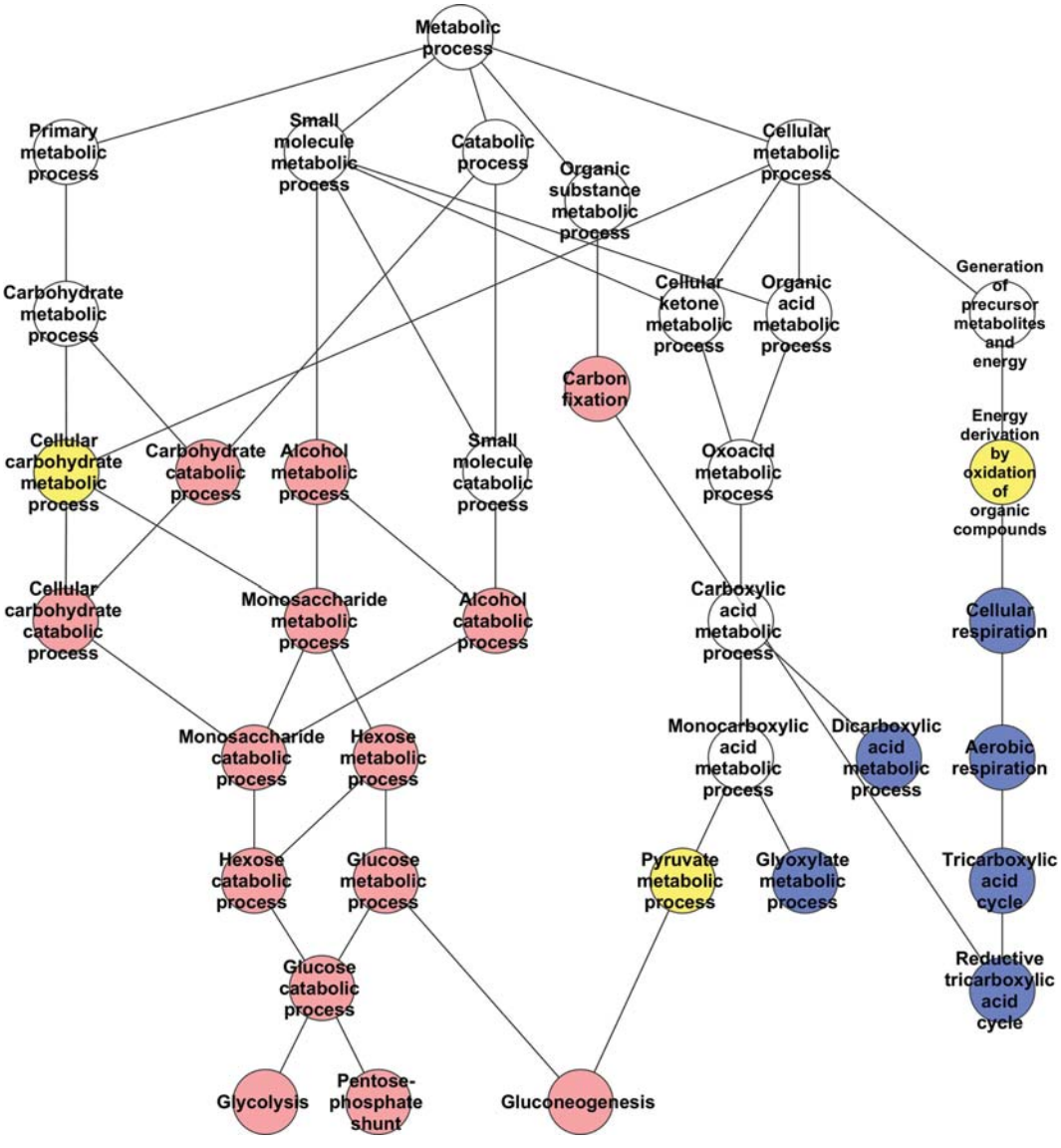

Figure 7. Energy category pathways network. A schematic demonstrating the hierarchy of relationships between the processes/pathways significantly correlated with the CAG repeat length (red), significantly altered in the absence of huntingtin (blue) or significantly altered in both full-length huntingtin genetic paradigms (yellow). The cellular component 'Mitochondrial matrix', significantly altered only in the huntingtin-null ES cell analysis, is not shown. Only directly related pathways are illustrated. The KEGG/GO annotations for the pathways are provided in Supplementary Material, Figure S3.

huntingtin. The highly interconnected character of these networks, which are impacted by altering both the full-length huntingtin polyglutamine repeat and the dose of the full-length huntingtin, predicts that, integrating across the network, both genetic paradigms might in some cases be expected to produce similar phenotypic outcomes despite emanating from different initial insults, whereas in other cases the phenotypic outcomes may be distinct.

DISCUSSION

The accumulated evidence indicates that the HD CAG repeat acts as a functional DNA polymorphism, encoding a polyglutamine region in the full-length huntingtin that exerts dominant effects that are graduated with CAG length across an allelic continuum. Yet HD homozygotes exist, despite expressing no normal-range full-length huntingtin, and conversely, huntingtin deficiency does not mimic HD. A parsimonious explanation is that the polyglutamine repeat confers a simple gain of a novel function, such that the full-length huntingtin is modulated, though not impaired, in a graded manner that yields dominant effects that are continuous with polyglutamine length.

Investigations of this hypothesis and alternative proposals, such as a gain of a dominant-negative loss of full-length huntingtin function, have been hampered by the lack of an appropriate series of CAG alleles in a cell culture system, for which there are also HD knock-out alleles. The isogenic allelic ES cell panel that we have generated now provides a suitable cell culture system. It comprises a series of heterozygous

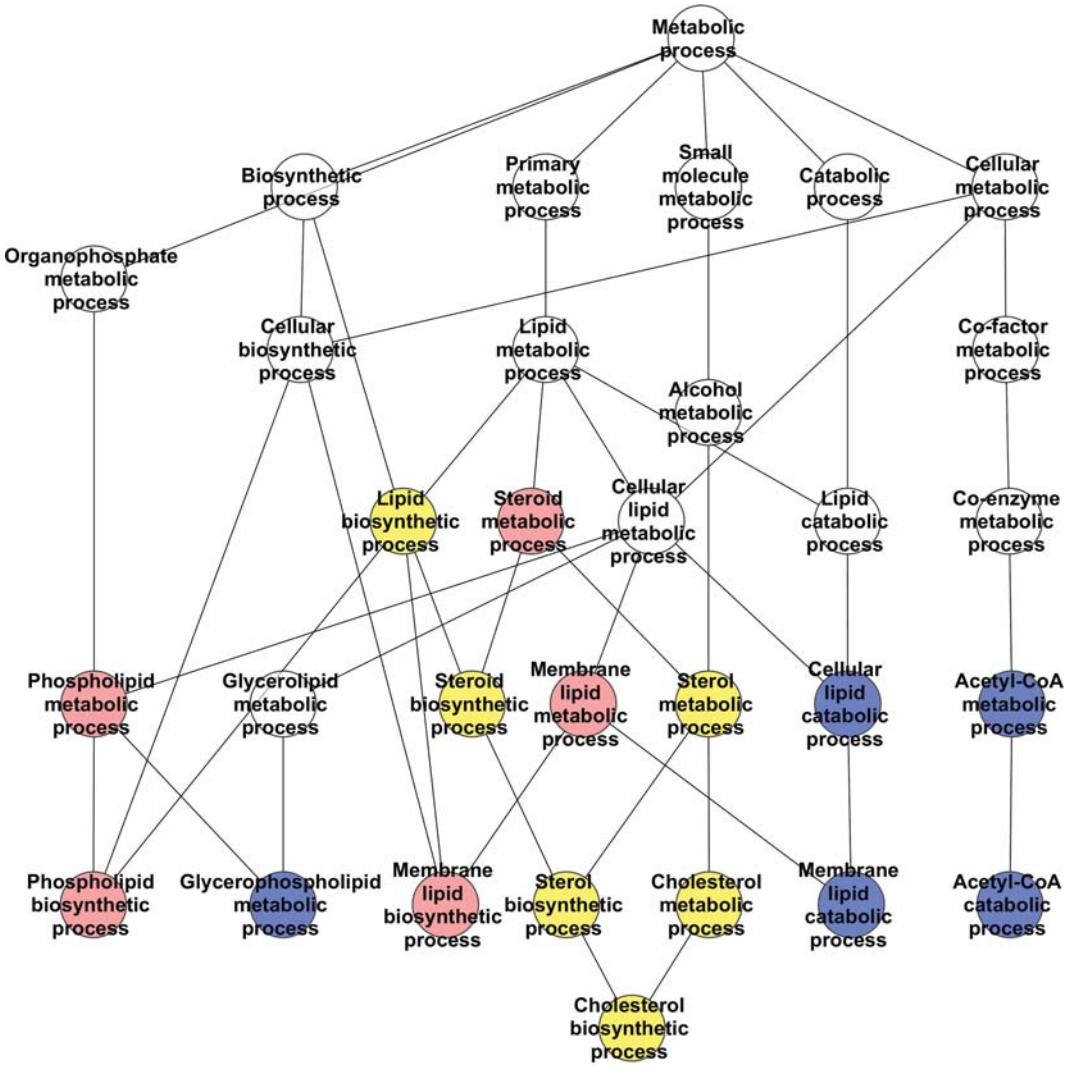

Figure 8. Lipid, sterol and lipoprotein metabolism category pathways network. A schematic demonstrating the hierarchy of relationships between the processes/pathways significantly correlated with the CAG repeat length (red), significantly altered in the absence of huntingtin (blue) or significantly altered in both full-length huntingtin genetic paradigms (yellow). The catalytic activity 'phospholipase A2', which is significantly changed only in the absence of huntingtin, is not depicted on the pathway annotation diagram. Only directly related pathways are illustrated. The KEGG/GO annotations for the pathways are provided in Supplementary Material, Figure S4.

CAG knock-in ES cell lines, appropriately expressing full-length huntingtins with 20, 50, 91 or 111 polyglutamine repeats (from endogenous alleles), augmenting the wild-type and huntingtin-null ES cell lines, previously reported. The members of this ES cell panel can undergo development, allowing studies in differentiated cell types, such as neuronal cells.

The allelic ES cell panel allows investigations to determine whether candidate phenotypes may (or may not) be dominant and progressive with CAG size. ATP/ADP ratios, continuously decreased with CAG size in human lymphoblastoid cell lines (18), were decreased with CAG length across the knock-in ES cell members, and ATP/ADP ratio was increased in the absence of full-length huntingtin, in knock-out ES cells, consistent with the proposal that the polyglutamine repeat enhances an as-yet uncharacterized role of full-length huntingtin in negatively regulating this energetic measure (18,32). The allelic CAG ES cell series, therefore, offers a resource with which to further assess purported HD-associated differences from studies in human and non-human systems to determine whether they conform to the dominant continuous effects of the HD CAG repeat, rather than emanating from other sources of variation that may distinguish HD and non-HD samples.

The discovery of new dominant CAG length-dependent effects can also be efficiently accomplished by phenotyping across the members of a CAG allelic panel. Continuous analysis, though not dichotomous analysis, efficiently uncovered genes with CAG-correlated expression from genome-wide data sets. The success of the continuous analytical approach, with four different CAG allele lengths on an isogenic genetic background, predicts that this strategy can be effective in identifying the dominant effects of the CAG repeat in human samples, though the increased genetic heterogeneity,

and higher proportion of expanded CAG alleles in the adult onset rather than the juvenile onset range, will likely require a larger panel representing a denser series of CAG alleles across the continuum. Knowledge of the dominant molecular, biochemical and cellular responses that emanate from the quantitative impact of the polyglutamine repeat on full-length huntingtin, especially in cells of neuronal lineages, should provide a better understanding of the molecular mechanism that initiates the pathogenic process to which these cells are vulnerable.

In our study, the CAG knock-in and huntingtin-null panel members allowed an evaluation of alternate hypotheses for the impact of the polyglutamine repeat on full-length huntingtin: a simple gain of a novel function versus a dominant-negative or a mixed gain/loss of function. The CAG-correlated gene set was strikingly distinct from the huntingtin-null gene set, failing to support a model involving a loss of function. However, this outcome was completely consistent with a simple novel gain-of-function hypothesis, which posits different mechanisms for the two genetic paradigms and does not require any overlap in the two gene sets to be valid. This finding joins the previous genetic evidence supporting a mechanism of a simple gain of a novel function, wherein the structural alteration of the full-length huntingtin by the polyglutamine repeat produces a graded effect on some action of huntingtin, though it does not impair the protein's inherent function. Whether the gain of function involves the graded modulation of a property/task intrinsic to the full-length huntingtin or, alternatively, adds a novel non-intrinsic property/task into full-length huntingtin's biological repertoire remains to be determined. Simple enhancement of an intrinsic action of huntingtin by the polyglutamine repeat is supported by the interrelated nature of the pathways that emerged from the two genetic huntingtin paradigms. However, the polyglutamine repeat might also confer a new property, because, while the huntingtin-null changes do to a certain extent capture the CAG repeat-correlated changes, the converse is not the case. Thus, our results support the view that the polyglutamine repeat may confer enhanced intrinsic huntingtin activity and/or confer some additional non-intrinsic property on the full-length huntingtin.

Indeed, rather than revealing a common mechanism, our analyses indicate that the distinct CAG-correlated and huntingtin-null genes, defined by the structure–function and deficiency strategies, respectively, identify instead an interrelated hierarchy of biological pathways. The pathways that were specifically correlated with CAG size were not predictive of the pathways altered by huntingtin knock-out. However, together, the pathways clustered into about a dozen biological categories or networks in realms consistent with previous reports of huntingtin function (41), some influenced more prominently by the full-length huntingtin polyglutamine repeat (energy, cholesterol/sterol/lipid, nucleotide metabolism, regulation of cell cycle/death, RNA metabolism/ribosomal process and cell structure/adhesion) (18,32,42–45) and some by huntingtin deficiency (reproduction/development, protein metabolism, chromatin regulation, transcription and translation, immune process and signal transduction) (28,37,46–50).

The energy metabolism network revealed the effects of the polyglutamine-size in full-length huntingtin on glycolysis and of huntingtin deficiency on the tricarboxylic acid (Krebs) cycle, respectively. However, few processes were shared, implying that the elevated or decreased ATP/ADP ratios, respectively, that result from these insults may result from distinct rate-limiting steps in each case. The lipid/sterol/lipoprotein metabolism network, with unique impacts of polyglutamine size in full-length huntingtin on phospholipid/lipid biosynthesis and huntingtin deficiency on lipid catabolism (β-oxidation) and acetyl-CoA catabolism, respectively, featured a high proportion of shared processes, notably lipid, steroid and cholesterol biosynthesis. Thus, the two distinct full-length huntingtin mechanisms, polyglutamine expansion versus protein deficiency, which altered the expression of completely different gene sets, both converged at the pathway level on cholesterol biosynthesis, strongly implying that decreased levels of cholesterol biosynthetic intermediates in cells expressing either normal or mutant huntingtin likely result via different mechanisms due to the effects on distinct rate-limiting steps within the same network (34,51).

The CAG-correlated genes and pathways, which conform to genetically defined properties expected of the consequences of the HD disease-initiating mechanism, demonstrate the wide physiological impact of varying the polyglutamine repeat in full-length huntingtin. Though a common regulator is formally possible, it seems unlikely that targeting any single candidate regulator will effectively mitigate most of the many hundreds of interconnected consequences of the CAG repeat. Instead, our results strongly support a system-wide approach to the discovery and validation of factors that may moderate the dominant effects of extending the polyglutamine region in full-length huntingtin. Moreover, for therapeutic strategies aimed at lowering the expression of the expanded CAG allele, our results in this proof-of-concept experiment in murine ES cells strongly suggest that understanding the biological processes perturbed by the lack of full-length huntingtin may be important, as such treatments might instead exacerbate the physiologic effects of the expanded CAG repeat.

MATERIALS AND METHODS

ES cell culture

Wild-type parental, huntingtin null $Hdh^{ex4/5/ex4/5}$ and $Hdh^{neoQ20/7}$, $Hdh^{neoQ50/7}$ $Hdh^{neoQ91/7}$ $Hdh^{neoQ111/7}$ mouse ES cell lines have been reported previously (9,14,25,27). ES cells were maintained on feeder layers of irradiated mouse embryonic fibroblasts (Global Stem Sciences) at 37°C in 5% CO_2 or on gelatin-coated plates (1% gelatin solution; Millipore). ES cell media (ESCM) typically contained Knock-Out D-MEM (Invitrogen), 15% FBS (Hyclone), 50 I.U/ml of penicillin, 50 μg/ml of streptomycin (Cellgro), 0.2 mM GlutaMax (Invitrogen), 0.1 mM MEM non-essential amino acids (Invitrogen), 0.1 mM 2-mercaptoethanol (Sigma) and 1000 U/ml of leukemia inhibitory factor (LIF) (Millipore). For ES cell lines with targeted alleles, the media also contained G418 (150–450 μg/ml). Cells were passaged by trypsinization (0.05% trypsin, 0.53 mM EDTA) (Cellgro) every 3 days. For

molecular analysis (protein, RNA, DNA), cells were grown on gelatin-coated plates in ESCM. Molecular analyses and analyses of nucleotide (ATP and ADP) levels were performed on independent cell cultures, grown under standard conditions.

To induce embryoid body (EB) formation, 5×10^6 ES cells were grown in the absence of feeder cells on 10 cm bacterial plates in ESCM without LIF. The day 4 EBs were characterized with germ-layer-specific markers using RT–PCR amplification assays as described below.

Adeno-Cre recombinase and identification of ES cells with neo-out CAG knock-in alleles

The *Hdh*$^{neo20/7}$, *Hdh*$^{neo50/7}$, *Hdh*$^{neo91/7}$ and *Hdh*$^{neo111/7}$ ES cells, in each case, were plated in 12-well plates at $\sim 2.5 \times 10^5$ cells/well, in G418 selection, and infected with 200 infectious units/cell Adeno-Cre (Ad5CMVCre). The following day, the selection was removed by changing to a medium lacking G418. Established colonies were subsequently plated into wells of duplicate 96-well plates, into media with G418 or media without G418. For each line, those G418-sensitive subclones that grew in the absence of G418, but not in the presence of G418, were propagated to establish PGKneo-minus lines for three to four subclones for each member of the allelic ES cell series. PCR amplification analysis confirmed the proper Cre-recombinase removal of the PGKneo cassette. DNA was purified using the Gentra Puregene Cell kit (Qiagen) and treated with RNase A, following the manufacturer's instructions. Primers to assess the presence of the PGKneo cassette were: Mouse mod-2 Neo-in F: 5′-GATCTCCTGTCATCTC ACCTTG-3′ and 5′-UTR R: 5′-CAGGCAGGCAGC AGTAGTTA-3′. Cycling conditions were as follows: 94°C for 5 min, followed by 30 cycles of 94°C for 30 s, 60°C for 30 s, 72°C for 90 s and a final extension at 72°C for 7 min. Primers to assess the absence of the PGKneo cassette were: Neo-out F: 5′-TCACTGCTTGGCTTTTTCCT-3′ and 5′-UTR R: 5′-CAGGCAGGCAGCAGTAGTTA-3′. Cycling conditions were as follows: 94°C for 5 min, followed by 30 cycles of 94°C for 30 s, 60°C for 30 s, 72°C for 1 min and a final extension at 72°C for 7 min.

Quantitative RT–PCR amplification assays

For RNA extraction, washed ES cell pellets were homogenized in TRIzol (Invitrogen) and total RNA isolated using phenol/chloroform. Following digestion with DNaseI recombinant RNase-free (Roche), RNA was reverse-transcribed to produce cDNA using Superscript III according to the manufacturer's guidelines (Invitrogen). An oligo-dT primer was used to prime cDNA synthesis. Each quantitative real-time PCR amplification reaction was performed in a total volume of 40 μl using 2× iQ SYBR Green Supermix (Bio-Rad) and 0.2 pmol primer. Primers were designed to the 3′ end of each transcript analyzed and all products were 70–100 bp in length. Cycling parameters were: 95°C for 2 min to denature followed by 40 cycles of 95°C for 15 s and 60°C for 1 min. Melting temperature analysis was performed at the end of each run to validate the specificity of the PCR amplicon. Assays were conducted in a 96-well plate format with 'no template' and 'no reverse transcriptase' controls and run on the iQ cycler (Bio-Rad). Three technical replicates were performed for each sample and all genes were compared with the reference gene, mouse β-actin. Primers were designed using Primer3 software (http://frodo.wi.mit.edu/).

Primers to assess EB primary germ layers were: *Afp* F: 5′-AGCAAAGCTGCGCTCTCTAC-3′ and *Afp* R: 5′-CCGA GAAATCTGCAGTGACA-3′, *Pdx1* F: 5′-GAAATCCA CCAAAGCTCACG-3′ and *Pdx1* R: 5′-TCTCCGGCTATA CCCAACTG-3′, *Bry* F: 5′-CCGGTGCTGAAGGTAAATGT -3′ and *Bry* R: 5′-TGACCGGTGGTTCCTTAGAG 3′, *Actc* F: 5′ GCTTTGGTGTGTGACAATGG-3′ and *Actc* R: 5′-AGAGACAGCACTGCCTGGAT-3′, *Pax6* F: 5′-AGGGGGAGAGAACACCAACT-3′ and *Pax6* R: 5′ GG TTGCATAGGCAGGTTGTT-3′, *Ncam1* F: 5′-AGCTG AAAACCAGCAAGGAA-3′ and *Ncam1* R: 5′-TTTTGTTTG TGTGGCATCGT-3′. Cycling conditions for *Afp*, *Actc*, *Pdx* and *Pax6* were 94°C for 5 min, followed by 30 cycles of 94°C for 30 s, 55°C for 30 s, 72°C for 45 s and a final extension at 72°C for 7 min. Cycling conditions for *Bry* are: 94°C for 5 min, followed by 30 cycles of 94°C for 30 s, 50°C for 30 s, 72°C for 45 s and a final extension at 72°C for 7 min. Cycling conditions for *Ncam1* are: 94°C for 5 min, followed by 30 cycles of 94°C for 30 s, 60°C for 30 s, 72°C for 45 s and a final extension at 72°C for 7 min.

Primers to validate microarray results were: *Mapt* F: 5′-GCTCGTTAGGGAACATCCAT-3′ and *Mapt* R: 5′- TC GACTGGACTCTGTCCTTG-3′, *Mll5* F: 5′-GAACAGTTT GAAGCAAATGGAT-3′ and *Mll5* R: 5′-CCTCATTCCCA AAAGTCCTC-3′, *Erdr1* F: 5′-AGTGATGTCACCCACG AAAG-3′ and *Erdr1* R: 5′-GTGGGGATGGCAGAGAC AT-3′, *Bhlhb2* F: 5′-CACCCCAAGATCCTTTCTGT-3′ and *Bhlhb2* R: 5′-GGAGATGGAACCCTTTTTAGC-3′, *Ccdc18* F: 5′-TGGTTTAAGTCAGGGAGGAAA-3′ and *Ccdc18* R: 5′-AGCACAGTACCAACAATTCCA-3′, *Abca1* F: 5′-TGT TGCATCCCTTTTTGTAGA-3′ and *Abca1* R: 5′-AAAGCA CAAAACCAGCTTCA-3′, *Mest* F: 5′-AGTGAGGGAGG AGCTTGCTA-3′ and *Mest R*: 5′-GCAGCCGATGAAA CTAAATG-3′, *Xlr* F: 5′-GGAAGCCAGAAAGCTAATGG-3′ and *Xlr* R: 5′-GATTGAACACCATCCTTTGC-3′, *Tgm2* F: 5′-AGAGCCTGGGAAGAATCAAA-3′ and *Tgm2* R: 5′-AA AAGAAACAGAACCGTGTGG-3′, *Lrp2* F: 5′-CTGAGC AAAAGGAAGCTGTG-3′ and *Lrp2* R: 5′-CAGTGTA GCCTGGAGTCGAA-3′, *Snapc1* F: 5′-TCCAACAGAA GAAAGGTGTCA-3′ and *Snapc1* R: 5′-GCATGCTCTTCC ATCTCACA-3′, *Utp14a* F: 5′-AAGGCTGTGGATCTGA CCTT-3′ and *Utp14a* R: 5′-CCCTCAGGGGCTTTAAT AAG-3′, *NfuI* F: 5′-TCCATCATCACCCTGAAGAG-3′ and *NfuI* R: 5′-TTCGTCATCATCCATCACCT-3′, *Hsd17b11* F: 5′-GAAAGGATCGTCCCTGAGAG-3′ and *Hsd17b11* R: 5′-GCTGCGTCACTTGTCTTTGT-3′, *Rpap2* F: 5′ GTTG CTGGAGGTGTCCACTA-3′ and *Rpap2* R: 5′-AGGGGA GAGAGTGGGAAAGT-3′, *Nicn1* F: 5′-AGTTAAGCCCCAC TGACAGG-3′ and *Nicn* R: 5′-GATCCTCTTTGCCCAAG TGT-3′, *Ngdn* F: 5′-CAGAGTCAGGAGGATCAGCA-3′ and *Ngdn* R: 5′-CCTTCGCAGTCCTTTCTCTC-3′, *β-actin* F: 5′-GACGGCCAGGTCATCACTAT-3′ and *β-actin* R: 5′-ATGCCACAGGATTCCATACC-3′. Cycling conditions are described previously.

Immunoblot analysis

Protein extracts were prepared from washed cell pellets by lysis on ice for 30 min in a buffer containing 20 mM HEPES (pH 7.6), 1 mM EDTA, 0.5% Triton X-100, protease inhibitor mixture (Roche) and 1 mM phenylmethyl sulfonyl fluoride. Lysates were mixed every 10 min during the incubation. The lysates were then cleared by centrifugation at 14 000g for 30 min and the supernatants collected. The protein concentration was determined using the Bio-Rad (detergent compatible) protein assay. Twenty-five micrograms of protein extract was mixed with 4× SDS sample buffer, boiled for 2 min and subjected to 6 or 10% SDS–PAGE. After electrophoresis, the proteins were transferred to nitrocellulose membranes (Schleicher & Schuell) and incubated for 30 min in a blocking solution containing 5% non-fat powdered milk in TBS-T (50 mM Tris–HCl, 150 mM NaCl, pH 7.4, 0.1% Tween-20). The membranes were probed overnight at 4°C with the primary antibody mAb2166 (Chemicon). After four 10 min TBS-T washes, the blots were incubated for 1 h at room temperature with horseradish peroxidase-conjugated anti-mouse antibodies. After an extensive 30 min wash, the membranes were processed using an ECL chemiluminiscence substrate kit (New England Biolabs) and exposed to autoradiographic film (Hyperfilm ECL; Amersham Bioscience). Notably, on SDS–PAGE immunoblots, anti-huntingtin antibodies are known to detect full-length huntingtin proteins differentially, based upon the length of the polyglutamine tract, though the reasons for this phenomenon are not yet known.

HPLC ATP/ADP measurement

Nucleotide extraction was as previously described (18,52). To normalize the amount of nucleotide, each pellet was solubilized with 1 N NaOH and the protein content was analyzed by Bio-Rad DC protein assay (Bio-Rad). HPLC-grade nucleotide standards (Fluka) were used to calibrate the signals. Internal standards were occasionally added to the samples to test recovery, which exceeded 90% for all nucleotides. Data were quantified by Breez software.

Microarray analysis

RNA extracted from ES cells using TRIzol reagent (Invitrogen) was further purified through RNeasy mini columns (Qiagen). All RNA samples passed quality control steps, including RNA purity check (OD 260/280 ratio) and Bioanalyzer analysis (Agilent). Total RNA (5 μg) was converted, using SuperScript II reverse transcriptase (Invitrogen), to cRNA, and labeled cRNA was prepared by *in vitro* transcription (Affymetrix). Twenty-five micrograms of labeled probe was hybridized to Affymetrix MG 430 2.0 arrays. Expression data were normalized using gcrma (R, 2.6.2; gcrma, 2.6.0), and significant probes were identified by nominal *P*-value ($P < 0.001$) and fold-change (absolute fold-change > 1.5) or Pearson's correlation coefficient (absolute correlation coefficient > 0.8). All microarray data have been deposited in NCBI's Gene Expression Omnibus (accession number GSE26001).

Gene set enrichment analysis

To test whether a set of significantly altered probes in knock-out ES cells was enriched in knock-in ES cells, GSEA (53) was performed using phenotype permutation procedures (1000 permutations). Similarly, we tested whether significantly correlated probes in knock-in ES cells were significantly enriched in knock-out ES cells using GSEA. For identification of significantly enriched pathways in knock-out and knock-in ES cells, pre-compiled gene sets from pathway databases (Biocarta and KEGG) and Gene Ontology were analyzed using the sigPathway program (54). Gene sets with sizes between 25 and 500 were selected, and gene sets showing undirectional enrichment were identified by gene set permutation (10 000) and phenotype permutation (1000) (false discovery rate, $q < 0.01$). To assess commonality between significant pathways in knock-out and CAG knock-in cells, the average of ranks of the top 20 knock-out significant pathways in the CAG knock-in data (i.e. enrichment score; 4.51) was compared with a distribution of averages of ranks obtained by randomly choosing the same number of pathways in knock-in data (10 000 permutations). Similarly, the average of ranks of the top 20 knock-in significant pathways in the knock-out data (i.e. enrichment score; 4.55) was compared with a distribution of averages of ranks of 20 randomly chosen pathways in knock-out data. Networks of significant pathways were hand-annotated, identifying shared pathway categories using the graphical view feature on the gene ontology website. Significant pathways from the KEGG database were annotated using the corresponding GO pathway. Networks were drawn using Cytoscape (version 2.7.0).

SUPPLEMENTARY MATERIAL

Supplementary Material is available at *HMG* online.

Conflict of Interest statement. None declared.

FUNDING

This work was supported by National Institute of Neurological Disorders and Stroke (grant number NS32765 to M.E.M.), The Massachusetts HD Center Without Walls (grant number NS16367 to J.F.G. and M.E.M.), i2b2 (grant number LM008748-01 to I.S.K.), the Huntington's Disease Society of America Coalition for the Cure Normal Function Team (to M.E.M. and J.F.G.), and an Anonymous Donor. J.M.W. was the recipient of the Milton Wexler Postdoctoral Fellowship from the Hereditary Disease Foundation. G.G. was the recipient of the Sir Keith Murdoch Fellowship from the American Australian Association. J.J. is the recipient of the Philip Wrightson Fellowship from the Neurological Foundation of New Zealand.

REFERENCES

1. Vonsattel, J.P. and DiFiglia, M. (1998) Huntington disease. *J. Neuropathol. Exp. Neurol.*, **57**, 369–384.

2. Huntington's Disease Collaborative Research Group (1993) A novel gene containing a trinucleotide repeat that is expanded and unstable on Huntington's disease chromosomes. *Cell*, **72**, 971–983.
3. McNeil, S.M., Novelletto, A., Srinidhi, J., Barnes, G., Kornbluth, I., Altherr, M.R., Wasmuth, J.J., Gusella, J.F., MacDonald, M.E. and Myers, R.H. (1997) Reduced penetrance of the Huntington's disease mutation. *Hum. Mol. Genet.*, **6**, 775–779.
4. Quarrell, O.W., Rigby, A.S., Barron, L., Crow, Y., Dalton, A., Dennis, N., Fryer, A.E., Heydon, F., Kinning, E., Lashwood, A. *et al.* (2007) Reduced penetrance alleles for Huntington's disease: a multi-centre direct observational study. *J. Med. Genet.*, **44**, e68.
5. Kenney, C., Powell, S. and Jankovic, J. (2007) Autopsy-proven Huntington's disease with 29 trinucleotide repeats. *Mov. Disord.*, **22**, 127–130.
6. Hendricks, A.E., Latourelle, J.C., Lunetta, K.L., Cupples, L.A., Wheeler, V., MacDonald, M.E., Gusella, J.F. and Myers, R.H. (2009) Estimating the probability of de novo HD cases from transmissions of expanded penetrant CAG alleles in the Huntington disease gene from male carriers of high normal alleles (27–35 CAG). *Am. J. Med. Genet. A.*, **149A**, 1375–1381.
7. Duyao, M., Ambrose, C., Myers, R., Novelletto, A., Persichetti, F., Frontali, M., Folstein, S., Ross, C., Franz, M., Abbott, M. *et al.* (1993) Trinucleotide repeat length instability and age of onset in Huntington's disease. *Nat. Genet.*, **4**, 387–392.
8. Snell, R.G., MacMillan, J.C., Cheadle, J.P., Fenton, I., Lazarou, L.P., Davies, P., MacDonald, M.E., Gusella, J.F., Harper, P.S. and Shaw, D.J. (1993) Relationship between trinucleotide repeat expansion and phenotypic variation in Huntington's disease. *Nat. Genet.*, **4**, 393–397.
9. Auerbach, W., Hurlbert, M.S., Hilditch-Maguire, P., Wadghiri, Y.Z., Wheeler, V.C., Cohen, S.I., Joyner, A.L., MacDonald, M.E. and Turnbull, D.H. (2001) The HD mutation causes progressive lethal neurological disease in mice expressing reduced levels of huntingtin. *Hum. Mol. Genet.*, **10**, 2515–2523.
10. Fossale, E., Wheeler, V.C., Vrbanac, V., Lebel, L.A., Teed, A., Mysore, J.S., Gusella, J.F., MacDonald, M.E. and Persichetti, F. (2002) Identification of a presymptomatic molecular phenotype in Hdh CAG knock-in mice. *Hum. Mol. Genet.*, **11**, 2233–2241.
11. Heng, M.Y., Detloff, P.J., Paulson, H.L. and Albin, R.L. (2010) Early alterations of autophagy in Huntington disease-like mice. *Autophagy*, **6**, 1206–1208.
12. Heng, M.Y., Tallaksen-Greene, S.J., Detloff, P.J. and Albin, R.L. (2007) Longitudinal evaluation of the Hdh(CAG)150 knock-in murine model of Huntington's disease. *J. Neurosci.*, **27**, 8989–8998.
13. Menalled, L.B. (2005) Knock-in mouse models of Huntington's disease. *NeuroRx*, **2**, 465–470.
14. Wheeler, V.C., Auerbach, W., White, J.K., Srinidhi, J., Auerbach, A., Ryan, A., Duyao, M.P., Vrbanac, V., Weaver, M., Gusella, J.F. *et al.* (1999) Length-dependent gametic CAG repeat instability in the Huntington's disease knock-in mouse. *Hum. Mol. Genet.*, **8**, 115–122.
15. Wheeler, V.C., Gutekunst, C.A., Vrbanac, V., Lebel, L.A., Schilling, G., Hersch, S., Friedlander, R.M., Gusella, J.F., Vonsattel, J.P., Borchelt, D.R. *et al.* (2002) Early phenotypes that presage late-onset neurodegenerative disease allow testing of modifiers in Hdh CAG knock-in mice. *Hum. Mol. Genet.*, **11**, 633–640.
16. Wheeler, V.C., White, J.K., Gutekunst, C.A., Vrbanac, V., Weaver, M., Li, X.J., Li, S.H., Yi, H., Vonsattel, J.P., Gusella, J.F. *et al.* (2000) Long glutamine tracts cause nuclear localization of a novel form of huntingtin in medium spiny striatal neurons in HdhQ92 and HdhQ111 knock-in mice. *Hum. Mol. Genet.*, **9**, 503–513.
17. Perlis, R.H., Smoller, J.W., Mysore, J., Sun, M., Gillis, T., Purcell, S., Rietschel, M., Nothen, M.M., Witt, S., Maier, W. *et al.* (2010) Prevalence of incompletely penetrant Huntington's disease alleles among individuals with major depressive disorder. *Am. J. Psychiatry*, **167**, 574–579.
18. Seong, I.S., Ivanova, E., Lee, J.M., Choo, Y.S., Fossale, E., Anderson, M., Gusella, J.F., Laramie, J.M., Myers, R.H., Lesort, M. *et al.* (2005) HD CAG repeat implicates a dominant property of huntingtin in mitochondrial energy metabolism. *Hum. Mol. Genet.*, **14**, 2871–2880.
19. Andrade, M.A. and Bork, P. (1995) HEAT repeats in the Huntington's disease protein. *Nat. Genet.*, **11**, 115–116.
20. Li, W., Serpell, L.C., Carter, W.J., Rubinsztein, D.C. and Huntington, J.A. (2006) Expression and characterization of full-length human huntingtin, an elongated HEAT repeat protein. *J. Biol. Chem.*, **281**, 15916–15922.
21. Seong, I.S., Woda, J.M., Song, J.J., Lloret, A., Abeyrathne, P.D., Woo, C.J., Gregory, G., Lee, J.M., Wheeler, V.C., Walz, T. *et al.* (2010) Huntingtin facilitates polycomb repressive complex 2. *Hum. Mol. Genet.*, **19**, 573–583.
22. Takano, H. and Gusella, J.F. (2002) The predominantly HEAT-like motif structure of huntingtin and its association and coincident nuclear entry with dorsal, an NF-kB/Rel/dorsal family transcription factor. *BMC Neurosci.*, **3**, 15.
23. Grinthal, A., Adamovic, I., Weiner, B., Karplus, M. and Kleckner, N. (2010) PR65, the HEAT-repeat scaffold of phosphatase PP2A, is an elastic connector that links force and catalysis. *Proc. Natl Acad. Sci. USA*, **107**, 2467–2472.
24. Ambrose, C.M., Duyao, M.P., Barnes, G., Bates, G.P., Lin, C.S., Srinidhi, J., Baxendale, S., Hummerich, H., Lehrach, H., Altherr, M. *et al.* (1994) Structure and expression of the Huntington's disease gene: evidence against simple inactivation due to an expanded CAG repeat. *Som. Cell Mol. Genet.*, **20**, 27–38.
25. Duyao, M.P., Auerbach, A.B., Ryan, A., Persichetti, F., Barnes, G.T., McNeil, S.M., Ge, P., Vonsattel, J.P., Gusella, J.F., Joyner, A.L. *et al.* (1995) Inactivation of the mouse Huntington's disease gene homolog Hdh. *Science*, **269**, 407–410.
26. Nasir, J., Floresco, S.B., O'Kusky, J.R., Diewert, V.M., Richman, J.M., Zeisler, J., Borowski, A., Marth, J.D., Phillips, A.G. and Hayden, M.R. (1995) Targeted disruption of the Huntington's disease gene results in embryonic lethality and behavioral and morphological changes in heterozygotes. *Cell*, **81**, 811–823.
27. White, J.K., Auerbach, W., Duyao, M.P., Vonsattel, J.P., Gusella, J.F., Joyner, A.L. and MacDonald, M.E. (1997) Huntingtin is required for neurogenesis and is not impaired by the Huntington's disease CAG expansion. *Nat. Genet.*, **17**, 404–410.
28. Zeitlin, S., Liu, J.P., Chapman, D.L., Papaioannou, V.E. and Efstratiadis, A. (1995) Increased apoptosis and early embryonic lethality in mice nullizygous for the Huntington's disease gene homologue. *Nat. Genet.*, **11**, 155–163.
29. Myers, R.H., Leavitt, J., Farrer, L.A., Jagadeesh, J., McFarlane, H., Mastromauro, C.A., Mark, R.J. and Gusella, J.F. (1989) Homozygote for Huntington disease. *Am. J. Hum. Genet.*, **45**, 615–618.
30. Wexler, N.S., Young, A.B., Tanzi, R.E., Travers, H., Starosta-Rubinstein, S., Penney, J.B., Snodgrass, S.R., Shoulson, I., Gomez, F., Ramos Arroyo, M.A. *et al.* (1987) Homozygotes for Huntington's disease. *Nature*, **326**, 194–197.
31. Brooks, S., Higgs, G., Jones, L. and Dunnett, S.B. (2010) Longitudinal analysis of the behavioural phenotype in Hdh((CAG)150) Huntington's disease knock-in mice. *Brain Res. Bull*. In press.
32. Clabough, E.B. and Zeitlin, S.O. (2006) Deletion of the triplet repeat encoding polyglutamine within the mouse Huntington's disease gene results in subtle behavioral/motor phenotypes in vivo and elevated levels of ATP with cellular senescence in vitro. *Hum. Mol. Genet.*, **15**, 607–623.
33. Zuccato, C., Belyaev, N., Conforti, P., Ooi, L., Tartari, M., Papadimou, E., MacDonald, M., Fossale, E., Zeitlin, S., Buckley, N. *et al.* (2007) Widespread disruption of repressor element-1 silencing transcription factor/neuron-restrictive silencer factor occupancy at its target genes in Huntington's disease. *J. Neurosci.*, **27**, 6972–6983.
34. Valenza, M., Carroll, J.B., Leoni, V., Bertram, L.N., Bjorkhem, I., Singaraja, R.R., Di Donato, S., Lutjohann, D., Hayden, M.R. and Cattaneo, E. (2007) Cholesterol biosynthesis pathway is disturbed in YAC128 mice and is modulated by huntingtin mutation. *Hum. Mol. Genet.*, **16**, 2187–2198.
35. Valenza, M., Rigamonti, D., Goffredo, D., Zuccato, C., Fenu, S., Jamot, L., Strand, A., Tarditi, A., Woodman, B., Racchi, M. *et al.* (2005) Dysfunction of the cholesterol biosynthetic pathway in Huntington's disease. *J. Neurosci.*, **25**, 9932–9939.
36. Zuccato, C., Tartari, M., Crotti, A., Goffredo, D., Valenza, M., Conti, L., Cataudella, T., Leavitt, B.R., Hayden, M.R., Timmusk, T. *et al.* (2003) Huntingtin interacts with REST/NRSF to modulate the transcription of NRSE-controlled neuronal genes. *Nat. Genet.*, **35**, 76–83.
37. Futter, M., Diekmann, H., Schoenmakers, E., Sadiq, O., Chatterjee, K. and Rubinsztein, D.C. (2009) Wild-type but not mutant huntingtin modulates the transcriptional activity of liver X receptors. *J. Med. Genet.*, **46**, 438–446.
38. Borrell-Pages, M., Zala, D., Humbert, S. and Saudou, F. (2006) Huntington's disease: from huntingtin function and dysfunction to therapeutic strategies. *Cell. Mol. Life Sci.*, **63**, 2642–2660.

39. Cattaneo, E., Rigamonti, D., Goffredo, D., Zuccato, C., Squitieri, F. and Sipione, S. (2001) Loss of normal huntingtin function: new developments in Huntington's disease research. *Trends Neurosci.*, **24**, 182–188.
40. Zuccato, C., Ciammola, A., Rigamonti, D., Leavitt, B.R., Goffredo, D., Conti, L., MacDonald, M.E., Friedlander, R.M., Silani, V., Hayden, M.R. *et al.* (2001) Loss of huntingtin-mediated BDNF gene transcription in Huntington's disease. *Science*, **293**, 493–498.
41. MacDonald, M.E. (2003) Huntingtin: alive and well and working in middle management. *Sci. STKE*, **2003**, pe48.
42. Caviston, J.P. and Holzbaur, E.L. (2009) Huntingtin as an essential integrator of intracellular vesicular trafficking. *Trends Cell. Biol.*, **19**, 147–155.
43. Faber, P.W., Barnes, G.T., Srinidhi, J., Chen, J., Gusella, J.F. and MacDonald, M.E. (1998) Huntingtin interacts with a family of WW domain proteins. *Hum. Mol. Genet.*, **7**, 1463–1474.
44. Godin, J.D., Colombo, K., Molina-Calavita, M., Keryer, G., Zala, D., Charrin, B.C., Dietrich, P., Volvert, M.L., Guillemot, F., Dragatsis, I. *et al.* (2010) Huntingtin is required for mitotic spindle orientation and mammalian neurogenesis. *Neuron*, **67**, 392–406.
45. Hilditch-Maguire, P., Trettel, F., Passani, L.A., Auerbach, A., Persichetti, F. and MacDonald, M.E. (2000) Huntingtin: an iron-regulated protein essential for normal nuclear and perinuclear organelles. *Hum. Mol. Genet.*, **9**, 2789–2797.
46. Kegel, K.B., Sapp, E., Alexander, J., Valencia, A., Reeves, P., Li, X., Masso, N., Sobin, L., Aronin, N. and DiFiglia, M. (2009) Polyglutamine expansion in huntingtin alters its interaction with phospholipids. *J. Neurochem.*, **110**, 1585–1597.
47. Lumsden, A.L., Henshall, T.L., Dayan, S., Lardelli, M.T. and Richards, R.I. (2007) Huntingtin-deficient zebrafish exhibit defects in iron utilization and development. *Hum. Mol. Genet.*, **16**, 1905–1920.
48. Truant, R., Atwal, R.S. and Burtnik, A. (2007) Nucleocytoplasmic trafficking and transcription effects of huntingtin in Huntington's disease. *Prog. Neurobiol.*, **83**, 211–227.
49. Valencia, A., Reeves, P.B., Sapp, E., Li, X., Alexander, J., Kegel, K.B., Chase, K., Aronin, N. and DiFiglia, M. (2010) Mutant huntingtin and glycogen synthase kinase 3-beta accumulate in neuronal lipid rafts of a presymptomatic knock-in mouse model of Huntington's disease. *J. Neurosci. Res.*, **88**, 179–190.
50. Zhang, H., Das, S., Li, Q.Z., Dragatsis, I., Repa, J., Zeitlin, S., Hajnoczky, G. and Bezprozvanny, I. (2008) Elucidating a normal function of huntingtin by functional and microarray analysis of huntingtin-null mouse embryonic fibroblasts. *BMC Neurosci.*, **9**, 38.
51. Battista, N., Bari, M., Tarditi, A., Mariotti, C., Bachoud-Levi, A.C., Zuccato, C., Finazzi-Agro, A., Genitrini, S., Peschanski, M., Di Donato, S. *et al.* (2007) Severe deficiency of the fatty acid amide hydrolase (FAAH) activity segregates with the Huntington's disease mutation in peripheral lymphocytes. *Neurobiol. Dis.*, **27**, 108–116.
52. Gines, S., Seong, I.S., Fossale, E., Ivanova, E., Trettel, F., Gusella, J.F., Wheeler, V.C., Persichetti, F. and MacDonald, M.E. (2003) Specific progressive cAMP reduction implicates energy deficit in presymptomatic Huntington's disease knock-in mice. *Hum. Mol. Genet.*, **12**, 497–508.
53. Subramanian, A., Tamayo, P., Mootha, V.K., Mukherjee, S., Ebert, B.L., Gillette, M.A., Paulovich, A., Pomeroy, S.L., Golub, T.R., Lander, E.S. *et al.* (2005) Gene set enrichment analysis: a knowledge-based approach for interpreting genome-wide expression profiles. *Proc. Natl Acad. Sci. USA*, **102**, 15545–15550.
54. Tian, L., Greenberg, S.A., Kong, S.W., Altschuler, J., Kohane, I.S. and Park, P.J. (2005) Discovering statistically significant pathways in expression profiling studies. *Proc. Natl. Acad. Sci. USA*, **102**, 13544–13549.

Appendix C

Reprint of:

Myre, M. A., Lumsden, A. L., Thompson, M. N., Wasco, W., MacDonald, M. E., Gusella, J. F. *Deficiency of huntingtin has pleiotropic effects in the social amoeba Dictyostelium discoideum*. PLoS Genet, 2011. **7**(4):e1002052.

Attributions

My question:

Pertaining to this manuscript, the question I personally sought to address was: Is the functional requirement for huntingtin in cell adhesion & the cytoskeleton conserved in *Dictyostelium*?

My research contributions:

I discovered a defect in the developmental acquisition of cell-cell adhesion in huntingtin deficient *Dictyostelium* (Figure 7) that was included in the manuscript reprinted here in Appendix C. Since that time, I have performed all of the experiments to characterize this defect in cell-cell adhesion, detailed in Chapter 4, and a manuscript of this work is in preparation.

Significance:

My research provides preliminary evidence that the function of huntingtin in cell adhesion may be conserved. I uncovered the existence of novel adhesion biology in early *Dictyostelium* development, developing two assay systems that can be used in future mechanistic studies.

OPEN ACCESS Freely available online PLoS GENETICS

Deficiency of Huntingtin Has Pleiotropic Effects in the Social Amoeba *Dictyostelium discoideum*

Michael A. Myre[1]*, Amanda L. Lumsden[1], Morgan N. Thompson[1], Wilma Wasco[2], Marcy E. MacDonald[1], James F. Gusella[1]

1 Molecular Neurogenetics Unit, Center for Human Genetic Research, Massachusetts General Hospital, Boston, Massachusetts, United States of America, **2** Genetics and Aging Research Unit, MassGeneral Institute for Neurodegenerative Disease, Massachusetts General Hospital, Charlestown, Massachusetts, United States of America

Abstract

Huntingtin is a large HEAT repeat protein first identified in humans, where a polyglutamine tract expansion near the amino terminus causes a gain-of-function mechanism that leads to selective neuronal loss in Huntington's disease (HD). Genetic evidence in humans and knock-in mouse models suggests that this gain-of-function involves an increase or deregulation of some aspect of huntingtin's normal function(s), which remains poorly understood. As huntingtin shows evolutionary conservation, a powerful approach to discovering its normal biochemical role(s) is to study the effects caused by its deficiency in a model organism with a short life-cycle that comprises both cellular and multicellular developmental stages. To facilitate studies aimed at detailed knowledge of huntingtin's normal function(s), we generated a null mutant of *hd*, the *HD* ortholog in *Dictyostelium discoideum*. *Dictyostelium* cells lacking endogenous huntingtin were viable but during development did not exhibit the typical polarized morphology of *Dictyostelium* cells, streamed poorly to form aggregates by accretion rather than chemotaxis, showed disorganized F-actin staining, exhibited extreme sensitivity to hypoosmotic stress, and failed to form EDTA-resistant cell–cell contacts. Surprisingly, chemotactic streaming could be rescued in the presence of the bivalent cations Ca^{2+} or Mg^{2+} but not pulses of cAMP. Although hd^{-} cells completed development, it was delayed and proceeded asynchronously, producing small fruiting bodies with round, defective spores that germinated spontaneously within a glassy sorus. When developed as chimeras with wild-type cells, hd^{-} cells failed to populate the pre-spore region of the slug. In *Dictyostelium*, huntingtin deficiency is compatible with survival of the organism but renders cells sensitive to low osmolarity, which produces pleiotropic cell autonomous defects that affect cAMP signaling and as a consequence development. Thus, *Dictyostelium* provides a novel haploid organism model for genetic, cell biological, and biochemical studies to delineate the functions of the HD protein.

Citation: Myre MA, Lumsden AL, Thompson MN, Wasco W, MacDonald ME, et al. (2011) Deficiency of Huntingtin Has Pleiotropic Effects in the Social Amoeba *Dictyostelium discoideum*. PLoS Genet 7(4): e1002052. doi:10.1371/journal.pgen.1002052

Editor: Gregory S. Barsh, Stanford University School of Medicine, United States of America

Received November 23, 2010; **Accepted** March 2, 2011; **Published** April 28, 2011

Funding: This study was funded by grants NINDS NS032765, Massachusetts HD Center Without Walls NS016367, Huntington's Disease Society of America Coalition for the Cure, and the CHDI Foundation. ALL received a fellowship from the Hereditary Disease Foundation. The funders had no role in study design, data collection and analysis, decision to publish, or preparation of the manuscript.

Competing Interests: The authors have declared that no competing interests exist.

* E-mail: myre@chgr.mgh.harvard.edu

Introduction

Huntington's disease (HD) is an autosomal dominant neurodegenerative disorder whose clinical manifestations include psychiatric disturbances, cognitive decline and characteristic involuntary movements, typically diagnosed in mid-life [1,2]. HD is caused by a CAG trinucleotide repeat expansion mutation (>35 units) that produces an elongated version of a normally polymorphic polyglutamine segment in huntingtin [3–5], a large 350 kDa ubiquitously expressed HEAT (*h*untingtin, *e*longation factor 3, the *A* subunit of protein phosphatase 2A, and *T*OR1) repeat protein.

Several lines of evidence indicate that the HD mutation confers a CAG length-dependent 'gain-of-function' that likely produces its distinctive neuropathology through a modulatory effect on some structural or functional feature of huntingtin [6–9]. HD homozygote individuals with two mutant *HD* genes, and therefore no wild-type huntingtin, develop the characteristic movement disorder with timing comparable to that seen in typical *HD* mutation heterozygote individuals, indicating the absence of a strong dosage effect. Moreover, complete deficiency of huntingtin causes developmental abnormalities and embryonic lethality in the mouse that can be fully rescued by mutant huntingtin, indicating that these fundamental normal functions of huntingtin are not abrogated by the HD mutation. Thus, defining the disease-producing 'gain-of-function' - either a polyglutamine-length dependent increase or deregulation of a normal huntingtin activity or the introduction of a novel polyglutamine-length dependent activity, will require an understanding of the protein's normal function(s).

Huntingtin is present throughout eukaryotic evolution except in fungi and plants and shows no close primary sequence homology to any other protein [6]. Therefore, one approach to huntingtin function is to investigate its orthologs in tractable experimental models. Manipulation of the *HD* gene homologs in model organisms has revealed that huntingtin is essential for normal embryonic development both in the mouse and in the zebrafish [10–13], is dispensable for *Drosophila* development [14] and is implicated in a variety of functions ranging from vesicle trafficking to chromatin silencing and gene expression [15–18]. However, though murine embryonic stem cells lacking huntingtin are viable

Author Summary

Genetic evidence in humans and mouse models of Huntington's disease suggests that the disease mutation confers a deleterious gain-of-function on huntingtin that acts through the deregulation of some aspect of the protein's normal function(s). While huntingtin's function is poorly understood, its evolutionary conservation makes investigation of its physiological role in lower organisms an attractive route that has yet to be fully exploited. Therefore, we have used *Dictyostelium discoideum* to study the consequences of huntingtin (*hd*) deficiency. Developing *Dictyostelium* cells chemotax to form a multicellular slug that forms a fruiting body, comprising dormant spores encased above dead stalk cells. We found that hd^- cells were hypersensitive to hypoosmotic stress. When starved, hd^- cells aggregate by accretion, showed disorganized F-actin, and failed to form EDTA-resistant cell–cell contacts. Surprisingly, chemotactic signaling was rescued with Ca^{2+} or Mg^{2+} but not pulses of cAMP. Development of hd^- mutants produced small fruiting bodies with round, defective spores, and when mixed with wild-type cells they didn't differentiate into spores. Our results are consistent with mammalian studies that show huntingtin is a multifunctional protein involved in many biochemical processes; and, importantly, they establish *Dictyostelium* as a valuable experimental organism for exploring in biochemical detail huntingtin's normal function(s).

in tissue culture, permitting multi-cellular developmental studies *in vitro* [10], investigation of huntingtin function in single cells versus multicellular stages of development would be expedited by an experimental organism with a short life-cycle, comprising cellular and multicellular developmental stages.

The soil amoeba *Dictyostelium discoideum* is a *bona fide* multicellular eukaryotic organism with a haploid genome and a relatively simple developmental program that serves as a model for basic biological research [19] and is emerging as a valuable tool for understanding gene function and pathogenic mechanisms in a variety of human disorders [20–24]. During development, *Dictyostelium* undergoes a series of coordinated morphological and physiological changes that are initiated by starvation and progress in defined stages over a 24 hour period. Within the first 6 hours of development, cells secrete, and undergo chemotaxis toward cyclic adenosine monophosphate (cAMP) to form aggregation centers. The secretion of cAMP promotes a G protein-coupled receptor signal/response cascade resulting in the formation of loose mounds comprising up to 100,000 cells [25,26]. As development continues, cells within the mound are directed to differentiate into either prestalk or prespore cells, leading to morphological changes that yield a multicellular stalk, supporting a ball of encapsulated dormant spores [27].

To explore huntingtin function in both single cells and multicellular structures of the same organism, we have characterized a *Dictyostelium* ortholog (*hd*) of the human *HD* gene, have generated a viable *hd*-null mutant and have delineated a number of consequent phenotypes. We present evidence to suggest that huntingtin is a multifunctional protein that plays a protective role during hypoosmotic stress, regulates cell shape and homophilic cell-cell adhesion through a cytoskeletal–based mechanism, modulates pre-spore/spore cell fate determination and affects spore dormancy in *Dictyostelium*. Interestingly, hd^- cells were found to have a requirement for bivalent cations in the medium for optimal chemotaxis and cell aggregation. Our findings establish *Dictyostelium* as a valuable experimental eukaryotic organism for exploring in biochemical detail huntingtin's normal function(s), as defined by the pleiotropic effects of huntingtin deficiency throughout the developmental life cycle.

Results

The *Dictyostelium* huntingtin ortholog

The *Dictyostelium discoideum* genome, examined via dictyBase (www.dictybase.org) [28], contains a single gene (DDB_G0272344) with evident sequence homology to human huntingtin. The *hd* locus is comprised of four exons, located on chromosome 2. Analysis of GenBank with psi-BLAST [29,30] placed the product of *hd* firmly within the huntingtin family (Figure 1A), with a length of 3,095 amino acids comparable to the 3,144 amino acids of human huntingtin. Structural analysis of huntingtin proteins has identified the presence of numerous HEAT and HEAT-like repeats thought to produce a large α-helical solenoid rather than a typical globular protein [6,15,31,32]. *Dictyostelium* huntingtin is also predicted to be α-helical across most of its length (Figure 1B) and, as in other organisms, BLASTP searches of GenBank revealed no significant sequence alignments with other *Dictyostelium* proteins. Interestingly, *Dictyostelium* huntingtin contains a polyglutamine tract of 19 residues (Figure 1B) that is comparable in size to that found in normal-range human huntingtin but is encoded by the trinucleotide repeat CAA interrupted by a single CAG codon, is not followed by a polyproline domain, is located further downstream of the initiator methionine (at residue 533 rather than residue 18 as in the human protein), and may reflect the unusually high number of predicted proteins (~34%) that contain homopolymer tracts of 15 residues or more in *Dictyostelium* [33].

Dictyostelium huntingtin was expressed throughout growth and development

To determine the spatial and temporal pattern of huntingtin mRNA expression throughout the life cycle (Figure 2A); we cloned the intergenic region up to the closest upstream gene (608 bp) and used it to replace the actin15 promoter in pTX-GFP and to direct expression of the green fluorescent protein (GFP), which was detected in all cell types of transformed AX3 wild-type *Dictyostelium* cells during growth and development (Figure 2B, 2C, 2D), a pattern that fits well with the developmental and cell-type specific mRNA expression data acquired through extensive microarray and RNA-seq analysis which is freely available in dictyBase (DDB_G0272344) [34]. To further characterize the function of huntingtin in *Dictyostelium*, we examined the existence of alternate transcripts using exon specific primers and reverse transcriptase polymerase chain reaction (RT-PCR). No alternatively spliced forms of mRNA could be detected using various primer sets specific for exons (exon 1–exon 4) during vegetative growth and development of AX3 cells (Figure 2E).

Huntingtin-null cells display pleiotropic phenotypes

To explore huntingtin function, we utilized homologous recombination to create multiple independent *Dictyostelium* strains carrying a disruption of the *hd* gene in the haploid genome (Figure 3A). The disruption cassette targeted *hd* such that a double-recombination event would remove 278 bp of exon 2 and insert a blasticidin resistance (*Bsr*) selection cassette (Figure 3B, 3C). Following transformation of parental AX3 cells and blasticidin selection, 150 independent resistant clones were isolated and those (16) with the properly targeted *hd* gene disruption were identified by PCR amplification of the expected genomic DNA products

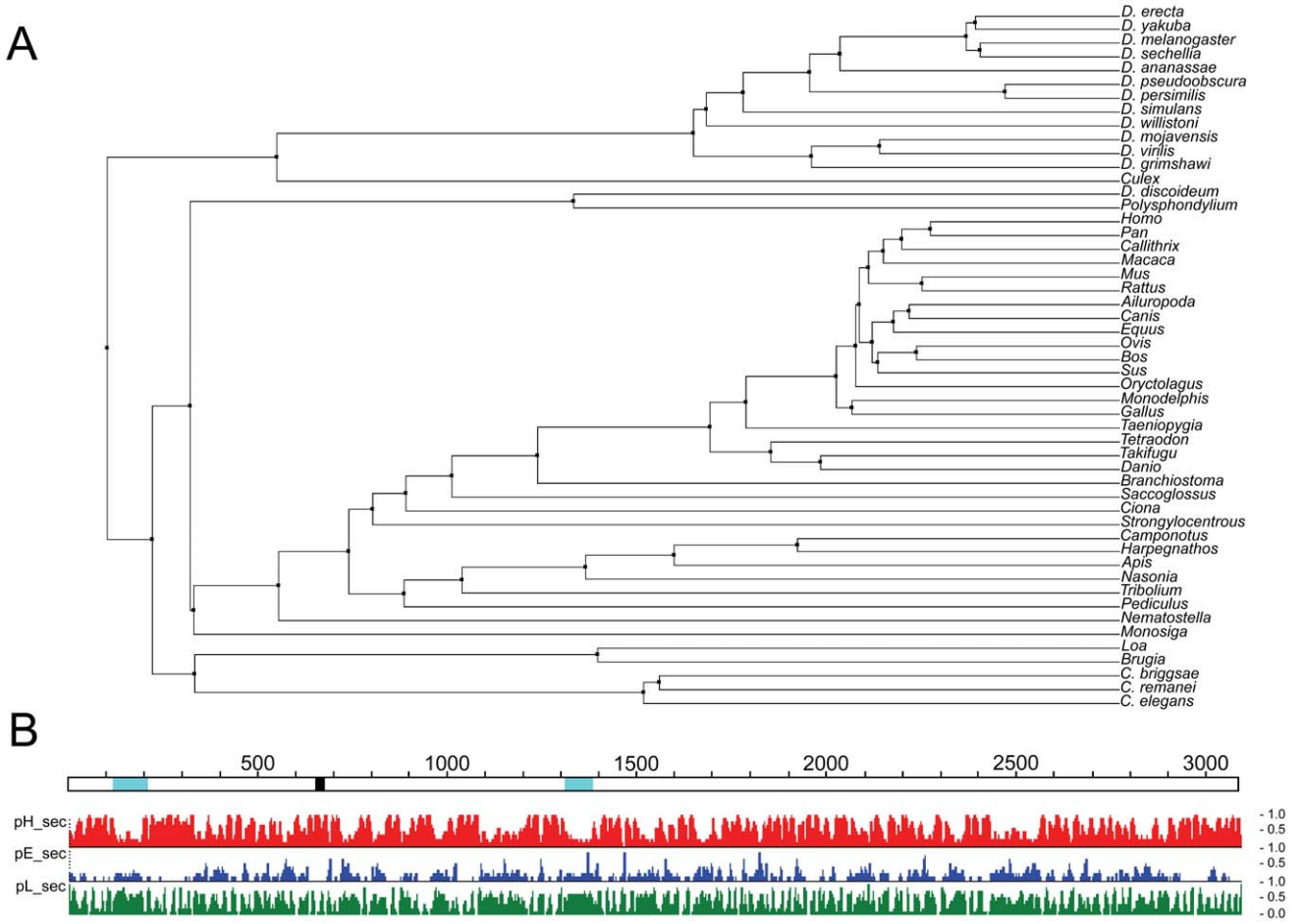

Figure 1. Phylogenetic and structural analysis of *Dictyostelium* huntingtin. A. A phylogenetic tree showing the relationship of *Dictyostelium* huntingtin to huntingtin proteins from 51 other organisms was prepared as the average distance tree using BLOSUM62 of a CLUSTALW alignment in JALVIEW (reference: Waterhouse, A.M., Procter, J.B., Martin, D.M.A, Clamp, M. and Barton, G. J. (2009) "Jalview Version 2 - a multiple sequence alignment editor and analysis workbench" Bioinformatics 25 (9) 1189–1191). B. *Dictyostelium* huntingtin (open line) is depicted with amino acid coordinates (above) above secondary structure predictions from PROF (www.predictprotein.org; B Rost, G Yachdav and J Liu (2004) The PredictProtein Server. Nucleic Acids Research 32(Web Server issue):W321–W326) where pHsec, pEsec and pLsec represent the probability (1 high, 0 low) for helix (red), strand (blue) and neither helix nor strand (green). Locations in the huntingtin schematic of natively unstructured regions predicted by NORSnet (Avner Schlessinger and Jinfeng Liu and Burkhard Rost (2007)) and of a 19 residue polyglutamine repeat are shown by cyan and black, respectively.
doi:10.1371/journal.pgen.1002052.g001

(Figure 3D). Proper targeting was also confirmed by Southern blot using DIG-labeled *Bsr* specific probes as well as by RT-PCR amplification of cellular mRNA which demonstrated that *hd* mRNA was absent (Figure 3E, 3F). Clonal isolates from multiple independent mutants possessing the same disruption and developmental phenotype (glassy sori and round spores) were obtained. One of these clones (httE13) was used in all subsequent experiments and is referred to as hd^- for clarity.

Actin cytoskeleton and contractile vacuole defects in hd^- cells

We did not observe differences in the growth properties of hd^- and wild-type cells when grown as adherent cultures in tissue culture dishes (data not shown). However, in contrast to wild-type cells, axenically grown shaking cultures of hd^- cells consistently grew faster with a doubling time of ~10 hours compared to the ~12 hour doubling time of wild-type cells (Figure S1), suggesting a physiological impact of the absence of huntingtin at the level of single cells. Plating of hd^- cells under non-nutrient, low ionic strength phosphate buffer (KK_2; ~40 mOsmol/L), elicited a cell rounding phenotype that suggested an actin-cytoskeleton defect, which we examined by staining for F-actin. The morphology of hd^- cells grown as an adherent culture in HL-5 medium was similar to that of wild-type cells (Figure 4A) and phalloidin staining showed a similar distribution of F-actin in extended pseudopods in both genotypes (Figure 4C). However, removal of nutrients and the addition of KK_2 buffer resulted in a rapid reduction in pseudopod formation (~20 minutes) and ultimately a failure to polarize only in the hd^- cells (Figure 4B). The rounded cell phenotype of hd^- cells was accompanied by a redistribution of F-actin from the cell cortex to the cytosol (Figure 4D).

As the extreme cell rounding observed in low osmotic buffer hinted at a potential defect in contractile vacuole osmoregulation, we assessed the ability of hd^- cells to respond to osmotic stress. When wild-type cells were placed in water, several small contractile vacuoles formed within 30 minutes and, over time, the cells compensated for the sudden change in their osmotic environment and gradually regained their original size, shape and cell-substratum adhesion (Figure 4E; Video S1). In contrast, hd^-

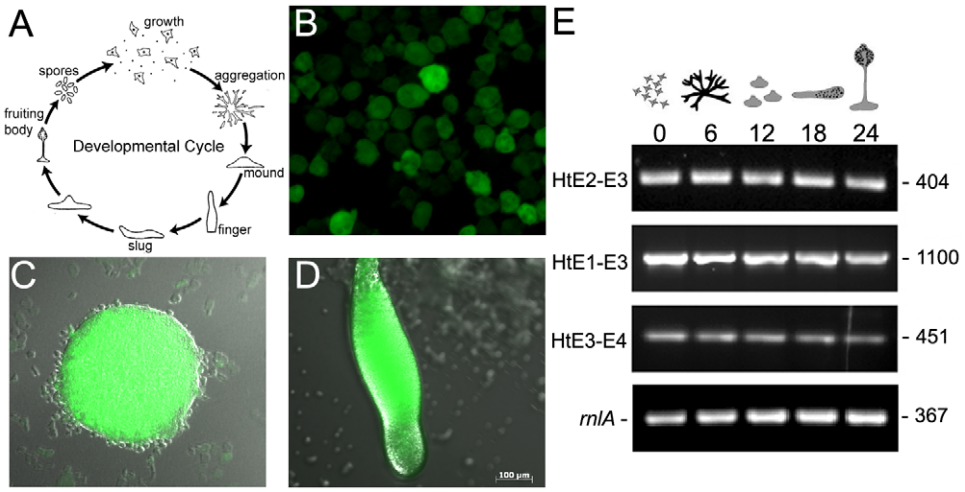

Figure 2. The predicted endogenous hd promoter drives expression of GFP during growth and development. (A) Developmental life cycle of *Dictyostelium discoideum*. Dictyostelium* spends most of its life as vegetative cells that prey upon bacteria and divide mitotically. When starved, the cells enter the developmental cycle that completes in a 24 hour period. During development, amoebae chemotactically aggregate towards secreted cAMP to form a hemispherical mound. Within the mound cells differentiate and sort out to form a motile slug. The slug ultimately forms a fruiting body comprised of a multicellular stalk supporting a ball of encapsulated dormant spores. (B) A cloned region of DNA sequence 595 bp upstream of the *hd* gene was used to replace the actin 15 promoter in the expression vector pTX-GFP. Wild-type AX3 cells were transformed with this construct and expression of GFP was assessed in vegetative cells; (C) mound structure showing GFP expression from *hd* promoter; (D) slug showing expression of GFP in both prestalk (anterior) and prespore (posterior) regions. Scale bar (µm) is shown at the *bottom right*. (E) *Dictyostelium* huntingtin is a single copy gene comprised of four exons. Total RNA was extracted from wild-type *Dictyostelium* strain AX3 during vegetative growth and 6-hour increments during synchronous development on nitrocellulose filters supported by filter pads soaked in DB buffer and developed at 21°C. The presence of alternate transcripts was analyzed with a combination of *hd* exon-specific primer sets, RT-PCR and resolved using ethidium bromide stained agarose gels. *rnlA* was used as a mRNA amplification control. Collection time points are shown in hours (*top*). *hd* exon boundaries are shown *on the left*. PCR product sizes (bp) are shown *on the right*. *Figure representing the developmental life cycle of *Dictyostelium* was adapted from *CC Creative Commons Attribution – Share Alike 3.0, David Brown & Joan E. Strassmann* and is freely available online for download at the dictyBase.
doi:10.1371/journal.pgen.1002052.g002

cells failed to form any visible vacuoles, but instead became round, swollen, lost their adhesion to the substratum and underwent complete lysis within 5–6 hours (Figure 4F; Video S2), indicating that contractile vacuole activity was dramatically compromised in hd^- cells under conditions of hypotonic stress. No difference was observed between wild-type and hd^- cells under hyperosmotic (400 mM sorbitol) conditions (data not shown).

Loss of huntingtin caused developmental delay and abnormal morphogenesis

To determine whether the mutant cells were capable of carrying out the full program of multicellular development, we assayed wild-type and hd^- cells by plating on filters. Wild-type cells formed numerous streaming aggregation centers by 6 hours that went on to form tight mounds by 12 hours, early culminants by 18 hours and fruiting bodies by 24 hours as expected (Figure 5). By contrast, hd^- mutant cells formed delayed aggregates, and by 12 hours had constructed comparatively loose mounds with supernumerary prestalk tips, which subsequently went on to form multiple slugs and small fruiting bodies (Figure 5). Thus, whereas wild-type cells had completed the developmental program by ~24 hours, the development of hd^- cells was delayed and asynchronous, resulting in the appearance of aborted intermediates and the formation of small fruiting bodies that develop glassy sori.

Huntingtin-deficient cells exhibited abnormal shape and motility during early development

A closer examination of the effects that loss of huntingtin has on the earliest stages of development revealed deficits in both the aggregation properties and cell-cell cohesiveness of wild-type and hd^- cells. When assayed on non-nutrient KK_2 agar or buffer-soaked nitrocellulose filters, wild-type cells migrated as streams to form aggregates by 6–8 hours (Figure 6A). The hd^- cells did not form streams that led to distinct aggregation territories, but rather form delayed aggregation territories by accretion (Figure 6B). We next examined the behavior of cells deposited at different cell densities under starvation buffer (non-nutrient phosphate buffer KK_2, pH 6.2) in order to get a better view of the streaming defect. When plated at 1×10^5 cells/cm^2, wild-type cells formed long streams of polarized, elongated cells that congregated into aggregation signaling centers (Figure 6C; Video S3). In contrast, hd^- cells adopted the rounded shape noted previously and ultimately failed to polarize, form aggregation centers or initiate streams (Figure 6D; Video S4). Yet, when assessed at high cell densities (5×10^6 cells/cm^2), hd^- cells managed to form aggregation centers, largely by accretion; however the mounds appear polarized (regular shape on one side, irregular with dark clumping cells on the other side) and many cell were excluded (Figure 6E, 6F).

The observed defects suggest two possibilities; 1) hd^- cells are defective in cAMP signaling, or 2) the extreme sensitivity of hd^- cells to conditions of low osmolarity negatively affects development. The secretion of periodic cAMP pulses is required to initiate *Dictyostelium* development [35] and so the addition of timed pulses of exogenous cAMP should facilitate early development in hd^- cells if they are defective in cAMP signaling. Pulsing wild type cells in KK_2 buffer with 75 nM cAMP every 6 minutes for a period of 4–5 hours accelerated the onset of chemotactic streaming, but equivalent cAMP pulses did not rescue the rounding or chemotactic streaming of hd^- cells (data not shown). We next assessed what effect the addition of bivalent

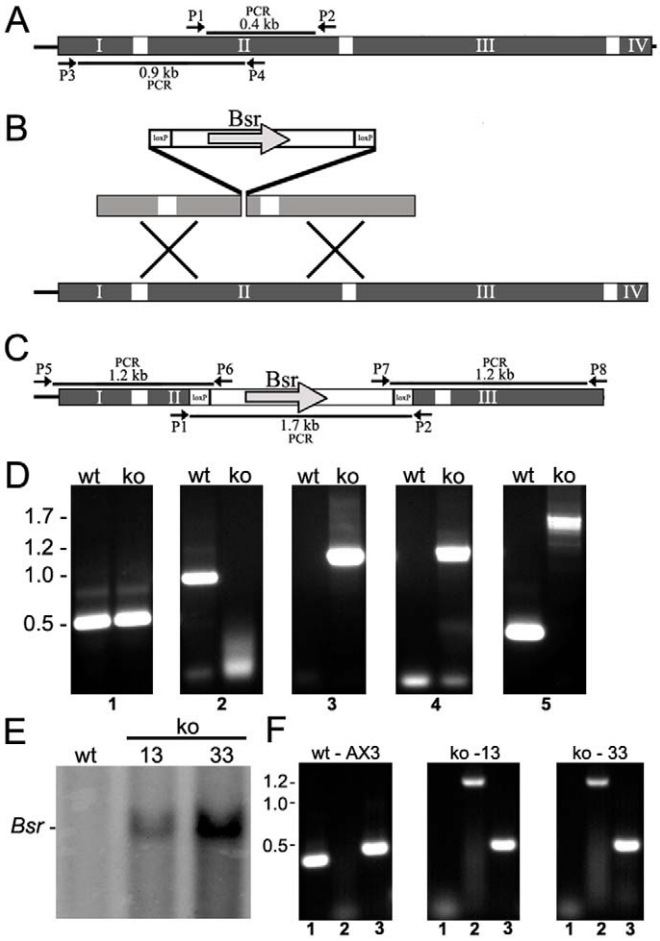

Figure 3. Targeted disruption of the *hd* gene by homologous recombination. (A) Physical map of the *hd* gene is shown. The four exons (*I, II, III and IV*) that comprise the *hd* gene are shown (*grey*) interrupted by three introns (*white* bars). PCR primers are shown as *arrows* at the positions in which they prime including amplicon sizes. The exon-intron boundaries are not to drawn to scale. (B) The targeting vector and sites of recombination are shown. The vector contains the Blasticidin S resistance gene (*Bsr*) that is flanked by loxP sites and allows for selection of transformed cells. (C) Physical map of the targeted deletion is shown. PCR primers are shown as *arrows* at the positions that they prime including amplicon sizes. (D) Genomic PCR of wild-type (*wt*) and *hd*$^-$ (*ko*) clones. Control PCR amplification of the sequence immediately upstream of the *hd* gene (*panel 1*); No amplification in clones carrying a targeted deletion of the *hd* gene which removes 278 bp of sequence from exon 2 (*panel 2*); PCR amplification of genomic DNA using primers that prime outside the vector (P5 or P8) and inside the *Bsr* cassette (P6 or P7), respectively (*panels 3 and 4*). No DNA is amplified from wild-type cells; PCR of genomic sequences that flank the insertion site (*panel 5*). The endogenous wild-type allele yields a fragment of ~400 bp whereas the knockout mutant yields a much larger fragment representing insertion of the *Bsr* cassette. Molecular weight markers are shown *on the left*. (E) Confirmation of gene disruption by Southern blot analysis. Genomic DNA from wild-type or two independent *hd*$^-$ clones (clones 13 and 33) were probed by Southern blot hybridization for the presence of *Bsr* sequences. (F) RT-PCR of total RNA isolated from wild-type and two independent *hd*$^-$ clones (clones 13 and 33). In each panel, *lane 1* represents the amplicon derived from priming the exon 2 deletion; lane 2 represents priming inside the *Bsr* cassette; and *lane 3* represents control RT-PCR reactions. Molecular weight markers are shown *on the left*.
doi:10.1371/journal.pgen.1002052.g003

cations (higher osmolarity) would have on cAMP signaling and chemotactic aggregation of *hd*$^-$ cells under KK_2 buffer. Interestingly, the addition of 1 mM $CaCl_2$ (Figure 6G, 6H), 1 mM $MgCl_2$ or 1 mM $MgSO_4^-$ (data not shown) rescued endogenous cAMP signaling and chemotactic aggregation of *hd*$^-$ cells (Video S5). However, the streams formed by *hd*$^-$ cells in the presence of bivalent cations were shorter and had a tendency to break and re-form when compared to wild type streams (Figure S2A, S2B). In addition, rescue of cAMP signaling and chemotactic aggregation of *hd*$^-$ cells in the presence of bivalent cations was inhibited by the addition of 1 mM ethylene glycol tetraacetic acid (EGTA) (Video S6).

To further assess cAMP signaling in *hd*$^-$ cells, we explored their aggregation properties on KK_2 agar containing caffeine (1, 2.5 and 5 mM), a compound shown to inhibit cAMP signaling in *Dictyostelium* [36]. *Hd*$^-$ mutant cells were equally sensitive and exhibited similar developmental phenotypes to wild type cells when treated with caffeine. Aggregation and development of wild type and *hd*$^-$ cells was severely inhibited at 5 mM caffeine and at 1 mM caffeine both wild type and *hd*$^-$ cells were capable of forming fruiting bodies (data not shown). We next assessed aggregation and development of wild type and *hd*$^-$ cells on KK_2 agar containing EGTA (1 mM or 2 mM). In contrast to caffeine treatment, development of wild type cells in the presence of 1 mM EGTA was unaffected (Figure 6I) whereas *hd*$^-$ cells failed to form chemotactic streams and arrested development as loose aggregates (Figure 6J). Taken together, our data suggest that *hd*$^-$ cells are not primarily defective in cAMP signaling but rather have a hypersensitivity to conditions of low osmolarity which affects cAMP signaling and thus development.

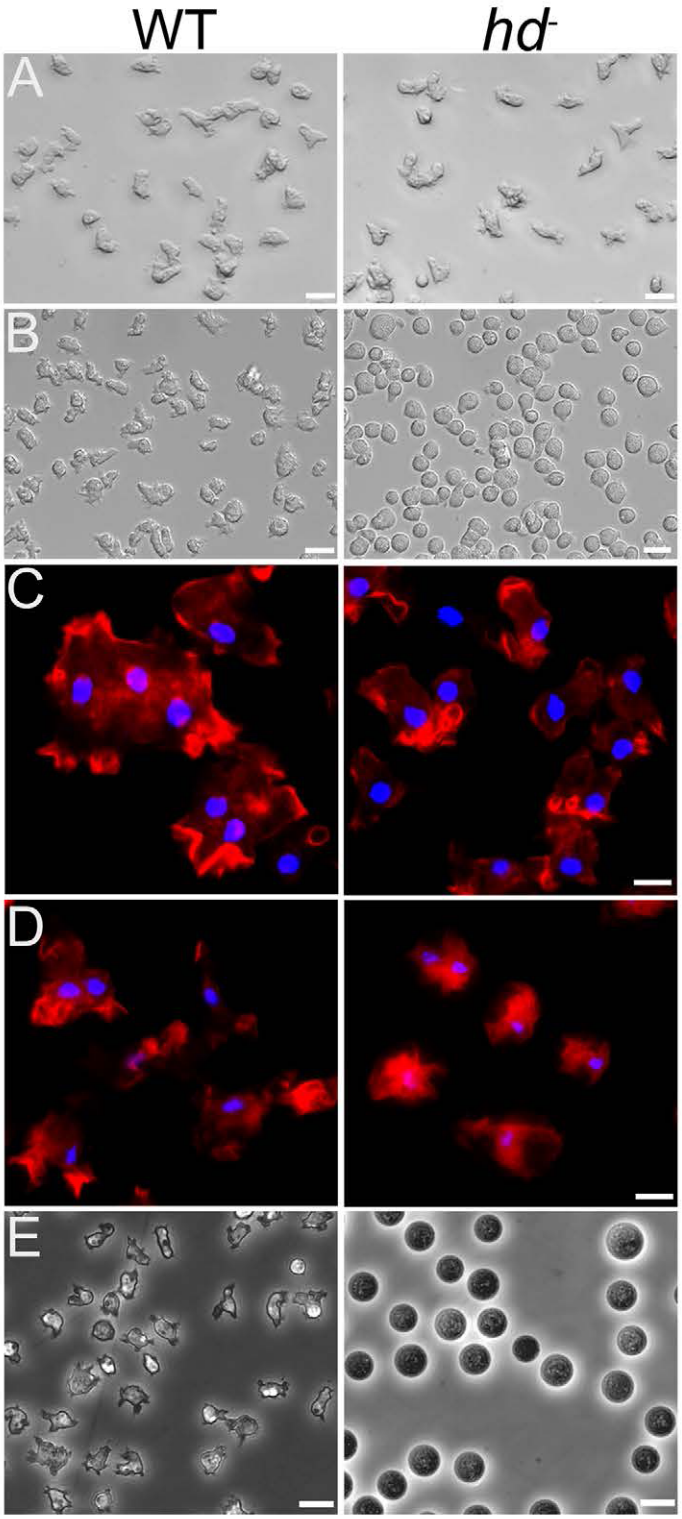

Figure 4. Removal of nutrients caused rounding of *hd*$^{-}$ cells and affects F-actin localization. (A) The morphology of *hd*$^{-}$ cells (*right panel*) grown and photographed as an adherent culture in HL-5 was similar to wild-type cells (*left panel*). Scale bars (20 μm) are shown on the *bottom right*. (B) Removal of nutrients (HL-5) and replacement with starvation buffer (KK_2) caused rounding of *hd*$^{-}$ cells. Cells were photographed 20 minutes after the addition of starvation buffer. Wild-type cells (*left panel*) displayed morphology similar to that observed for cells in HL-5 whereas all *hd*$^{-}$ cells immediately adopted a rounded morphology (*right panel*). Scale bars (20 μm) are shown on the *bottom right*. (C) Aberrant localization of F-actin in starved *hd*$^{-}$ cells. Vegetative wild-type cells (*left panel*) and *hd*$^{-}$ cells (*right panel*) collected from axenic medium (HL-5) were deposited into Lab-tek chambered cover glass (8 well) at 1×10^5 cells/cm^2 and allowed to grow overnight in HL-5 at 21°C. For F-actin staining, the cells were fixed with 4% formaldehyde in PDF buffer and then stained with Texas red-phalloidin. Arrows indicate membrane extensions enriched with F-actin. (D) Localization of F-actin in cells submerged in starvation buffer (KK_2). One hour after starvation in KK_2, wild-type cells retained their normal amoeboid morphology (*left panel*); *hd*$^{-}$ cells remained rounded and exhibited a redistribution of F-actin away from the cell cortex as it concentrated in the cytosol (*right*

panel). Nuclei were stained with Hoechst 33342. Scale bars (5 μm) are shown on the *bottom right*. (E) *hd*$^-$ mutants were impaired in osmoregulation. Wild-type (wt) and (F) huntingtin-null (*hd*$^-$) cells were grown in cell culture dishes with HL-5 media. The media was exchanged with dH_2O and the cells were examined after 1 hour. Wild-type cells initially rounded and showed partial swelling under the hypoosmotic conditions, but quickly recovered the ability to crawl and change shape. In contrast, *hd*$^-$ cells were completely round and swollen in dH_2O, and barely remained attached to the culture dish. The *hd*$^-$ cells began to rapidly lyse after ~3 hours of this treatment and underwent complete lysis by 6 hours suggesting that the mutants may retain some very low level of osmoregulation. Scale bar 10 μm.
doi:10.1371/journal.pgen.1002052.g004

The cell-cell adhesion properties of *hd*$^-$ cells in the absence or presence of 10 mM ethylenediaminetetraacetic acid (EDTA) mirrored those observed for wild-type cells during the first 3 hours of development (Figure 7). However, after ~4 hrs of development, wild-type cells began to attain EDTA-resistant cell-cell contacts whereas *hd*$^-$ cells not only failed to acquire EDTA-resistant cell-cell contacts but also began to display an overall loss in cell-cell cohesion as judged by an increase in the number of single cells assayed in the absence of EDTA (Figure 7). Even by 24 hours, neither EDTA-resistant adhesion in *hd*$^-$ cells nor recovery of their cohesion properties in suspension developed (data not shown). Thus, stringent conditions exacerbated *hd*$^-$ cell developmental deficits, revealing aberrant cell polarization, aggregation and motility consistent with abnormal cell shape, cytoskeletal function and cell-cell adhesion properties.

hd$^-$ mutants exhibited abnormal prespore/spore cell differentiation

Though streaming and aggregation of *hd*$^-$ cells were abnormal and overall development was delayed, multiple prestalk tips formed atop most of the developing *hd*$^-$ mounds. Each of these tips elongated into a finger structure, suggesting the possibility of aberrant prestalk/prespore cell differentiation (Figure 8A, 8B), and eventually produced a fruiting body with a glassy sorus containing a reduced spore complement when developed on KK_2 agar or with a lawn of *Klebsiella* on SM agar (Figure 8C, 8D). In contrast to wild-type fruiting bodies, the numbers of spores in *hd*$^-$ sori decreased as the fruiting bodies aged, resulting in a glassy sorus; this suggested a potential defect in spore formation or alternatively, spore dormancy. We used electron microscopy to examine the fine structure of the elliptical wild-type spores and round mutant *hd*$^-$ spores from 72 hr fruiting bodies (Figure 8E, 8F). The EM images revealed the premature germination of spores in the sori of *hd*$^-$ fruiting bodies. In stark contrast to the dormant wild-type spores, the *hd*$^-$ sori contained a mixture of apparently dormant spores with three wall layers, swollen spores, swollen spores with thin spore walls about to release amoebae, and nascent amoebae (Figure 8F). Our data suggest that shortly after fruiting body formation *hd*$^-$ spores are unable to maintain dormancy, or alternatively, fail to achieve dormancy possibly through poor differentiation properties and germinate within the sorus. Consequently, we assessed the ability of *hd*$^-$ cells to differentiate into stalk and spore cells in low cell density monolayer culture [37]. In response to 10–100 nM of the stalk cell inducer, differentiation inducing factor 1 (DIF-1), *hd*$^-$ mutants were able to produce stalk cells as efficiently as wild-type cells (data not shown). However, in response to the sporulation inducer 8-Br-cAMP (5–15 mM), a cell permeable analogue of cAMP, sporulation in the mutants was delayed ~24 hours compared to wild-type cells (Figure 8G). *hd*$^-$ cells collectively formed spore cells at ~40% efficiency relative to wild-type controls after 48 hours differentiation (Figure 8G).

hd$^-$ mutants produced spores with abnormal morphology and reduced viability

At least some spores produced by development of *hd*$^-$ organisms were capable of germination and formation of viable amoebae. The spore coats of both wild-type and *hd*$^-$ cells also stained brightly with Calcofluor, demonstrating the normal presence of cellulose in the mutant spores (data not shown). To test the relative viability of the *hd*$^-$ mutant spores, we compared their germination rates with wild-type spores. Spores harvested from sori of each cell line were mixed with *Klebsiella*, deposited on SM agar plates and the number of plaques that formed was scored. Spores harvested from wild-type sori displayed an average survival rate of 82±3.4%, whereas *hd*$^-$ spores demonstrated a dramatically reduced mean survival rate of 20±2.2% (Figure 9). This did not appear to be due to reduced resilience of *hd*$^-$ mutant spore coats,

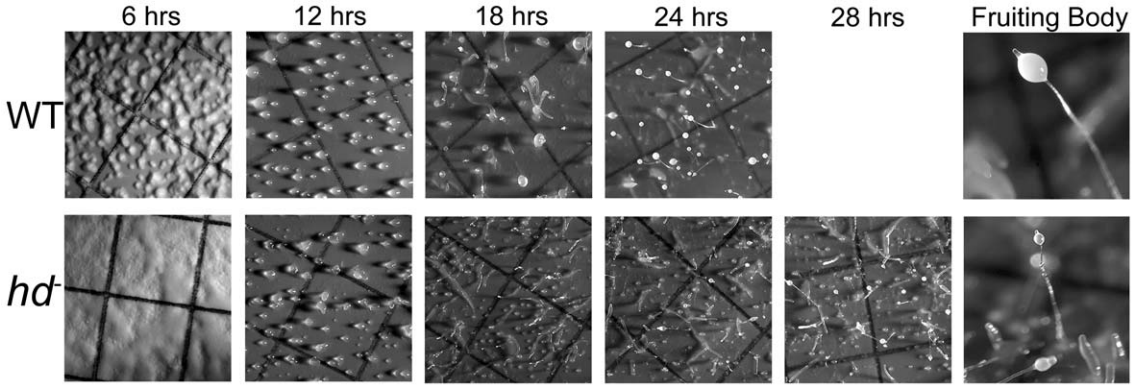

Figure 5. *hd*$^-$ mutants exhibited asynchronous delayed development. Exponentially growing wild-type and *hd*$^-$ cells (2×10^6 cells/mL) were washed three times with DB buffer, resuspended at a density of 5×10^7 cells/mL, deposited on black nitrocellulose filters supported by filter pads soaked in DB buffer and developed for 28 hours at 21°C. All photographs are top view. Wild-type cells developed distinct aggregation territories after 6 hours whereas *hd*$^-$ null cells displayed a much smoother appearance and the noticeable absence of streams. By 12 hours *hd*$^-$ cells formed mounds that tended to produce multiple tips. Further development of *hd*$^-$ cells proceeded in a delayed asynchronous manner resulting in the presence of various intermediate structures and small aborted mounds. The developmental time points in hours are shown *at the top*.
doi:10.1371/journal.pgen.1002052.g005

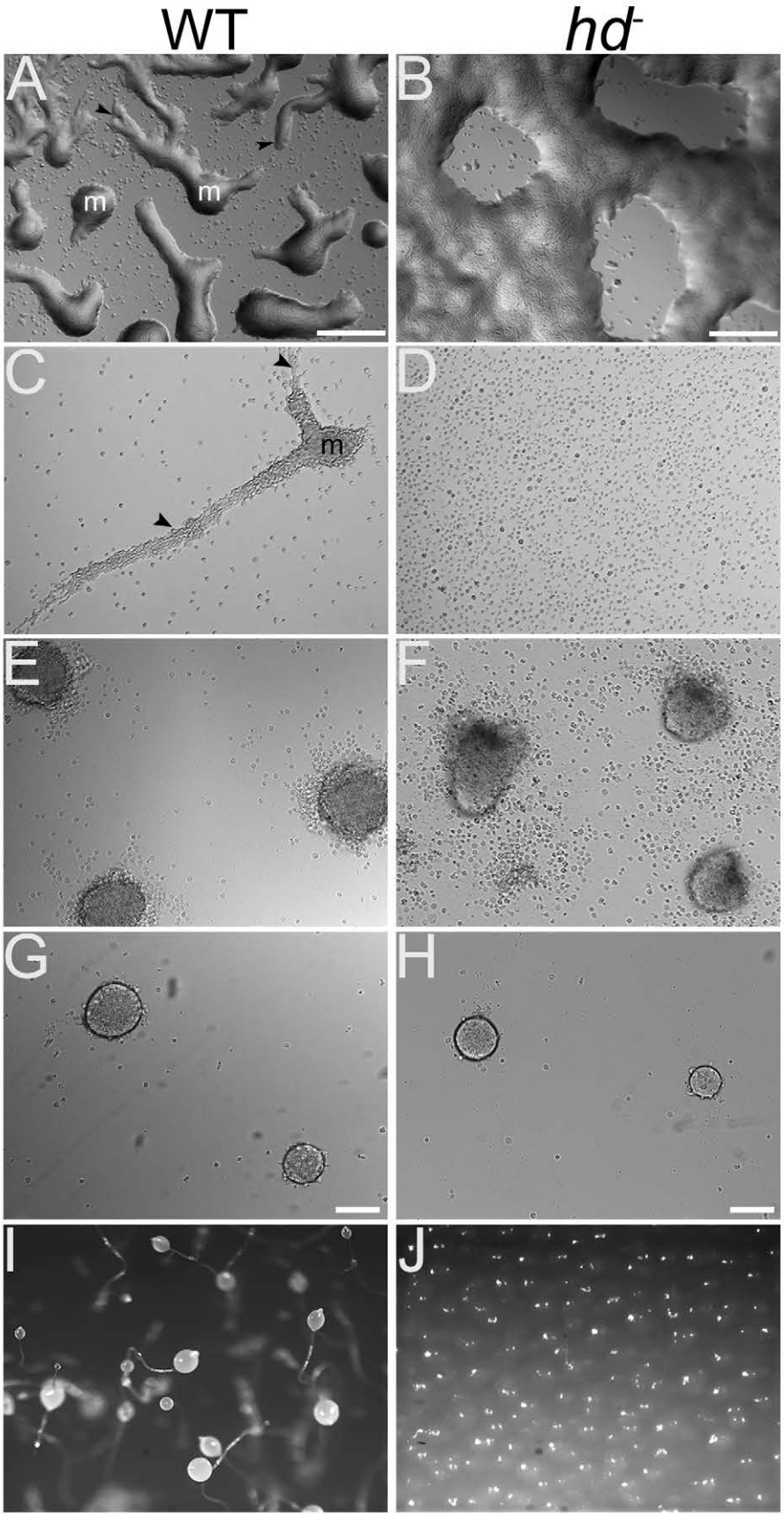

Figure 6. *hd*$^{-}$ cells displayed aggregation defects and failed to stream under submerged culture. Wild-type and *hd*$^{-}$ cells (1×10^6 cells/mL) were deposited on non-nutrient KK_2 agar plates and visualized by brightfield microscopy. Images are top view. (A) Wild-type cells migrated in

streams (*arrows*) to form aggregation territories (*m*) by ~6 hours. (B) *hd*$^-$ cells did not form well-defined streams, but rather clusters of cells that formed aggregation centers largely by accretion. Scale bar 100 μm. (C) Wild-type and (D) *hd*$^-$ cells (1×10^5 cells/cm^2) were submerged under KK_2 and allowed to develop for 6 hours. Streams (*arrows*) of wild-type cells moving into an aggregation center (*m*) were readily apparent (*left panel*) whereas *hd*$^-$ cells failed to stream (*right panel*). (E) Wild-type and (F) *hd*$^-$ cells were submerged under buffer at high density (5×10^6 cells/cm^2) and imaged after 20 hours. Under these conditions, wild-type cells readily formed distinct organized mounds; high density partially restored the ability of *hd*$^-$ cells to form aggregation territories but with an irregular polarized shape. (G) Wild-type and (H) *hd*$^-$ cells (1×10^5 cells/cm^2) were submerged under KK_2 in the presence of 1 mM $CaCl_2$ and imaged after 20 hours. Under these conditions exogenous calcium rescues early development of *hd*$^-$ cells. Scale bar 100 μm. (I) Development on KK_2 agar in the presence of EGTA. After 24 hours, wild type cells form fruiting bodies whereas development of *hd*$^-$ cells (J) is blocked in the presence of 1 mM EGTA.
doi:10.1371/journal.pgen.1002052.g006

as spore viability of both wild-type and *hd*$^-$ mutant spores was not differently altered by treatment with the non-ionic detergent NP-40 (0.5%) and brief heat treatment (45°C) (Figure 9).

Developmental defects in huntingtin-deficient organisms are cell-autonomous

To distinguish whether the developmental defects observed in *hd*$^-$ cells were cell autonomous or non-cell autonomous, we followed the cell fate of *hd*$^-$ cells during chimera development in mixed cell cultures. Mutant *hd*$^-$ cells and wild-type cells carrying an act15/GFP construct, which marks all cells, were prepared and mixed in ratios of 1:1, 1:3 or 1:9 with unmarked cells of the opposite genotype (or of the same genotype as controls). As expected, the deficits revealed by *hd*$^-$ cells in assays at the single cell stage (e.g., cell rounding, actin cytoskeleton rearrangement, sensitivity to osmotic shock) or early in development (cell-cell adhesion) were not rescued by the presence of wild-type cells in co-culture (data not shown). Similarly, in developing co-aggregates of cells developed under starvation buffer, *hd*$^-$ cells failed to populate the central region of the developing aggregate, consistent with the inability of wild-type cells to correct the observed failure in the initiation of intracellular cAMP signaling pathways required to trigger aggregation (Figure 10A) or, possibly, the onset of cell-cell adhesion properties in *hd*$^-$ cells.

We then studied cell pattern organization of live cells during the slug stage, where prestalk cells primarily populate the anterior region and prespore cells occupy the slug posterior [38]. In the context of an excess of unmarked wild-type cells (3:1 ratio), GFP-marked *hd*$^-$ cells

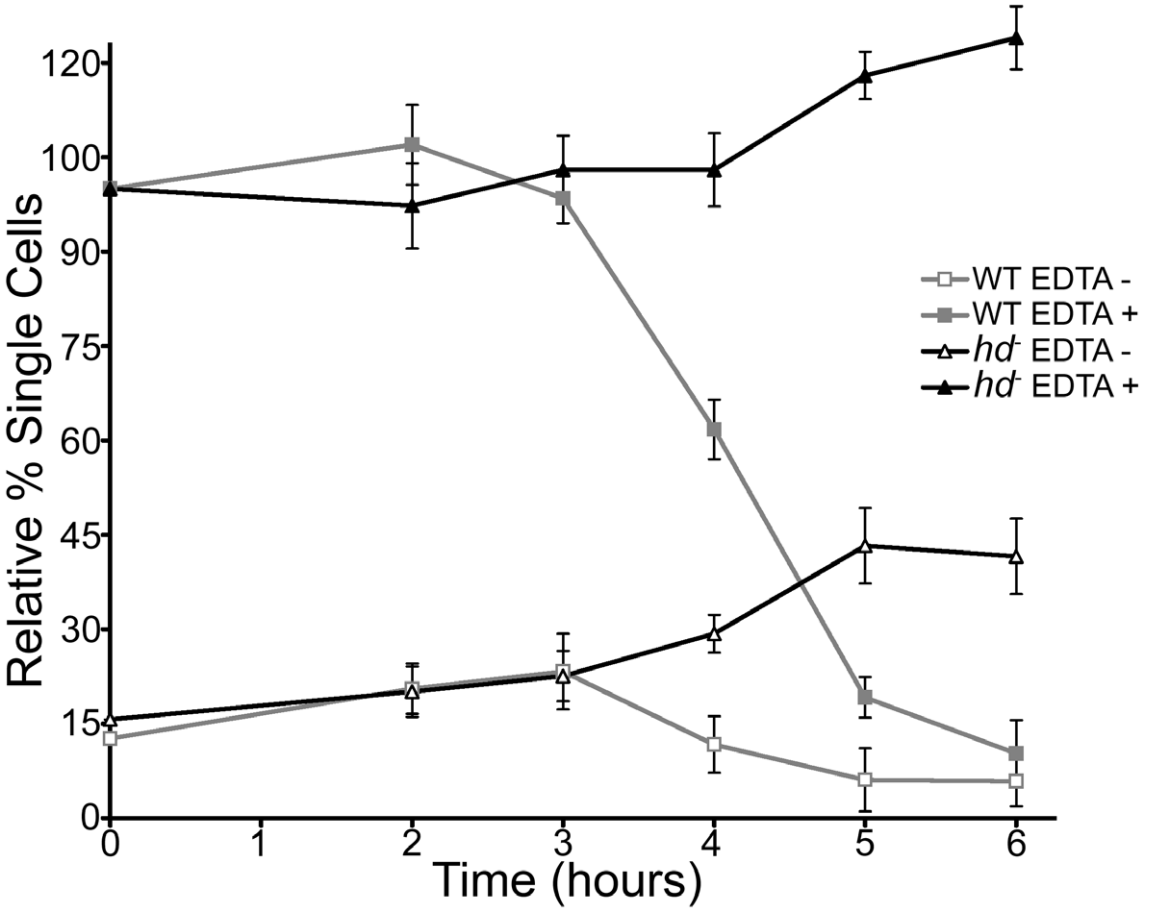

Figure 7. Loss of EDTA-resistant adhesion in *hd*$^-$ cells. Wild-type and *hd*$^-$ cells (5×10^6 cells/mL) were developed in Soerensen's buffer at 150 rpm and 21°C. Samples were collected at the start of the assay and at one hour time points over a period of 6 hours. For each collection point, cells were dissociated by vortexing and then incubated in the presence or absence of 10 mM EDTA for 30 minutes, fixed with 2% glutaraldehyde (10 min.) and single cells were counted in triplicate using a hemocytometer. All experiments were performed in duplicate at least three times and the mean value for single cells in duplicate samples, expressed as percentage of total cells was plotted over time.
doi:10.1371/journal.pgen.1002052.g007

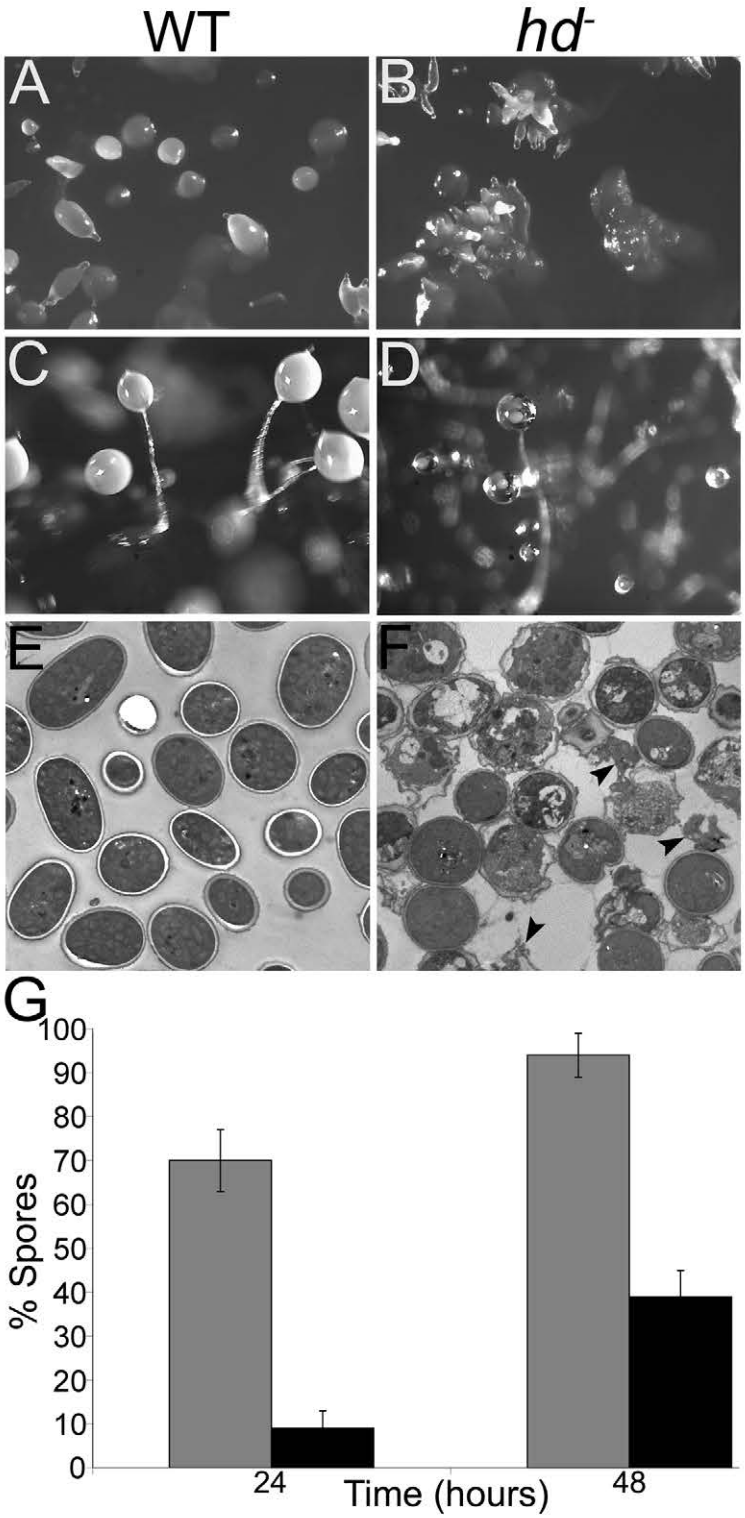

Figure 8. *hd*⁻ cells formed mounds with multiple prestalk-tips and fruiting bodies with a glassy sorus. (A) Wild-type mounds formed mounds that develop a single tip which proceeded to form an elongated finger structure. (B) Multiple prestalk-tips formed atop most *hd*⁻ mounds that went on to form comparably small individual finger structures. Cells were developed on SM agar with a lawn of *Klebsiella*. Images are top view. (C) Terminal structures of wild-type (*left panel*) and (D) *hd*⁻ null cells (*right panel*). After 36–48 hours, the sori of *hd*⁻ cells became progressively glassy in appearance and contained very few spores. (E) *hd*⁻ spores spontaneously germinated within the sorus. Wild-type and *hd*⁻ spores were collected and fixed (see Materials and Methods) for imaging using electron microscopy. Wild-type sori contained intact elliptical dormant spores with well-defined spore coats and without the presence of amoebae. (F) Spores collected from *hd*⁻ fruiting bodies showed a heterogeneous mixture of round spores that represented the various stages of germination. Swollen spores, swollen spores with thin spore walls about to release amoebae, and nascent amoebae (*arrows*) are shown. (G) *hd*⁻ mutants displayed defects in prespore/spore cell differentiation. Wild-type and *hd*⁻ cells were starved at low density in monolayer culture in the presence of 15 mM 8-Br-cAMP to induce sporulation, viewed by brightfield microscopy and the number of

spores formed was counted. The percentage of differentiated wild-type (*grey bars*) and *hd*$^{-}$ (*black bars*) spore cells was calculated from the total cells after 24 and 48 hour incubation periods. On average, *hd*$^{-}$ cells collectively formed spore cells at ~30% efficiency relative to wild-type controls after 48 hours. Bars indicate standard errors that are derived from three independent experiments, each with three replicates.
doi:10.1371/journal.pgen.1002052.g008

within chimeric slugs were distributed within the prestalk zone (pstO), rearguard and anterior-like cells (ALC), which suggests that they have a greatly reduced ability to form prespore cells in the presence of wild-type cells (Figure 10B). In the complementary experiment, GFP-marked wild-type cells co-developed with *hd*$^{-}$ cells populated primarily the prespore region at cell ratios of 1:1 or lower (Figure 10C). In both comparable control experiments, GFP fluorescence was observed throughout the entire slug. Furthermore, this trend was also seen in terminally differentiated chimeric fruiting bodies with wild-type cells predominantly found in the spore mass whereas *hd*$^{-}$ cells occupied the tip and lower cup region, stalk and basal disc (Figure 10D, 10E). Thus, although *hd*$^{-}$ cells were capable of forming spores when developed as a pure population (albeit poorly, with reduced viability), the presence of wild-type cells in a chimeric organism did not rescue but rather reduced the contribution of *hd*$^{-}$ cells to spore formation.

Discussion

Huntingtin is notable for its role in HD, where an expanded polyglutamine tract near the amino terminus of human huntingtin produces late-onset progressive neurodegeneration, likely through a modulatory effect of the polyglutamine region on the structure and/or function of the protein. In this study, we have investigated the fundamental function(s) of huntingtin in the haploid eukaryote *Dictyostelium discoideum*, by characterizing deficiency phenotypes in the single and multicellular phases of development of this social amoeba. The deletion of the *hd* gene, using targeted homologous recombination, was compatible with cell growth but produced pleiotropic cell autonomous phenotypes that demonstrated that mutant cells could not efficiently complete the processes necessary for coordinated synchronous development of a multicellular organism. The pleiotropic effects of huntingtin deficiency could be the result of loss of a single activity or could be separate effects due to the protein having multiple functions. Further experimentation will be required to resolve these options, but the multiple phenotypes, at both single cell and multicellular stages, offer several routes to further explore the issue.

Our findings suggest that huntingtin participates, directly or indirectly, in actin cytoskeleton-membrane dynamics that affect cell shape. The mechanical properties of the cytoplasm are important determinants of cell shape and permit cells to change

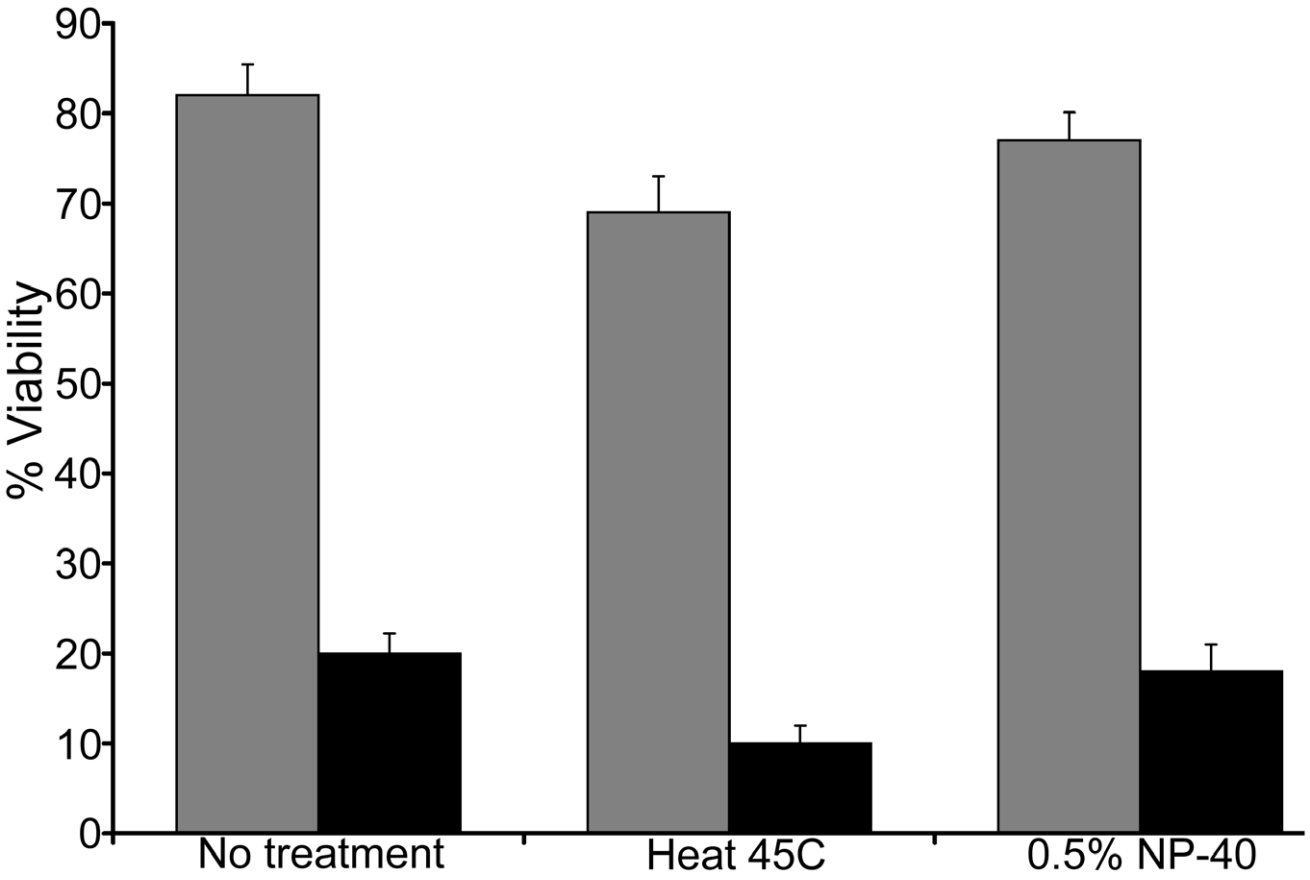

Figure 9. *hd*$^{-}$ cells produced spores with reduced viability. The viability of wild-type (*grey bars*) and *hd*$^{-}$ (*black bars*) spores was assessed. Spores were untreated, heated to 45°C for 10 minutes or incubated with 0.5% NP40 detergent for 5 minutes and aliquots of 100 spores were plated in triplicate onto SM-5 agar plates in a suspension of bacteria and grown for 7 days at 21°C. The relative viability of *hd*$^{-}$ spores was assessed by counting the number of clear plaques formed on the bacterial lawns. Results are representative of three independent experiments.
doi:10.1371/journal.pgen.1002052.g009

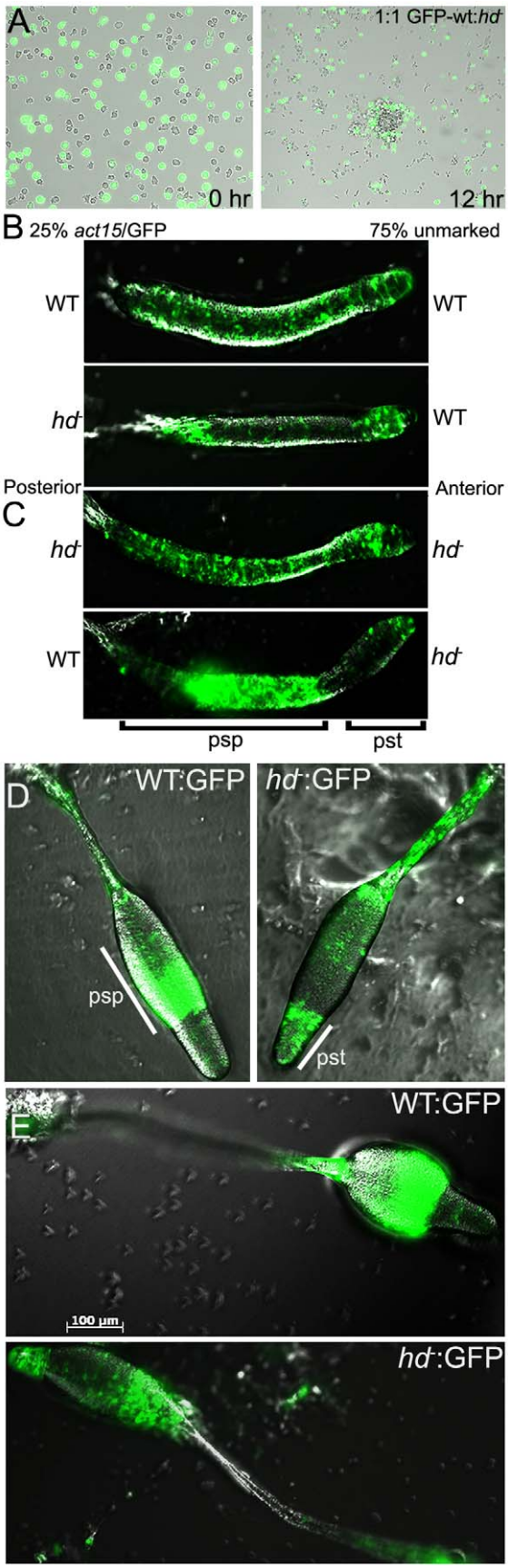

Figure 10. Huntingtin regulates prespore/spore differentiation cell-autonomously. GFP was expressed in wild-type cells and their position in chimeric aggregation territories with unlabelled *hd*$^-$ cells was monitored. (A) Mixed (1:1) cell suspensions were submerged (1×10^5 cells/cm^2) under KK_2 buffer (left panel). After 12 hours, aggregation centers were imaged under brightfield and fluorescence using an inverted microscope. *hd*$^-$ cells failed to populate the central region of aggregation territories but were instead localized to the periphery of the mound. Images are representative of three independent experiments. (B) Wild-type and *hd*$^-$ cells that express GFP were mixed 1:3 or less with unmarked wild-type cells as indicated and cellular organization in live cells during the slug stage was assessed. GFP-labeled wild-type cells were mixed with the same genotype as a control (*top panel*); GFP-labeled *hd*$^-$ cells populated the prestalk regions of the slug (*lower panel*). (C) GFP-labeled *hd*$^-$ cells were mixed with the same genotype as a control (*top panel*); GFP-labeled wild-type cells populated the prespore regions of the slug (*lower panel*). Slugs are positioned with their indicated posterior prespore (psp) zones to the left and anterior prestalk (pst) zones to the right. (D) *hd*$^-$ cells marked with an actin/GFP reporter plasmid were mixed with unmarked wild-type cells in a 1:3 ratio and allowed to develop into fruiting bodies. Developing structures (late culminant) were imaged by DIC and fluorescent microscopy. Wild-type cells marked with GFP (*left panel*) predominantly occupied the prespore/spore region; *hd*$^-$ cells marked with GFP failed to populate the prespore region and were overrepresented in the upper cup, lower cup and basal disc (*right panel*). Psp – *prespore*; Pst – *prestalk*. (E) Terminal fruiting structures were viewed by DIC and fluorescent microscopy. Wild-type cells expressing GFP (*top panel*); *hd*$^-$ cells expressing GFP (*lower panel*). Results are representative of three independent experiments for all panels shown. Scale bar 100 µm.
doi:10.1371/journal.pgen.1002052.g010

the cytoplasm from a rigid to a dynamic actin network that can greatly influence cell motility [39]. Huntingtin under certain conditions appears to act as an essential facilitator of this process. Whereas *hd*$^-$ cells displayed apparently normal cell shape, pseudopod formation, F-actin localization and random motility in nutrient-rich media, when assayed in the absence of nutrients (under developmental buffer), they failed to produce membrane extensions, were abnormally round and lacked cortical F-actin, although at high cell density, rounded *hd*$^-$ cells managed to form delayed aggregation territories by accretion. These observations could also reflect the loss of an excitatory signaling pathway during development of *hd*$^-$ cells, as the phenotypes resemble those exhibited by *Dictyostelium* null mutants for adenylyl cyclase that overexpress the catalytic subunit of protein kinase A (PKA) [40] or cells expressing the constitutively active inhibitory heterotrimeric G-protein Gα9 [41]. Addition of exogenous pulses of 75 nM cAMP at 6 minute intervals over a period of 4–5 hours did not rescue the aggregation defect in our *hd*$^-$ cells (data not shown), though it is plausible that high cell density partially rescues mound formation by increasing cell-cell contacts. However, cAMP signaling and subsequent chemotactic aggregation could be rescued through the addition of bivalent cations (Ca^{2+} or Mg^{2+}) to the medium, which suggests the possibility that *hd*$^-$ cells exhibit depleted cationic stores. Our findings support the notion that huntingtin may facilitate proper Ca^{2+}- Mg^{2+}-dependent actin cytoskeleton remodeling that determines cell shape, but that the detection of this role critically depends upon the conditions in which the cells are evaluated.

A second function for huntingtin is maintenance of cellular integrity under conditions of osmotic stress. Contractile vacuoles are intracellular membrane organelles involved in osmoregulation, function as a highly efficient acidic Ca^{2+}-store that is required for cAMP-induced Ca^{2+}-influx and are found in free-living amoebae and protozoa [42–44]. Normally, wild-type cells growing in culture media contain a few moderately active contractile vacuoles that maintain the osmotic balance of the cell. The contractile

vacuole system functions as a "bladder" during conditions of hypoosmotic stress, where it collects fluid (water and neutral amino acids) in a network of tubular channels that associate with the cortical actin network to allow for transient fusion with the plasma membrane and expulsion of its contents to the extracellular environment [45,46]. The behavior and survival rate of *hd*$^-$ cells in response to hyperosmotic conditions is similar to wild-type cells (data not shown). However, contractile vacuole activity in response to hypoosmotic stress is completely abolished in *hd*$^-$ cells, and renders the cells sensitive to conditions of low ionic strength. These effects were consistently associated with a retraction of F-actin from the cell cortex to the cytosol, suggesting that in the absence of huntingtin, inefficient actin cytoskeleton remodeling may underlie the failure of the tubular network to convert into the contractile vacuole. This could involve abnormal formation of the vacuole and failure to discharge, or altered regulation of F-actin binding proteins, as there are examples of both. Cells deficient for MEGAP1 and MEGAP2, members of the Pombe/Cdc15 homology (PCH) family of proteins involved in actin cytoskeletal reorganization, are sensitive to hypoosmotic conditions because they are defective in the tubulation and the associated emptying of contractile vacuoles [47]. Whereas MEGAP-null cells fail to form tubules from vacuoles and therefore accumulate the latter, we suggest that *hd*$^-$ cells cannot effectively osmoregulate due to the inability of the tubule system to convert to vacuoles. Indeed, *Dictyostelium* double mutants lacking two F-actin crosslinking proteins, α-actinin and gelation factor, display a general weakening of the cortical cytoskeleton and, like *hd*$^-$ cells, do not exhibit the normal polarized morphology of wild-type cells during aggregation and are sensitive to hypoosmotic shock [48]. Our data further suggest that the defective CV system in *hd*$^-$ cells renders cells not only sensitive to extreme hypoosmotic shock, but secondarily affects intracellular ion homeostasis as the CV has been shown to function as a major Ca^{2+}-store [42,44] as well as being tightly linked to Ca^{2+}/Mg^{2+}-containing mass dense granules [43]. As a consequence, unless these cations are provided exogenously *hd*$^-$ cells appear unable to initiate cAMP-induced Ca^{2+}-transients that may act in a feedback loop to positively reinforce cAMP relay [44] leading to chemotaxis. Moreover, in contrast to wild type cells, development of *hd*$^-$ cells on non-nutrient agar was blocked by EGTA and, interestingly, was not differentially sensitive to low concentrations of caffeine (data not shown) suggesting that a defect in cAMP signaling, if present, is relatively minor in comparison to their sensitivity to low osmolarity and/or cation chelation. We posit that huntingtin likely acts very early in establishing CV activity or integrity under hypoosmotic conditions. It may act indirectly, or it may function directly as a regulatory scaffold in this setting to drive assembly of the cortical cytoskeleton with CV-associated proteins during the conversion of tubule to vacuoles. Importantly, several proteins associated with the contractile vacuole network and involved in membrane protein trafficking are related to human proteins, suggesting that some functions of the contractile vacuole network have been preserved during the evolution of higher eukaryotes [45,49].

The cell-cell adhesion properties of *hd*$^-$ cells are similar to wild-type cells during the first 3 hours of development, but as development proceeds *hd*$^-$ cells fail to acquire EDTA-resistant contacts. This suggests that *hd*$^-$ cells retain the ability to form early functional adhesion sites but not the EDTA-resistant sites characteristic of aggregating chemotactic cells. Cell-cell contact plays an important role in differentiation and gene expression in *Dictyostelium* [50–52]. EDTA-resistant cell-cell binding is mediated by the expression of glycoprotein gp80 at the onset of aggregation [53,54]. Interestingly, the expression of gp80 is greatly augmented by pulsatile cAMP signaling and the formation of EDTA-sensitive cell-cell contacts [51,55]. Taken together, the apparently normal EDTA-sensitive adhesion properties of *hd*$^-$ cells, their inability to initiate signaling centers at densities where wild-type cells can, and the rescue of cAMP relay and streaming by the addition of exogenous cations suggest that *hd*$^-$ cells potentially lack the Ca^{2+}-Mg^{2+}-dependent excitatory intracellular signal transduction pathways that upregulate gp80 EDTA-resistant adhesion complexes, or that they are deficient in transporting gp80 to the cell surface.

We also provide compelling evidence to suggest huntingtin modulates prespore cell fate choice. In the context of either an equal ratio or excess ratio (3:1 and 9:1) of unmarked wild-type cells, GFP-marked *hd*$^-$ cells within chimeric slugs are distributed within the prestalk zone (pstO), and as rearguard and anterior-like cells (ALC) which suggests they have a significantly reduced ability to form prespore cells when challenged in the presence of wild-type cells. This could be due to a defect in the mutant cells in cell-cell interaction, either through extracellular signaling or direct contact relative to the efficient homotypic interactions of wild-type cells. Indeed, this difference in differentiation might be explained by the adhesion defect in *hd*$^-$ cells as, in chimeras with wild-type, gp80-null cells are also directed preferentially toward the prestalk pathway [56]. Differential differentiation of huntingtin deficient cells during development has also been observed in vertebrates. In zebrafish, reduced expression of huntingtin differentially targets development of telencephalic neurons compared to mid- and hindbrain [57]. In mouse chimeras, *Hdh*$^{-/-}$ cells also preferentially colonize the hypothalamus, midbrain, and hindbrain during relative to the telencephalon and the thalamus during early development [58]. Thus, like these latter neuronal populations, *Dictyostelium* cells require huntingtin for the proper development of viable spores in the presence of wild-type cells.

The culmination of *Dictyostelium* multicellular development permits survival of the organism through the production of environmentally resistant spores and the complex organization of actin filaments in *Dictyostelium* spores contributes to their ellipsoid shape and dormancy [59]. *hd*$^-$ mutants produced abnormally round spores, which exhibited decreased viability, suggesting that they were poorly differentiated or had a defect in the actin-cytoskeleton. Moreover, electron microscopic examination of the fine structure of spores from wild-type and *hd*$^-$ fruiting bodies suggested that the formation of the glassy sorus was likely a result of the premature germination of spores and the resulting death of newly emerged amoebae. Spore dormancy is maintained via active biological processes including high osmolarity, actin dynamics, production of the germination inhibitor discadenine and active PKA which in concert function to insure a viable supply of spores [60–62]. Since *hd*$^-$ amoebae are sensitive to changes in osmolality, display aberrant F-actin staining and show compromised sporulation when subjected to constitutive PKA activation *via* 8-Br-cAMP *in vitro*, it is plausible that in the absence of huntingtin, imprecise cytoskeletal architecture and signaling from PKA required to maintain or enter dormancy might also be defective at this late stage of development.

Our data do not provide a simple definition for a single normal function for huntingtin, but, as huntingtin deficiency in *Dictyostelium* produces pleiotropic effects throughout the life cycle, our findings are consistent with the consensus from mammalian studies that huntingtin is a multifunctional protein that can impact upon many biochemical processes. In *Dictyostelium*, defects in CV activity or integrity leading to a disruption in ion homeostasis affecting the cytoskeleton, cell shape and cell-cell adhesion would all predictably interfere with many aspects of chemotactic aggregation and development. Defining the degree to which the phenotypes

reported here are connected by common underlying biochemical deficits or, alternately, reflect different functions of huntingtin will require detailed molecular investigation. However, the existence of a *Dictyostelium* ortholog of human huntingtin, the viability of the null *hd*$^-$ mutant, and its discrete, readily assayed deficiency phenotypes indicate that this haploid organism provides an effective genetic model system to identify molecular and cellular processes affected by the loss of huntingtin function. While the latter is of fundamental biological interest considering the unique nature of this ancient large α-solenoid HEAT protein, delineating which of these functions are conserved in mammals and determining whether they are altered by expansion of the polyglutamine tract in human huntingtin will also provide much needed insights into the mechanism by which mutant huntingtin triggers HD pathogenesis.

Materials and Methods

Cell culture and development

Wild-type *Dictyostelium discoideum* AX3 cells were grown in association with *Klebsiella aerogenes* on SM plates, axenically in tissue culture plates or as shaking cultures in HL-5 medium (Formedia) at 21°C. To assess growth rates, shaking cultures (150 rpm) of AX3 or *hd*$^-$ null mutant cells were suspended in HL-5 at a density of 1×10^4 cells/mL and grown at 21°C. Cells were counted in triplicate using a hemocytometer. For synchronous development exponentially growing cells ($\sim2\times10^6$ cells/mL) were washed three times from the nutrient source with DB buffer (5 mM Na_2HPO_4, 5 mM KH_2PO_4, 1 mM $CaCl_2$, 2 mM $MgCl_2$, pH 6.5) by centrifugation at 1500 rpm for 5 min, resuspended at a density of 5×10^7 cells/mL, deposited on black nitrocellulose filters supported by filter pads soaked in DB buffer and developed at 21°C. Growth curves were determined for the *hd*$^-$ strain, and parental (wild-type) strain AX3. Shaking (150 rpm) cultures were grown axenically in HL-5 at 21°C. Exponentially growing cultures were used to inoculate four 50 mL cultures for each strain, starting at 1×10^5 cells per mL and counted daily using a hemocytometer. For development under buffer (KK_2), cells were grown in 6-well tissue culture dishes in HL-5 to a density of $\sim5\times10^5$ cells/cm^2. Cells were washed twice with KK_2 and then allowed to develop under KK_2 or KK_2 supplemented with 1 mM $CaCl_2$, 1 mM $MgCl_2$, 1 mM $MgSO_4$ or were provided with 75 nM pulses of cAMP every 6 minutes for a period of 4 hours [41]. For development and assessment of streaming behavior cells were washed twice with KK_2 and then deposited on agar at a density of $\sim5\times10^5$ cells/cm^2 on non-nutrient 1.5% agar plates (KK_2 buffer pH 6.4) or KK_2 supplemented with caffeine (1, 2.5 and 5 mM) or 1 mM EGTA.

Disruption of the *hd* gene by homologous recombination

The targeting construct for disruption of the *hd* gene was made by standard cloning procedures in the floxed-Bsr gene disruption vector pLPBLP [63]. PCR was used to amplify genomic sequences flanking and within the coding region of the *hd* gene. The 5′ targeting region of *hd* was amplified using primers 5′CCCGGTACCATGGATCTTATTCG3′ and 5′-CCCAAGCTTCCAATGATAATATA3′ which incorporate restriction sites (underlined) for *Kpn*I and *Hind*III, respectively to facilitate cloning into the vector pLPBLP. The 3′ targeting region of the *hd* gene was amplified using primers 5′CCCCTGCAGTTCTCCACCAATCT3′ and 5′CCCGGATCCGTTATATGATCGG3′ which incorporate restriction sites (underlined) for *Pst*I and *BamH*I, respectively to facilitate directional cloning into pLPBLP. For electroporation, 5×10^6 cells in 100 µL of ice cold buffer H-50 (20 mM HEPES, 50 mM KCl, 10 mM NaCl, 1 mM $MgSO_4$, 5 mM $NaHCO_3$, 1 mM NaH_2PO_4) was mixed with 10 µg of linearized gene-targeting DNA and electroporated twice, waiting for about 5 sec between pulses, using a Bio-Rad Gene Pulser (0.85 kv, 25 µF) (Bio-Rad, Hercules, CA) [64]. The next day, the media was replaced with fresh HL-5 supplemented with 10 µg/ml blasticidin. Single colonies were collected and replica-plated into multiple 96-well plates. Genomic DNA was extracted exactly as described [65], and targeted gene disruptions were identified initially by several PCR reactions using a combination of primers (Table S1). Clonal isolates from multiple independent mutants possessing the same disruption and sporulation phenotype were obtained. One of these clones (httE13) was used in all subsequent experiments. Southern blot hybridizations using Bsr DIG-labeled probes were used for definitive confirmation of gene disruption. The *Bsr* fragment from pLPBLP was agarose gel purified and used to make a DIG-labeled probe using the DIG-High Prime starter kit from Roche. Hybridization was carried essentially as described in the DIG-DNA Detection manual (Roche). Blots were washed at room temperature and then at 68°C, equilibrated in detection buffer, incubated in disodium 3-(4-methoxyspiro {1,2-dioxetane-3,2′-(5′-chloro)tricyclo[3.3.1.1]decan}-4-yl) phenyl phosphate (CSPD) for 15 minutes at 37°C and developed using enhanced chemiluminescence XOMAT Kodak film.

RT-PCR analysis of *hd* splice variants

The analysis of total RNA for *hd* alternate splice variants was performed using exon-specific primers and RT-PCR. Total RNA was collected from vegetative cells and at 6-hour increments during development using the Qiagen RNeasy kit followed by on-column DNase digestion (Qiagen). The *hd* transcript was detected using the Qiagen One-Step RT-PCR kit as per the manufacturer's recommendations using primer pairs listed in Table S2.

Conventional and fluorescence microscopy

Growing cells were harvested and deposited into Lab-tek chambered cover glass (8 well) at 1×10^5 cells/cm^2 and allowed to grow overnight in HL-5 at 21°C. For F-actin staining, the media was aspirated and cells were fixed with 4% formaldehyde in PDF buffer (20 mM KCl, 11 mM K_2HPO_4, 13.2 mM KH_2PO_4, 1 mM $CaCl_2$, 2.5 mM $MgSO_4$, pH 6.4) at room temperature for 15 minutes, permeabilized with 0.025% TX-100 in PDF buffer for 15 minutes, followed by a brief wash in PDF buffer. Cellular F-actin was stained by incubating the fixed cells with Texas-Red-conjugated phalloidin (Molecular Probes, Eugene, OR) at a concentration suggested by the manufacturer for 25 minutes at room temperature and washed three times with PBS prior to viewing. To assess the effects of nutrient removal, the HL-5 was aspirated and replaced with KK_2 buffer (16.5 mM KH_2PO_4 and 3.8 mM K_2HPO_4). After starving cells for 1 hr, the cells were fixed and processed for F-actin staining as described above. Nuclei were stained with Hoechst 33342. Images were taken on an inverted NIKON microscope TE2000 (NIKON Instruments, Dallas, TX) with either 4×, 20×, 40× objectives or a 63× 1.4 NA PlanFluor oil immersion objective and Quantix camera (Roper Scientific, AZ) controlled by NIS Elements and processed with Adobe Photoshop software (Adobe, San Jose, CA).

Spore viability assays

The viability of wild-type and *hd*$^-$ spores were assayed by harvesting approximately 2×10^8 cells and plating onto 10 cm non-nutrient 1.5% agar plates (KK_2 buffer pH 6.4). Spores from mature fruiting bodies were harvested using sterile pipette tips

containing 10 µL of spore buffer (40 mM KH_2PO_4, 20 mM KCl, 2.5 mM $MgCl_2$), washed twice by centrifugation at 12,500 g for 2 minutes at room temperature and counted with a hemocytometer. Aliquots of 100 spores were heated to 45°C for 10 minutes, incubated with 0.5% NP40 detergent (Sigma-Aldrich, St Louis, MO) for 5 minutes or incubated with spore buffer alone for 5 minutes as a control. Spores were washed and plated in triplicate onto SM-5 agar plates in a suspension of bacteria (either *E. coli* B/R or *K. aerogenes*) and grown for 7 days at 21°C. The viability of spores was assessed by counting the number of clear plaques formed on the bacterial lawns for each treatment. Relative viability was measured as the percentage of hd^- plaques formed compared to wild-type cells for all conditions.

Submerged-monolayer assay

The submerged-monolayer assay was modified from an assay described previously [66]. For stalk cell induction, vegetative cells were washed once with KK_2 buffer and three times with stalk buffer (10 mM morpholineethanesulfonic acid [MES], 2 mM NaCl, 10 mM KCl, 1 mM $CaCl_2$, 5 mM cAMP and 200 µg of penicillin-streptomycin per ml, pH 6.2). The cells were then plated into 24-well tissue culture plates at a density of 10^4 cells/cm^2 and incubated in the presence or absence of 10–100 nM differentiation-inducing factor (DIF-1). A calcofluor solution (0.01%) was added to the wells for 5 min., removed and the cells were observed immediately by microscopy. Only the cells that were vacuolated and stained by calcofluor were counted as stalk cells [67]. For spore cell induction, wild-type cells and hd^- cells were washed once with KK_2 buffer and three times with spore buffer (10 mM MES, 20 mM NaCl, 20 mM KCl, 1 mM $CaCl_2$, 1 mM $MgCl_2$) and then incubated in spore buffer supplemented with 5–15 mM 8-Br-cAMP for 24 and 48 hours [68] and visualized in bright field microscopy. Relative sporulation percentage was calculated as described for the stalk cell assay. Assays were performed three independent times, each with three replicates.

Development of chimeric mixture of GFP-labeled wild-type and hd^- cells

In *Dictyostelium*, chimeras are readily produced by mixing cells of different genetic backgrounds and allowing them to co-aggregate to form a chimeric mound [69]. For chimera aggregation, development and tracing cell lineages, wild-type and hd^- cells were transfected with pTX-GFP and selected in 10 µg/mL G418. GFP-marked and unmarked cells were mixed at varying percentages prior to deposition under buffer or development on non-nutrient agar as described above.

Electron microscopy (EM)

To examine spores under electron microscopy, greater than 2×10^8 wild-type and huntingtin-null spores were harvested and resuspended in 2% glutaraldehyde (EM grade) in spore buffer and incubated for 1–2 hours at 21°C. After this fixation, the spores were washed in spore buffer and processed for electron microscopy (EM). Electron micrographs were prepared using the CHGR Microscopy Core.

Generation of DdHtt (595):GFP reporter construct

Dictyostelium expression vector pTX-GFP was digested with restriction enzymes *Sal*I and *Kpn*I, releasing its actin15 promoter and the first 11 codons of the ORF containing an 8× His tag [70]. A region of DNA sequence including 595 bp 5′ to *hd* ORF and the first 42 bp of the ORF was amplified from *D. discoideum* (AX3) genomic DNA using forward primer DdHtt_F608+SalI (5′- AATATGTGTCGACCTACAGTTATTAAATAAATTG-CAATAAAGGTGC-3′) and reverse primer DdHtt_R_Pro+*Kpn*I (5′-TCCTCTGTGGTACCTGGTGATGCTGATAATATATC-TAATCCACG-3′). The product was digested with restriction enzymes *Sal*I and *Kpn*I to facilitate ligation into the vector upstream and in frame with the GFP ORF sequence. The resulting vector therefore expresses the first 14 amino acids of *hd* fused upstream of GFP, under the control of the predicted minimal *hd* promoter sequence. The vector was transformed into AX3 cells as previously described [71].

Cell–cell adhesion assay

Cell-cell adhesion was assessed as previously described [72]. Briefly, cells were grown axenically to a density of $2–5\times10^6$ cells/mL, washed twice in ½ volume of ice cold Soerensen buffer (SB), resuspended in 0.4 initial volume of SB and vortexed, then immediately counted in order to adjust the concentration of cells to 5×10^6 cells/mL. Cells were incubated in an Erlenmeyer flask at 150 rpm and 21°C and samples were collected at various time points over a period of 6 hours. For each collection point, cells were incubated in the presence or absence of 10 mM EDTA for 30 minutes and fixed with 2% glutaraldehyde. Single cells were counted using a hemocytometer. All experiments were performed in duplicate and the mean value for single cells in duplicate samples, expressed as percentage of total cells was plotted over time.

Osmotic shock

Control (wild-type) or hd^- cells were grown HL-5 and the medium was replaced with low ionic buffer (KK_2), water (hypotonic) or 400 mM sorbitol in KK_2 (hyperosmotic). At various time points samples were taken, diluted into KK_2 phosphate buffer containing *K. aerogenes* and plated onto SM agar plates to assay for viability. Cell lysis upon osmotic shock was also observed visually by brightfield microscopy. All experiments were performed in triplicate.

Supporting Information

Figure S1 Comparison of growth rates between wild-type and hd^- cells. Cells were inoculated into fresh HL-5 medium at an initial density of 5×10^4 cells/ml and incubated at 21°C with shaking at 150 rpm on an orbital shaker. Cell counts were performed every 24 hours, under a microscope, using a hemocytometer. The graph represents the average of the readings of the four flasks for each strain, at each time-point. Hd^- cells grow with a doubling-time of ~10 hours compared to the ~12 hours doubling time of wild-type control cells in suspension culture.
(TIF)

Figure S2 The addition of bivalent cations to the medium rescues cAMP relay and streaming of hd^- cells. (A) Wild-type and (B) hd^- cells (1×10^5 cells/cm^2) were submerged under KK_2 in the presence of 1 mM $CaCl_2$ and allowed to develop for 6 hours. Long streams of wild-type cells are seen moving into aggregation centers (*left panel*). In the presence of Ca^{2+}, hd^- cells are now capable of streaming but form much smaller streams (*right panel*).
(TIF)

Table S1 Primers used for preliminary genomic DNA PCR screening of *hd-null* cells. Sequences of primers presented in the 5′-3′ direction that were used to initially identify putative hd^- cells.
(DOCX)

Table S2 Primers used to detect the presence of alternatively spliced *hd* mRNA transcripts during growth and development.

Sequences of primers presented in the 5′-3′ direction that was used in RT-PCR reactions to detect the presence of alternatively spliced *hd* transcripts from wild-type AX3 purified total RNA.
(DOC)

Video S1 Osmoregulation of wild-type *Dictyostelium* cells during hypoosmotic conditions. Growth media was replaced with water and cells were imaged using brightfield microscopy. After 2 hours in water, images were taken every 20 seconds over a period of 1 hour with a frame rate of 50 msec.
(AVI)

Video S2 Lysis of *Dictyostelium hd*$^-$ cells during hypoosmotic conditions. Growth media was replaced with water and cells were imaged using brightfield microscopy. After 2 hours in water, images were taken every 20 seconds over a period of 1 hour with a frame rate of 50 msec.
(AVI)

Video S3 Pulsatile cAMP signaling and chemotactic streaming of wild-type *Dictyostelium* cells. Pulsatile signaling of cAMP appears as dark, periodic propagating waves moving from right to left across the field of view prior to the onset of chemotactic streaming. Cells were imaged using brightfield microscopy and images were captured every 15 seconds over a period of 6 hours. Video is representative of the time between 5 and 6 hours with a frame rate of 50 msec.
(AVI)

Video S4 *Dictyostelium hd*$^-$ cells do not exhibit pulsatile cAMP signaling or chemotactic streaming into aggregation territories. *Hd*$^-$ cells fail to initiate pulsatile waves and consequently do not stream into aggregation centers. Cells can be seen randomly colliding to form loose aggregates. Cells were imaged using brightfield microscopy and images were captured every 15 seconds over a period of 8 hours. Video is representative of the time between 5 and 6 hours with a frame rate of 50 msec.
(AVI)

Video S5 Rescue of pulsatile cAMP signaling and chemotactic streaming of *Dictyostelium hd*$^-$ cells by addition of bivalent cations. Under KK_2 buffer *Hd*$^-$ cells fail to initiate pulsatile waves and consequently do not stream into aggregation centers. However, addition of 1 mM $CaCl_2$ (shown here) rescues pulsatile signaling and partially rescues chemotactic streaming. The streams formed by *hd*$^-$ cells under these conditions tend to break and are shorter than that seen with wild-type cells. Cells were imaged using brightfield microscopy and images were captured every 15 seconds over a period of 6 hours. Video is representative of the time between 5 and 6 hours with a frame rate of 50 msec.
(AVI)

Video S6 EGTA blocks calcium rescue of *hd*$^-$ early development. *Dictyostelium hd*$^-$ cells do not exhibit pulsatile cAMP signaling or chemotactic streaming into aggregation territories when incubated with 1 mM $CaCl_2$ in the presence of 1 mM EGTA. *Hd*$^-$ cells failed to initiate pulsatile waves and consequently do not stream into aggregation centers, become rounded and can be seen randomly colliding. Cells were imaged using brightfield microscopy and images were captured every 15 seconds over a period of 8 hours. Video is representative of the time between 5 and 6 hours with a frame rate of 50 msec.
(AVI)

Acknowledgments

We thank the Dicty Stock Center for supplying the parental *Dictyostelium* AX3 strains and pTX-GFP plasmid.

Author Contributions

Conceived and designed the experiments: MAM JFG. Performed the experiments: MAM ALL MNT. Analyzed the data: MAM MEM JFG. Contributed reagents/materials/analysis tools: MAM WW MEM JFG. Wrote the paper: MAM JFG.

References

1. Vonsattel JP, Myers RH, Stevens TJ, Ferrante RJ, Bird ED, et al. (1985) Neuropathological classification of Huntington's disease. J Neuropathol Exp Neurol 44(6): 559–577.
2. Martin JB, Gusella JF (1986) Huntington's disease: Pathogenesis and management. N Engl J Med 315(20): 1267–1276.
3. Gusella JF, Wexler NS, Conneally PM, Naylor SL, Anderson MA, et al. (1983) A polymorphic DNA marker genetically linked to Huntington's disease. Nature 306(5940): 234–238.
4. Gusella JF, MacDonald ME (1995) Huntington's Disease. Semin Cell Biol 6: 21–28.
5. The Huntington's Disease Collaborative Research Group (1993) A novel gene containing a trinucleotide repeat that is expanded and unstable on Huntington's Disease chromosomes. Cell 72: 971–983.
6. Andrade MA, Bork P (1995) HEAT repeats in the huntingtin protein. Nat Genetics 11(2): 115–116.
7. Gusella JF, MacDonald ME (2006) Huntington's disease: Seeing the pathogenic process through a genetic lens. Trends Biochem Soc 31(9): 533–540.
8. MacDonald ME, Gusella JF (1996) Huntington's disease: Translating a CAG repeat into a pathogenic mechanism. Curr Opin Neurobiol 6(5): 638–643.
9. Gusella JF, MacDonald ME (2000) Molecular genetics: Unmasking polyglutamine triggers in neurodegenerative disease. Nat Rev Neurosci 1(2): 109–115.
10. Duyao MP, Auerbach AB, Ryan A, Persichetti F, Barnes GT, et al. (1995) Inactivation of the mouse Huntington's disease gene homolog Hdh. Science 269: 407–410.
11. Nasir J, Floresco SB, O'Kusky JR, Diewert VM, Richman JM, et al. (1995) Targeted disruption of the Huntington's disease gene results in embryonic lethality and behavioral and morphological changes in heterozygotes. Cell 81(5): 811–823.
12. Zeitlin S, Liu JP, Chapman DL, Papaioannou VE, Efstratiadis A (1995) Increased apoptosis and early embryonic lethality in mice nullizygous for the Huntington's disease gene homologue. Nat Genet 11(2): 155–163.
13. Lumsden AL, Henshall TL, Dayan S, Lardelli MT, Richards RI (2007) Huntingtin-deficient zebrafish exhibit defects in iron utilization and development. Hum Mol Genet 16(16): 1905–1920.
14. Zhang S, Feany MB, Saraswati S, Littleton JT, Perrimon N (2009) Inactivation of *Drosophila* Huntingtin affects long-term adult functioning and the pathogenesis of a Huntington's disease model. Dis Model Mech 2(5–6): 247–266.
15. Seong IS, Woda JM, Song JJ, Lloret A, Abeyrathne PD, et al. (2009) Huntingtin facilitates polycomb repressive complex 2. Hum Mol Genet 19(4): 573–583.
16. Cattaneo E, Rigamonti D, Goffredo D, Zuccato C, Squitieri F, et al. (2001) Loss of normal huntingtin function: New developments in Huntington's disease research. Trends Neurosci 24(3): 182–188.
17. Harjes P, Wanker EE (2003) The hunt for huntingtin function: interaction partners tell many different stories. Trends Biochem Sci 28: 425–433.
18. Cattaneo E, Zuccato C, Tartari M (2005) Normal huntingtin function: An alternative approach to Huntington's disease. Nat Rev Neurosci 6(12): 919–930.
19. Loomis WF (1982) The Development of *Dictyostelium discoideum* Academic Press, New York USA.
20. McMains VC, Myre M, Kreppel L, Kimmel AR (2010) *Dictyostelium* possesses highly diverged presenilin/gamma-secretase that regulates growth and cell-fate specification and can accurately process human APP: a system for functional studies of the presenilin/gamma-secretase complex. Dis Model Mech 3(9–10): 581–594.
21. Rehberg M, Kleylein-Sohn J, Faix J, Ho TH, Schulz I, et al. (2005) *Dictyostelium* LIS1 is a centrosomal protein required for microtubule/cell cortex interactions, nucleus/centrosome linkage, and actin dynamics. Mol Biol Cell 16(6): 2759–2771.
22. Hägele S, Köhler R, Merkert H, Schleicher M, Hacker J, et al. (2000) *Dictyostelium discoideum*: a new host model system for intracellular pathogens of the genus Legionella. Cell Microbiol 2(2): 165–171.
23. Maselli AG, Davis R, Furukawa R, Fechheimer M (2002) Formation of Hirano bodies in *Dictyostelium* and mammalian cells induced by expression of a modified form of an actin-crosslinking protein. J Cell Sci 115(9): 1939–1949.
24. Wilczynska Z, Barth C, Fisher PR (1997) Mitochondrial mutations impair signal transduction in *Dictyostelium discoideum* slugs. Biochem Biophys Res Commun 234(1): 39–43.
25. Parent CA, Devreotes P (1996) Molecular genetics of signal transduction in *Dictyostelium*. Annu Rev Biochem 65: 411–440.

26. Soderbom F, Loomis B (1998) Cell-cell signaling during *Dictyostelium* development. Trends Microbiol 6(10): 402–406.
27. Williams JG, Duffy KT, Lane DP, McRobbie SJ, Harwood AJ, et al. (1989) Origins of the prestalk-prespore pattern in *Dictyostelium* development. Cell 59(6): 1157–1163.
28. Chisholm RL, Gaudet P, Just EM, Pilcher KE, Fey P, et al. (2006) dictyBase: The model organism database for *Dictyostelium discoideum*. Nucleic Acids Res 34: 423–427.
29. Altschul SF, Madden TL, Schäffer AA, Zhang J, Zhang Z, et al. (1997) Gapped BLAST and PSI-BLAST: a new generation of protein database search programs. Nucleic Acids Res 25: 3389–3402.
30. Schäffer AA, Aravind L, Madden TL, Shavirin S, Spouge JL, et al. (2001) Improving the accuracy of PSI-BLAST protein database searches with composition-based statistics and other refinements. Nucleic Acids Res 29: 2994–3005.
31. Takano H, Gusella JF (2002) The predominantly HEAT-like motif structure of huntingtin and its association and coincident nuclear entry with dorsal, an NF-kB/Rel/dorsal family transcription factor. BMC Neurosci 3: 15.
32. Tartari M, Gissi C, Lo Sardo V, Zuccato C, Picardi E, et al. (2008) Phylogenetic comparison of huntingtin homologues reveals the appearance of a primitive polyQ in sea urchin. Mol Biol Evol 25(2): 330–338.
33. Insall R (2005) The *Dictyostelium* genome: The private life of a social model revealed? Genome Biol 6(6): 222.
34. Parikh A, Miranda ER, Katoh-Kurasawa M, Fuller D, Rot G, et al. (2010) Conserved developmental transcriptomes in evolutionarily divergent species. Genome Biol 11(3): R35.
35. Kimmel AR (1987) Different molecular mechanisms for cAMP regulation of gene expression during *Dictyostelium* development. Dev Biol 122: 163–71.
36. Brenner M, Thoms SD (1984) Caffeine blocks activation of cAMP synthesis in *Dictyostelium discoideum*. Dev Biol 101: 136–146.
37. Kay RR (1987) Cell differentiation in monolayers and the investigation of slime mold morphogens. Methods Cell Biol 28: 433–448.
38. Williams JG (2006) Transcriptional regulation of *Dictyostelium* pattern formation. EMBO Rep 7(7): 694–698.
39. Chung CY, Funamoto S, Firtel RA (2001) Signaling pathways controlling cell polarity and chemotaxis. Trends Biochem Sci 26(9): 557–566.
40. Wang B, Kuspa A (1997) *Dictyostelium* development in the absence of cAMP. Science 277: 251–254.
41. Brzostowski JA, Johnson C, Kimmel AR (2002) Galpha-mediated inhibition of developmental signal response. Curr Biol 12(14): 1199–1208.
42. Zhu Q, Clarke M (1992) Association of calmodulin and an unconventional myosin with the contractile vacuole complex of *Dictyostelium discoideum*. J Cell Biol 118(2): 347–358.
43. Marchesini N, Ruiz FA, Vieira M, Docampo R (2002) Acidocalcisomes are functionally linked to the contractile vacuole of *Dictyostelium discoideum*.. J Biol Chem 277(10): 8146–8153.
44. Malchow D, Lusche DF, Schlatterer C, De Lozanne A, Müller-Taubenberger A (2006) The contractile vacuole in Ca^{2+}-regulation in *Dictyostelium*: its essential function for cAMP-induced Ca^{2+}-influx. BMC Dev Biol 6: 31–38.
45. Gerisch G, Heuser J, Clarke M (2002) Tubular-vesicular transformation in the contractile vacuole system of *Dictyostelium*. Cell Biol Int 26(10): 845–852.
46. Steck TL, Chiaraviglio L, Meredith S (1997) Osmotic homeostasis in *Dictyostelium discoideum*: excretion of amino acids and ingested solutes. J Eukaryot Microbiol 44(5): 503–510.
47. Heath RJ, Insall RH (2008) *Dictyostelium* MEGAPs: F-BAR domain proteins that regulate motility and membrane tubulation in contractile vacuoles. J Cell Sci 121(7): 1054–1064.
48. Rivero F, Köppel B, Peracino B, Bozzaro S, Siegert F, et al. (1996) The role of the cortical cytoskeleton: F-actin crosslinking proteins protect against osmotic stress, ensure cell size, cell shape and motility, and contribute to phagocytosis and development. J Cell Sci 109(Pt 11): 2679–2691.
49. Du F, Edwards K, Shen Z, Sun B, De Lozanne A, et al. (2008) Regulation of contractile vacuole formation and activity in *Dictyostelium*. EMBO J 27(15): 2064–2076.
50. Sesaki H, Wong EF, Siu CH (1997) The cell adhesion molecule DdCAD-1 in *Dictyostelium* is targeted to the cell surface by a nonclassical transport pathway involving contractile vacuoles. J Cell Biol 138(4): 939–951.
51. Desbarats L, Brar SK, Siu CH (1994) Involvement of cell-cell adhesion in the expression of the cell cohesion molecule gp80 in *Dictyostelium discoideum*. J Cell Sci 107(Pt 6): 1705–1712.
52. Brar SK, Siu CH (1993) Characterization of the cell adhesion molecule gp24 in *Dictyostelium discoideum*. J Biol Chem 268(33): 24902–24909.
53. Muller K, Gerisch G (1978) A specific glycoprotein as the target site of adhesion blocking Fab in aggregating *Dictyostelium* cells. Nature 274(5670): 445–449.
54. Muller K, Gerisch G, Fromme I, Mayer H, Tsugita A (1979) A membrane glycoprotein of aggregating *Dictyostelium* cells with the properties of contact sites. Eur J Biochem 99(2): 419–426.
55. Gerisch G, Fromm H, Huesgen A, Wick U (1975) Control of cell-contact sites by cyclic AMP pulses in differentiating *Dictyostelium* cells. Nature 255(5509): 547–549.
56. Ponte E, Bracco E, Faix J, Bozzaro S (1998) Detection of subtle phenotypes: the case of the cell adhesion molecule csaA in *Dictyostelium*. Proc Natl Acad Sci USA 95(16): 9360–9365.
57. Henshall TL, Tucker B, Lumsden AL, Nornes S, Lardelli MT, et al. (2009) Selective neuronal requirement for huntingtin in the developing zebrafish. Hum Mol Genet 18(24): 4830–4842.
58. Reiner A, Del Mar N, Meade CA, Yang H, Dragatsis I, et al. (2001) Neurons lacking huntingtin differentially colonize brain and survive in chimeric mice. J Neurosci 21(19): 7608–7619.
59. Sameshima M, Kishi Y, Osumi M, Mahadeo D, Cotter DA (2000) Novel actin cytoskeleton: actin tubules. Cell Struct Funct 25(5): 291–295.
60. Saran S, Schaap P (2004) Adenylyl cyclase G is activated by an intramolecular osmosensor. Mol Biol Cell 15(3): 1479–1486.
61. van Es S, Virdy KJ, Pitt GS, Meima M, Sands TW, et al. (1996) Adenylyl cyclase G, an osmosensor controlling germination of *Dictyostelium* spores. J Biol Chem 271(39): 23623–23625.
62. Virdy KJ, Sands TW, Kopko SH, van Es S, Meima M, et al. (1999) High cAMP in spores of *Dictyostelium discoideum*: association with spore dormancy and inhibition of germination. Microbiology 145(Pt 8): 1883–1890.
63. Faix J, Kreppel L, Shaulsky G, Schleicher M, Kimmel AR (2004) A rapid and efficient method to generate multiple gene disruptions in *Dictyostelium* discoideum using a single selectable marker and the Cre-loxP system. Nucleic Acids Res 32(19): e143.
64. Pang KM, Lynes MA, Knecht DA (1999) Variables controlling the expression level of exogenous genes in *Dictyostelium*. Plasmid 41: 187–197.
65. Charette SJ, Cosson P (2004) Preparation of genomic DNA from *Dictyostelium discoideum* for PCR analysis. Biotechniques 36(4): 574–575.
66. Harwood AJ, Plyte SE, Woodgett J, Strutt H, Kay RR (1995) Glycogen synthase kinase 3 regulates cell fate in *Dictyostelium*. Cell 80(1): 139–148.
67. Harrington BJ, Raper KB (1968) Use of a fluorescent brightener to demonstrate cellulose in the cellular slime molds. Appl Microbiol 16(1): 106–113.
68. Kubohara Y, Arai A, Gokan N, Hosaka K (2007) Pharmacological evidence that stalk cell differentiation involves increases in the intracellular $Ca^{(2+)}$ and $H^{(+)}$ concentrations in *Dictyostelium discoideum*. Dev Growth Differ 49(3): 253–264.
69. Houle J, Balthazar J, West CM (1989) A glycosylation mutation affects cell fate in chimeras of *Dictyostelium discoideum*. Proc Natl Acad Sci USA 86(10): 3679–3683.
70. Levi S, Polyakov M, Egelhoff TT (2000) Green fluorescent protein and epitope tag fusion vectors for *Dictyostelium discoideum*. Plasmid 44(3): 231–238.
71. Myre MA, O'Day DH (2002) Nucleomorphin: A novel, acidic, nuclear calmodulin-binding protein from *Dictyostelium* that regulates nuclear number. J Biol Chem 277(22): 19735–19744.
72. Bozzaro S, Merkl R, Gerisch G (1987) Cell adhesion: its quantification, assay of the molecules involved, and selection of defective mutants in *Dictyostelium* and *Polysphondylium*. Methods Cell Biol 28: 359–385.